Extent, timing and nature of retreat of the British-Irish Ice Sheet offshore of north-western Ireland during and following the Last Glacial Maximum

WEILBACH, KASPER

Extent, timing and nature of retreat of the British-Irish Ice Sheet offshore of north-western Ireland during and following the Last Glacial Maximum

Kasper Weilbach

A thesis submitted for the degree of Doctor of Philosophy

August 2017

Re-submitted with corrections June 2018

Supervisors: Colm O'Cofaigh, Jerry Lloyd, Sara Benetti, Paul Dunlop & John Howe

Department of Geography

University of Durham

Abstract

There has been a long history of research that has attempted to reconstruct the extent and dynamics of the British-Irish Ice Sheet (BIIS) during the last glacial cycle. Early reconstructions of ice extent in Ireland were based on terrestrial evidence, and advocated a relatively restricted ice sheet during the Last Glacial Maximum (LGM) that did not cover the whole of the island. More recent investigations from the continental shelf around Britain and Ireland reveal evidence for a much larger ice sheet, confluent with the Fennoscandian Ice Sheet in the North Sea and extending westwards onto the Atlantic continental shelf. However, offshore chronological control on the timing of ice sheet advance and retreat remain poor for many sectors of the continental shelf, particularly west and north-west of Ireland.

This thesis brings together high-resolution multibeam swath bathymetry, sub-bottom profiler data, and sedimentological, micropalaeontological and geochronological data, in order to reconstruct the extent, timing and dynamics of the last ice sheet in Donegal Bay and the adjoining north-western Irish continental shelf. This area is of interest due to its location adjacent to the North Atlantic and the Gulf Stream branch of the thermohaline circulation, making this sector of the BIIS sensitive to external forcing. The new data in this thesis show evidence for the extension of a grounded ice sheet to the shelf edge at or shortly after 26.3 cal ka BP, and thus during the LGM. Foraminiferal assemblages and lithofacies show that subsequent retreat took place in a glacimarine environment, and acoustic stratigraphic data show that the retreat was characterised by several still stands and re-advances, creating a series of arcuate moraines across the shelf. Chronological data constrain initial retreat from the shelf edge to before 24.8 cal ka BP, with formation of a large moraine at the mouth of Donegal Bay dated to between 20.2 and 17.9 cal ka BP.

The results and interpretations presented in this thesis thereby offers a new interpretation of the extent, timing and nature of the north-western sector of the BIIS, offshore of Donegal Bay and across the adjacent continental shelf, during the LGM and the subsequent deglaciation.

Contents

List of Figures

List of Tables

Declaration:

I declare that this thesis contains the research and results of work carried out by myself, except where otherwise stated, at Durham University between October 2013 and September 2016, as part of my PhD. Where results or interpretations of other authors and from previous work have been presented, references have been duly acknowledged. This work has not previously been submitted to this or any other university.

Copyright Statement:

Acknowledgements

This Ph.D project received funding through the People Programme (Marie Curie Actions) of the European Union's Seventh Framework Programme FP7/2007-2013/ under REA grant agreement n^o: 317217, and from the Britice-Chrono project funded by the UK National Environment Research Council grant NE/J007196/1. The CE08 research survey was carried out under the Sea Change Strategy with the support of the Marine Institute and the Marine Research Sub-programme of the National Development Plan 2007-2013. For research cruise CE08, the Geological Survey of Ireland lent the vibrocore for core acquisition and the INFOMAR programme (www.infomar.ie) provided additional funding in support of cruise activities.

I would like to express my gratitude towards my supervisors, Professor Colm O'Cofaigh and Dr. Jeremy Lloyd, for continuous supervision and advice during the many phases of this thesis, none the least for the numerous corrections needed during the writing process. I would also extend my gratitude towards my supervisors based at other institutions: Dr. Sara Benetti and Dr. Paul Dunlop from Ulster University and Dr. John Howe from the Scottish Association for Marine Science, for advice and guidance throughout the project. I would also like to thank Ulster University for allowing me to undergo a secondment at their facilities in Coleraine NI.

Further I would like to thank the Britice-Chrono project for allowing me to participate in the JC106 cruise. In that regard I would also like to thank the crew of the RRS James Cook and the BGS team for ensuring the success of the cruise.

I would like to thank Dr. Louise Callard for countless identifications of foraminifera whenever my own knowledge was insufficient, and for good advice and counselling with the chronological and palaeoenvironmental interpretations in this project.

Finally I would like to thank my colleagues in the GLANAM project, first and foremost my colleagues in the Durham office, for numerous discussions, advices, guidance, help with technical issues, and countless coffee breaks. Secondly the rest of the GLANAM group for interesting workshops, conferences, and for bringing fresh eyes to the project when needed.

1. *Introduction*

1.1 Rationale

According to the fifth assessment report of the Intergovernmental Panel on Climate Change (IPCC), the global cryosphere had an overall net loss of 226 Gt yr^{-1} in the period of 1971 to 2009 (Figure 1.1), and as high as 275 Gt yr^{-1} from 1993 to 2009 (Figure 1.1) (Stocker *et al.*, 2013). The Greenland ice sheet had an average loss of 34 Gt yr^{-1}, in the period of 1992 to 2001 with an increase to 215 Gt yr^{-1} from 2002 to 2011. The Antarctic Ice Sheet experienced an average loss of 30 Gt yr^{-1} from 1992 to 2001 with an average increase to 147 Gt yr^{-1} from 2002 to 2011. (Stocker *et al.*, 2013).

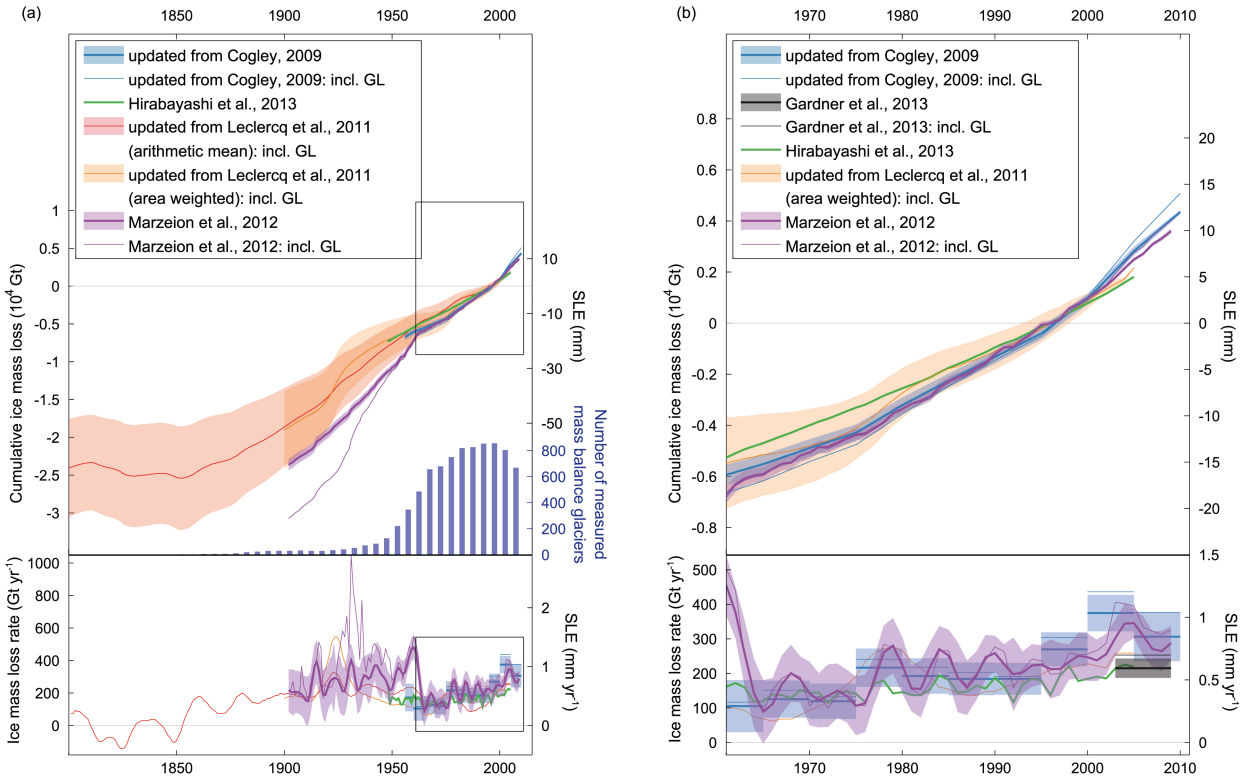

Figure 1.1: Global cumulative and annual glacier mass change for (a) 1801-2010 and (b) 1961-2010. The cumulative estimates are all set to zero mean over 1986-2005. Estimates are based on glacier length variations, from area-weight extrapolations of individual directly and geodetically measured glacier mass budgets, and from modelling with atmospheric variables as input. (Vaughan *et al.*, 2013)

Coinciding with this ice loss, is an average increase in global atmospheric temperature, ocean temperatures and mean sea level. Over the period from 1880 to 2012, there has been an increase in global atmospheric temperature of 0.85^{o}C with the largest average increase happening in the 2003 to 2012 period (Stocker *et al.*, 2013). Globally, surface waters in the oceans have warmed by on average 0.11^{o}C from 1971 to 2010, and it is very likely that sea level rise has increased from 1.7 mm yr^{-1} between 1901 and 2010, to 2.0 mm yr^{-1} between 1971 and 2010 and even as high as 3.2 mm yr^{-1} between 1993 and 2010 (Stocker *et al.*, 2013). The underlying cause of these climatic changes have been interpreted as both natural and anthropogenic in origin, but cumulative emissions of anthropogenic CO_2 and other greenhouse gasses, is likely to be one of the main drivers of global mean surface temperature increase (Myhre *et al.*, 2013; Stocker *et al.*, 2013). By the end of the 21st century, cryospheric loss is predicted to be between 15 to 55% based on the low estimates and 35 to 85% based on high estimates. At the same time, total global mean sea level rise is predicted to be between 0.6 to 1 m (Figure 1.2), and ocean warming is predicted to be between 0.6 and 2.0^{o}C (Stocker *et al.*, 2013).

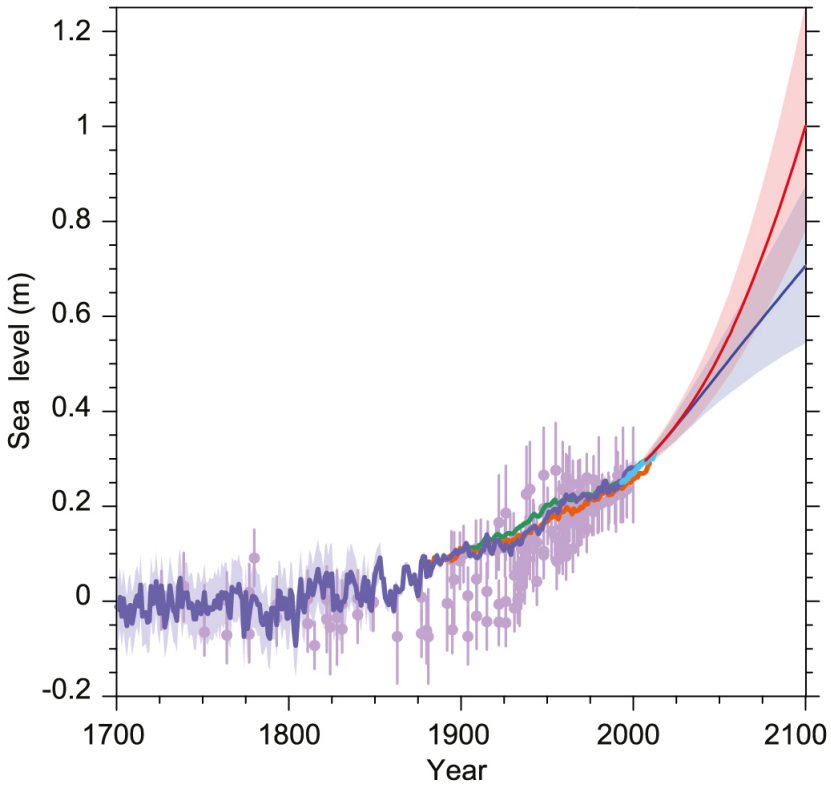

Figure 1.2: Compilation of paleo sea level data, tide gauge data, altimeter data and central estimates and likely ranges for projections of global mean sea level rise for minimum (blue) and maximum (red) estimations by 2100, all relative to pre-industrial values. (Church *et al.*, 2013)

Predictions on future dynamic behaviour of marine-terminating ice sheets based on numerical models, are often constrained by the short time period of modern observations. Gaining a better constraint on: chronology, grounding-line position, retreat rate and relative sea level, over centuries to millennia on individual ice sheets or ice sheet sectors, can thereby provide input data to better constrain model predictions (Clark *et al.*, 2012a; Bentley *et al.*, 2014; Lecavalier *et al.*, 2014; Stroeven *et al.*, 2016). With its relatively small size and location adjacent to the Gulf Stream branch of the thermohaline circulation (known to have undergone large and rapid oscillations during the Quaternary), the British-Irish Ice Sheet (BIIS) is likely to have been sensitive to external forcing, and potentially experienced a highly dynamic behaviour during deglaciation. It therefore serves as a good analogue for how marine-based ice sheets deglaciate (Clark *et al.*, 2012a).

The presence of an marine-terminating sector can have an important control on the dynamics and stability of large ice sheets (Bamber *et al.*, 2007; Rignot *et al.*, 2010; Joughin *et al.*, 2014). Understanding the effect of ongoing global warming on marine-terminating ice sheets is of considerable importance, due to the potential inherent instability of these ice masses and their potential impact on global sea level (Bamber *et al.*, 2007; Clark *et al.*, 2012a). Studying the dynamics of the BIIS in general and the marine-terminating NW Ireland sector in particular will help improve understanding of the links between large ice sheets and climate change. Whilst it is believed that external forcing, such as changes in solar insolation, is required to initiate deglaciation on a global scale, controls on the dynamics of smaller ice sheets or marine-terminating glaciers are believed to reflect a complex combination of factors, such as changes in sea surface temperatures, increased ice calving through sea level rise and changes in atmospheric temperature (Clark *et al.*, 2012a). As both the Greenland and Antarctic ice sheets have experienced significant ice mass loss over the past decades, there is a need to understand these recent trends and how they will impact sea level in a warming world (Clark *et al.*, 2012a).

The global LGM is traditionally defined as the most recent interval in Earth history when global ice sheets reached their maximum integrated volume (Mix *et al.*, 2001; Clark *et al.*, 2009b). This has traditionally been assessed by two independent methods estimating changes in sea level from direct observational evidence of past sea level relative to the present, or indirectly from temporal variations in oxygen isotopic composition of the mean ocean water (mow), δ^{18}O_*mow* (Mix *et al.*, 2001; Lambeck *et al.*, 2014). The associated eustatic sea level history has been measured based on the U/Th dated Barbados Relative sea level (RSL) curve (Peltier & Fairbanks, 2006), and recently a more precise RSL curve has been put together, comprising data from other Caribbean locations along with data from Tahiti, Papua New Guinea, Northwest Australia, New

Zealand, the western Indian Ocean, the Great Barrier Reef, and the Sunda Shelf between Vietnam and Malaysia (Lambeck *et al.*, 2014) (Figure 6.3). This curve show a ∼120-130 m drop in sea level (SL) between ∼30.0 ka BP and 19.0 ka BP. with the maximum lowstand SL at ∼ 21.0 ka BP (Lambeck *et al.*, 2002, 2014; Peltier & Fairbanks, 2006; Clark *et al.*, 2009b). This constrains the onset of the global LGM to between ∼30.0 ka BP (Lambeck *et al.*, 2014) and ∼26.5 ka BP (Clark *et al.*, 2009b) and the termination to ∼19.0 ka BP (Clark *et al.*, 2009b; Lambeck *et al.*, 2014).

$\delta^{18}O\_mow$ is a measure of stored ^{18}O-depleted ice on land. This can be measured on benthic foraminifera from deep sea sediment cores (Waelbroeck *et al.*, 2002), or directly in the ice cores from, for example, the Greenland Ice Sheet (Svensson *et al.*, 2006; Rasmussen *et al.*, 2008). Benthic foraminiferal $\delta^{18}O$ records from the North Atlantic, show an enrichment in ^{18}O leading up to the LGM followed by a depletion (Waelbroeck *et al.*, 2002).

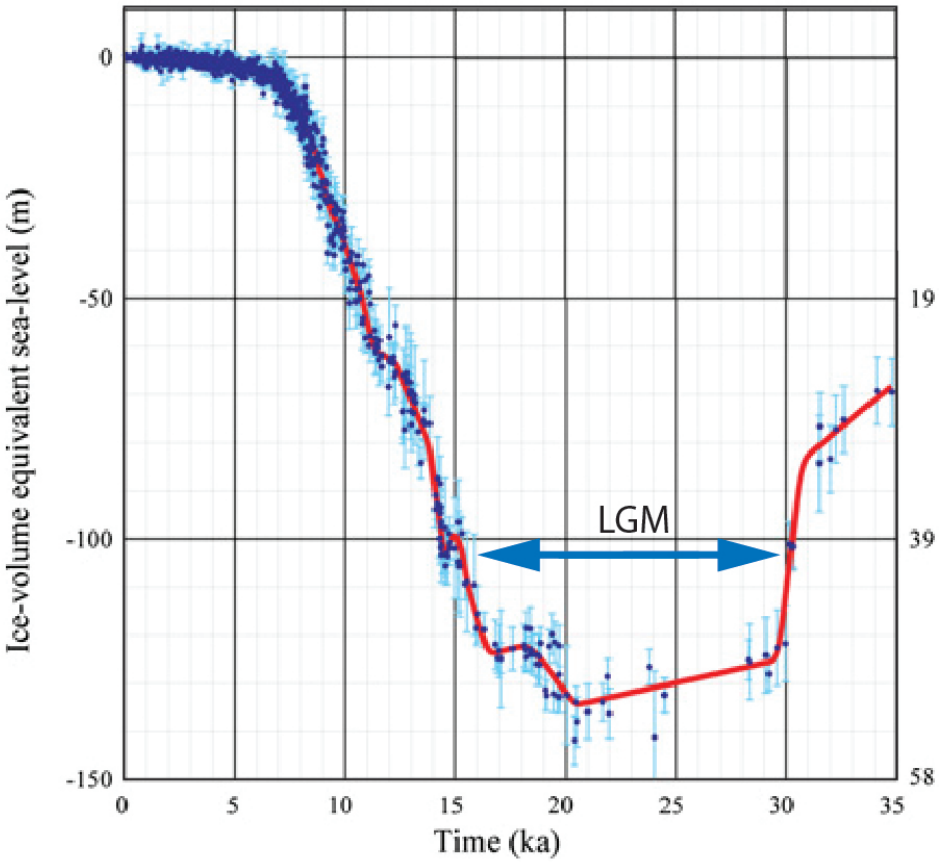

Figure 1.3: Composite global RSL curve from corals from Barbados, Tahiti, Papua New Guinea, Northwest Australia, New Zealand, the western Indian Ocean, the Great Barrier Reef, and the Sunda Shelf. After Lambeck *et al.* (2014).

1.2 Aim

The overall aim of this thesis is to reconstruct the extent, timing, and nature of the British-Irish Ice Sheet (BIIS) on the continental shelf offshore of North-west Ireland during the Last Glacial Maximum (LGM). This area is of particular interest due to its location adjacent to the North Atlantic, and the Gulf Stream branch of the thermohaline circulation, which experienced large and rapid oscillations during the Quaternary (Clark *et al.*, 2012a) potentially caused by adjacent ice sheets, through icebergs and meltwater fluxes (Ó Cofaigh *et al.*, 2012). In order to achieve the overall aim the following research questions were formulated:

1: What was the timing of the maximum extent of the last BIIS on the continental shelf offshore of NW Ireland and did this occur during the LGM or an earlier glaciation? How does this compare to other sectors of the BIIS and the LGM more widely?
2: What was the timing and cause(s) of ice retreat across the shelf, and how does this compare to other sectors of the BIIS?
3: What was the nature of the depositional environment during deglaciation? Did the ice sheet retreat in a marine-based or terrestrial-based setting?
4: What can be inferred about the retreat dynamics from the distribution and age of glacial landforms on the continental shelf?

To answer these questions a multi-proxy approach was adopted, investigating geophysical, sedimentological and micro-palaeontological data collected across the continental shelf offshore of North-west Ireland. In the following chapters, these data will be presented and through interpretations and discussions, a conclusive chapter will asses if the aims of the thesis can be answered.

2. *Background*

2.1 Onset of the Quaternary

During the Mesozoic era and well in to the early Cenozoic, the Earth was in a greenhouse state unable to sustain any large scale glaciations. During the last 55 million years, earth has experienced significant cooling, especially in polar and high latitude regions (Ruddiman, 2001), leading to the development of major high and mid-latitude glaciation. One of the drivers of this cooling is thought to be changing continental configuration due to plate tectonics, specifically closing of the Tethys sea, and collision of the Indian sub-continent with Eurasia, creating the Tibetan plateau (Ruddiman, 2001). Climate models suggest that there was a large decrease in temperature over the uplifted plateau, and that this change in temperature and altered circulation patterns had a further cooling effect over the northern oceans, particularly in the middle and high latitudes (Kutzbach *et al.*, 1993; Owen, 2013). This was augmented by increased albedo and chemical weathering of the uplifted plateau, both of which worked as a positive feedback, further driving global cooling (Owen, 2013). Oxygen isotope data acting as a proxy for ice volume together with plate-tectonic reconstructions, suggest that the onset of the present icehouse state started around 36.5 to 30 million years ago, with the opening of the Tasmanian gateway separating Australia from Antarctica and the opening of the Drake Passage between South America and Antarctica (Smith & Pickering, 2003; Coxall *et al.*, 2005; Scher *et al.*, 2015). The opening of these gateways eventually led to the development of the Antarctic Circumpolar Current, thermally isolating Antarctica and allowing for the development of the Antarctic Ice Sheet (Smith & Pickering, 2003; Coxall *et al.*, 2005).

In the early Pleistocene, Northern Hemisphere Glaciation (NHG) intensified, leading to the glacial - interglacial cycles typified by the Quaternary (Naafs *et al.*, 2010). The onset of this is in part, believed to be tied to the final closure of the Central American Seaway, which stopped the equatorial interchange of Pacific and Atlantic deep water, forcing warm saline water from the Caribbean to high northern latitudes, and thus starting the North Atlantic Deep Water production (Warren, 1983; Smith & Pickering, 2003). This process increased evaporation and supply of moisture in the high latitudes, which led to increased build up of continental ice sheets (Lear *et al.*, 2003; Bartoli *et al.*, 2005), further increased by the ice-albedo positive feedback effect.

In the late Quaternary, the past ∼800,000 years, climate has been dominated by the Earth's orbital eccentricity, causing glacial-interglacial cycles of about 100,000 to 110,000 years in the Northern Hemisphere (Petit *et al.*, 1999; Ruddiman, 2001). Ice-rafted debris (IRD) records from deep sea sediment cores from the eastern North Atlantic, indicate that growth and decay of continental ice sheets has occurred several times during MIS 4-2, in the so called Heinrich (H) events. These events refer to periods with high IRD in the sediment cores, and indicate the presence of marine based ice margins. During MIS 4-2, six 'H' events have been identified: H6 at ∼60 ka BP, H5 at ∼45 ka BP, H4 at ∼39 ka BP, H3 at ∼30 ka BP, H2 at ∼25 ka BP and finally H1 following the LGM at ∼19 ka BP (Scourse *et al.*, 2009). In North America the growth of three individual ice sheets, the Laurentide, the Cordilleran and Innuitian ice sheets, began between 33 ka and 30 ka PB, and reached their maximum extent between 29 ka and 24 ka PB (Clark & Mix, 2002; Dyke *et al.*, 2002). However, IRD records from deep sea sediment cores, show that the Laurentide Ice Sheet (LIS), deposited sediment in the ocean during all six H events (Peck *et al.*, 2007), and that it thus had a marine-based ice margin on several occasions during MIS 4-2, and not only began to grow during the onset of the LGM. This indicates a highly dynamic ice sheet, with several growth and decay cycles throughout MIS 4-2, and with an unstable ice margin at its maximum extent (Knutz *et al.*, 2001).

In Greenland, ice core records indicate that the Greenland ice sheet existed continuously throughout MIS 5-2 (Dansgaard *et al.*, 1993), and fluctuations in $\delta\ ^{18}O$ show that climate in the North Atlantic underwent rapid changes, possibly due to instability in ocean/atmosphere circulation in the region (Dansgaard *et al.*, 1993). This is argued to be a reason for the instability in the LIS margins, indicated by the presence of LIS IRD throughout the H-events (Knutz *et al.*, 2001; Peck *et al.*, 2007). Isotopic composition of IRD from the Porcupine Bank west of Ireland, deposited between H5 and H4, show a potential influence in provenance of eastern Greenland and Gulf of St. Lawrence (Peck *et al.*, 2007), indicating that ice sheets in these regions developed marine margins at some point during MIS 3.

2.2 Onset of the British and Irish Ice Sheet (BIIS)

There have been numerous attempts to reconstruct the extent and dynamics of the BIIS, during the last glacial cycle e.g. Geikie (1878); Boulton *et al.* (1985); Bowen *et al.* (1986, 2002); McCabe (1987); Hall & Bent (1990); Ballantyne *et al.* (1998b,a); Ballantyne (2010); Sejrup *et al.* (2005); Bradwell *et al.* (2008); Clark *et al.* (2012a); Peters *et al.* (2015). However, there has often been very little consensus between these different reconstructions (Ballantyne, 2010). While some early interpretations show the BIIS as an

independent ice sheet with restricted extent (Bowen *et al.*, 1986, 2002) (Dashed line on Figure 2.1), recent marine investigations from the continental shelf around Ireland and Britain reveal a much larger ice sheet, confluent with the Fennoscandian Ice Sheet, and with westward extension onto the Atlantic continental shelf (Sejrup *et al.*, 2005; Bradwell *et al.*, 2008; Clark *et al.*, 2012a; Ó Cofaigh *et al.*, 2012; Peters *et al.*, 2015; Ballantyne & Ó Cofaigh, 2017) (Figure 2.1).

In the mid to late nineteenth century the Geological Survey of Ireland recorded and mapped the occurrence of glacially-related features across Ireland (Portlock, 1843; Close, 1866; Traill, 1875; Carvill Lewis, 1894; Praeger, 1896; Hinch, 1913) in an attempt to describe and interpret Irish glaciation. These terrestrial observations provided an early insight into the problems with landform genesis, which up until then had been based on the biblical view of a flooding -or "diluvial" event (McCabe, 1987) and thus, the landforms and deposits were regarded as the product of deposition in water (Edwards & Warren, 1985). Through observations of the morphology and location of glacial landforms in Ireland, along with observations and records of sedimentary sequences, primarily in coastal exposures (McCabe, 1987), it is now accepted that glaciers were the main agent shaping the landscape. Throughout the twentieth century, mapping of glacial landforms and stratigraphy continued to be the main tool for reconstructing ice sheet dynamics and flow patterns and for estimating their extent and timing (Bowen *et al.*, 1986; McCabe, 1987, 2008). More recently, however, understanding of the extent, dynamics and chronology of the last Irish Ice Sheet has undergone significant revision through a number of different approaches (Ballantyne & Ó Cofaigh, 2017). First the increased access to and use of satellite imagery and digital elevation models (Greenwood & Clark, 2009a,b; Clark *et al.*, 2012a); second, the increased use of offshore geophysical data and sediment coring, especially on the continental shelf (Sejrup *et al.*, 2005; Scourse *et al.*, 2009; Benetti *et al.*, 2010; Dunlop *et al.*, 2010; Ó Cofaigh *et al.*, 2012; Peters *et al.*, 2015, 2016); and third, the development and application of new and improved dating techniques such as accelerator mass spectrometry (AMS) radiocarbon dating, optically-stimulated luminescence (OSL) dating, and cosmogenic nuclide surface exposure dating (Bowen *et al.*, 2002; Ballantyne *et al.*, 2006; Clark *et al.*, 2009a,b; Stroeven *et al.*, 2016). The last cold stage in Ireland is traditionally named the Midlandian, and chronologically it correlates with the British Devensian Stage and the North-west European Weichselian Stage (Bowen *et al.*, 1986; McCabe, 1987). The Midlandian is further subdivided into the Early (MIS 5d-4 ca. 116 to 58 ka), Middle (MIS 3 ca. 58-31 ka) and Late Midlandian (MIS 2 ca. 31-11.7 ka) (Ballantyne & Ó Cofaigh, 2017). Our knowledge of the BIIS during the Early and Middle Midlandian (MIS 5d-3), is primarily based on marine sediment cores, as most of the onshore glacial evidence was erased by the subsequent LGM ice sheet advance (Bowen *et al.*, 1986; McCabe, 1987, 1999; Chiverrell & Thomas, 2010). Isotopic

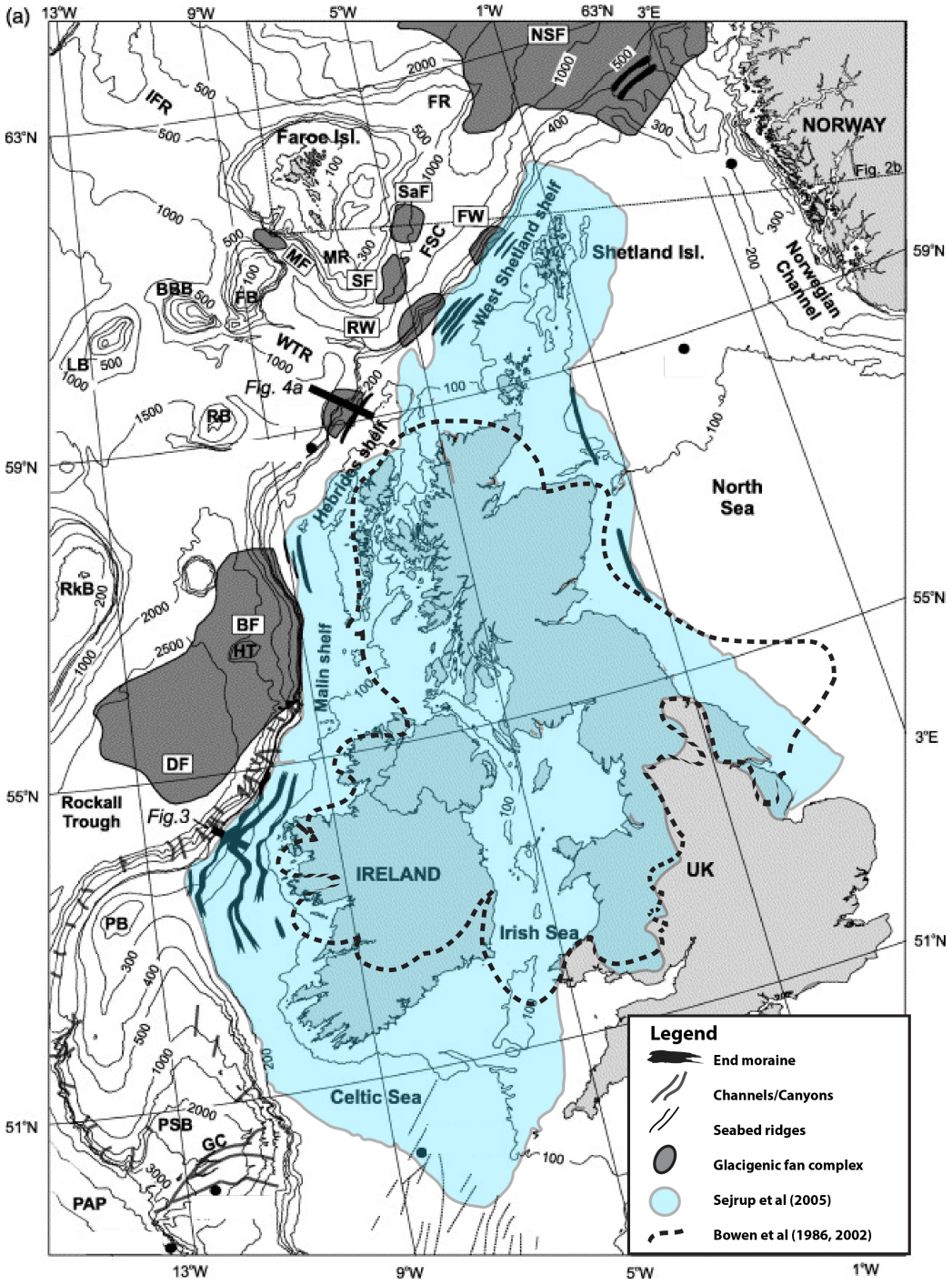

Figure 2.1: The two interpretations of the BIIS extent during the LGM. Dashed line is the interpretation of Bowen *et al.* (1986) while the light blue represent the extensive shelf edge interpretation of Sejrup *et al.* (2005) This large LGM extent is interpreted based on offshore locations of end-moraines, channels and canyons and glacigenic fan complexes. Modified from (Sejrup *et al.*, 2005) and based on (Ballantyne, 2010).

composition of individual IRD grains from sediment cores west and north of Britain and Ireland show that, while Heinrich events ('H events') are dominated by North American sediment, inter 'H' event sediment is dominated by material with a clear British and Irish provenance, as early as between H5 and H4, 45 ka BP (Knutz *et al.*, 2001; Peck *et al.*, 2007; Scourse *et al.*, 2009), or perhaps even as early as during MIS 4, 70 ka BP (Chiverrell & Thomas, 2010; Hibbert *et al.*, 2010). This is a clear indication that an early BIIS was present at some locations in Britain and/or Ireland, with a sufficient size and a marine margin to deliver IRD to the shelf from MIS 4 through to the final stage of MIS 2 (Peck *et al.*, 2007; Scourse *et al.*, 2009; Hibbert *et al.*, 2010; Chiverrell & Thomas, 2010). The exact composition and configuration of this early BIIS are not well understood (Hibbert *et al.*, 2010), but IRD samples from the Barra-Donegal Fan, indicate the presence of an ice sheet with marine calving margins in Scotland, which delivered material to this fan system as early as H6 and with a continuous presence of ice from H5 to post-LGM deglaciation (Knutz *et al.*, 2001; Scourse *et al.*, 2009). The isotopic composition of H4 and H5 IRD from the Porcupine Bank indicate a provenance from the Irish shelf (Peck *et al.*, 2007) and thus the presence of a local, marine-terminating Irish ice sheet at this time. Based on IRD records and glacimarine sediments, it is therefore apparent that a long lived, dynamic and climatically-sensitive early BIIS existed from MIS 3 or 4 and into MIS 2 (Scourse *et al.*, 2009), with localised ice domes at several locations in Britain and Ireland. An increase in IRD concentration in the cores during MIS 2 (Hibbert *et al.*, 2010), indicate that these ice domes merged into a single BIIS sometime after 29 ka BP, with several shelf edge advances from ∼27 ka PB to ∼24 ka BP when the BIIS reached its maximum extent (Scourse *et al.*, 2009).

2.3 LGM glaciation in Ireland

The maximum extent of the Irish Ice Sheet during the LGM was for long believed to have been marked by a moraine complex in southern Ireland, called the South Ireland End Moraine (SIEM) (Bowen *et al.*, 1986; Ballantyne, 2010). This interpretation implied the presence of an ice free swath across southern Ireland and in several areas to the west. End moraines in western Ireland were assumed to mark the limit of LGM ice, with ice free peninsulas in the west and north-west (Bowen *et al.*, 1986, 2002; McCabe, 1987). An alternative suggestion was that they were the product of earlier glacial advances and were not subsequently overrun (McCabe *et al.*, 2007b). Late Midlandian re-advances after the LGM are believed to have created extensive fields of sub-glacial landforms across Ireland, especially in the north-west, where well developed drumlin fields are present (Knight *et al.*, 2004).

In more recent years, this view of a more restricted Irish Ice Sheet at the LGM has been questioned and there is now a broad consensus that during the LGM, Ireland was covered by an ice sheet that extended onto the adjacent continental shelf, and as far as to the shelf edge (Sejrup *et al.*, 2005; Ballantyne, 2010; Dunlop *et al.*, 2010; Clark *et al.*, 2012a; Ó Cofaigh *et al.*, 2012; Ballantyne & Ó Cofaigh, 2017). Based on sedimentary evidence and recent dating of coastal stratigraphic sequences in southern Ireland, it is now believed that most of southern Ireland was ice covered during the LGM. These reconstructions show the ice sheet extended south of the Scilly Islands (Scourse *et al.*, 2000, 2009; Brooks *et al.*, 2008; Ballantyne, 2010), and possibly to the shelf edge (Praeg *et al.*, 2015). The SIEM is now regarded as an ice-marginal retreat moraine, deposited during northward ice retreat following the LGM (Ó Cofaigh & Evans, 2001, 2007; Ballantyne & Ó Cofaigh, 2017). Based on geomorphological evidence for the upper limits of glaciation in the Wicklow Mountains in Ireland, these mountains supported an independent ice dome (Ballantyne *et al.*, 2006; Ballantyne, 2010). Summits over 725 m are inferred to have either remained as nunataks, or to have supported a thin cover of cold-based ice, preserving underlying tors and block-fields (Ballantyne *et al.*, 2006). In western and north-western Ireland, the LGM ice thickness has been estimated to be up to ∼700 m (Ballantyne *et al.*, 2007, 2008). This further implies an ice sheet that extended beyond the present coastline and onto the adjacent continental shelf, and based on the ice thickness Ballantyne *et al.* (2007) estimated that the ice sheet extended at least 20 km west offshore, thus far exceeding the previous interpretation of limited Irish LGM extent, with end moraines on the western Irish peninsulas. It is now broadly accepted that the glacial limits of the LGM ice sheet are to be found at the continental shelf edge (Benetti *et al.*, 2010; Dunlop *et al.*, 2011; Ó Cofaigh *et al.*, 2012), however, the question of chronology of advance and retreat remain largely unknown for most of the Irish continental shelf.

2.4 Geology and geomorphology of NW Ireland, Donegal bay and the adjacent continental shelf

Donegal Bay in north-western Ireland, is a broad and open bay (Figure 2.2). The coastal areas of the bay border four counties; Co. Donegal to the north and east, Co. Leitrim to the south-east, Co. Sligo to the south-east and south, and Co. Mayo to the south and south-west. To the west, and north-west, the bay opens into the North Atlantic. The northern coast is bordered by an approximately 40 km long peninsula with Malin Beg as the western-most point in Co. Donegal. To the south, the Mayo and Sligo coast stretches approximately 100 km westward (Figure 2.2), Killala Bay forms a broad and open bay stretching south for

about 10 km, on the south side of Donegal Bay (Figure 2.2). The inner part of Donegal Bay is a shallow narrow embayment, with water depths down to about 80 meters at the mouth of the bay. The coastal area surrounding Donegal Bay generally lies below 80m a.s.l. but it is flanked by uplands of up to 200 m. a.s.l. (Knight & McCabe, 1997a). These upland areas lead to the mountainous areas of north-western Ireland (see below). The low lying coastal area immediately to south-east and east of Donegal Bay is dominated by Carboniferous limestone and shale with smaller areas of Carboniferous sand- and mudstone (GSI, 2017) (Figure 2.3).

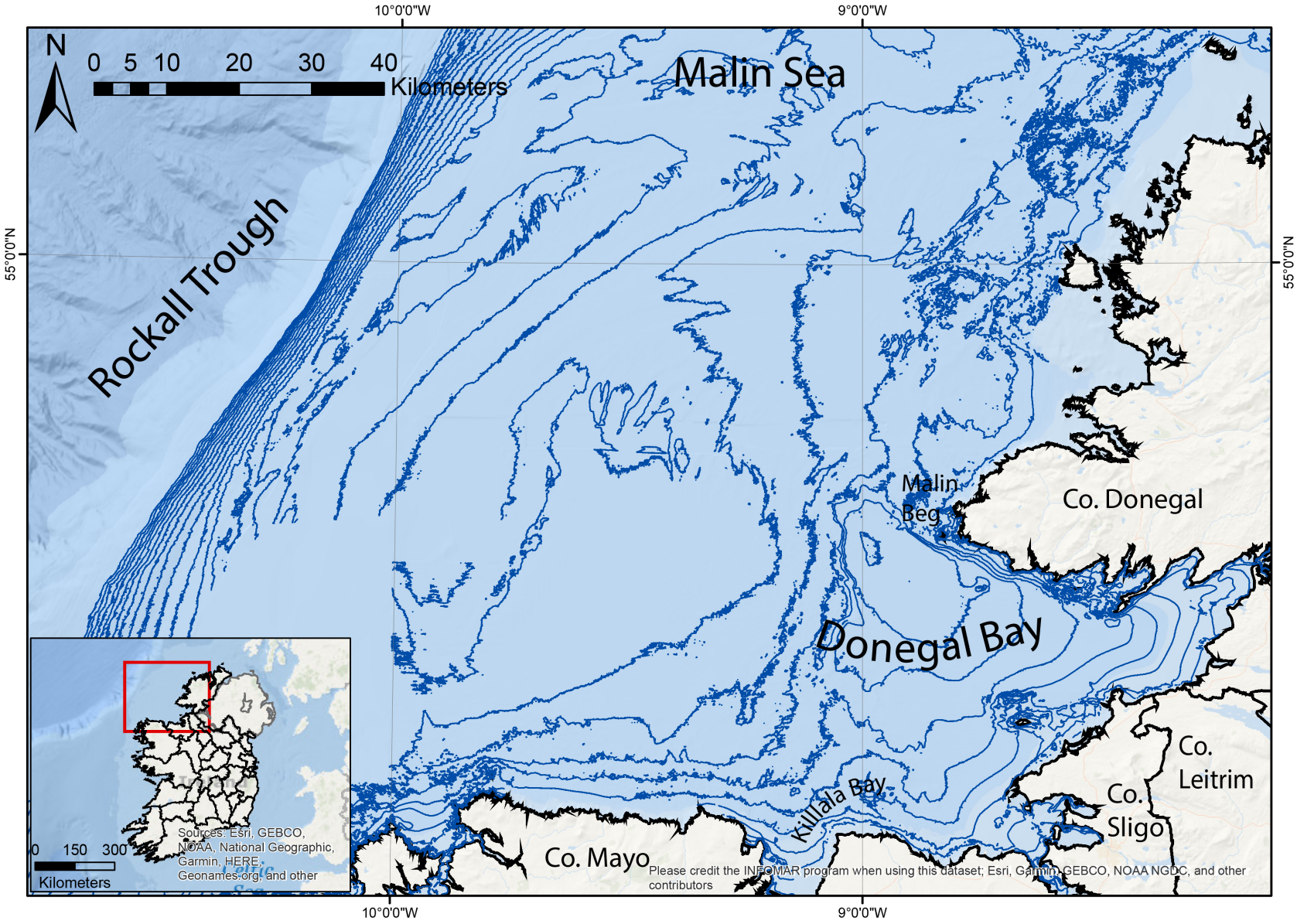

Figure 2.2: Location map of Donegal Bay and adjacent continental shelf to the north-west. To the north and east: Co. Donegal. To the south-east: Co. Sligo and to the south-west Co. Mayo. (© Government of Ireland).

Donegal Bay is surrounded by five mountainous areas. In Co. Donegal, to the north-west, the Derryveagh and Blue-Stack Mountains form a mountainous massif, with peaks over 650 m. Further west towards Malin Beg, the Glengesh plateau forms the northern coast of Donegal Bay (Figure 2.3). This plateau is dominated by the peak of Slieve League at 596 m. These three mountain massifs are dominated by pre-Cambrian metamorphic schist and gneisses, with some intrusive Silurian-Devonian granite (Figure 2.3). To the south and east of Donegal Bay, in Co. Sligo are the Benbulbin mountains. This massif forms a 400-500 m high plateau comprised of Carboniferous limestone. To the west of the Benbulbin mountains, the Ox mountains run south-west about 40 km, from near Sligo Town to the south of Killala Bay. The Ox mountains are composed of pre-Cambrian metamorphic schist and gneisses, which are also found in western Mayo (Figure 2.3). The north-east/south-west orientation of the Ox mountains, follow the overall orientation of the faultlines in Ireland, and in particularly in the north-west (Figure 2.3). Many faults can be followed from Fair Head in Northern Ireland, to Clew Bay in western Ireland, in a fault zone called the Fair head - Clew Bay fault zone (Max & Riddihough, 1975; Chew D. *et al.*, 2004). This fault zone is a continuation of the Scottish Great Glen fault line (Max & Riddihough, 1975), and constitutes part of the great Caledonian shear zone in Ireland.

In Ireland more than 40,000 glacial landforms have been identified (Greenwood & Clark, 2008, 2009a), and a large number of these have been interpreted as sub-glacial landforms, such as drumlins and ribbed moraines. The orientation of flow-parallel, streamlined subglacial landforms, such as drumlins has traditionally been used to reconstruct local ice flow patterns (Knight & McCabe, 1997a; Greenwood & Clark, 2009a). This is especially the case in central and north-west Ireland, where these bedforms are found in abundance. For example figure 2.6 shows the drumlin fields around Donegal Bay. Here a highly streamlined landscape is seen, which has been used to interpret the flow directions of the late Midlandian ice sheet in the area (Knight & McCabe, 1997a; Greenwood & Clark, 2009a).

From detailed mapping of striations, erratics and drumlin orientation, there is widespread agreement that the Donegal mountains at some point supported and nourished an independent ice dome (Ballantyne *et al.*, 2007). This idea was first proposed by Charlesworth (1924) and it has since been widely supported and accepted (Colhoun, 1971; Knight & McCabe, 1997b; McCabe, 1987; McCabe & Clark, 2003; McCabe *et al.*, 2005; Ballantyne *et al.*, 2007). The position of the ice divide and radial flow directions within the ice dome, have been placed along a north-south trending line, from the Derryveigh Mountains to the Blue Stack Mountains (Figure 2.4). To the east and south-east, the ice dome merged with the adjacent ice sheet covering mainland Ireland (Figure 2.4) (Ballantyne *et al.*, 2007), and to the north, north-west, west and

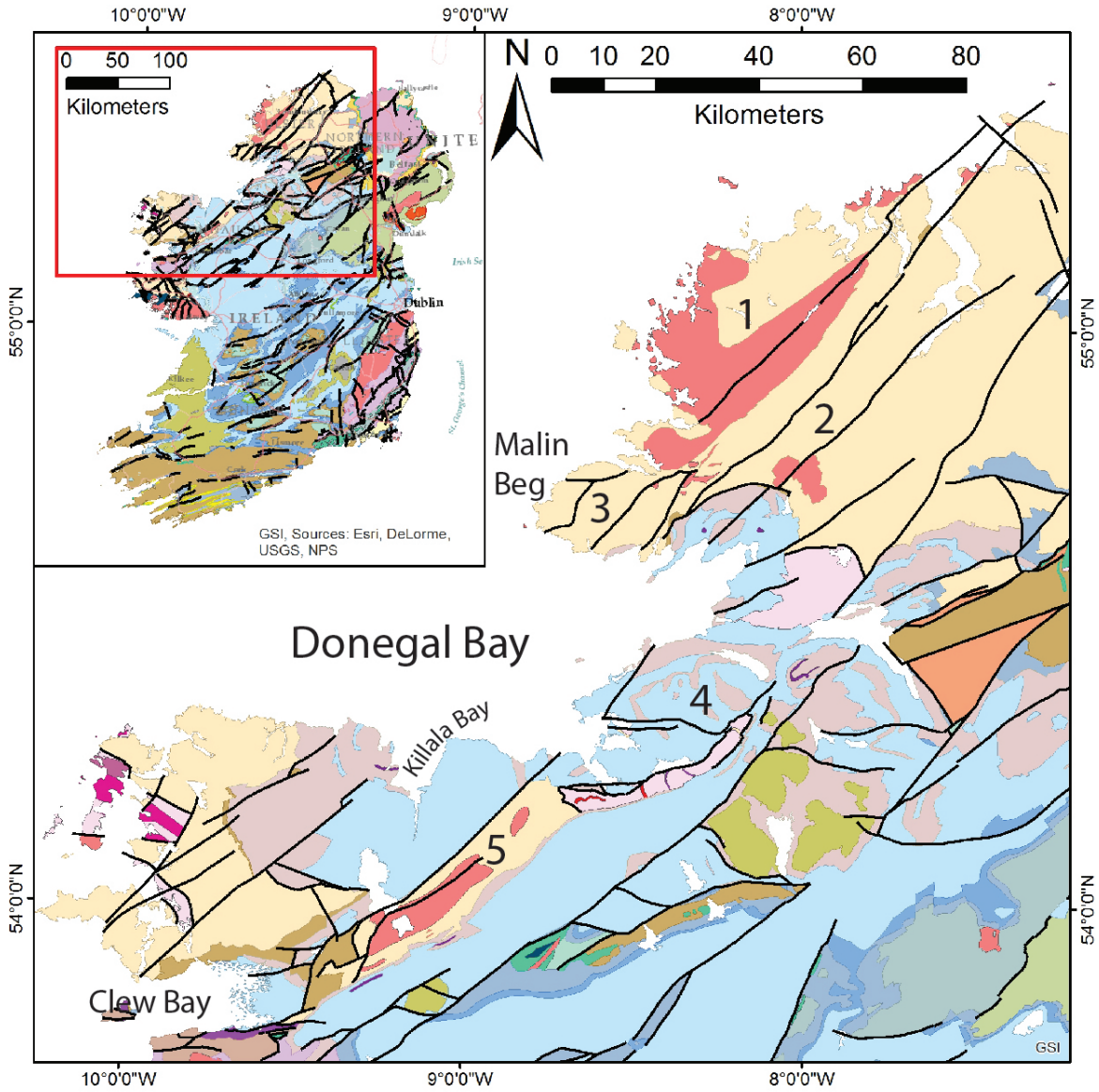

Legend- dominating lithologies in Ireland

- Bedrock Faults
- Palaeocene basalt lava
- Carboniferous shale, sandstone, siltstone & coal
- Carboniferous limestone & calcareous shale
- "Old Red Sandstone", Devonian sandstone, conglomerate & mudstone
- Siluro-Devonian granitie
- Late Ordovician-Silurian deep marine greywacke, mudstone
- Carboniferous sandstone, mudstone & evaporite
- pre-Cambrian metamorphic schist and gneiss

Figure 2.3: Geological map of Donegal Bay and Ireland. 1: Derryveagh Mountains. 2: Blue-stack Mountains. 3: Glengesh Plateau. 4: Benbulbin Mountains. 5: Ox Mountains.(GSI, 2017)

south-west, ice is believed to have streamed down from the mountains and extended beyond the present coastline (Figure 2.4) (Knight & McCabe, 1997a; McCabe *et al.*, 1993, 2005). This is particularly clear in Co. Donegal and near Donegal town, where the south-west flow direction is shown by the vast drumlin fields covering the upland, all with an overall north-east to south-west orientation (Figure 2.6) (Knight & McCabe, 1997a). Mapping of the drumlin orientation in the Donegal uplands (Figure2.6), reveals two overall drumlin orientations: north-east to south-west trending, and east to west (Knight & McCabe, 1997a; Greenwood & Clark, 2008, 2009a), interpreted to indicate changes to the ice divide of the Donegal ice dome during build up.

On the Donegal Bay southern coast, on the Mayo coastline, a sequence of raised glacimarine sediments, up to 80 m OD, are exposed in river valleys and gully complexes at several locations along the coast (Figure 2.5). The sequence consists of three lithofacies associations, with an over consolidated basal till at the base, a glacimarine mud drape overlying this and a deltaic gravel complex at the top (McCabe *et al.*, 1986, 2005, 2007b). Palaeoenvironmental analysis of the sequence reveals reworked shell fragments of *Arctic islandica* in the basal till ((McCabe *et al.*, 2007b), while in the overlying mud drape, unbroken and paired valves of *Macoma calcarea* and *Elpihidium clavatum* benthic foraminifera interpreted as *in situ*, have been found suggesting a glacimarine environment (McCabe *et al.*, 1986, 2005, 2007b). Clast composition in the basal till and striae orientation in the underlying bedrock, indicate ice advance from the south-east extending offshore onto the continental shelf (McCabe *et al.*, 1986, 2005, 2007b). AMS radiocarbon dating of both macro and microfossils from the exposed sequence at Glenulra (Figure 2.5), show that these glacimarine lithofacies were deposited between 40 and 19 ka BP and therefore indicate the presence of a local marine-terminating ice sheet, perhaps as early as 20 ka prior to the LGM (McCabe *et al.*, 2007b). However the reliability of some of these dates make such an interpretation questionable (Ballantyne & Ó Cofaigh, 2017), and will be further discussed in chapter 6.

Cosmogenic ^{10}Be exposure ages, dating between ∼18.4 and ∼15.9 ka BP from coastal sites at Malin Beg, Bloody Foreland and Malin Head, imply that the Donegal ice dome extended over these sites during the LGM (Ballantyne *et al.*, 2007). Further exposure ages from rock slope failures in the Donegal mountains imply de-glaciation of the mountains after ∼17.4 ka BP to ∼16.3 ka BP depending on the local ^{10}Be production rate (Ballantyne *et al.*, 2013). This means that the Donegal ice dome must have been of LGM age, and that the de-glaciation of the coast and ice retreat up into the mountains occurred between ∼ 18 ka to ∼17.4 ka BP.

Based on trimline evidence from the Donegal mountains, Ballantyne *et al.* (2007) reconstruct the Donegal

ice dome to have had a thickness of at least 700 m at the ice centre. Based on these thickness estimations, flow reconstruction of the ice dome suggest that over the present coastline, ice thickness must have been ∼500 m, which was argued by Ballantyne *et al.* (2007) to mean that the ice sheet must have extended offshore by at least 20 km.

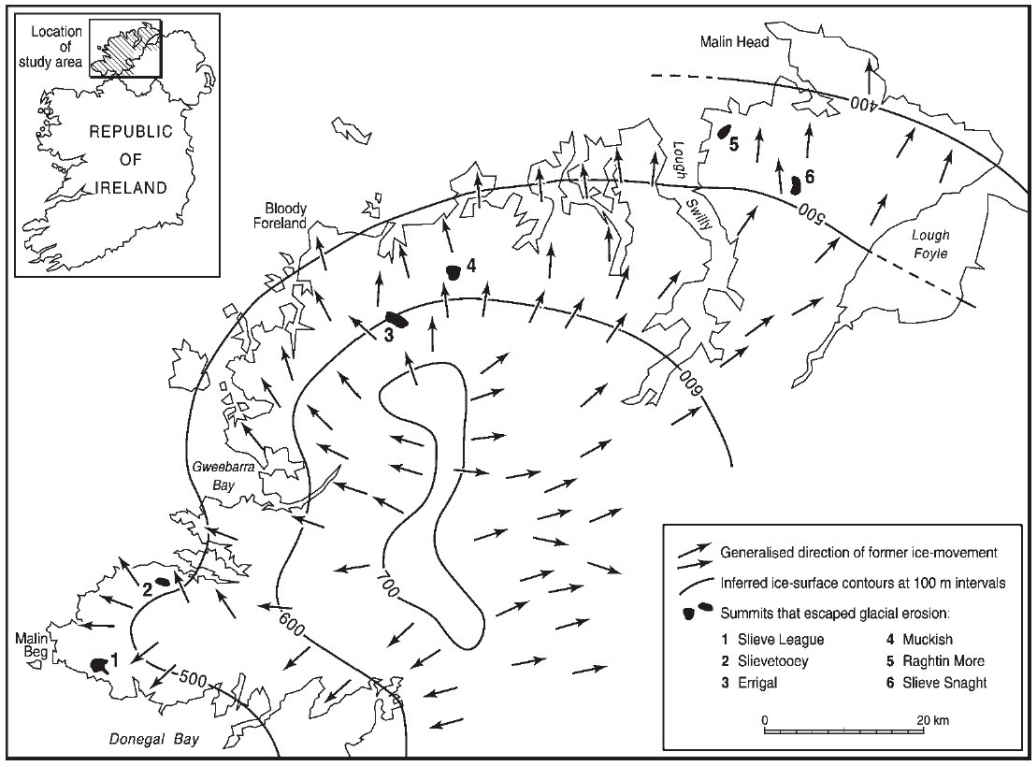

Figure 2.4: Three- dimentional reconstruction of the Donegal Ice dome, and internal radial flow directions. Reconstructed based on upper limits of glacial erosion evidence. General direction of ice movement is from Charlesworth (1924). From Ballantyne *et al.* (2007).

2.5 Offshore studies of BIIS north-western extent

Much of the previous research on the late Pleistocene glaciation of Ireland has been based on terrestrial investigations of glacial geomorphology, sedimentology and stratigraphy. The offshore investigation of glaciation has, until recently, been sparse due to technical limitations, and any evidence for offshore glacial extent was attributed to earlier glacial periods (Bowen *et al.*, 2002). With the development of high resolution multi-beam swath bathymetry, acoustic sub-bottom profiling tools, and offshore coring techniques, it has become possible to investigate submerged and buried glacial landforms, not only in coastal waters, but across the

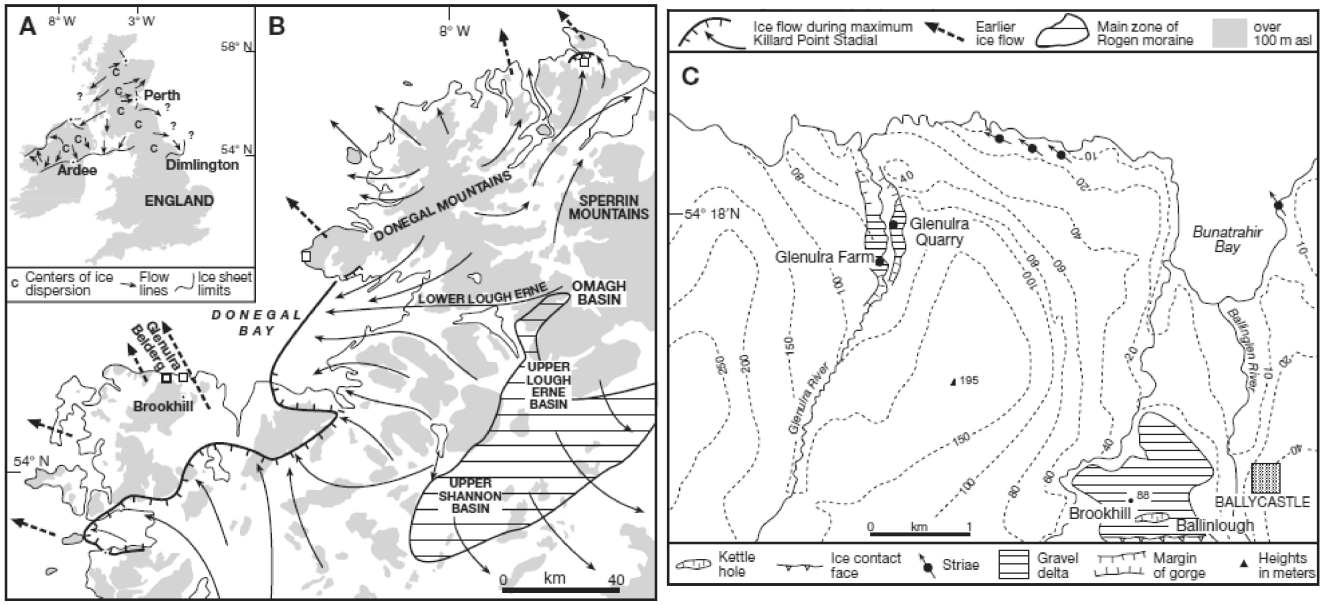

Figure 2.5: The Co. Mayo coast facing Donegal Bay to the north. Raised glacimarine sediments have been found at several locations, among those, at Glenulra where AMS radiocarbon dating of macro and microfossils indicate deposition between 40 and 19 ka BP. From (McCabe *et al.*, 2007b).

entire continental shelf, and adjacent slope.

Early investigations of the Irish continental shelf using marine geophysical data, have identified large arcuate ridges to the north and west of Ireland (Sejrup *et al.*, 2005; Benetti *et al.*, 2010; Dunlop *et al.*, 2010; Ó Cofaigh *et al.*, 2012; Peters *et al.*, 2015). These were interpreted as end moraines by King *et al.* (1998), and have since been confirmed by Sejrup *et al.* (2005) based on seismic data. Since 1999 the Irish Government has collected high resolution marine geophysical data, in order to fully map Ireland's Exclusive Economic Zone (Benetti *et al.*, 2010; Ó Cofaigh *et al.*, 2012). This has produced a large amount of data on seafloor morphology of the continental shelf, and has documented nested end- and recessional-moraines, lateral moraines, drumlin swarms, and extensive areas of iceberg scouring, in the Malin sea to the north of Ireland, on the shelf north-west of Donegal Bay, and on the Porcupine bank west of Ireland (Benetti *et al.*, 2010; Dunlop *et al.*, 2010, 2011; Ó Cofaigh *et al.*, 2012; Peters *et al.*, 2015). This has led to new interpretations of the extent and timing of the LGM ice cover, especially in the western and north-western Ireland, extending out into the North Atlantic as far as the shelf edge (Benetti *et al.*, 2010; Dunlop *et al.*, 2010, 2011; Ó Cofaigh *et al.*, 2012; Peters *et al.*, 2015, 2016).

The continental shelf offshore of north-west Ireland and Donegal Bay stretches approximately 150 km to the west and north-west to the shelf break, bordering the Rockall Trough (Figure 2.2). To the north, the

continental shelf extends for about 100 km, and continues into the Malin Sea (Figure 2.2), and to the south, the shelf extends further westward, broadening to the Porcupine Bank west of Ireland. Multibeam swath bathymetry and backscatter data, were acquired in this area between 2002 and 2008 by the Marine Institute and the Geological Survey of Ireland, on the research vessels the RV Celtic Explorer and RV Celtic Voyager (Benetti *et al.*, 2010; Dunlop *et al.*, 2010, 2011; Ó Cofaigh *et al.*, 2012). The multibeam swath bathymetry from the north-west of Ireland can be seen on figure 2.7. The data reveal large scale glacial features on the shelf to the west and north-west of Donegal Bay and north of Co. Donegal, and indicate flow from the Donegal ice dome across the coast line and onto the shelf (Figure 2.4).

Most prominent are a number of elongate north-east to south-west orientated ridges, distributed over the shelf from the mouth of Donegal Bay, in ∼60 m water depth, to the shelf edge, in ∼120 m water depth, shown in light blue on figure 2.8. The ridges become longer and more pronounced with distance from the Irish mainland, with the two western-most ridges most pronounced with a length of ∼125 km and a width of up to 11 km (Dunlop *et al.*, 2011; Ó Cofaigh *et al.*, 2012) (Figure 2.8). Further east, the ridges are arcuate shaped and are spaced closer together, up a few km apart. (Figure 2.8). These ridges range from 1.5 to 9 km in length, 1 to 3.5 km in with and have a amplitude of 1 to 4 meters. (Ó Cofaigh *et al.*, 2012). These nested arcuate ridges have been interpreted as moraines recording a grounded ice-sheet retreat across the shelf, punctuated by occasional minor re-advances (Ó Cofaigh *et al.*, 2012). The two larger moraines at the shelf break are interpreted as recording the grounding of a large ice sheet, possibly of LGM age, although prior to the present study there was no direct dating of these features. (Benetti *et al.*, 2010; Ó Cofaigh *et al.*, 2012).

In the southern part of Donegal Bay just north of Killala Bay, a second series of ridges have been identified, (shown in lilac on figurte 2.8). These ridges are shorter than the north-east to south-west orientated ridges described across the shelf. They have an overall east-west orientation, and extend some 15-20 km north into Donegal Bay from Killala Bay. The ridges are superimposed on the larger shelf ridges, indicating that they were deposited after the first set of ridges(Benetti *et al.*, 2010; Dunlop *et al.*, 2011).

North of Donegal Bay, two areas of streamlined well defined elongated mounds are seen on the seabed (Ó Cofaigh *et al.*, 2012), on figure 2.8, these are shown in red. These mounds all have the same north-west to south-east orientation, vary in height from 1 to 5.5 m, and have a short steep eastern side and a long slope on the western side. These mounds have been interpreted as drumlins, and record offshore directed ice flow from the Donegal Ice dome (Figure 2.4) (Benetti *et al.*, 2010; Ó Cofaigh *et al.*, 2012). The appearance of glacial ridges and landforms at the shelf edge, and subsequent retreat moraines across the shelf, indicate

that the Donegal Ice dome extended much further offshore than the previously estimated 20 km, based on terrestrial trimline evidence (Ballantyne *et al.*, 2007), with an ice mass that extended about ∼150 km from Donegal Bay to the shelf edge. Based on the pattern of the glacial landforms identified on the Irish continental shelf, it is thus believed that the LGM ice sheet extended to the continental shelf edge, (Benetti *et al.*, 2010; Dunlop *et al.*, 2010, 2011; Ó Cofaigh *et al.*, 2012).

In the Malin Sea north of Ireland (Figure 2.2), extensive moraine fields have been reported from across the Malin Shelf, extending to the shelf edge Dunlop *et al.* (2010); Sacchetti *et al.* (2012). These moraines provide direct evidence for the grounding of an ice sheet on the continental shelf, and their northwest-southeast aligned orientation suggests ice flow from Scotland, north east of the Malin sea (Dunlop *et al.*, 2010; Sacchetti *et al.*, 2012). This is supported by the IRD record from the Barra-Donegal Fan system, which received material from this grounded ice sheet at the shelf edge between 29 ka BP to 27 ka BP (Scourse *et al.*, 2009; Dunlop *et al.*, 2010). In addition this provides a maximum constraint on the age of the formation of the moraines across the Malin shelf suggesting deposition during retreat back to the Scottish coast (Dunlop *et al.*, 2010).

West of Ireland, the Porcupine Bank forms a dome-like westward extension of the Irish continental shelf, with water depths ranging from ∼155 to 200 m (Peters *et al.*, 2015). Bathymetric investigations reveal a series of sinuous ridges on the outer shelf (Peters *et al.*, 2015). Until recently, no analysis of the glacial sedimentology or palaeoenvironment had been completed in this area, and furthermore, no chronological control of the BIIS advance onto the shelf west of Ireland existed (Peters *et al.*, 2015). Through geomorphic, sedimentary and micropaleontological data from the Porcupine Bank, Peters *et al.* (2015, 2016), interpret the ridges to be moraines or grounding-zone wedges, thus confirming the presence of BIIS on the Porcupine Bank, and extending the margin of the BIIS by up to 80 km further west than previously believed. Dating of this westward extension is based on coral fragments from highly consolidated till, and indicate glaciation on the shelf after 24,720 cal. BP (Peters *et al.*, 2015, 2016).

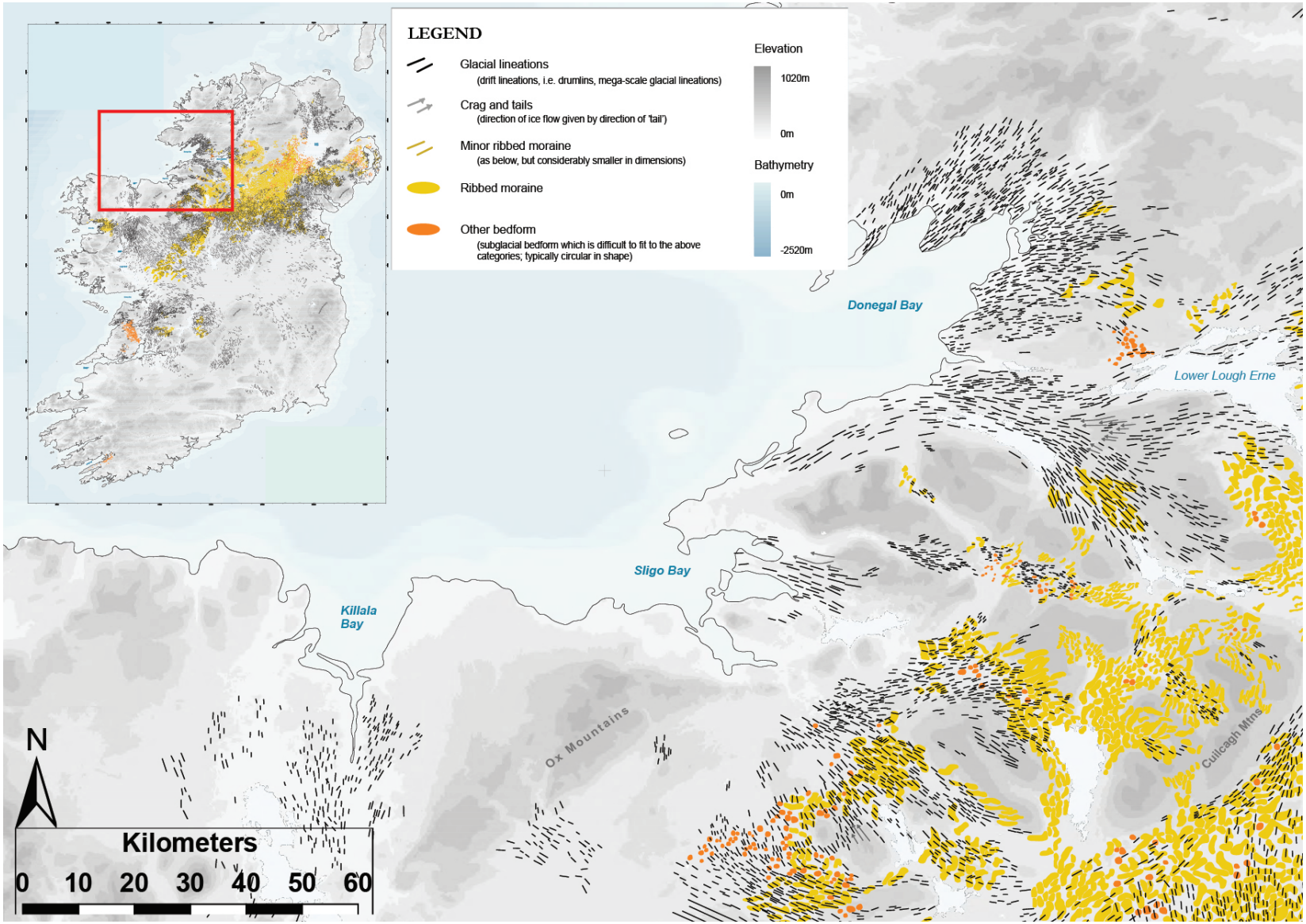

Figure 2.6: A clear streamlining of the landscape can be seen in the orientation of drumlins and landforms around Donegal Bay. Two overall orientations can be seen: north-east to south-west, and east to west, indicating two flow directions. (After Greenwood & Clark 2008)

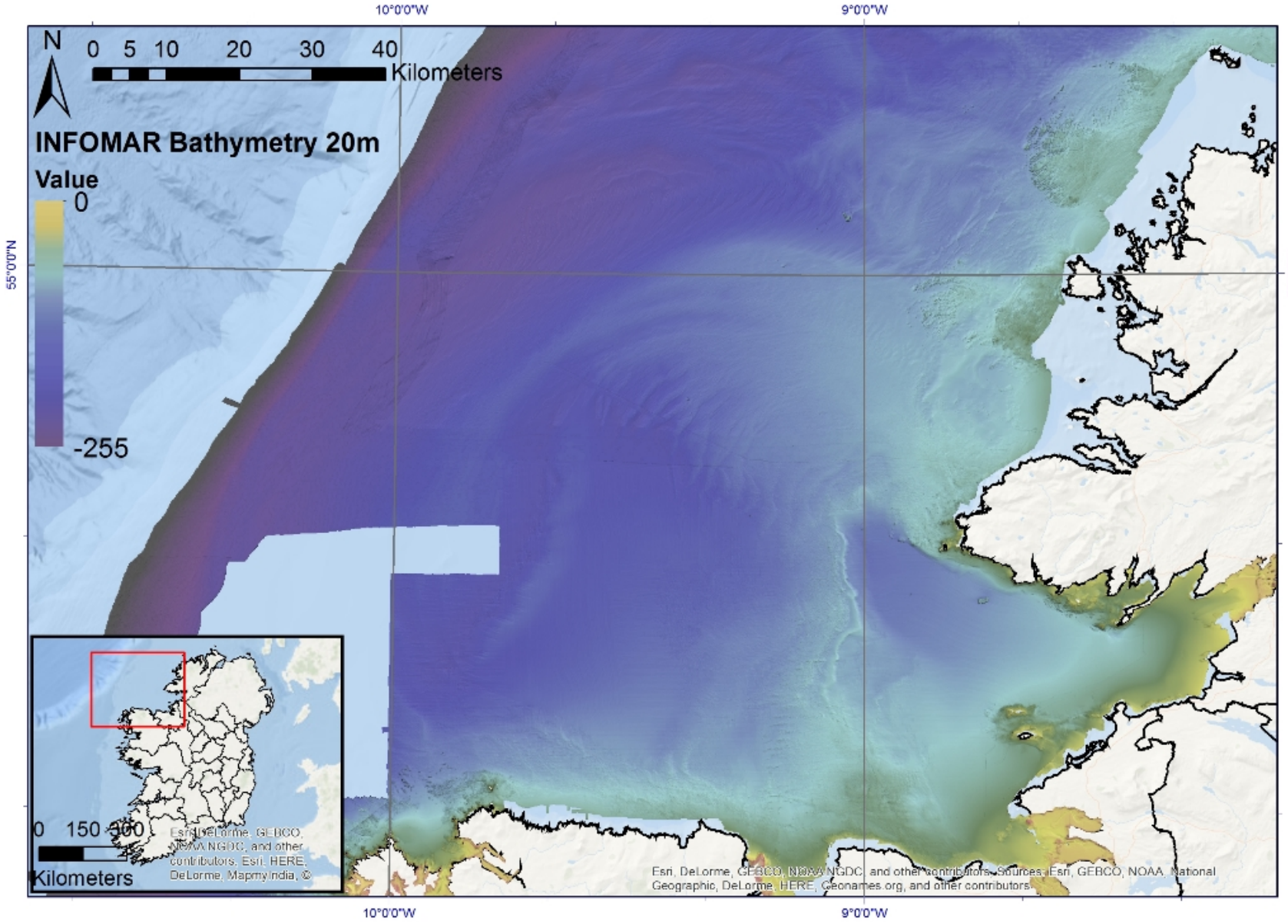

Figure 2.7: Multibeam swath bathymetry coverage in Donegal Bay and the adjacent continental shelf, collected by the vessels RV Celtic Voyager and RV Celtic Explorer between 2002 and 2008. Bathymetric data accessible from www.infomar.ie.

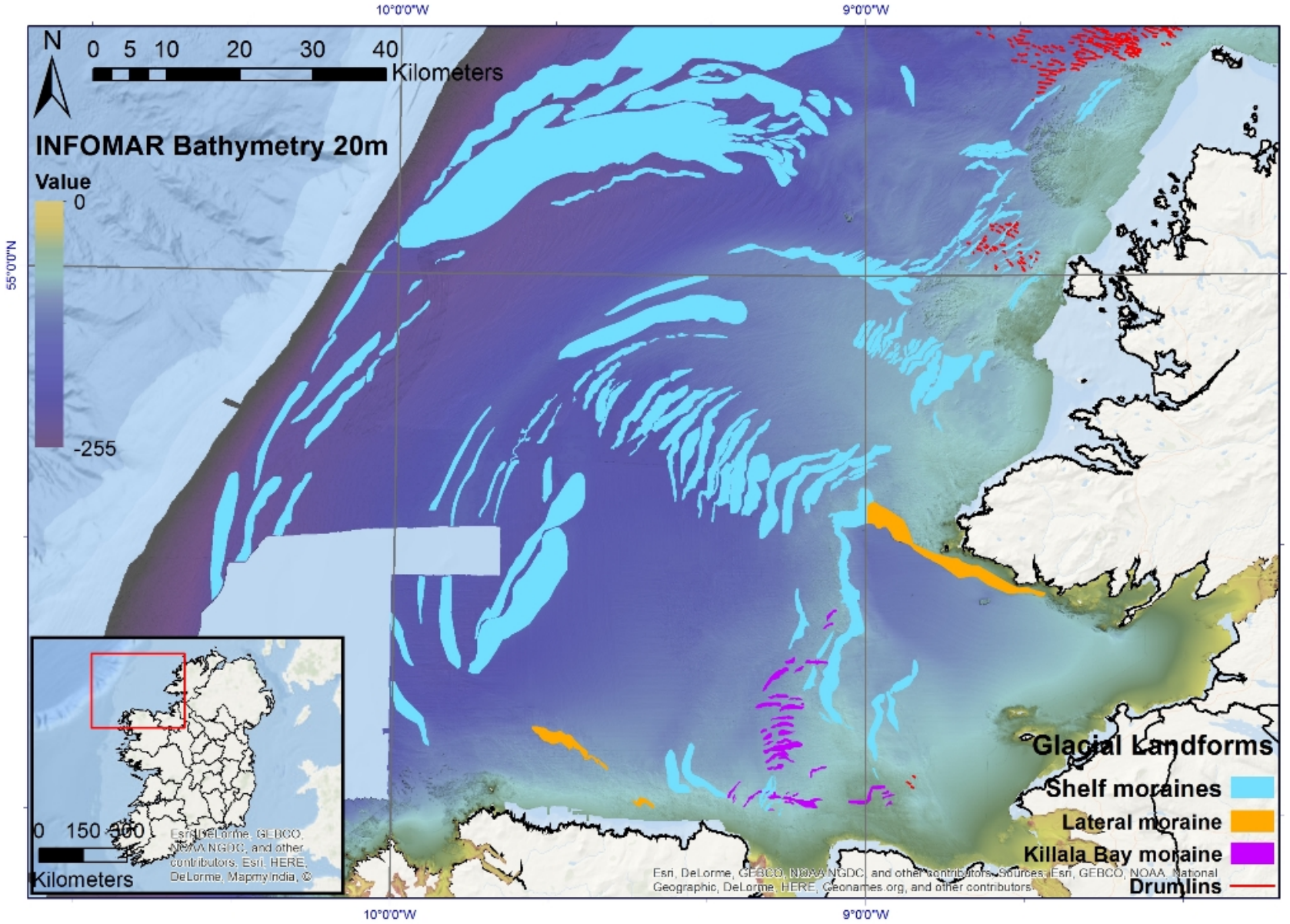

Figure 2.8: Interpretations of the Multibeam swath bathymetry across the continental shelf offshore Donegal Bay. (After Benetti *et al.* 2010.) Bathymetric data accessible from www.infomar.ie

3. *Methods*

In order to answer the research questions put forward in Chapter (1.2), this thesis employs a multi proxy-approach to build a coherent reconstruction of the glacial history of Donegal Bay and the adjacent continental shelf. Three main methods have been employed: 1) geophysical data analysis; 2) sediment coring and analysis; 3) foraminiferal analysis. Geophysical data collection across the study area consisted of multibeam swath bathymetry and sub-bottom profiling. These data provide spatial information on the geomorphology of the continental shelf, information on acoustic stratigraphy and sediment thicknesses, distribution of acoustic facies and depositional environments. Analysis of sediment cores across the study area provide information on sediment composition and thickness, sediment lithofacies, and physical properties. Finally micropalaeontological analysis from selected sediment cores provides information on paleoenvironments constrained by twenty two new AMS radiocarbon dates on bivalves and foraminifera. These methods collectively allow the reconstruction of ice sheet extent, the timing and style of ice sheet retreat and associated depositional environment(s) offshore of NW Ireland from the LGM through to deglaciation.

3.1 Multibeam swath bathymetry

The bathymetry of the seabed can to some extent be compared with a topographic map on land. The aim of a bathymetric map is to produce a picture of the morphology of the seabed in as high a resolution as the data permits (Monahan, 2009). This makes bathymetry a very useful tool to describe the geomorphology of the seabed. Multibeam swath bathymetry uses a hull-mounted sonar system to transmit an array of sound pulses, or pings, in a fan beneath a research vessel (Figure 3.1). The resolution of individual beams is typically 1° to 3°, and angular sectors range from ±20° to ±70° to either side of the vessel(De Moustier & Matsumoto, 1993). The energy transmitted is bounced back from the seabed and, depending on the depth of the water they pass through, will reach the vessel at slightly different times. This allows the seafloor depths and thus the bathymetry to be calculated across the width of the sonar beam under the vessel (Figure 3.1). The extent of data coverage on the seafloor, called the swath, can be as high as 7 times the water depth, but more typically, the swath width is about twice the water depth (Monahan, 2009). The usual approach to data collection is for the vessel to move back and forth in order to cover the whole of the seafloor in a given study area.

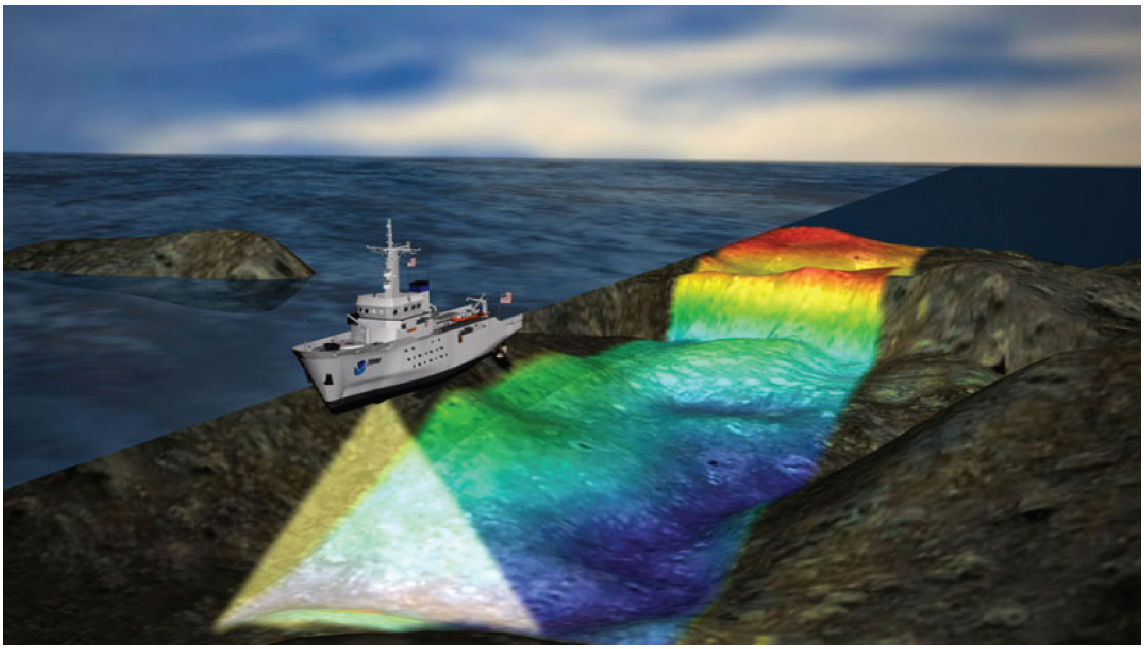

Figure 3.1: Principle of multibeam swath collection (Taschek, 2011).

The continental shelf offshore of NW Ireland was surveyed between 2002 and 2008 by the Marine Institute and Geological Survey of Ireland (INSS), now the Integrated Mapping for the Sustainable Development of Ireland's Marine Resource (INFOMAR) (Ó Cofaigh *et al.*, 2012) (Figure 2.7). Multibeam swath bathymetry was acquired using hull-mounted Simrad EM1002S and EM3002 systems by the research vessel RV Celtic Voyager, and by an EM1002 on the research vessel RV Celtic Explorer (Benetti *et al.*, 2010; Dunlop *et al.*, 2011; Ó Cofaigh *et al.*, 2012). The frequencies were 95 kHz for the EM1002S and up to 300 kHz for the EM3002 (Dunlop *et al.*, 2011). The horizontal and vertical accuracy ranges from 10 to 50 cm, depending on water depth (Benetti *et al.*, 2010; Ó Cofaigh *et al.*, 2012). Bathymetry data was processed in CARIS/Hydrographic Information Processing systems (HIPS) and Sonar Image Processing Software (SIPS), and data collected in water depths between 10 and 230 m was corrected for tidal influence using Polpred Continental Shelf Model CS3-30HC and tide gauge data (Dunlop *et al.*, 2011). For the purposes of this thesis, bathymetry data was acquired from INFOMAR using an ArcGIS server and data analysis was done using ArcGIS 10.2. Presentation and interpretation of the bathymetry data have previously been carried out by Benetti *et al.* (2010) and Ó Cofaigh *et al.* (2012), and interpretations of the glacial geomorphology in the study area, are based on these data.

3.2 Sub-Bottom Profiling

Sub-bottom profiling is based on reflected seismic waves and can be used to produce a seismic stratigraphy. Seismic stratigraphy is the study of stratification and depositional facies interpreted from seismic, or acoustic data. Seismic reflectors can be used to identify stratification patterns, and grouped into seismic facies, can contribute to the interpretation of depositional environment and to recognize and correlate depositional sequences (Mitchum *et al.*, 1977a). (Mitchum *et al.* 1977b p.53) defines a depositional sequence (Figure 3.2 as: *"a stratigraphic unit composed of a relatively conformable succession of genetically related strata and bounded at its top and base by unconformities or their correlative conformities"* The sequence shows the depositional environments in a stratified succession, as different internal seismic reflectors, or acoustic facies. Seismic reflectors appear with sufficient density-velocity contrast between sedimentary layers in the sub-surface. A sedimentary layer will therefore have its own acoustic characteristics, or impedance, compared to layers above or below (Veeken, 2007). The interface between sedimentary boundaries, sedimentary bedding planes or unconformities will therefore appear as reflectors in the data, and based on the seismic facies parameters: configuration, continuity, amplitude and frequency of the reflectors, individual acoustic facies can be identified.

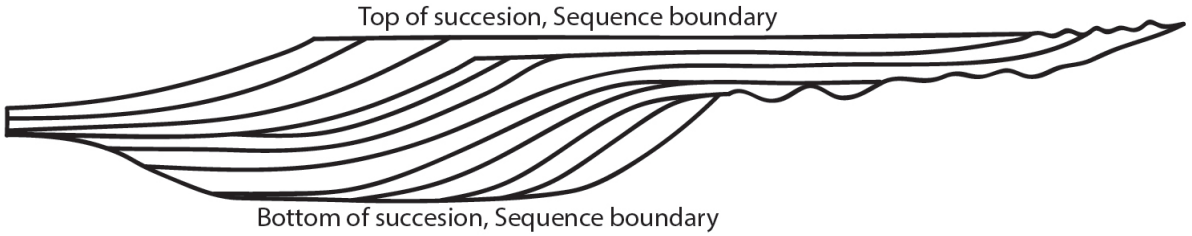

Figure 3.2: Example of a simplified depositional sequence. (After Mitchum *et al.* 1977a)

Seismic facies parameters: The reflection configuration is related to the bedding pattern, the depositional processes, erosion and the original paleotopography and to the fluid content of the sediment.
Continuity is related to bedding continuity and therefore also to the environment of deposition and depositional processes.
Amplitude is a measure for the velocity-density contrast, bed spacing, lithological contrast and fluid content.
The reflection frequency gives a measure of bed thickness and fluid content. (Veeken, 2007)

Depending on sedimentary or environmental conditions, or structural movement in the substrata, the reflectors can have a series of characteristic geometries.

Erosional truncation (Figure 3.3) is seen towards the upper boundary of a depositional sequence, and is seen as lateral termination of reflectors by erosion (Mitchum *et al.*, 1977b). Truncation can in some cases be mistaken for toplap, but where toplap is a depositional feature, truncation is erosional.

Toplap (Figure 3.3) refers to reflectors pinching out and terminating against the upper boundary of a depositional sequence. This mainly occurs as a result of non-deposition, for example as a result of low sea level, and thereby lack of accommodation space. Toplap is generally associated with shallow marine or deltaic deposits (Mitchum *et al.*, 1977b).

Concordance can be seen both in relations to the top or bottom of a sequence or stratigraphic boundary (Figure 3.3). This pattern is seen when the sediments follow the underlying or overlying strata. Concordance is usually the result of deformation of the sedimentary layers, after deposition.

Onlap (Figure 3.3) is seen when initially horizontal or slightly inclined reflectors pinch out against the underlying facies. In order for onlap to occur, the underlying facies must be more inclined than the onlapping reflectors. This feature is often seen in relations to rising sea-level, with high sedimentation rate, where onlapping reflectors can be seen as transgressive surfaces in coastal deposits (Vail *et al.*, 1977).

Downlap (Figure 3.3) is seen as inclined reflectors terminating downwards on a horizontal, or less inclined underlying facies boundary. Downlap normally occurs in a direction away from sediment supply, and is related to a prograding system where sediment supply is sufficient and accommodation space is available for sedimentation. Downlap is therefore often expressed as prograding forsets.

A two dimensional seismic profile may in some instances show downlap, but in intersecting profiles shows onlap at the same location. In the same way, horizontal reflectors in one profile, can show dipping, and thereby downlapping reflectors in an intersecting profile (Mitchum *et al.*, 1977b). In order to see the true bedding plane, the seismic profile must therefore be taken in the dip direction, thereby showing the strata in the strike plane, or perpendicular to the bedding plane. As two dimensional seismic do not always show the strata perpendicular to the bedding plane, the true geometry of the strata can therefore be difficult to see, and the geometry of the reflectors can be described as *apparent* downlap. Onlapping reflectors are most likely to be seen as base discordance towards the bottom of the depositional sequence(Mitchum *et al.*, 1977a).

As this thesis only encompasses two dimensional seismic profiles, with very few intersecting profiles, the

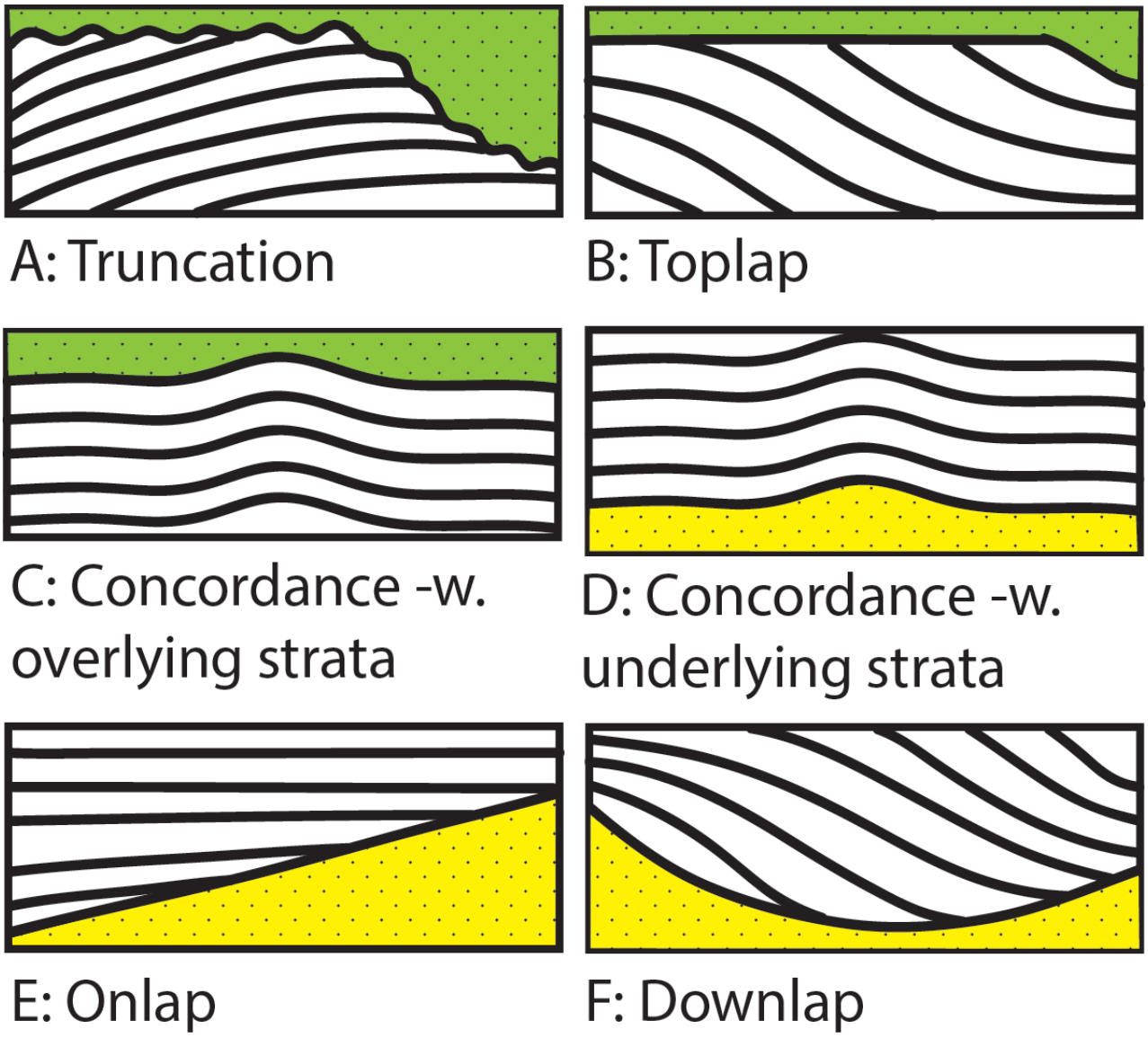

Figure 3.3: A: Erosional truncation. Reflectors of underlying strata are cut off by erosion. B: Toplap. Reflectors pinch out under the sequence boundary. C/D: Concordance. Reflectors follow the underlying/overlying strata. E: Onlap. Reflectors terminate in the inclined underlying strata. F: Downlap. reflectors are seen to terminate against the underlying strata. After Mitchum *et al.* (1977b)

geometry of the reflectors will automatically be regarded as *apparent*.

Based on previous interpretations of the swath bathymetry data (Benetti *et al.*, 2010; Dunlop *et al.*, 2011; Ó Cofaigh *et al.*, 2012), targets for collection of acoustic sub bottom profiles were selected in Donegal Bay and across the shelf (Figure 3.4). Data were acquired in the summer of 2014 as part of the NERC-funded

BRITICE CHRONO research cruise JC106. Data were acquired on board the RRS James Cook, using a hull-mounted Kongsberg SBP 120 Sub-bottom profiler system. The system operates at a 3.5 kHz frequency and provides information on acoustic stratigraphy and sediment thickness down to a depth of about 50 m below seafloor in glacial sediments (Beaman & Harris, 2003; Ó Cofaigh *et al.*, 2012). Data acquisition was done using SeiSee to convert data into Seg-Y files, and Excel to convert shotpoints from arc seconds to lat-long decimal degrees with an accuracy of 7 decimal places. Data was then imported to IHS Kingdom as 2D survey lines.

Interpretation of the SBP data was carried out using IHS Kingdom. Reflectors separating acoustic facies were set as stratigraphic boundaries and sediment thickness was calculated based on the P-wave velocity measured on the sediment cores (see section 3.3.1). Based on the technical specifications of the Kongsberg SBP system and the P-wave velocity, vertical resolution of the sediment thickness was calculated to approximately 30 cm (Kongsberg, 2016).

3.3 Core collection

Twenty seven sediment cores were collected and analysed for this study. Core sites were selected based on the acquired multibeam swath bathymetry and SBP data, and cores were collected from the outer shelf moraine and shelf break, the mid-shelf basin and the inner bay basin. Cores were obtained during two cruises: the Marine Institute/INFOMAR cruise CE08 of the Irish research vessel Celtic Explorer in 2008 (core names beginning with CE08), and cruise JC106 of the RRS James Cook in 2014 (core names beginning with JC106). The core locations are shown in figure 3.4.

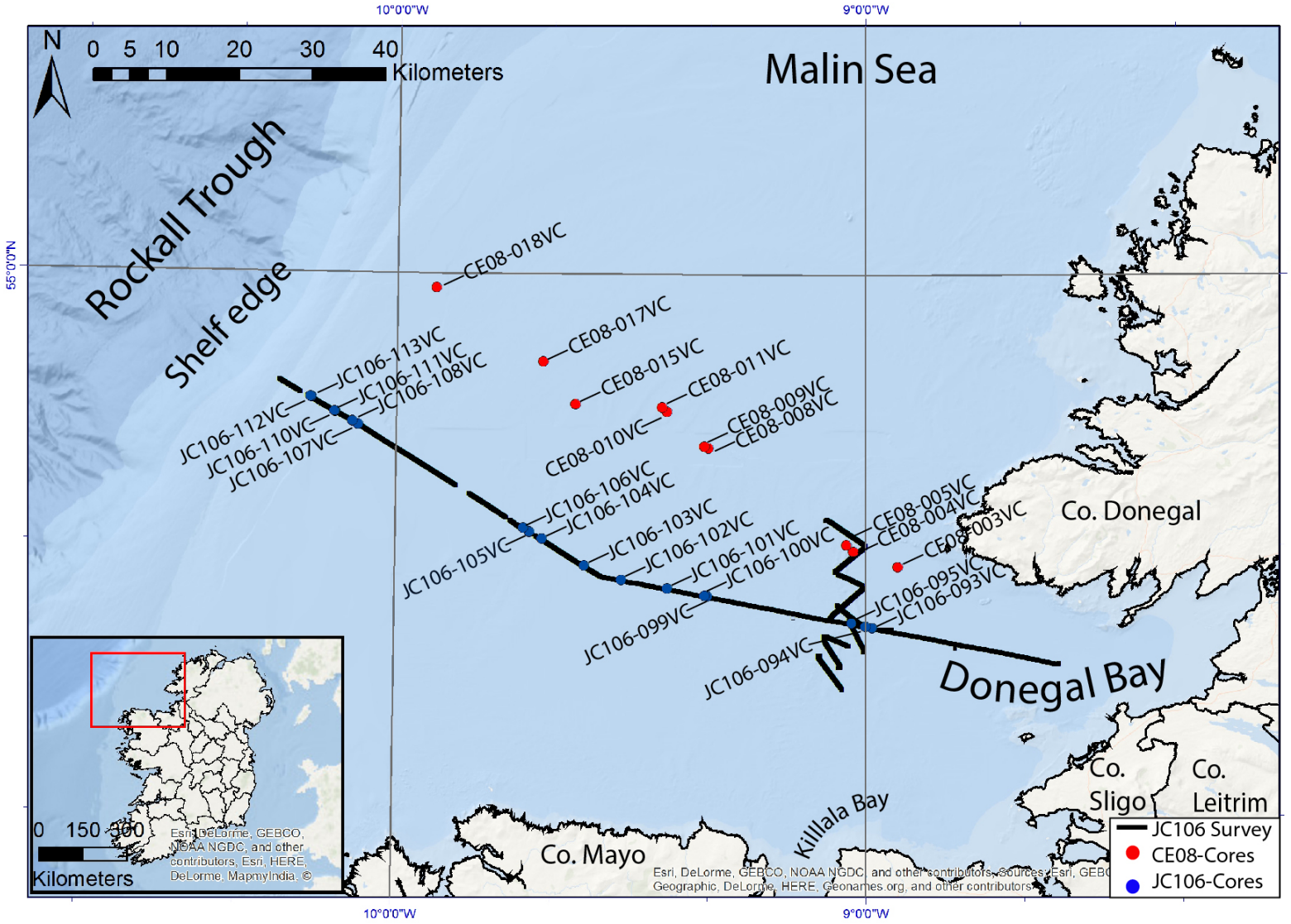

Figure 3.4: SBP profile lines collected across the shelf on the JC106 cruise in the summer 2014, and location of cores across the shelf, collected during two cruises, the CE08 cores in the north transect, and JC106 in the south transect.

From the Celtic Explorer cruise, ten cores were analysed in this thesis. The cores were located in a north-west to south-east transect in the northern part of the study area (Figure 3.4).

From the JC106 cruise a total of 20 cores were obtained from the study area, of which 17 were analysed for this thesis. These cores are located in a west-east transect from the outer shelf moraine over the mid shelf basin to the Donegal Bay Moraine (DBM) and the inner bay basin, in a line to the south of the CE08 cores (Figure 3.4).

On the Celtic Explorer, the sediment cores were retrieved from the seabed using a 6 m long vibrocorer from the Irish Geological Survey, and on the CJ106 cruise a similar vibrocorer from the British Geological Survey also with a 6 m core barrel was used. The vibrocorer was lowered to the seabed, where the core barrel is forced into the sediment by a vibrating motor, penetrating through soft to semi consolidated sediments. Penetration in over consolidated sediments, or in clast rich gravel with an individual clast size greater than the diameter of the core barrel (70 mm) is limited, and cores recovered from these sediments are often shorter than 6 m. Most cores had a recovery of 1-5 m. Upon retrieval from the seabed, the core barrel was removed from the vibrocorer and the inner plastic liner, containing the sediment is pushed out of the core barrel, and cut into 1 m long sections. The cut core sections were labelled with the cruise name, core number, coring method, core section and depth. In the case of JC106, after cutting and labelling the cores were put in a temperature controlled container for at least 12 hours before being scanned with a GEOTEK© MSCL scanner.

All cores were split into two halves, an ARCHIVE for storing, and a WORKING for further analysis. Working halves were visually logged and where the sediment was consolidated, shear strength was measured using a torvane. The cores were photographed and any visible macro-fossils were collected before the working and archive halves were packed together. Both halves of the core section were then stored in a cold container at 4°C until further use.

3.3.1 Core logging

As described above, sediment cores from the JC106 cruise were scanned using a GEOTEK© MSCL scanner shortly after retrieval. The GEOTEK© MSCL scanner provides high resolution non-destructive incremental measurements of four physical parameters in the sediment; P-wave velocity, Magnetic susceptibility, Gamma density and Electrical resistivity (Weber *et al.*, 1997; Gunn & Best, 1998; Rothwell & Rack, 2006). These parameters provide information about the physical properties of the sediment.

The P-wave velocity in the sediment is used in the conversion of time to depth in the SBP data, and thus

provides the information needed to calculate sediment thickness and depth of reflectors in the acoustic data.

Magnetic susceptibility is a measure of the ease of which a material can be magnetized (Robinson, 1993; Gunn & Best, 1998). It provides a measure of the abundance of ferro and/or paramagnetic minerals, such as magnetite, pyrrhotite, hematite, pyrite and others. Relatively high abundance of these minerals produce high magnetic susceptibility values, while relatively high abundance of organic or biogenic material such as calcite or silica results in low magnetic susceptibility (Robinson, 1993; Rothwell & Rack, 2006). Ferro and paramagnetic minerals are often related to terrigenous detritus such as glacial deposits and IRD, and magnetic susceptibility spikes in the sediment have been used as a proxy for glaciations (Chi & Mienert, 1996). In contrast organic and biogenic material is often related to marine sedimentation. Relative changes in magnetic susceptibility can therefore be used as a proxy for sediment provenance and palaeoclimate (Chi & Mienert, 1996; Rothwell & Rack, 2006).

Gamma density is a measure of bulk density of the sediment, and can therefore be used as a measure of sediment mass (m) per. unit volume (V) and is expressed as grams per. cubic centimetre (g/cc)(GEOTEK, 2016). Gamma density is measured by emitting a beam of gamma rays at 0.662 MeV, from a Caesium-137 source, through the centre of the sediment core to a detector on the opposite side (Gunn & Best, 1998). The gamma density can be used as an indicator of porosity changes and changes in core lithology (Rothwell & Rack, 2006; GEOTEK, 2016).

The electrical resistivity can be used as a proxy for pore-fluid properties, identification of lithological changes and for core to core correlation (GEOTEK, 2016).

MSCL data was cleaned using Excel and C2 software, removing flawed values primarily from the end of individual core sections, due to end caps corrupting the data. Graphs were drawn up using the C2 software and correlated with lithological logs.

Detailed sedimentary logs were constructed from the working halves of both the CE08 and the JC106 sediment cores upon return to Durham University. Information was recorded on sedimentary structures grain size, lithology, sorting and shear strength, in order to identify lithofacies (cf.Eyles *et al.* 1983). A lithofacies can be defined as a section of sediments with a distinctive combination of these properties along with thickness, geometry, and the presence or absence of certain fossils (Eyles & Lazorek, 2013). Each lithofacies is therefore characterized by the individual properties of the sediment, and can be used as a basis for the interpretation of depositional environments.

X-radiographs of the core lithofacies were made on a selection of cores showing significant changes in lithofacies composition in order to provide further information on sedimentary and deformation structures.

The Celtic Explorer (CE08) cores were x-rayed at the Royal Victoria Infirmary hospital in Newcastle. In these x-rays, denser material such as clasts or shells, is shown as light in colour. X-rays of the JC106 cores were obtained using a GEOTEK© MSCL-XCT scanner. This scanner shows denser material as dark or opaque. X-ray images from the two cruises will therefore show up in reverse of each other, as seen on figure 3.5. The GEOTEK© MSCL-XCT was operated at between 95v and 105v (GEOTEK, 2016) and scanned the cores in 1 cm increments as 16bit grayscale TIFF images. GEOTEK© conversion software stitches the images and exports them as 8bit greyscale image files.

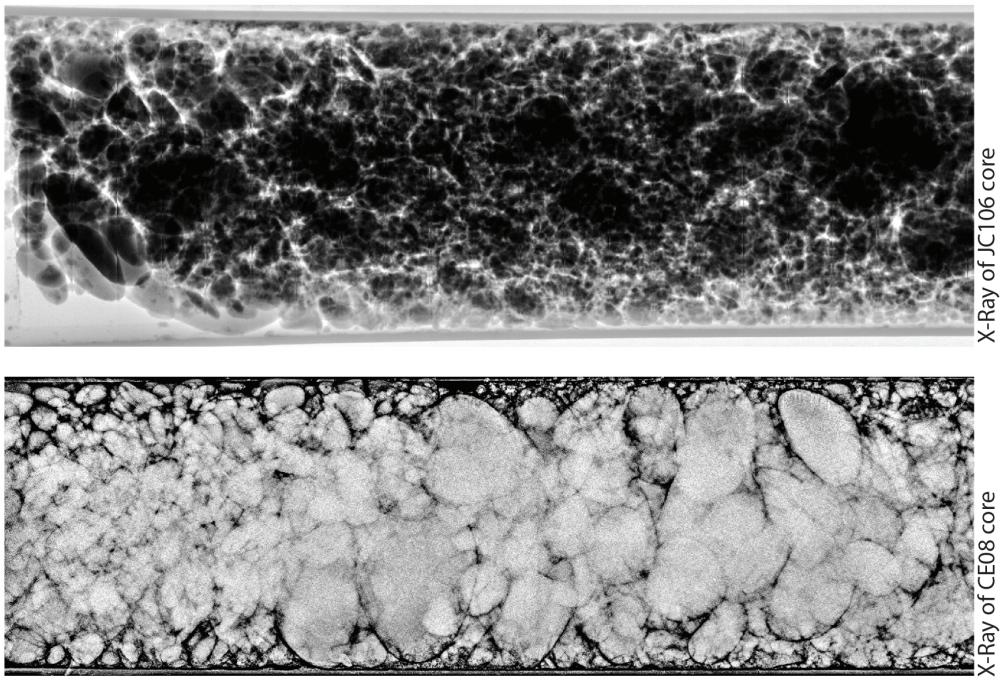

Figure 3.5: Examples of X-ray images form the CE08 and the JC106 cruises. Both X-Ray images show the same lithofacies, clast-supported gravel.

3.4 Micropalaeontological analysis

Micropalaeontological analysis was conducted on a total of 55 samples from five sediment cores. Two cores (cores CE08-010 and JC106-102) were sampled at 16 cm increments through most the core length. This interval was chosen in order to be able to decrease the increments by even numbers (8 4 and 2 cm), if any significant changes should be found across two samples. Another three cores (cores CE08-003, CE08-018 and JC106-095) were sampled at varying increments across key changes in lithofacies. For each sample 5 to 7 ml

of sediment, measured by water displacement, was left to soak in distilled water for 24 hours. Where the sediment was consolidated or clay content was high, 10 ml of a dispersant, Sodium Meta Hexaphosphate were added to the sample. After soaking, samples were wet sieved through a 500μm and a 63μm sieve, removing the relatively coarser and finer grained particles. The $\geq$63μm fraction was chosen in order to give a more precise taxonomic analysis, since the number of species and individuals will decrease with an increasing sieve size (Murray, 2006; Schonfeld *et al.*, 2012). After sieving, samples were left to dry in an oven at 40 or 60 °C for at least 24 hours or until they were completely dehydrated.

Foraminifera were dry picked from the sediment using a Leica MZ75 binocular microscope. Large bulk samples were split in order to get a sample size with an estimated 300 foraminifera tests needed for a taxonomic analysis (Murray, 2006). Individuals were counted and identified to species level, and percentages of each species were calculated against the total number of foraminifera in a sample. Data was processed in C2 and a Fisher α diversity statistic was calculated, (Fisher & Williams, 1943; Murray, 1991, 2006). The Fisher α diversity statistic gives a relation between the number of species and the number of individuals in a sample of animal population (Fisher & Williams, 1943).

3.4.1 Identification of foraminifera

Foraminifera are single celled amoebas (Phylum Protista, Class Foraminiferida (Murray, 2006)), which secrete calcareous shells, or agglutinate sediment particles into a shell called the test (Leoblich & Tappan, 1987). They are globally distributed and occur in all marine environments (Loubere & Austin, 2007), and species are commonly restricted by very specific marine conditions. Due to their small size, relatively high abundance, characteristic shells, and specific habitat preferences, foraminifera are useful palaeoenvironmental indicators (Leoblich & Tappan, 1987). Taxonomically, foraminiferas are sub-divided into three groups based on the nature of the test-wall: organic tests, agglutinated tests and calcareous tests (Loubere & Austin, 2007). A number of agglutinated and calcareous species have been found in the samples prepared for this thesis, and will be described and used in a palaeoenvironmental reconstruction.

Globally, more than 10,000 foraminiferal species have been identified based on the architecture of their test (Loubere & Austin, 2007). Foraminiferal tests are characterised by a great diversity of architecture. Growth of the test begins with an initial chamber (proloculus), with further chambers connected by an aperture, and separated by a septum. Chambers are typically added in some form of spiral, and can form complex shapes depending of coiling, chamber shape and axial orientation. The species are thus identified by the visual characteristics. Typical identification markers (Figure 3.6) are size, the placement and characteristics

of the aperture, presence or absence of a central boss, chamber configuration, characteristics of the sutures, spiral geometry, texture of the test, presence or absence of pores and/or papillae, and overall ornamentation of the test.

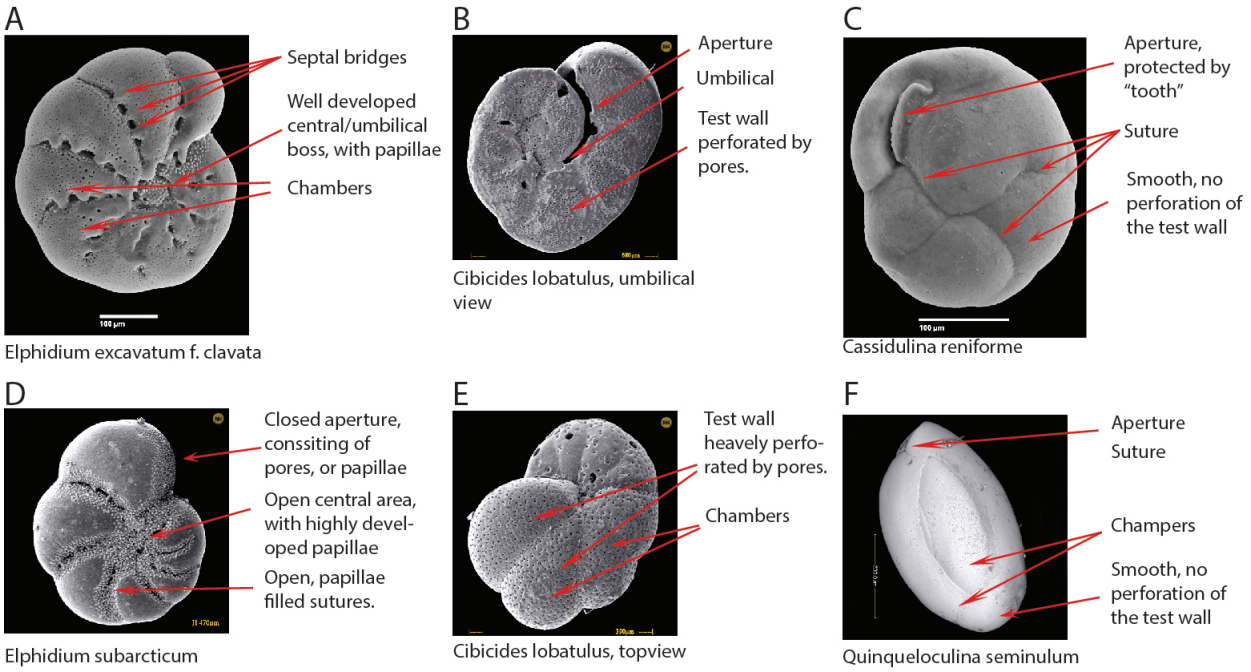

Figure 3.6: Examples of foraminiferal species and their characteristics. The species shown are commonly found in samples for this thesis. From Foraminifera.eu (2017).

Some foraminifera species can have very similar test architecture, especially species within the same *Genus*, even though they may require very different living conditions. One example are the species *Cassidulina reniforme* and *Cassidulina obtusa* (Figure 3.7). These two species are the same size and their tests have similar morphology. Both are calcareous, and the test consists of biserial, planar spiral enrolled chambers (Armstrong & Brasier, 2005). Due to the configuration of the chambers, the orientation of the sutures are also identical, but small differences can be seen in the characteristics of the sutures. In *C. reniforme*, the sutures are seen as broad depressions on the surface of the test, occasionally very shallow. In *C. obtusa*, on the other hand, sutures can be seen as thin, deep and well defined, giving the test an inflated look (Sejrup & Guilbault, 1980). The differences in sutures, however, are not always apparent, and therefore cannot be used as a definitive means to distinguish between them. In one aspect, however, the two species do have a distinct difference. Sejrup & Guilbault (1980) found that foraminifera identified as *genus Cassidulina* from Arctic environments have a well developed flap, or "tooth" attached to the upper edge of the last chamber,

blocking the aperture. This tooth is usually low at its umbilical end and higher at the peripheral end, where it often is cut off abruptly. This species has been identified as *C. reniforme*. *Genus Cassidulina* found in more boreal conditions, lack this tooth, but have a characteristic fold in the aperturial face. Along the base of the aperture a low, lip-like flap of uneven height can sometimes also be seen, giving the aperture a thin and elongate appearance. This species has been identified as *C obtusa*. To distinguish between the two species is important as the species are rarely seen together, and *C. reniforme* is a glacimarine indicator.

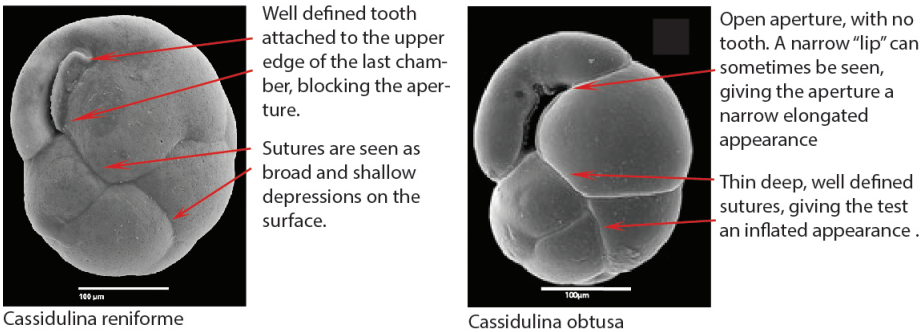

Figure 3.7: Differences of Cassidulina reneforme and Cassidulina obtusa. From Foraminifera.eu (2017).

Another challenge for identification is when one species can contain several forms. In that case individual tests can grade into one form or another and thereby show characteristics of both forms. An example is *Elphidium excavatum*. This species is highly adaptable and opportunistic (Murray, 1991; Kowalczuk *et al.*, 2013), and adapts both epifaunal and infaunal strategies to survive and thrive near ice-marine interfaces with high sedimentation rates, changing salinity and an average water temperature $\leq 1°C$ (Murray, 1991; Hald & Steinsund, 1996; **?**). It is planispiral with seven to nine chambers distinct deep sutures, in some cases with septal bridges and a granular (papillae) texture in the umbilical region (Feyling-Hanssen, 1972). *E excavatum* with a boss in the umbilical region are known as the form *clavata*. This boss can vary in size, shape and height, and in some cases it can consists of several smaller bosses, or even well developed papillae. *E excavatum* with developed papillae in the sutures are known as the form *selseyenses*. In the umbilical region, one or even more small bosses can be seen, or sometimes highly developed papillae (Feyling-Hanssen, 1972). As described above, the two forms often appear similar, and confusion between them is common. In previous studies *Elphidium excavatum f. clavata* was even interpreted as a juvenile form of *Elphidium*

excavatum f. selseyenses (Feyling-Hanssen, 1972). It is however important to make a distinction between the two forms, as *Elphidium excavatum f. selseyenses* are common in boreal environments (Feyling-Hanssen, 1972; Murray, 1991), while *Elphidium excavatum f. clavata* are a common glacimarine indicator (Murray, 1991; Hald & Steinsund, 1996; Korsun & Hald, 1998), and therefore important for this thesis.

Only benthic foraminifera were individually identified for this thesis, due to their close connection with the environment they live in (Murray, 2006), while plantonic species were added as a total count.

3.5 Radiocarbon dating

Radiocarbon is constantly produced in the atmosphere by cosmic radiation reacting with Nitrogen 14 to produce Carbon 14 (^{14}C) (Libby *et al.*, 1949). ^{14}C is radioactive and has a half-life of 5780 years, and through metabolism of CO_2 from the air, ^{14}C is incorporated in to the tissue of living organisms (Libby *et al.*, 1949). Upon death the constant replenishment of ^{14}C in the tissue stops, and the amount of ^{14}C in the tissue decays following the half-life constant of 5780 years. Using accelerator mass spectrometry (AMS), the amount of ^{14}C in a fossil can be measured, and a date of death can be calculated to a maximum of ∼50,000 years (Ramsey *et al.*, 2012), which in turn gives a date for the deposition of the enclosing sediment, provided no further reworking has taken place. The rate of ^{14}C production in the atmosphere is not constant, due to geomagnetic and solar modulation of the cosmic-ray flux (Reimer *et al.*, 2013), and so the use of calibration curves is necessary to obtain a precise date of a measured radio-carbon sample. In the Northern hemisphere, calibration with tree-ring chronologies is well established to as far back as 13.9 cal ka BP (Reimer *et al.*, 2013). In order to calibrate the radiocarbon curve further back in time, varved sediments from Lake Suigetsu in Japan have been used to obtain a calibration curve to the end of the ^{14}C dating range (Ramsey *et al.*, 2012; Reimer *et al.*, 2013). Using tree rings or varved lake sediments gives a very accurate calibration, since each annual layer or ring can be visually identified and organic material from that layer dated. Both these methods are, however, terrestrially-based calibration methods, and when dating marine sediments these calibrations cannot be used due to a delayed response in the incorporation of atmospheric ^{14}C into the ocean (Stuiver & Braziunas, 1993; Reimer *et al.*, 2013). In order to calibrate marine ^{14}C samples, marine calibration curves have been created by dating corals and speleotherms using U-Th (Reimer *et al.*, 2013). U-Th dating is not influenced by the varying factors ^{14}C is, and the dates can thereby be compared with the measured ^{14}C data, and calibration curves created. The latest and most precise marine calibration curve

is the Marine13 curve, which takes into account a 400 year global marine reservoir effect (Reimer *et al.*, 2013). Due to spatial and temporal uncertainties between the reservoir age and the global 400 year marine reservoir effect, three different ΔR values (the difference between the local reservoir age and the global 400 year correction) have been calculated: +0, +300 and +700 years, but the dates presented in table 4.9 and used in the actual text are all calibrated ages with a ΔR value of 0.

Samples for radiocarbon dating consisted of both macro-fossils and foraminifera. In the case of the macro-fossils, whole valves and large shell fragments identified as marine species were collected from the sediment immediately after cores were split (See chapter 3.3). Additional samples for radiocarbon dating were selected from sections with significant lithological changes in the sediment cores and where sufficient foraminifera were present to obtain a date. Preparation of foraminiferal samples for dating followed the same procedure as described for micropalaeontological analysis (See chapter 3.4), although sample size was on the order of 10 times larger. In samples with a high amount of silt, a 125μm sieve was used, in order to separate finer material from slightly larger foraminifera. This reduced the picking time of foraminifera significantly. Sampling targeted deglacial glacimarine sediments, in order to date ice sheet retreat and reworked shells in tills to provide a maximum age for till formation and ice sheet advance. Material was taken from the middle part of the core, avoiding the edges and core liner, where sediment might have been drawn down by the coring method. Dating is possible with carbonate sample sizes down to $\geq$5 mg, but for a more precise dating, >10 mg of carbonate material is desirable. In glacimarine sediments biological productivity and hence foraminiferal abundance can be low. Therefore it was necessary to use samples with mixed benthic species for dating rather than monospecific samples, as it was not possible to pick enough material from just one benthic species in each sample. Furthermore, no samples contained only one benthic species. In cases where foraminifera samples did not yield the required amount for dating, the sample size was increased through the addition of material from immediately above or below the original sample. Samples were sent to the AMS laboratory at the Scottish Universities Environment Research Centre (SUREC) and analysed using a 5MV tandem spectrometer. All ages are presented as cal ka BP (Calibrated kilo anno Before Present). Before Present relates to the date AD 1950.

4. *Results*

Data collected and presented in this thesis cover a range of spatial and temporal scales ranging from the regional scale of modern seafloor bathymetry, to longer term sub-bottom stratigraphic profiling, to millennial/centennial point data from sediment cores. Multibeam swath bathymetry data collected in the area between 2002 and 2008 was the basis for the sub-bottom profile (SBP) data collection across the shelf in 2014 on board the RRS James Cook. Sites selected for sediment coring on board the Celtic Explorer was based on INSS pinger data collected together with the multibeam swath bathymetry, and core sites for the RRS James Cook in 2014 were based on the geophysical data collected during that cruise. Sedimentary logs were produced based on the physical and visual properties of the sediment cores. These were used to develop a strategy for sub-sampling of the cores for detailed palaeoenvironmental (foraminiferal) analysis, and radiocarbon dating. This chapter presents the geophysical data (swath bathymetry and SBP data), followed by the sediment lithofacies from the cores and then detailed foraminiferal analysis from selected cores.

4.1 Multibeam Swath Bathymetry

Multibeam swath bathymetry data from the study area collected between 2002 and 2008 by INFOMAR, were presented and interpreted by Benetti *et al.* (2010), Dunlop *et al.* (2011) and Ó Cofaigh *et al.* (2012). In order to provide the broader context for the SBP and sediment core data presented in this thesis, the swath bathymetry data are here re-produced. Interpretations of the seafloor morphology are based on these earlier publications. The seafloor morphology in the study area (Figure 2.8), has been interpreted to be the result of glacial retreat from the shelf edge to Donegal Bay (Benetti *et al.*, 2010; Dunlop *et al.*, 2011; Ó Cofaigh *et al.*, 2012). As described in section 2.5 the continental shelf extends about 150 km to the shelf edge. The regional topography is characterized by relatively low gradients. The multibeam swath bathymetry data show a series of prominent NE-SW aligned and nested sediment ridges which are predominantly arcuate in planform, although some of the longer ridges have straight sections (Ó Cofaigh *et al.*, 2016). These ridges have been interpreted as moraines recording retreat of a grounded ice-sheet across the shelf, punctuated by occasional minor re-advances, which can be seen on figure 2.8 (Ó Cofaigh *et al.*, 2012). The two largest moraines are located at the shelf edge and stretches discontinuously along the shelf break for about 125 km

(Figure 2.8). This moraine is widest at its NW end, where it is up to 11 km wide and 14 m high, becoming increasingly narrower and lower as it extents to the SE, where it is ∼0.5 km wide and 6 m high (Dunlop *et al.*, 2011; Ó Cofaigh *et al.*, 2012, 2016). Another moraine of similar dimensions is nested just east of this, although its western end is bifurcated into a series of finger-like ridges 0.5-2 km wide and up to 7 km long. About 18 km further inshore, a suite of well-developed nested arcuate moraines can be seen. These moraines extend across the shelf forming a stepped sequence for about 45 km towards the mouth of Donegal Bay (Figure 2.8). They range from 1.5 to 9 km in length, 1 to 3.5 km in with and have a amplitude of 1 to 4 m. To the south, in a low lying morphologically smooth and featureless area, the moraines are no longer visible. These moraines tend to be asymmetrical with a steeper landward side and a gentle seaward side (Ó Cofaigh *et al.*, 2016). The most prominent moraine is located at the mouth of Donegal Bay, here named the Donegal Bay Moraine, (the DBM). It extends continuously for about 35 km, is 1-2.5 km wide and have a hight of 15 to 20 m. It have a sharp crest, and a steep landward slope, with a more gentle seaward slope. On the southern end of the DBM a series of minor, east-west orientated ridges are superimposed on the moraine (Figure 2.8).

4.2 Sub-Bottom Profile results

SBP data were acquired in a single, approximately 115 kilometre long profile line across the shelf from Donegal Bay to the shelf break, and in a series of shorter profiles crossing the DBM from various angles, primarily north-west to south-east and north-east to south-west (Figure 3.4). The 115 kilometre long profile and a selection of the profiles crossing the DBM are described here. The acoustic penetration across the profiles varies between 45 and 65 milliseconds (ms) based on the underlying acoustic facies.

The signal penetration depth can be calculated based on the acoustic penetration (45 to 65 ms) and P-wave velocity measurements from the sediments. P-wave velocities in the sediment cores vary between 1500 m per second (m/s) and 1800 m/s, with an average P-wave velocity of 1738 m/s (see MSCL results associated with sediment cores, section 4.5). As depth in the SBP data is shown as a measure of Two Way Time (TWT) the acoustic penetration has to be divided by 2 in order to get a proper time to depth conversion. However, since the actual acoustic penetration is not constant at any place in the profiles, in order to get a constant time to depth conversion, the average P-wave velocity is used in this calculation instead. Therefore, 1738/2=869. This gives a depth of 869 m per second, or 0.869 m per ms. This implies that one ms in the profiles is equivalent to 0.869 m. The actual depth penetration in the profiles can therefore be calculated as

approximately 45ms*0.869m=39.1m and 65ms*0.869m =56.4m The vertical penetration across the profiles is therefore between ∼39 to ∼56 m. According to the Kongsberg technical specifications for the TOPAS 120 system, a maximum vertical resolution of 0.3 ms can be expected (Kongsberg, 2016). It can therefore be calculated that the vertical resolution for the SBP data is 1/3 of the depth of one ms, or 0.869m/3 = 0.29m. The vertical resolution in the SBP is therefore ca. 30cm and sedimentary units thinner that this may not be possible to detect in the data.

4.2.1 Acoustic Facies

The survey lines running approximately 115 km from east to west across the shelf from Donegal Bay to the shelf edge, have been visualised as a single profile (Figure 4.1). Based on the SBP data presented in that profile and with SPB data from profiles from the DBM (Figures 4.1 to 4.7), three acoustic facies can be distinguished in addition to a strong seafloor reflector. Figure 4.1 illustrates the large scale variability in acoustic facies in the area, and zoomed in sections of the profile (Figures 4.2 to 4.7) display the three facies. The profile across the shelf can be divided into four sections; from west to east are (1) outer shelf moraine and shelf break, (2) mid-shelf basin, (3) Donegal Bay Moraine (DBM) and (4) inner bay basin. Each section contains one or more acoustic facies.

Facies A

Facies A constitutes the deepest lying acoustic facies over most of the study area. It is massive and has a moderate to strong amplitude in the acoustic data. On the mid-shelf (Figure 4.3) the facies extends to a depth of approximately 66 ms (56 m), but in most of the study area the acoustic data does not penetrate deeper than 45-50 ms (40-43 m), and the base of the facies is not visible. Facies A has a very pronounced topography and in several places this facies onlap or pinch out against the overlying facies B and C. It occurs across the study area and in high lying areas including the DBM (Figure 4.4) and on the outer shelf moraine (Figure 4.2), where Facies A crops out under the seafloor reflector. Similar structureless acoustic facies, characterized by a chaotic appearance and a lack of stratification have been found underlying stratified facies on contemporary glaciated continental margins and Arctic fjords and basins (Gilbert, 1985; Syvitski & Praeg, 1989; Syvitski, 1991; Hein & Syvitski, 1992). This facies seems to be widely distributed as the deepest lying facies in the entire inner bay basin (4) and mid-shelf area (2). Towards the outer shelf (1), the facies becomes less topographically distinct and pinches out under the seafloor reflector (Figure 4.2).

Facies B

Facies B overlies Facies A and is acoustically well stratified. It occurs in the inner bay basin (4), (Figure 4.7) and in the mid-shelf basin (2), (Figure 4.3). Towards the outer shelf it pinches out as the underlying Facies A crops out at the seafloor (Figure 4.2). The thickest sequences of Facies B are found within depressions in the underlying facies. This is best seen in the mid-shelf basin (Figure 4.3). East of the DBM and in the inner bay basin (Figure 4.7) Facies B reaches thicknesses of up to 45 ms (40 m), while it is up to 28 ms (25 m) thick in the mid-shelf basin (Figure 4.3). Facies B is characterised by near horizontal reflectors that typically onlap the topography of the underlying Facies A and infill topographic lows (figures 4.7 and 4.3). The top of Facies B is truncated by Facies C and, in some cases, the seafloor reflector.

Facies C

Facies C is acoustically weak or transparent. It is seen throughout the study area as a thin layer immediately beneath the seafloor reflector (Table 4.1). The facies occurs in the inner bay basin and mid-shelf basin (Figures 4.7 and 4.3), and also occurs as lenses draped onto the sides of both the DBM and the outer shelf moraine. However, on the outer shelf close to the shelf break this facies is not present (Figure 4.2). In the mid-shelf basin, Facies C has a thickness of up to 5 ms (4.5 m), but pockets of 8 ms (7 m) are seen as well (Figure 4.3). In coastal areas and the inner bay, thicknesses of up to 9 ms (8 m) are more common (Figure 4.7).

Seafloor

Throughout the study area, a very strong seafloor reflector truncates the acoustic facies. It has a constant thickness of 1 to 2 ms depending on the contrast used in the IHS Kingdom software. Nowhere is it penetrated by any of the underlying acoustic facies. Reflectors of the underlying facies do in some places top lap the base of the seafloor reflector, or are truncated by the seafloor reflector.

Table1

Facies	Acoustic signature	Description
Seafloor		Strong reflector at the top of the seismic data. This reflector can be seen throughout the study area, and has a thickness of approximately 1 to 2ms.
C	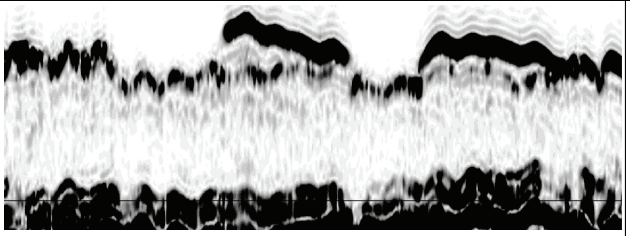	Acoustically weak or transparent facies. Seen under the seafloor, never underlying other facies. Found in most of the study area especially in the inner bay and mid shelf basins. Its thickness is between ∼0.8 m and ∼7 m and up to 9 m thick in coastal areas.
B	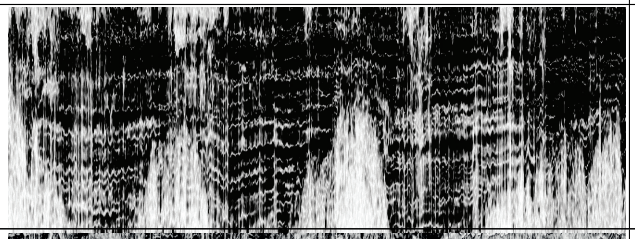	Acoustically well stratified. Seen in the inner bay and basins east and west of the DBM. The thickness is defined by the underlying topography. Maximum thickness up to ∼24 m. The facies is infilling underlying topography.
A	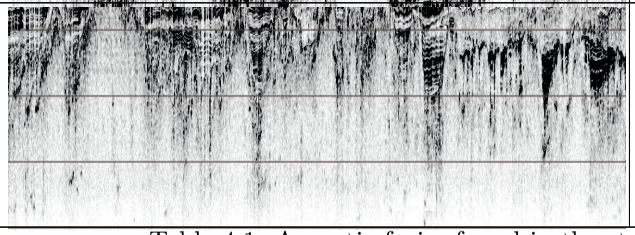	Massive structureless facies, constitutes the deepest lying stratigraphic unit in the study area. It has a very pronounced topography across the shelf and the overlying facies B infill the topography of facies A in several places.

Table 4.1: Acoustic facies found in the study area

4.3 SBP Profiles

As described above, the 115 km long profile across the shelf from Donegal Bay to the shelf break (Figure 4.1), can be divided into four sections: outer shelf moraine and shelf break, mid-shelf basin, DBM and inner bay basin. These sections are based on the sea bed morphology and characteristics of the SBP data, and will be described individually below.

4.3.1 Outer shelf moraine

In the western part of the profile (Figures 4.1 4.2), Facies A is dominating and is truncated by the seafloor reflector under a shallow ridge system. Facies B is seen pinching out in the eastern most part of the profile (Figure 4.2), where the ridge rises about 20 meters over the mid-shelf basin (Figure 4.2). An up to ∼5 m thick veneer of Facies C can be seen on each side of this ridge. As described by Sejrup *et al.* (2005) and Clark *et al.* (2012a) a series of large landforms interpreted as moraines are found on the western shelf edge of Britain and Ireland. This land-form is interpreted as one of these moraines and named the outer shelf moraine (Benetti *et al.*, 2010; Ó Cofaigh *et al.*, 2012) (Figure 4.2). The moraine is consisting primarily of Facies A, with the before mentioned veneers of Facies B on the sides. It is approximately 23 km wide and has gentle slopes born on its eastern and western facing sides. The western slope extends to the shelf break (Figure 4.2).

4.3.2 Mid-shelf basin

The mid-shelf basin, shown in figure 4.3, is an area of subdued relief that stretches approximately 35-40 km from the DBM to the outer shelf moraine. It has an average water depth of about 100 m. Throughout the basin, Facies C occur under the seafloor reflector, with a thickness of approximately 4.5 ms (4 m), but pockets of up to 8 ms (7 m) are seen (Figure 4.3). It is underlain by the acoustically well stratified Facies B, which ranges from less than 1 ms and up to 29 ms (25 m) depending on the topography of the underlying facies A. The horizontal reflectors of Facies B are seen to onlap Facies A (Figure 4.3), and to infill depressions of this facies. Facies A has a clear topographic expression in this basin, and comprises a series of buried landforms, 23-28 ms (20-25 m) high and 500-1000 m wide. This topography occur throughout the mid-shelf basin, with an increasing height and width towards west. In the middle of the basin (Figure 4.3C), at a depth of approximately 11.5 ms (10 m), a wedge of Facies A is seen overlying pockets of Facies B. This wedge

has a thickness between 4.5 and 11.5 ms (4-10 m) and can be traced for about 9 km towards the DBM where the underlying horizontal reflectors of Facies B can no longer be traced.

4.3.3 Donegal Bay Moraine

The mid-shelf basin is bounded to the east by the DBM, which also separate it from the inner bay basin. The ridge of the DBM is at about 60 meters of water depth, and the DBMs eastern slope rises up from the inner bay basin to a hight of about 30 meters over the basin floor. The DBM consists of two ridges; a 2.5 km wide eastern ridge with a steep eastern slope rising up from the basin floor, and a western ridge with an irregular topography (Figure 4.4). This western ridge is approximately 14 km wide and has a gentle west facing slope, gradually extending down into the mid-shelf basin (Figure 4.4). Acoustic penetration on the eastern flank of the DBM is good and reflectors of Facies B can be followed from the inner bay basin to a depth of approximately 46 ms (40 m) beneath the seafloor, immediately east of the DBM (Figure 4.4). Immediately under the eastern ridge, acoustic penetration is weak and only a faint lamination can be observed, which can be attributed to multibles or echoes of the seabed. Between the two ridges of the DBM, an isolated pocket of Facies B is seen lying close to the seafloor reflector (Figure 4.4). Under the eastern ridge a strong reflector with a distinct topography can be seen. This reflector is discontinuous, and can only be followed in two sections for about 300 and 600 m. Acoustic penetration into the western ridge is good, and Facies A can be seen to a depth of approximately 32 m under the seafloor (Figure 4.4). On the western slope of the moraine, a strong but segmented reflector is seen going through Facies A, with a faint lamination seen underneath. This lamination has some similarities with Facies B but is much weaker and segmented compared to other areas where Facies B is seen.

To get a better understanding of the acoustic stratigraphy of the DBM, a series of cross profiles were acquired over the eastern ridge of the moraine. Two profiles taken in an north-west to south-east direction, profiles 0542 and 4648 (Figures 4.5 and 4.6) provide excellent penetration through the ridge, and show a more complex interior architecture of the DBM. The isolated pocket of Facies B, seen on the western side of the rise on Figure 4.4, can be traced in these two profiles under the moraine to the east, and is seen almost connecting with the thick successions of Facies B on the eastern flank. In profile 0542 (Figure 4.5), the pocket of Facies B has an onlapping appearance on the eastern flank of the western ridge, but to the east, is more chaotic. The strong discontinuous reflector under the moraine is more extensive in these two profiles, both to the north-west and south-east of the ridge. In profile line 0542 (Figure 4.5) the reflector can be seen folded over it-self from the south-east, and in profile line 4648 (Figure 4.6), the reflector forms

a 10 m high NW facing scarp east of DBM.

4.3.4 Inner Bay Basin

The inner bay basin stretches from the nearshore coastal area approximately 25 km west where it is bounded by the DBM (Figure 4.7). In the eastern part of the profile, water depths reach about 80 m. In this part of the study area, Facies C reaches thicknesses of up to 10 ms (8 m) close to the coast, and overlies the acoustically well stratified Facies B, which reaches thicknesses of up to 28 ms (25 m). Reflectors of Facies B are truncated by the lower boundary of Facies C, and near horizontal reflectors can be followed east as they onlap the underlying Facies A. Towards the east, several "spikes" or blank zones can be seen in the data. These protrude upwards from Facies A, and penetrates both facies B and C in several places (Figure 4.7). These share characteristics with gas blanking rather than actual topography (Riedel *et al.*, 2002). To the west, however, a distinct land-form can be seen buried under Facies B. Facies A follows the overall topography of the seafloor reflector towards the east. In the eastern most part of the profile, the horizontal reflectors of Facies B, are more or less in concordance with the topography of Facies A, and no onlap is seen. To the west, towards the DBM, Facies B extends from the inner bay basin to a depth of approximately 46 ms (40 m) under the seafloor (Figure 4.4). Towards the bottom, parallel reflectors of Facies B is in concordance with the underlying topography of Facies A, but closer to the seafloor reflectors are seen to onlap the flank of the moraine down to a depth of about 25 m.

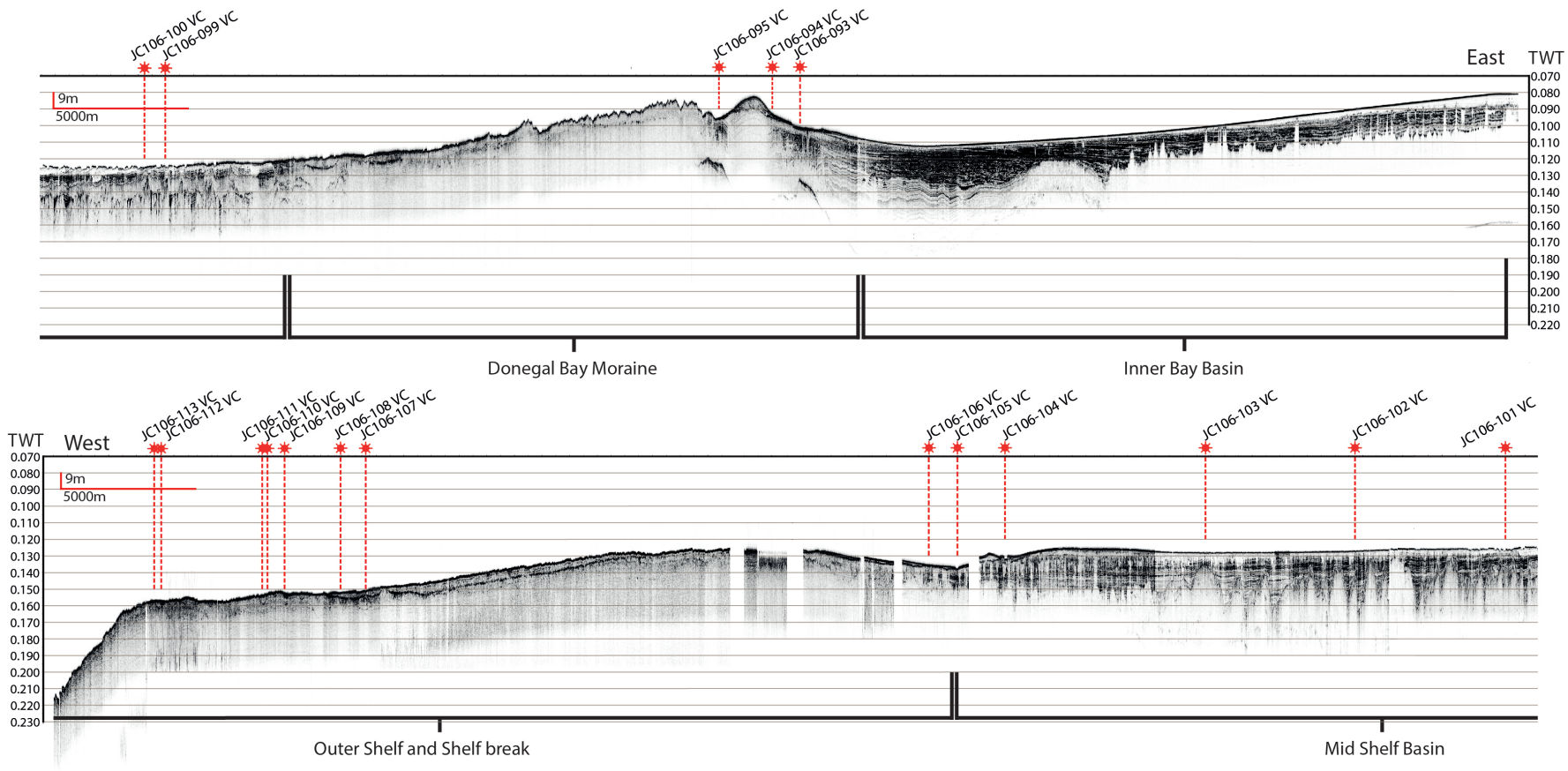

Figure 4.1: Sub-bottom profile across Donegal Bay and the adjoining shelf extending about 150 km from the inner bay in the east to the shelf break in the west. Note Two Way Time in seconds.

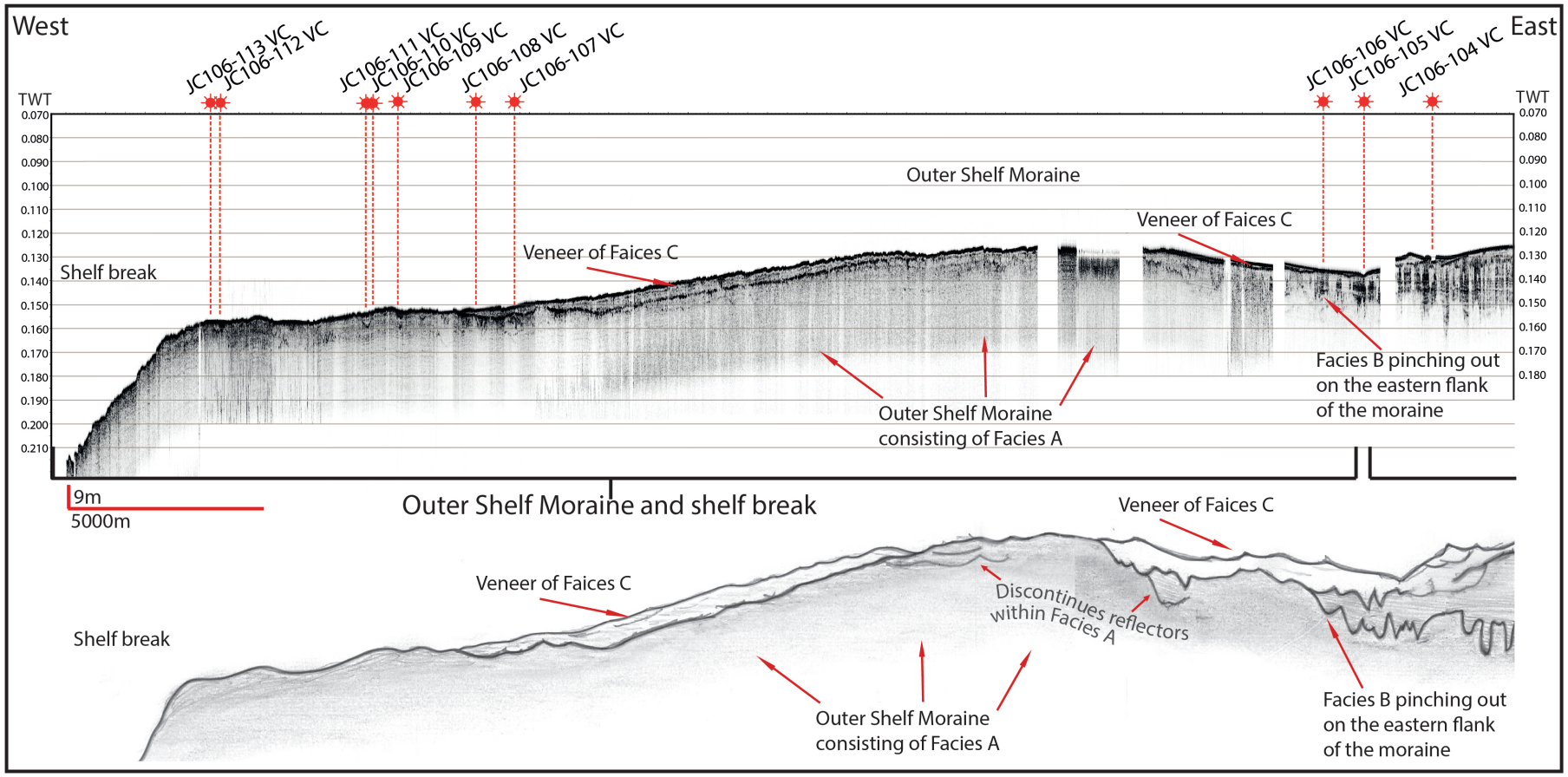

Figure 4.2: Outer Shelf Moraine and shelf break. The outer shelf is comprised of Acoustic Facies A, with a veneer of Acoustic Facies C on the east and west side of the outer shelf moraine. Note Two Way Time in seconds on the Acoustic profile. The hand drawn sketch have some exaggeration to the hight in order to better visualise the acoustic facies and contacts.

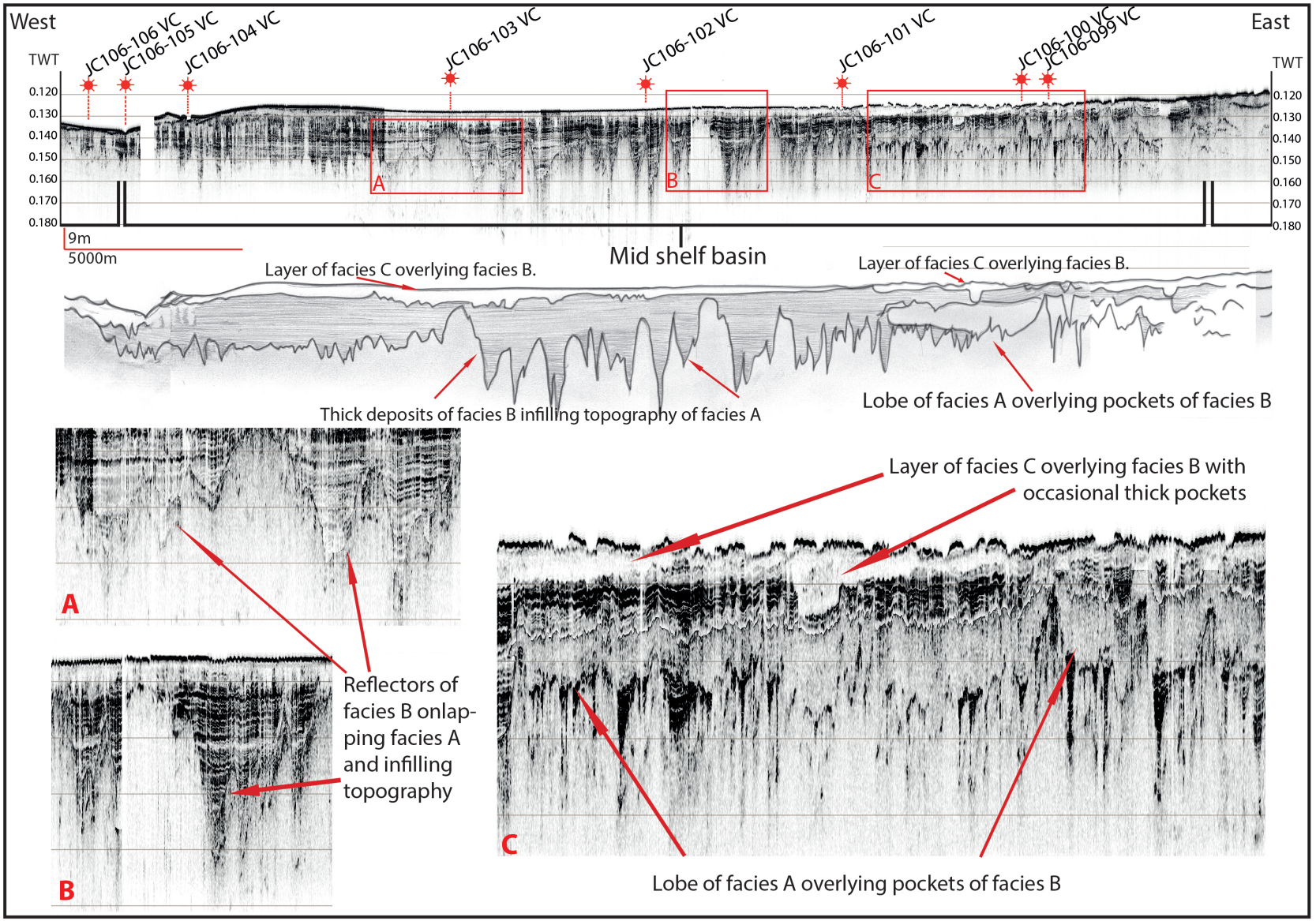

Figure 4.3: Sub-bottom profile from the mid-shelf basin. It is clearly seen how Facies B stratigraphially overlies Facies A (inset figures A and B on the Acoustic profile). Note Two Way Time in seconds on teh Acoustic profile. The hand drawn sketch have some exaggeration to the hight in order to better visualise the acoustic facies and contacts. It is clearly seen how Facies B infill the topography of Facies A.

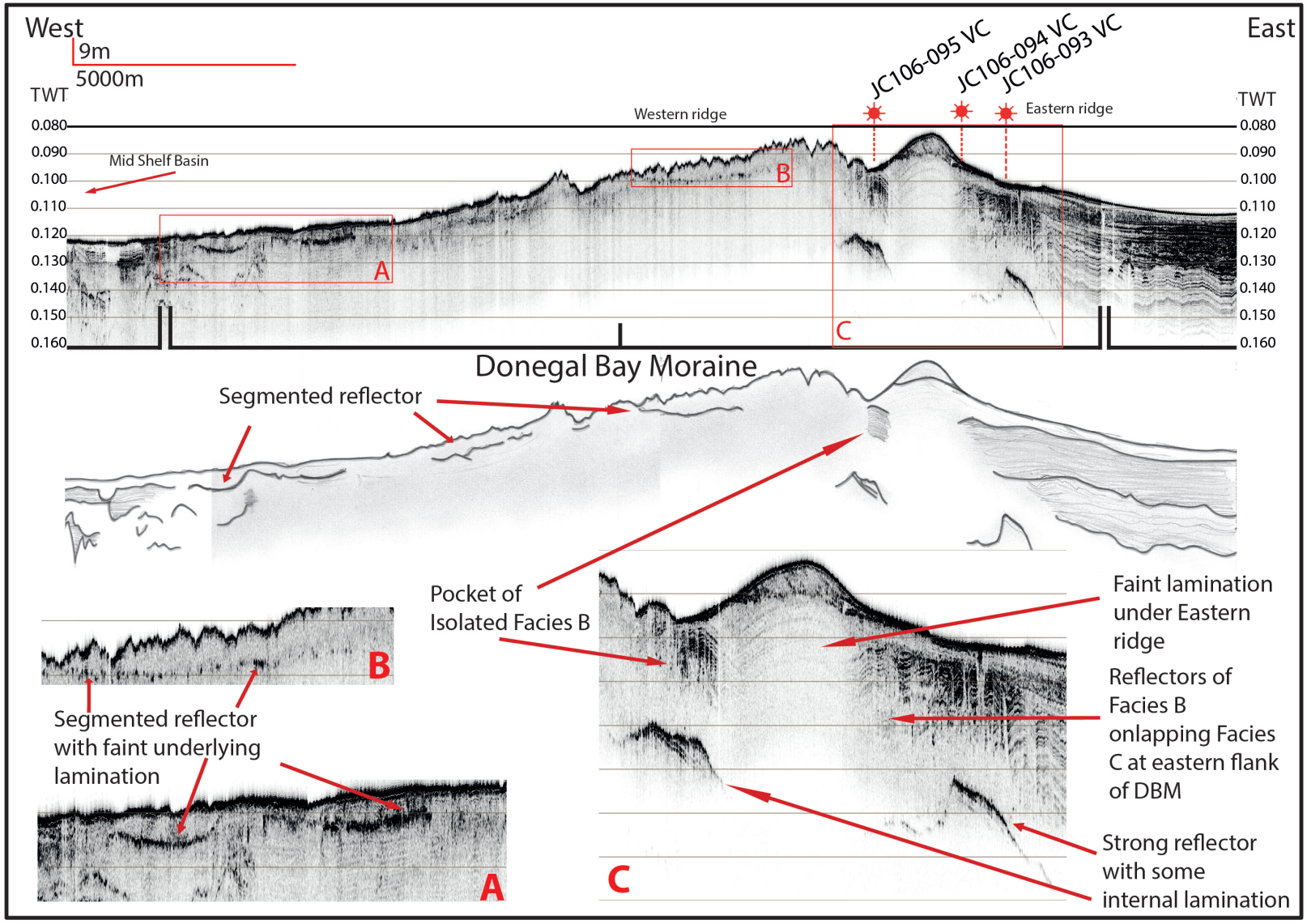

Figure 4.4: Donegal Bay Moraine. The two parts of the moraine are clearly seen as an eastern ridge with a steep east-facing slope, and a western ridge, with a gentle west-facing facing slope. Note Two Way Time in seconds on the Acoustic profile. The hand drawn sketch have some exaggeration to the hight in order to better visualise the acoustic facies and contacts.

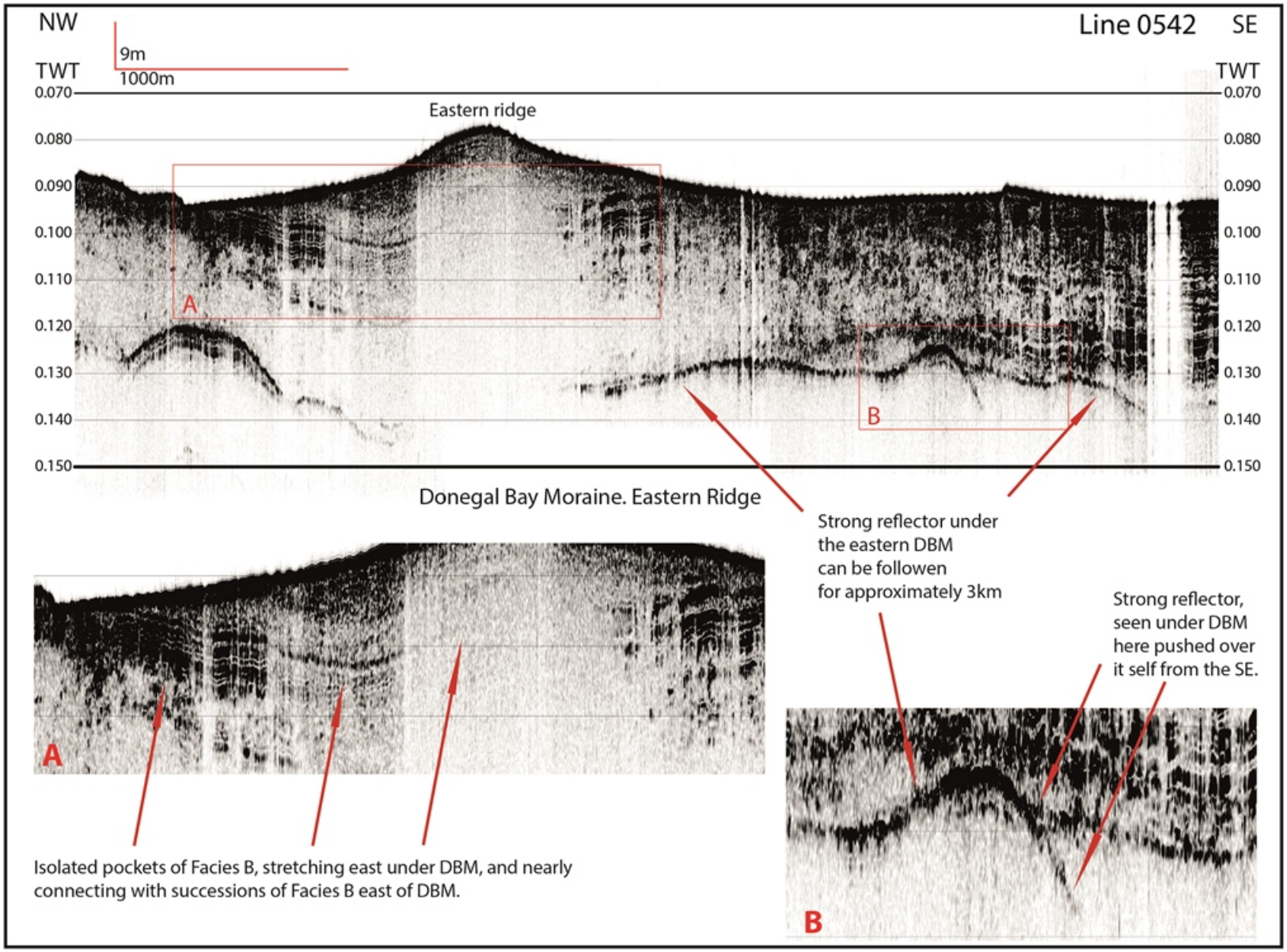

Figure 4.5: Profile line 0542, showing the eastern ridge of the DBM from south-east to north-west. Here the strong reflector deep under the moraine is seen over-folded from the south-east, and the isolated pockets of Facies B east of the ridge, can be seen under the ridge. Note Two Way Time in seconds.

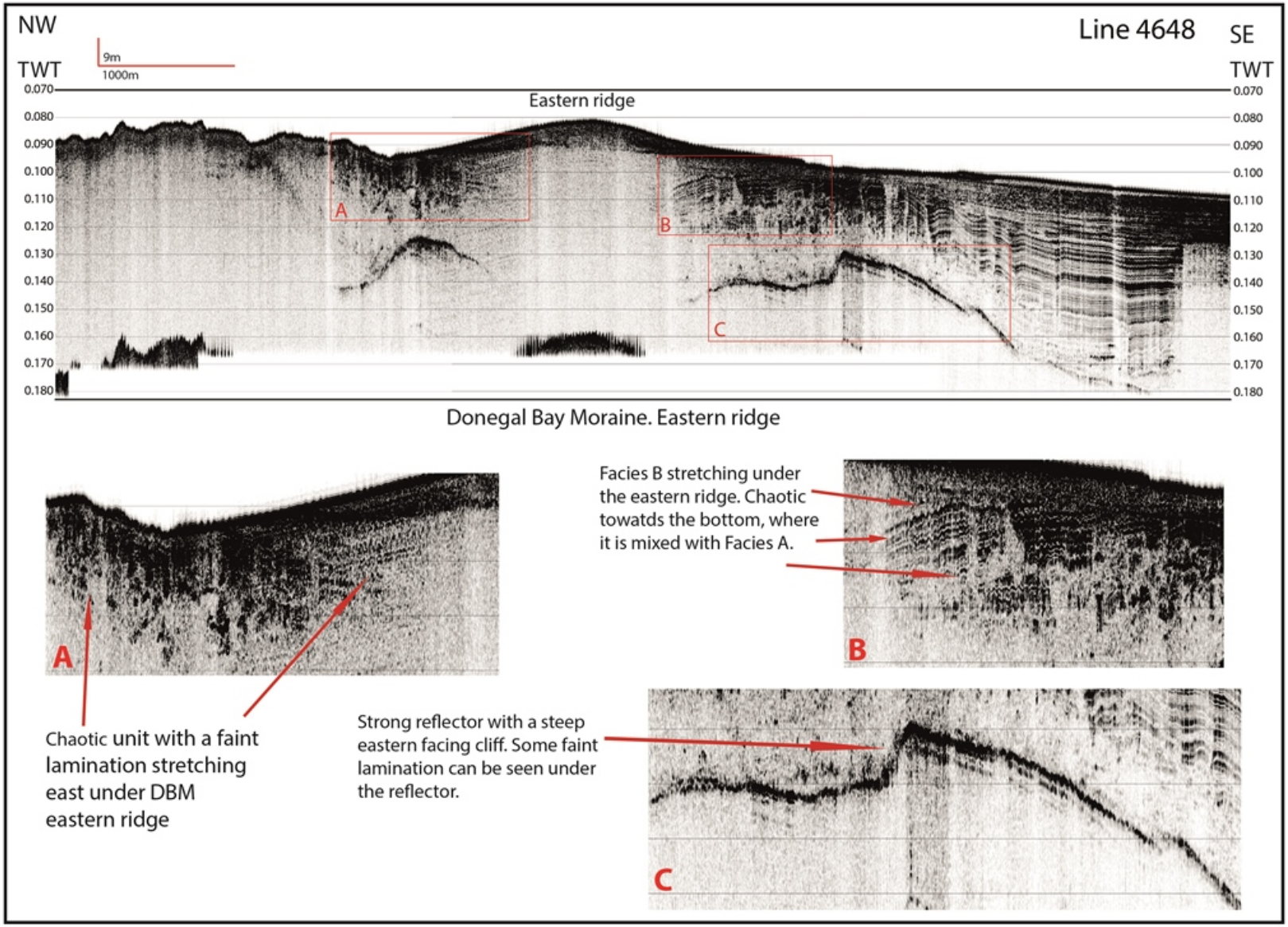

Figure 4.6: Profile line 4648, showing the eastern ridge of the DBM from south-east to north-west. The strong reflector is clearly seen under the ridge, and a steep 10 m high NW ridge face are seen. Note Two Way Time in seconds.

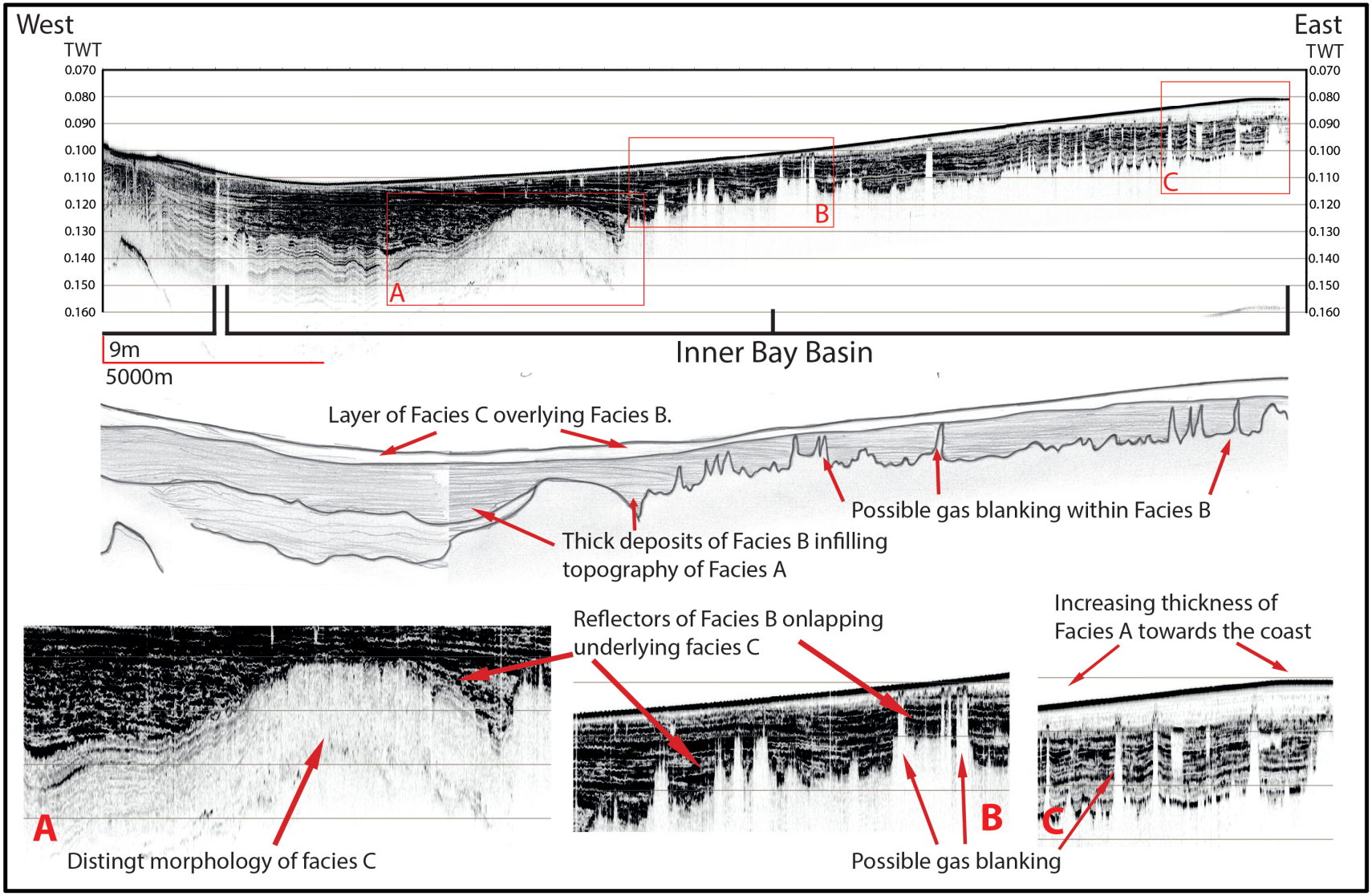

Figure 4.7: Sub-bottom profile of the inner bay basin. Thick successions of Acoustic facies B are seen east of DBM and further towards the east, where it onlap the underlying topography. Note Two Way Time in seconds on the Acoustic profile. The hand drawn sketch have some exaggeration to the hight in order to better visualise the acoustic facies and contacts. Here it is clearly seen how Facies B onlap Facies A towards the east.

4.4 Sedimentology

Twenty seven vibro-cores were collected from the study area, in two east–west orientated transects across the shelf, one in the north, and one in the south (Figure 3.4). For JC106 cores, core sites were selected where only a thin veneer of acoustic Facies C was seen on top of the strata so as to penetrate and recover acoustic facies A and B in the cores. The SBP-data was therefore used to identify areas where it was believed that the sediment cores could penetrate both acoustic facies B and A. Table **??** shows details of the location, water depth and recovery for each core site. Cores were split on-board (see chapter 3) and split cores were logged according to the following characteristics: texture, grain size, lithology, structures, sorting and shear strength. As MSCL measurements were conducted on board the RRS James Cook immediately after coring, only the JC106 cores have been scanned using this method. X-radiographs from a selection of cores were used to image finer sedimentary detail and structures. Sedimentary logs were created for all of the sediment cores, and a series of lithofacies were identified.

Table2

Core name	Latitude	Longitude	Water depth	Recovery	MSCL Xray*	Location description
CE08-003	54.6415	-8.9324	88 m	512cm	N/Y	Layered sediments
CE08-004	54.6601	-9.0260	82 m	275cm	N/Y	Inshore DBM
CE08-005	54.6679	-9.0414	67 m	67.5cm	N/N	Moraine crest
CE08-008	54.7869	-9.3348	90 m	326cm	N/Y	Behind moraine
CE08-009	54.7891	-9.3428	90 m	75cm	N/N	Moraine crest
CE08-010	54.8316	-9.4233	97 m	578cm	N/Y	Trough of Moraine
CE08-011	54.8370	-9.4332	95 m	139cm	N/Y	Moraine crest
CE08-015	54.8403	-9.6179	97 m	275cm	N/Y	Trough, sediment wedge
CE08-017	54.8926	-9.6872	93 m	130cm	N/N	Moraine crest
CE08-018	54.9822	-9.9172	122 m	100cm	N/Y	Behind shelf edge moraine
JC106-093	54.564968	-8.986291	82 m	345cm	Y/N	Eastern flank of DBM
JC106-094	54.566811	-9.000824	76 m	65cm	Y/N	Eastern flank of DBM
JC106-095	54.570897	-9.030010	78 m	220cm	Y/Y	In crest of DBM
JC106-099	54.603632	-9.335645	99 m	476cm	Y/N	Topographic flat, mid shelf
JC106-100	54.604055	-9.341606	99 m	494cm	Y/Y	Topographic flat, mid shelf
JC106-101	54.613074	-9.420683	100 m	552cm	Y/Y	Topographic flat, mid shelf
JC106-102	54.623453	-9.518898	101 m	250cm	Y/N	Topographic flat, mid shelf
JC106-103	54.640625	-9.597222	102 m	147cm	Y/N	Topographic flat, mid shelf
JC106-104	54.673223	-9.687324	102 m	93cm	Y/N	Behind shelf edge moraine
JC106-105	54.68195	-9.7139667	108 m	574cm	Y/Y	Behind shelf edge moraine
JC106-106	54.686707	-9.727714	123 m	391cm	Y/Y	Behind shelf edge moraine
JC106-107	54.813056	-10.080486	117 m	120cm	Y/N	Shelf edge moraine

JC106-108	54.817046	-10.093455	120 m	42cm	Y/Y	Shelf edge moraine
JC106-110	54.828589	-10.130138	123 m	30cm	Y/N	Shelf edge moraine
JC106-111	54.828983	-10.131347	123 m	30cm	Y/N	Shelf edge moraine
JC106-112	54.845130	-10.181365	125 m	94cm	Y/Y	Shelf edge moraine
JC106-113	54.845694	-10.183001	N/A	20cm	Y/N	Shelf edge moraine

Table 4.2: Information on sediment cores used in this thesis. CE08 cores were collected on the Celtic Explorer in 2008. JC106 cores were collected on the James Cook, in 2014 *MSCL/X-ray Y=Yes N=No

4.5 Core descriptions

As described above, sediment cores were collected in two transects, one in the north and one in the south of the study area. The northern transect of cores were collected on the Celtic Explorer in 2008 (cores prefixed CE08) and the southern transect on the RRS James Cook in 2014 (cores prefixed JC106). Cores from the northern transect generally are shorter and tend to be characterised by more coarse grained sediments, while cores from the southern transect tend to have long successions of fine grained sediments. The core logs are presented from west to east, from the outer shelf, to the inner bay.

4.5.1 Outer shelf cores

Cores JC106-113, JC106-112, JC106-111, JC106-110, JC106-108, JC106-107 and CE08-018 were all collected on the outer shelf (Figures 3.4 and 4.1), either directly on, or in front of, the outer shelf moraine. The average water depth at the outer shelf moraine is 120 meters. Core logs for the seven cores are shown in figures 4.8 and 4.9.

JC106-113

Core JC106-113 is 0.2 meters long (Figure 4.8), and the shortest of the cores collected in the study area. It is the western-most core, collected on the western flank of the outer shelf moraine, ∼3 km from the shelf break (Figures 3.4 and 4.2),

20-10 cm (Guf): Matrix-supported gravel. Normal graded. Clasts are pebble size.

10-0 cm (Suf): Upwards fining coarse sand. Few clasts. Gradual uneven lower boundary.

JC106-112

Core JC106-112 has a length of 0.94 m, and was collected on the western flank of the outer shelf moraine, 120 m east of JC106-113 (Figures 4.2 and 3.4). The core consists of two lithofacies.

94-34 cm (Dmm): Massive matrix-supported diamicton with a matrix of silt and fine sand. Abundant clasts ranging in size from sub cm to few cm. Shear strength measurements increases down core, with measurements of 70 kPa at 40 cm, to 185-220 kPa towards the base of the core in 94 cm depth. .

34-0 cm (Gm): Clast-supported gravel. Matrix is coarse sand. Clast size range from 1 to 4 cm. Sharp lower boundary .

JC106-111

Core JC106-111 is 0.30 m long. It was collected on the western flank of the outer shelf moraine, ∼3.7 km east of core JC106-112 (Figures 4.2 and 3.4).

30-17 cm (Dmm): Massive matrix-supported firm diamicton with abundant clasts. Shear strength measurement in 25 cm depth, result in 87.5 kPa.

17-14 cm (Gms): Matrix-supported gravel, silty matrix. Sharp lower boundary.

14-0 cm (Gm): Clast-supported gravel. Matrix, where present, is coarse sand. A few shell fragments are present. Gradational lower boundary.

JC106-110

Core JC106-110 has a length of 0.3 m. It was collected ∼ 90 m up slope of core JC106-111 on the western flank of outer shelf moraine (Figures 4.2 and 3.4).

30-16 cm Fm/Dmm): Massive matrix-supported firm diamicton with few sub cm clasts. Shear strength decreases down core, from 75 kPa at 21 cm depth to 37.5 kPa at 29 cm depth.

16-14 cm (Fm): Massive silt with shell fragments. Mixing zone between overlying gravel and underlying silt. Sharp lower boundary.

14-8 cm (Sm): Very coarse sand with occasional clasts. Gradational lower boundary. (Sm).

8-0 cm: Coarse to very coarse sand, abundant shell fragments and clasts. Gradational lower boundary. (Sm/Gms).

JC106-108

Core JC106-108 is 0.42 m long. It was collected ∼ 2 km east of core JC106-110 on the western slope of the outer shelf moraine (Figures 4.2 and 3.4).

42-18 cm (Dmm): Massive matrix-supported firm diamicton with occasional clasts. Shear strength measurements range from 137 kPa to 140 kPa.

18-13 cm (Gms): Matrix-supported gravel. Matrix consists of silt. Mixing zone between overlying gravel, and underlying silt.

0-13 cm: Clast-supported gravel. No matrix present. Clast size ranges from sub cm to 3-4 cm long. Gradational lower boundary. (Gm).

JC106-107

Core JC106-107 is 1.2 m long. It was collected ∼950 m up slope of core JC106-108, on the western flank of the outer shelf moraine, (Figure 4.2). The entire core consists of one lithofacies.

120-0 cm (Gm): Clast-supported gravel. Clast size varies from sub-cm to pebbles, and occasional larger clasts. At the base no matrix is present, but from 50 cm depth and upwards, some muddy matrix is present. Shell fragments are scattered throughout.

CE08-018

Core CE08-018 is 1 m long. it is the northern most core described (Figure 3.4). The core is collected on the outer shelf moraine, and is dominated by coarse grained lithofacies.

100-70 cm (Sh): Fine sand with faint laminae of silt and clay. Few clasts are present.

70-65 cm (Gm): Clast-supported granule gravel. No matrix present. Some shell fragments. Sharp lower boundary.

65-50 cm (Sm): Massive medium sand, with abundant clasts. Gradational lower boundary.

50-43 cm (Sm): Massive medium to coarse sand, with some silt in the top of the unit. Sharp lower boundary.

43-37 cm (Fl): Silt with sandy lamina. Gradational lower boundary.

37-20 cm (Gms): Matrix-supported gravel, with small clasts. Matrix is coarse sand and shell fragments.

Whole shells present. Sharp lower boundary.

20-0 cm (Sm): Massive coarse sand containing shell fragments and whole shells. Occasional clasts present. Gradational lower boundary.

4.5.2 Mid shelf cores

From the mid-shelf basin between the DBM and the outer shelf moraine (Figure 3.4), fourteen cores were collected. From west to east these cores are labelled JC106-106, JC106-105, JC106-104, CE08-017, CE08-015, JC106-103, JC106-102, CE08-011, CE08-010, JC106-101, CE08-009, CE08-008, JC106-100 and JC106-099. Core logs are shown on figures 4.10, 4.11, 4.12, 4.13, 4.14 and 4.15. The average water depth in the area is approximately 100 m.

JC106-106

Core JC106-106 is 3.91 m long. It was collected immediately east of the outer shelf moraine (Figure 4.3) from the mid-shelf basin (Figure 3.4).

391-366 cm: Silt with a gradational upper boundary.

366-310 cm (Sm): Massive sand, with occasional clay laminae at 340 cm and 355 cm depth. Gradational lower boundary to silt.

310-282 cm (Fm): Massive clayey silt. Gradational lower boundary.

282-280 cm (Fm): Mixed clay and sand, gradational lower and upper boundary.

280-264 cm (Sh): Laminated fine to medium sand. X-rays reveal occasional bivalves.

264-260 cm (Fm): Massive silty sand.

260-228 cm (Sm): Medium structureless sand. Occasional clay lenses. Gradational lower boundary.

228-192 cm (Fl/Fm): Silt with lamina of clay. Laminated in top of unit that gradually fade away and unit becomes massive at the base.

192-162 cm (Suf/Sh): Upwards fining fine to very fine sand. X-ray reveals increased lamination towards the base, starting at 180 cm depth. Gradational lower boundary.

162-150 cm (Fm): Massive silt and clay. Sharp lower boundary.

150-141 cm (suc): Upwards coarsening very fine to medium sand. Gradational lower boundary.

141-134 cm (Fm): Massive clay rich silt. Sharp lower boundary.

134-110 cm (Sm): Massive fine sand. X-rays reveal a chaotic appearance that gradually disappears down through the unit. Gradational and uneven lower boundary.

110-104 cm (Fm): Massive clay. Sharp lower boundary.

104-97 cm (Sm): Massive very fine sand. Sharp lower boundary.

97-86 cm (Fl): Diffusely laminated silty clay with occasional shell fragments.

86-62 cm (Sm): Massive medium sand. X-rays reveal a single bi-valved shell. Gradational lower boundary.

62-49 cm (Fl): Laminated clay-rich silt. Sharp lower boundary.

49-24 cm (Gm): Clast-supported gravel. Very little matrix. Clast size varies from sub-cm. to 3-4 cm. Sharp lower boundary.

24-0 cm (Sm): Massive medium sand with a sharp lower boundary. On X-rays clasts from underlying facies are seen in the lower part of the unit.

JC106-105

Core JC106-105 has a length of 5.74 m, and is one of the longest cores collected in the study area. It was collected ∼1 km east of core JC106-106 on the outer part of the mid-shelf basin (Figures 4.3 and 3.4).

574-546 cm (Fl): Laminated clay with laminae of silt.

546-528 cm (Sh): Horizontally laminated sand. Sharp lower boundary.

528-514 cm (Fm): Massive silty clay. Gradational lower boundary.

514-512 cm (Sm): Massive sand.

512-492 cm (Fl): Laminated clay and silt. Silt becomes more dominant at the top of the unit. X-ray reveals paired bivalve at 504 cm depth. Sharp lower boundary.

492-487 cm (Sh): Laminated sand. Sharp upper and lower boundary

487-449 cm (Fm/Fl): Clay with some silt and sand mixed in. On x-ray the silt and sand have a horizontal laminated appearance.

449-444 cm (Sh): Massive sand, on x-rays faint lamination is revealed. Sharp upper and lower boundaries

444-303 cm (Fm): Mixed unit of silt and clay, becoming more massive from 380-444 cm depth. X-rays reveals shell at 342 cm depth. The unit contains an interbed of massive sand at 330 cm depth.

303-262 cm (Suc): Upwards coarsening sand, with occasional shell fragments. X-ray reveals paired bivalved shells, and sharp uneven lower boundary.

262-233 cm (Fm): Silt, coarsening upwards towards the top. X-rays reveal uneven layers of clay.

233-228 cm (Fm): Massive clay, sharp but uneven boundaries.

228-219 cm (Sm): Massive fine sand with occasional single valves. Sharp but uneven boundaries.

219-187 cm (Sh/Fl): Fine sand, with clay beds at 190 cm, 205 cm and 217 cm depth.

187-170 cm (Fm): Massive clay and silt. Sharp lower boundary.

170-161 cm (Sh): Laminated sand, sharp but uneven lower boundary.

161-148 cm (Fm): Structureless clayey silt. Sharp lower boundary.

148-139 cm (Sh): Laminated sand. Gradational lower boundary.

139-119 cm (Fm): Structureless clayey silt. The unit becomes sandier towards the base. Gradational lower boundary.

119-113 cm (Sh): Faintly laminated fine sand.

113-92 cm (Fm): Massive clayey silt. Sharp lower boundary.

92-77 cm (Sh): Laminated fine sand. Gradational lower boundary.

77-73 cm (Fm): Massive silt. Sharp lower boundary.

73-66 cm (Suc): Upwards coarsening fine sand. Gradational lower boundary.

66-50 cm (Fm): Massive clayey silt with some sand. Gradational lower boundary.

50-40 cm (Sh): Fine sand with a horizontal bed of clay at 45 cm depth. X-rays reveal faint horizontal lamination in the sand. Gradational lower boundary.

40-10 cm (Fm): Chaotic and structureless clayey silt with some sand and occasional clasts. Sharp lower boundary.

10-0 cm (Gm): Clast-supported gravel, with a muddy matrix. Erosional lower boundary.

JC106-104

Core JC106-104 is 0.93 m long. It was collected ∼2 km east of core JC106-105, on the outer part of the mid-shelf basin (Figures 4.3 and 3.4).

93-89 cm (Sh): Laminated sand with silt laminae.

89-71 cm (Sm): Massive fine sand. Gradational lower boundary.

71-65 cm (Fm): Massive clay. Sharp lower boundary.

65-55 cm (Sm): Massive fine sand. Uneven lower boundary.

55-0 cm (Gm): Clast-supported granule gravel. clasts are well rounded. No matrix. Some large shell fragments and whole valves are present. Sharp erosion lower boundary.

CE08-017

Core CE08-017 is 1.30 m long. It is one of the western-most cores collected in the mid-shelf basin (Figure 3.4). The core is collected on the western side of a moraine crest.

130-30 cm (Guf): Upwards fining clast-supported gravel that grades from cobbles and large pebbles through to granules and very coarse sand.

30-0 cm (Suf): Upwards fining coarse to medium sand. Abundant small clasts and shell fragments. Sharp lower boundary.

CE08-015

Core CE08-015 is 2.75 m long. It was collected in a trough between two moraines (Figure 3.4).

275-190 cm (Sm): Massive medium to fine sand. Increasing abundance of clasts towards the top.

190-174 cm: Gap in core- no sediment.

174-168 cm (Gm): Granulated, well sorted, clast-supported gravel. Rounded clasts with little matrix.

168-166 cm (Sm): Massive sand. Sharp upper and lower boundaries

166-100 cm (Guc): Matrix-supported gravel. Inversely graded. Poorly-sorted matrix consisting of clay, silt and sand with occasional shell fragments.

100-99 cm (Fl): Laminated silt. Sharp upper and lower boundaries.

99-82 cm (Suf/Sh): Upwards fining medium to fine sand. Faint lamination. Sharp lower boundary.

82-72 cm: Gap in core- no sediment.

72-20 cm (Sm): Massive medium to fine sand. Occasional shell fragments.

20-0 cm: Gap in core - no sediment.

JC106-103

Core JC106-103 is 1.47 m long. It was collected ∼7 km east of core JC106-104 (Figures 4.3 and 3.4).

147-90 cm (Suf/Sm): Massive fine to medium sand. Two beds of silt at 110 cm and 122 cm depth. The upper 5 cm of the massive sand (from 95 to 90 cm depth) fines upwards to very fine sand and silt.

90-80 cm (Suf/Fm): Upwards fining sand to clay.

80-66 cm (Fm): Massive clay.

66-0 cm (Suf): Upwards fining medium to fine sand. Abundant singular valves and shell fragments increasing down core.

JC106-102

Core JC106-102 is 2.5 m long. It was collected ∼5.5 km east of core JC106-103, from the mid-shelf basin (Figures 4.3 and 3.4).

250-76 cm (Fl): Laminated clay with laminae of fine sand. 1 cm thick beds of fine to medium sand are found at 100 cm, 130 cm, 200 cm 210 cm 242 cm and 249 cm depth.

76-47 cm (Fl): Clay and silt with inter bedded sand becomming progressively sandier towards the top. Gradational lower boundary.

47-40 cm (Fm): Massive clay. Sharp lower boundary.

40-27 cm (Sh): Laminated medium sand, with clay laminae. Gradational lower boundary.

27-17 cm (Fm): Massive silt. Sharp boundary.

17-10 cm (Sm): Massive sand, fine to medium. Sharp lower boundary.

10-0 cm (Fm): Massive silt with. Sharp lower boundary.

CE08-011

Core CE08-011 is 1.39 m long. It was collected on a moraine crest (Figure 3.4). 139-25 cm (Dmm): Massive matrix-supported diamicton. the diamicton is soft in the top, but firm further down. Abundant in clasts. (Dmm).

25-20 cm (Sm): Massive coarse sand. Sharp lower boundary.

20-12 cm Gm): Poorly sorted clast-supported gravel. Matrix is coarse sand. Sharp lower boundary.

12-8 cm (Gms): Matrix-supported gravel. Clasts are pebble size. Matrix of coarse sand. Sharp lower boundary. (Gms)

8-0 cm (Suf): Upwards fining coarse to medium sand. Sharp lower boundary.

CE08-010

Core CE08-010 is 5.78 m long, and the longest of the mid shelf cores. It was collected from a trough between two moraines (Figure 3.4).

578-550 cm (Dmm): Massive matrix-supported diamicton. Matrix consists of very firm silt and clay. Abundant clasts.

550-535 cm (Suf): Upwards fining fine to very fine sand. Occasional clasts.

535-520 cm (Suc): Upwards coarsening poorly sorted mix of silt and sand. Occasional clasts.

520-506 cm (Sm): Massive fine sand. Occasional clasts.

506-492 cm (Fm): Massive clay and silt.

492-479 cm (Suf): Upwards fining coarse to fine sand.

479-475 cm (Suc): Upwards coarsening fine to coarse sand. Gradual lower boundary.

475-460 cm (Suf): Upwards fining medium to very fine sand. Occasional large clasts and small shell fragments present. Sharp lower boundary.

460-453 cm (Fm): Soft massive clay.

453-447 cm (Sm): Massive fine sand. Occasional small clasts. Sharp lower boundary.

447-380 cm (Fm): Massive silt. sharp lower boundary.

380-370 cm (Sm): Medium sand, with occasional clsts. Sharp uneven lower boundary.

370-345 cm (Fm): Massive silt. Sharp lower boundary.

345-290 cm (Gms): Matrix-supported gravel. Matrix consists of coarse sand. Some shell fragments present. Sharp uneven boundary.

290-280 cm (Fm): Massive clay and fine silt. Sharp uneven lower boundary.

280-270 cm (Sm): Fine to medium sand, Lenses of silt are present. Sharp lower boundary.

270-230 cm (Fm): Massive clay. Sharp uneven lower boundary.

230-210 cm (Suf): Upwards fining medium to fine sand, well sorted, few clasts. Sharp lower boundary.

210-190 cm (Fm): Massive clay. One lamina of fine sand at 201 cm. Large clast at 190 cm. Sharp lower boundary.

190-182 cm: Gap in core -no sediment.

182-177 cm (Sh): Laminated fine sand, with lamina of medium sand in 177 cm. Occasional shell fragments. (Sh).

177-170 cm (Fm): Soft massive silt. Gradational lower boundary.

170-162 cm (Sh): Laminated fine sand with small shell fragments. Gradational lower boundary.

162-155 cm (Suc): Upwards coarsening fine to medium sand. One lamina of silt. Occasional shell fragments and clasts around 155-160 cm. Sharp lower boundary.

155-150 cm (Fl): Clay, with laminae of fine sand. Sharp lower boundary.

150-135 cm (Guc): Matrix-supported inversely graded, gravel. Matrix consists of silt and clay. Sharp lower boundary.

135-55 cm (Gm): Clast-supported gravel with local silty clay matrix. Abundant shell fragments. Sharp lower boundary.

55-22 cm (Gms): Matrix-supported gravel. Matrix consists of granulated sand, with increase of silt and clay towards the base. Gradational lower boundary.

22-12 cm (Gm): Clast-supported gravel with some matrix of coarse sand. Gradational lower boundary.

12-0 cm (Sm): Very coarse massive sand, occasional shell fragments and whole shells. Gradational lower boundary.

JC106-101

Core JC-106-101 is 5.55 m long. It was collected ∼6.5 km east of core JC106-102, from the mid-shelf basin (Figures 3.4 and 4.3).

555-88 cm (Fl): Clay with horizontal laminae of silt and fine sand. Occasional bedding from 88 cm to 300 cm depth.

88-12 cm (Fmd): Massive clay and silt, with abundant clasts. Shear strength increase downwards, from 40 kPa at 30 cm depth, to 62.5 kPa at 80 cm depth. X-ray reveals sharp lower boundary.

12-0 cm (Gm): Clast-supported gravel, clast size ($\leq$1 cm). Shell fragments are present. Sharp lower boundary.

CE08-009

Core CE08-009 is 0.75 m long. It was collected at a moraine crest (Figure 3.4). It consists of two lithofacies.

75-52 cm (Guf): Upwards fining clast-supported gravel.

52-0 cm (Sm): Massive very coarse sand with some shell fragments and clasts. Gradational lower boundary.

CE08-008

Core CE08-008 is 3.26 m long, and was collected ∼0.5 km south-west of core CE08-009, behind a moraine (Figure 3.4). It consists of three lithofacies.

326-115 cm (Dmm): Massive matrix-supported diamicton. Matrix gets increasingly firmer down core. Abundant in clasts.

115-10 cm (Guf): Normally graded clast-supported gravel. Some shell fragments. Sharp lower boundary.

10-0 cm (Sm): Medium to coarse sand, abundant sub cm clasts, poorly sorted. Sharp lower boundary.

JC106-100

Core JC106-100 is 4.94 m long. It was collected from the mid-shelf basin, in a topographically flat area, ∼5 km east of core JC106-101 (Figure 4.3).

494-310 cm (Fmd): Massive clay, abundant clasts. Shear strength measurements gives values of 25 to 37.5 kPa.

310-83 cm (Fl): Clay with laminae of silt and fine sand. Very few clasts present. Sharp lower boundary.

83-74 cm (Gm): Clast-supported gravel. Very little matrix, clast size ¿1 cm. Sharp lower boundary.

74-66 cm: Matrix-supported gravel, clast size ¿1 cm. Sharp lower boundary. (Gms).

66-36 cm (Sh): Sand with faint lamination. Sharp lower boundary.

36-0 cm (Suf): Upwards fining coarse to medium sand with abundant shell fragments. Sharp lower boundary.

JC106-099

Core JC106-099 have a length of 4.76 m. It was collected on the topographically flat area of the mid-shelf basin, ∼0.4 km east of JC106-099, (Figures 4.3 and 3.4).

476-435 cm (Fl): Inter-bedded silts and clays. Individual beds are 5-10 cm thick.

435-32 cm (Fl): Clay with silt laminae. Sharp lower boundary.

23-21 cm (Gms): Matrix-supported gravel. Sharp lower boundary.

21-7 cm (Fl: Clay with lamina of silt. Sharp lower boundary.

7-0 cm (Gm): Clast-supported gravel. Sharp lower boundary.

4.5.3 Inner bay cores

Cores CE08-005, JC106-095, CE08-004, CE08-003, JC106-093 and JC106-094 were all collected from the inner bay basin, east of, or directly on top of the eastern ridge of the DBM. A common feature of all these cores, with the exception of core JC106-095, is the dominance of sandy facies especially in the upper parts of the cores. Core logs for the cores collected in the inner bay basin can be seen on figures 4.16 and 4.17.

CE08-005

Core CE08-005 is 0.67 m long and was collected on the crest o the DBM (Figure 3.4). It consists of two lithofacies, with no clear boundary in between.

67-0 cm (Guf): Normal graded clast supported gravel fining upwards into more matrix-supported gravel above 33 cm depth.

JC106-095

Core JC106-095 has a length of 2.2 m. It was collected from the top of the DBM, (Figures 4.4 and 3.4).

220-214 cm (Fm): Massive clay.

214-133 cm (Fl): Silt with clay beds at 145 cm and 170 cm depth. Rare clasts.

133-131 cm (Sm): Massive sand. Sharp lower boundary.

131-115 cm (Fl): Laminated silt and clay. Gradational lower boundary.

115-56 cm (Fm): Clay and silt, with horizontal beds of fine sand at 80 cm, 93 cm and 110 cm depth. Gradationall lower boundary.

56-54 cm (Sm): Bedding of fine sand. Sharp lower boundary.

54-49 cm (Fm): Massive clay. Sharp lower boundary.

49-32 cm (Suf): Upwards fining, very fine sand to silt. Gradational lower boundary.

32-0 cm (Guc): Inversely graded, clast-supported gravel. Sharp lower boundary.

CE08-004

Core CE08-004 is 2.75 m long, and was collected just inshore of the DBM (Figure 3.4).

275-236 cm (Fl): Sandy silt with clay laminae. Occasional clasts present.

236-220 cm (Gm): Clast-supported gravel. Occasional shell fragments. Sharp lower boundary. (Gm)

220-198 cm (Sm): Massive coarse sand. Occasional clasts, increasing in abundance down core. Sharp lower boundary.

198-135 cm (Gm): Clast-supported gravel with poorly sorted pebbles. Sandy matrix locally present. Sharp lower boundary.

135-0 cm (Sm): Massive coarse sand. Occasional shell fragments and small clasts. Increasing abundance of clasts down core. Gradational lower boundary.

JC106-094

Core JC106-094 is 0.65 m long and was collected ∼2 km east of core JC106-095, on the eastern flank of the DBM (Figure 4.4).

65-0 cm (Sm): Massive medium sand. From 0 to 25 cm, three large clasts are present. Abundant clast from 55 cm to 65 cm depth. (Sm).

JC106-093

Core nr. JC106-093 is 3.45 m long, and was collected ∼1 km east of core JC106-094, also on the eastern flank of the DBM (Figures 4.4 and 3.4). 345-90 cm (Sm): Massive fine to medium sand. Occasional shell fragments present.

90-15 cm (Suf): Upwards fining medium to fine sand.

15-0 cm (Gms): Matrix supported gravel. Matrix consists of coarse sand. Uneven lower boundary due to large clasts.

CE08-003

Core CE08-003 is the eastern-most core (Figure 3.4), and with a length of 5.12 m the longest of the cores collected in the inner bay basin.

512-505 cm (Fl): Silt with laminae of clay.

505-490 cm (Fl): Silt with clay laminae. Sharp lower boundary.

490-450 cm (Fl): Silt with a lamina of fine sand at 470 cm. Gradational lower boundary.

450-440 cm (Sm): Massive fine sand. Sharp uneven lower boundary.

440-430 cm (Fl): Laminated silty clay. Sharp lower boundary.

430-410 cm (suf): Upwards fining, fine sand with laminae of silt towards the top. Shell fragments along lower boundary. Sharp lower boundary.

410-375 cm (Fl): Silt with fine sand laminae. Gradational lower boundary.

375-230 cm (Sm): Fine massive sand. Abundant shell fragments throughout. Gradational lower boundary.

230-215 cm: Gap in core- no sediment.

215-140 cm (Sm): Fine massive sand. Abundant shell fragments.

140-116 cm: Gap in core- no sediment.

116-40 cm (Suf): Upwards fining, fine to very fine sand. Occasional shell fragments. Abundant shell fragments present along lower boundary.

40-25 cm: Gap in core- no sediment.

25-10 cm (Sm): Massive very fine to fine sand, occasional shell fragments.

10-0 cm: Gap in core- no sediment.

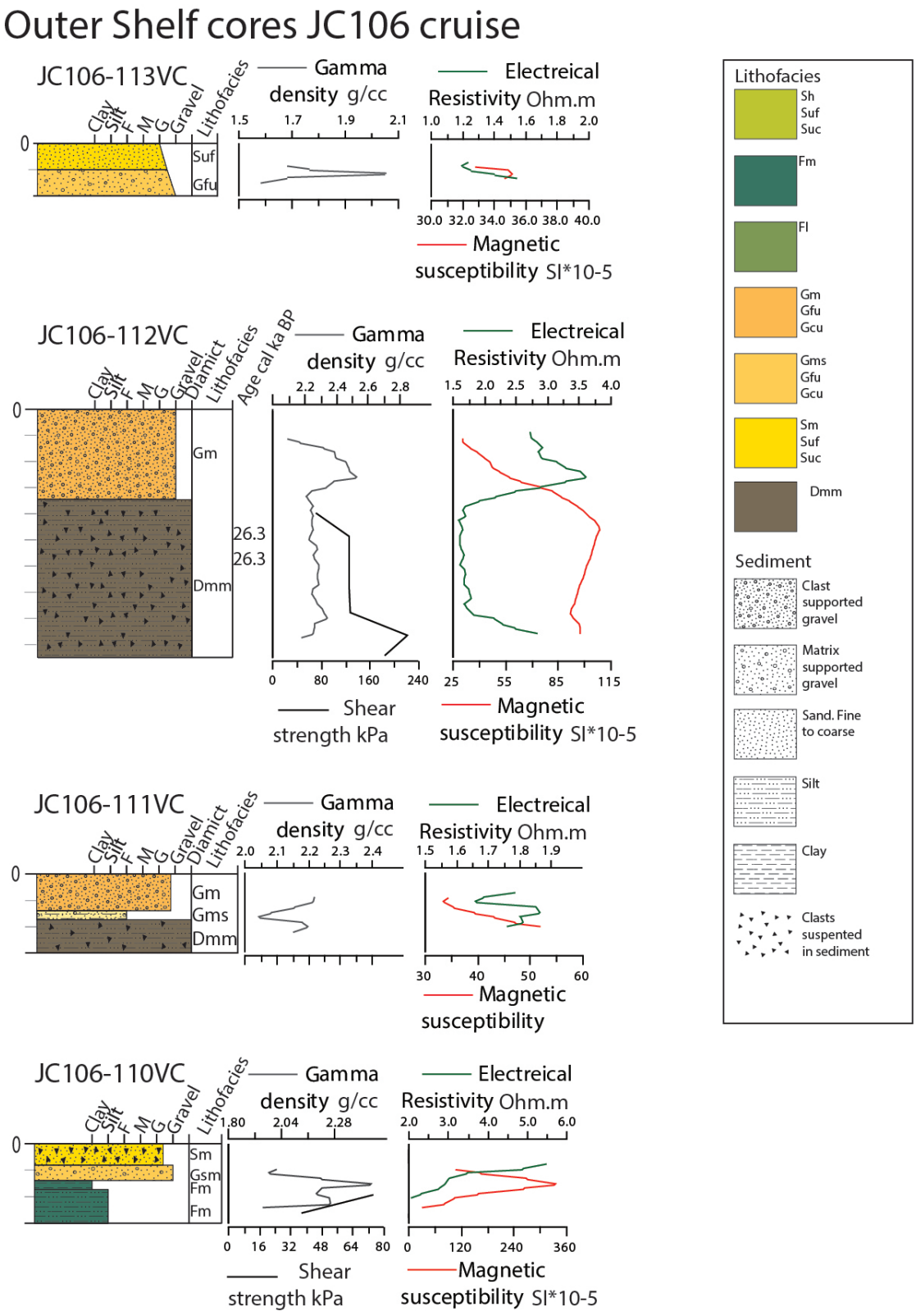

Figure 4.8: Core logs from the outer shelf, with MSCL data from the JC106 cores.

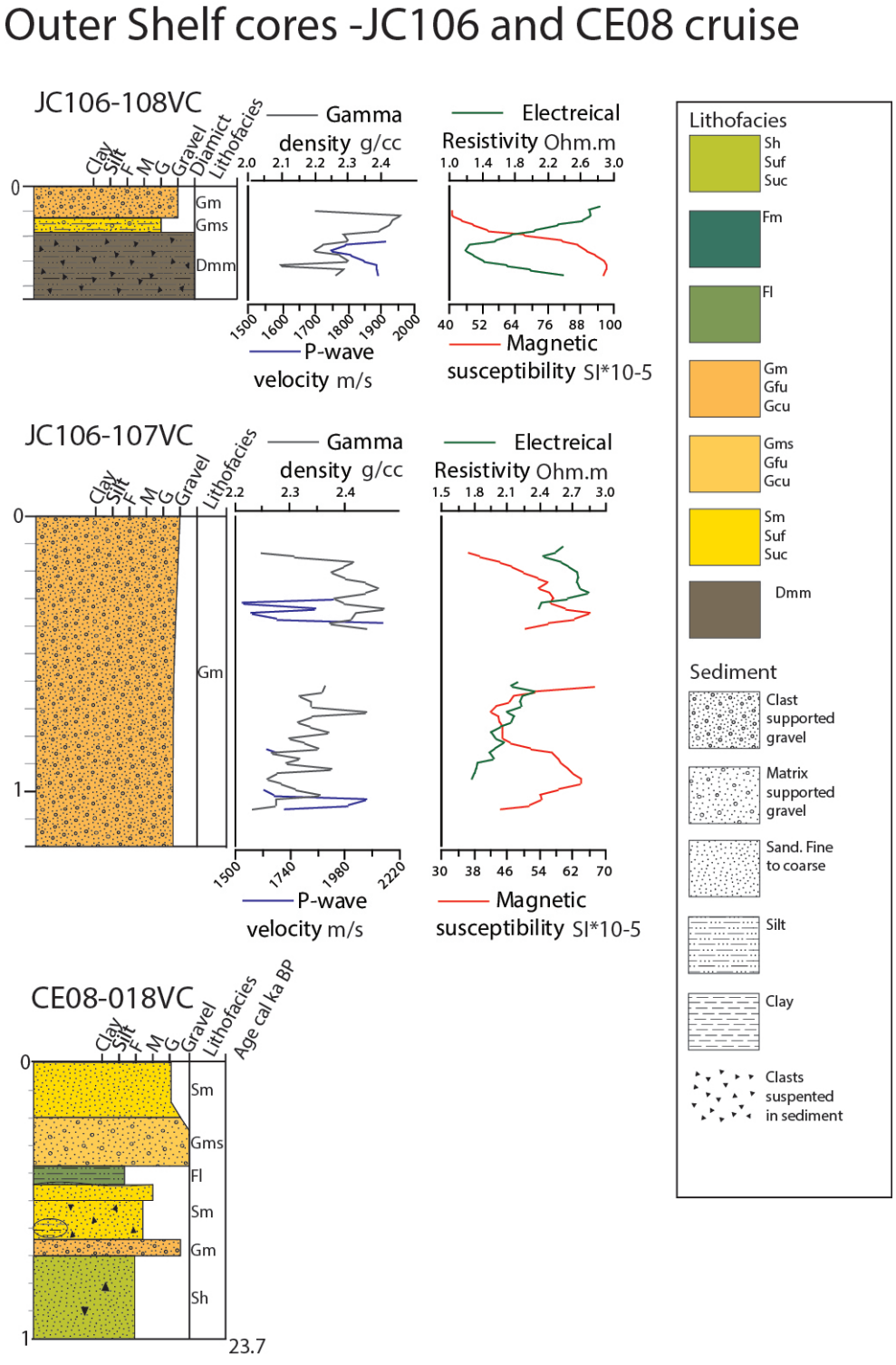

Figure 4.9: Core logs from the outer shelf, with MSCL data from the JC106 cores.

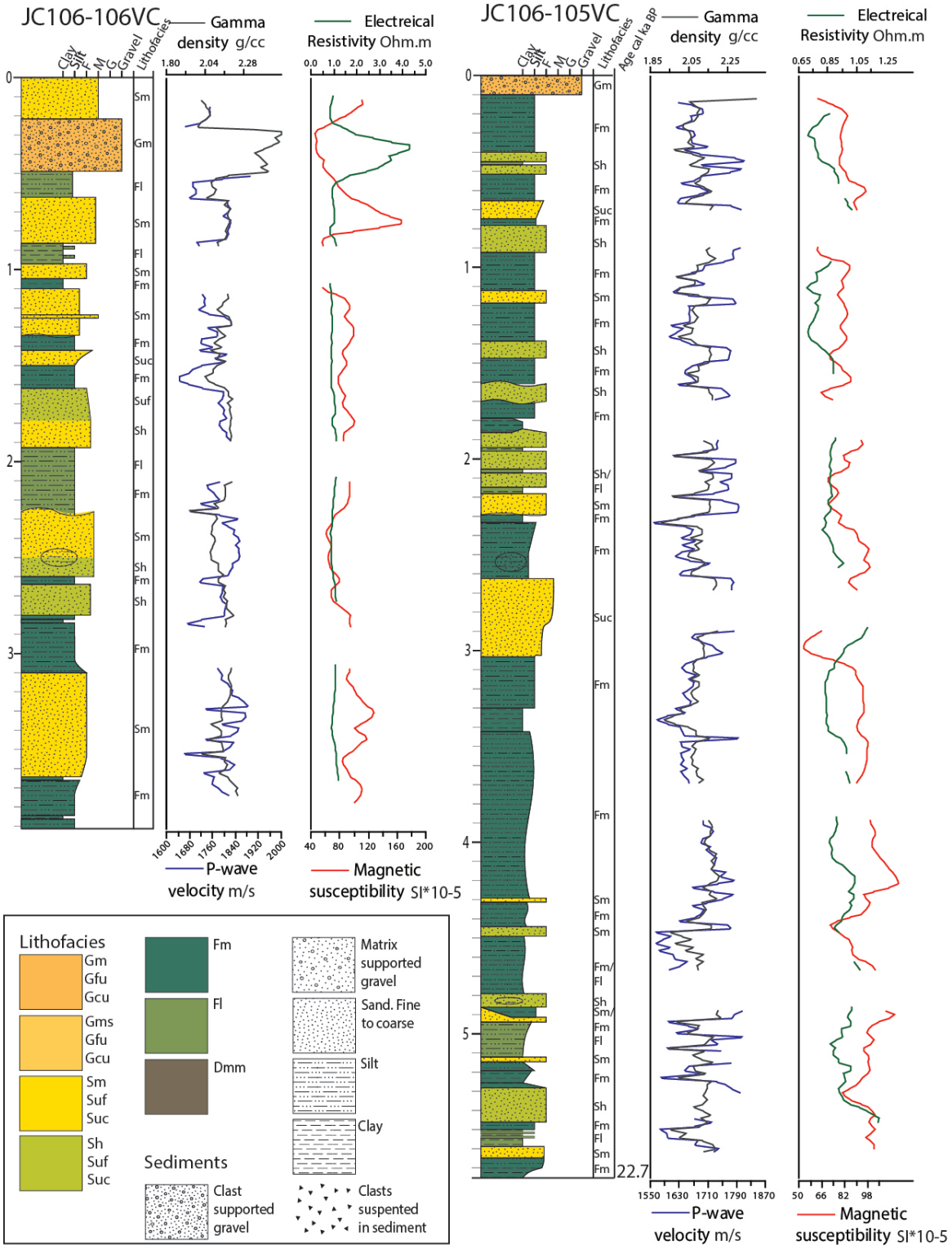

Figure 4.10: Core logs of the cores JC106-106 and JC106-105 with MSCL data.

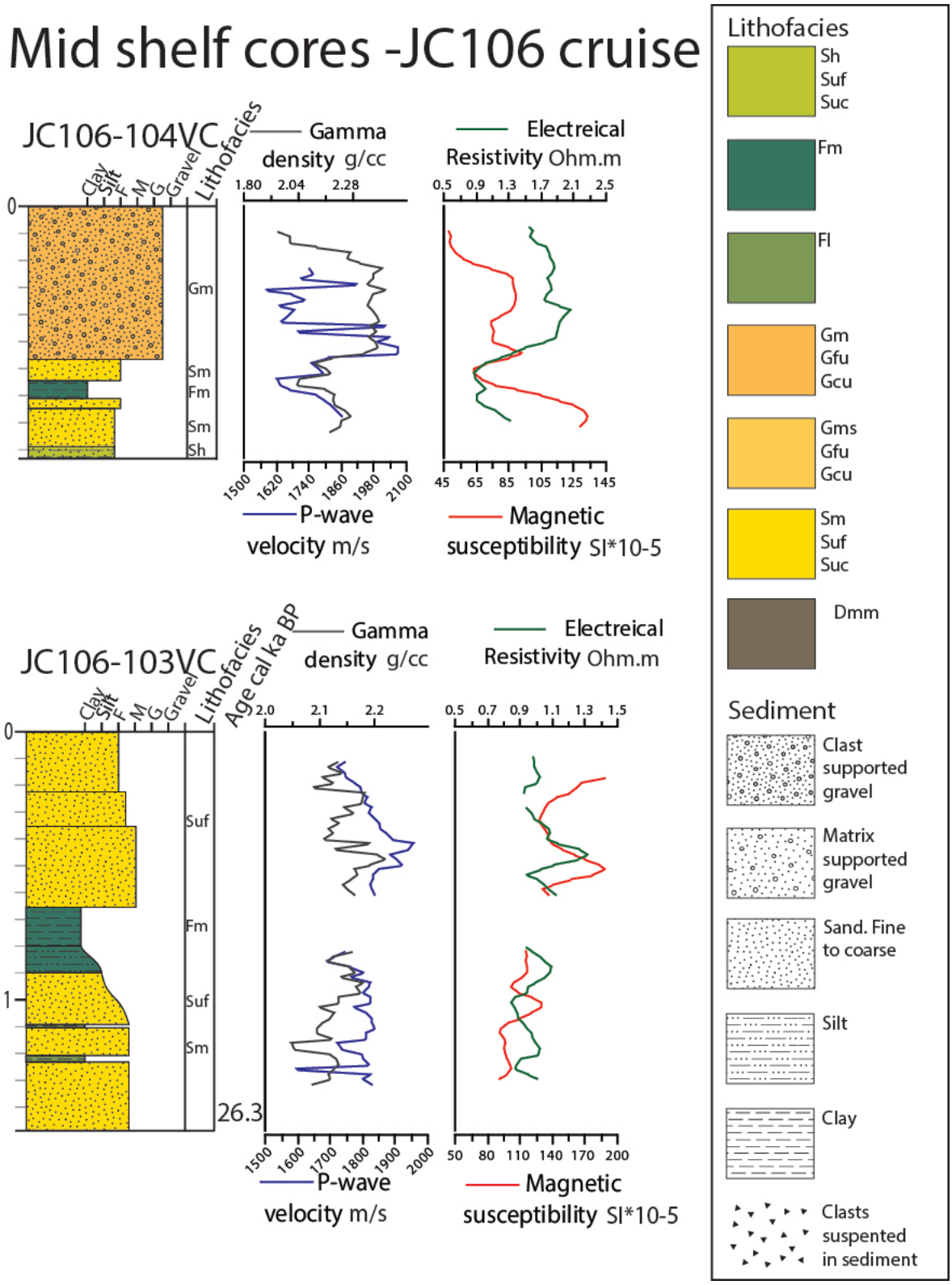

Figure 4.11: Core logs of the cores JC106-104 and JC106-103 with MSCL data.

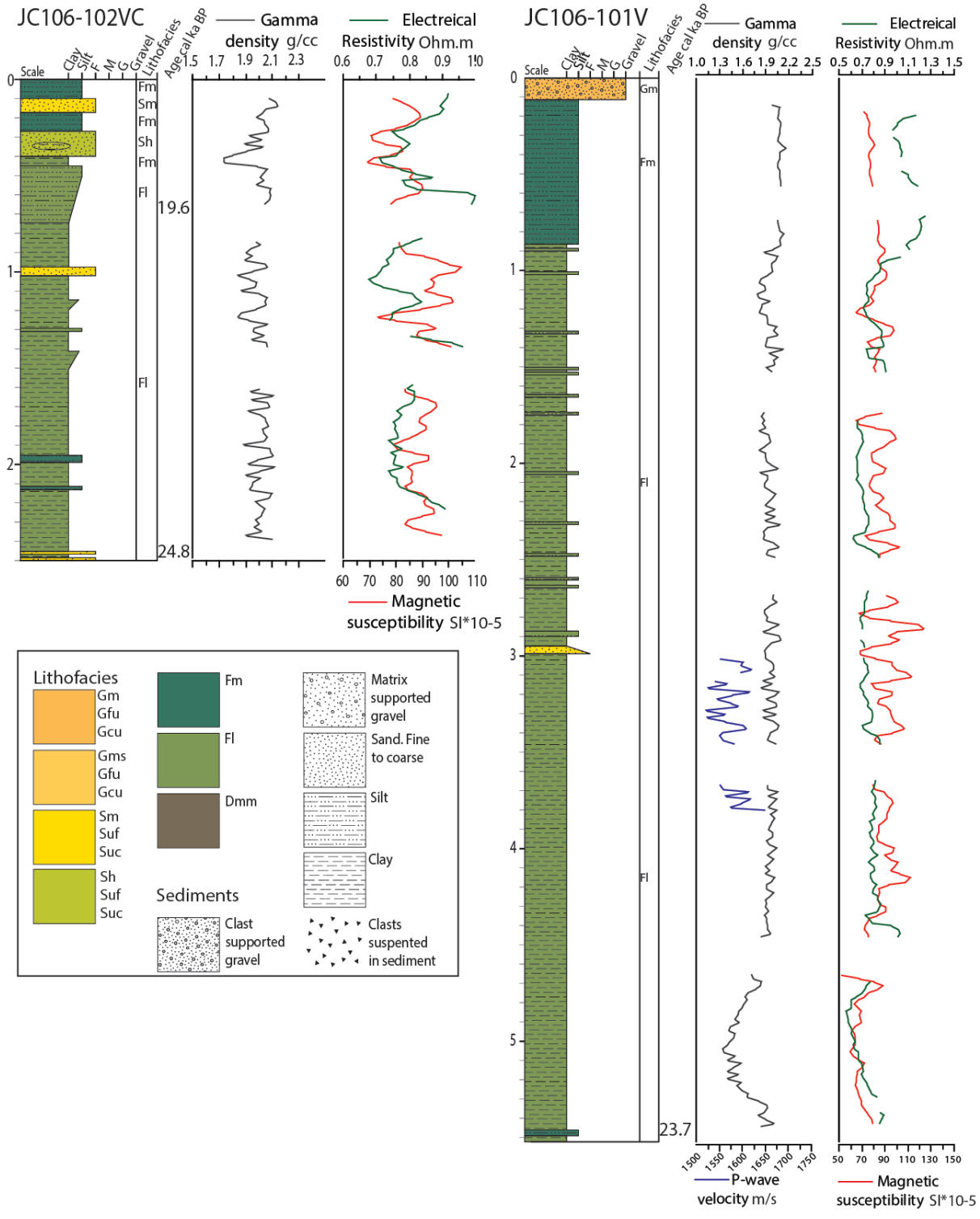

Figure 4.12: Core logs of the cores JC106-102 and JC106-101 with MSCL data.

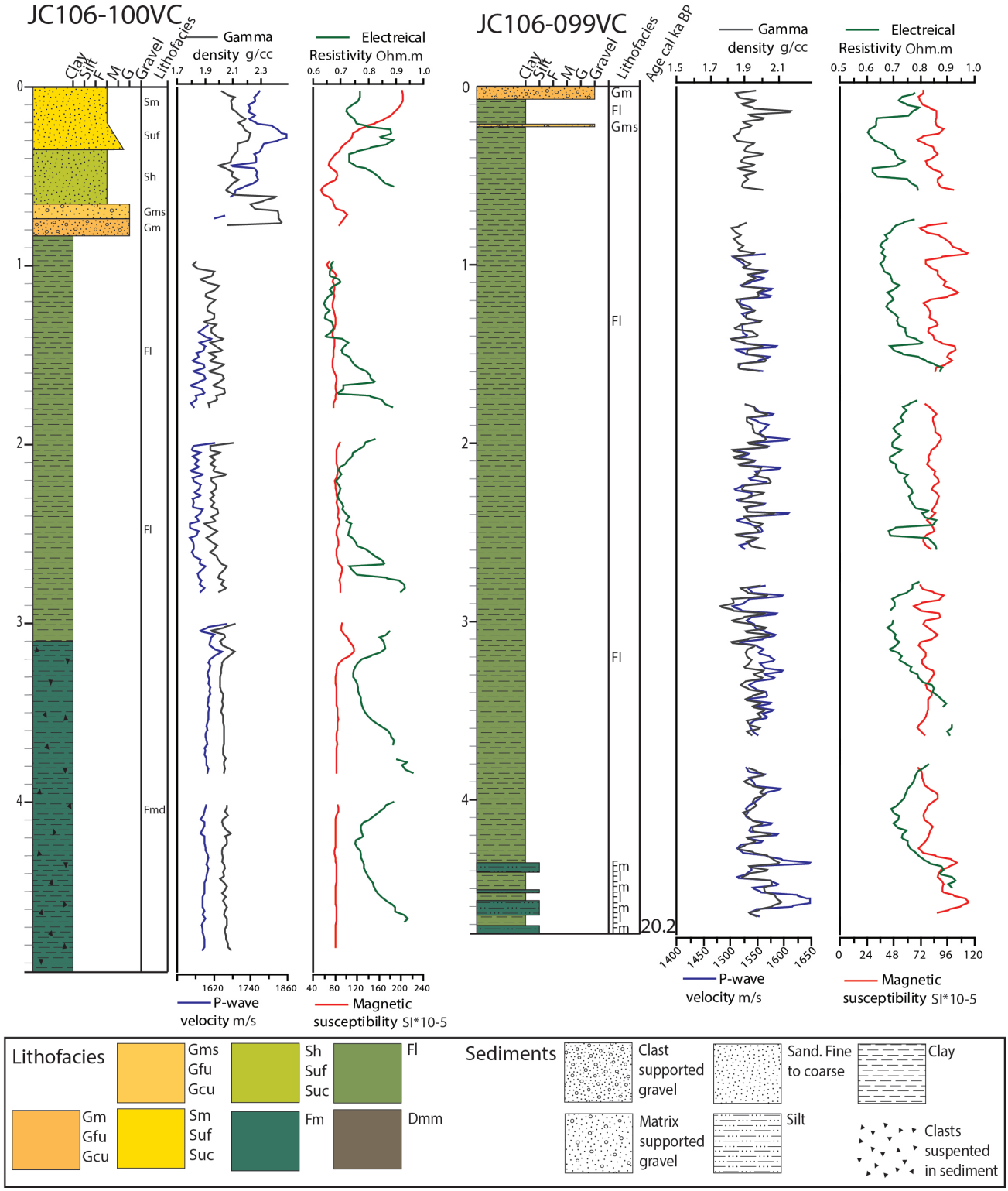

Figure 4.13: Core logs of the cores JC106-100 and JC106-99 with MSCL data.

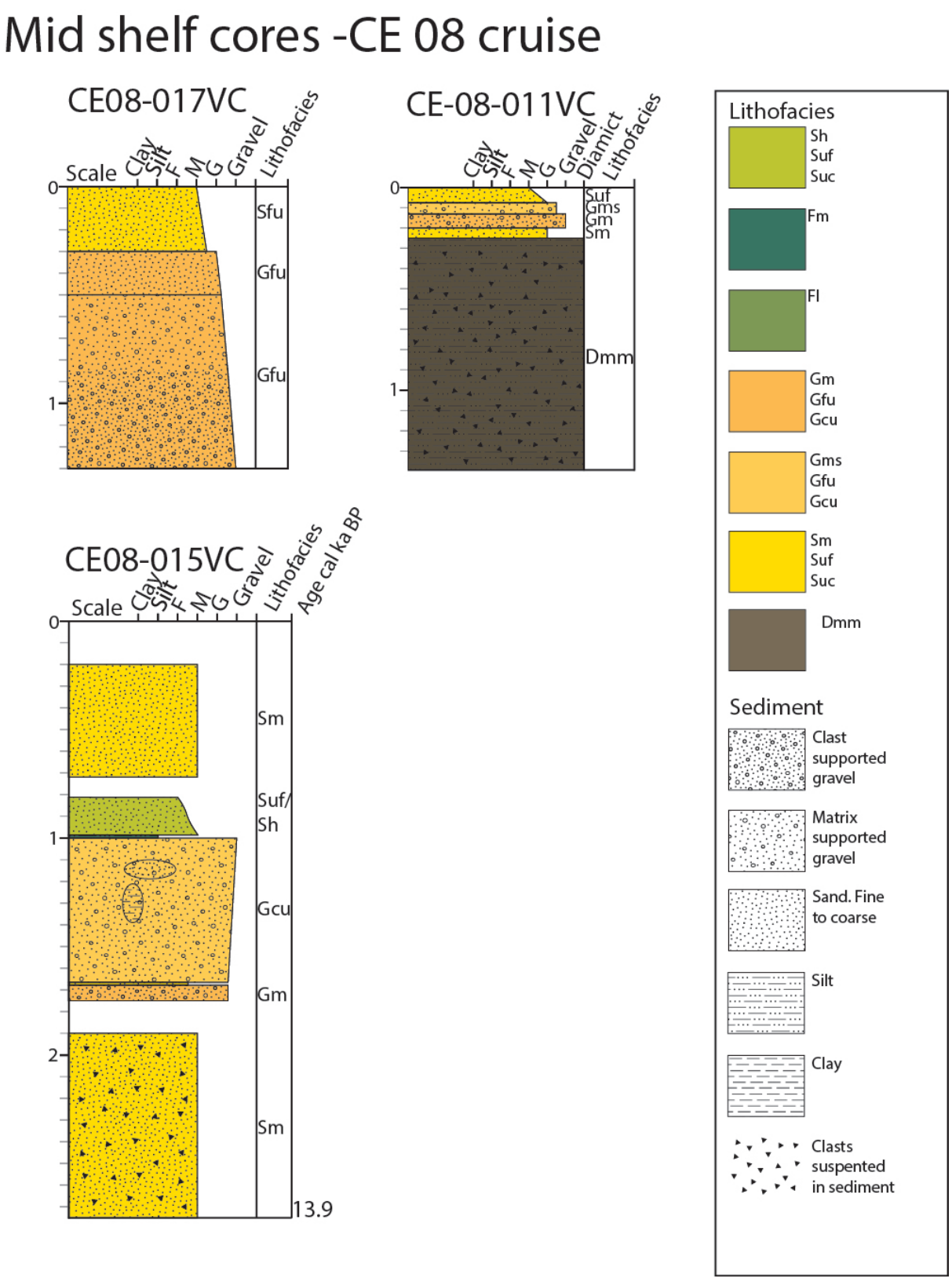

Figure 4.14: Core logs of the cores CE08-017, CE08-015 and CE08-011.

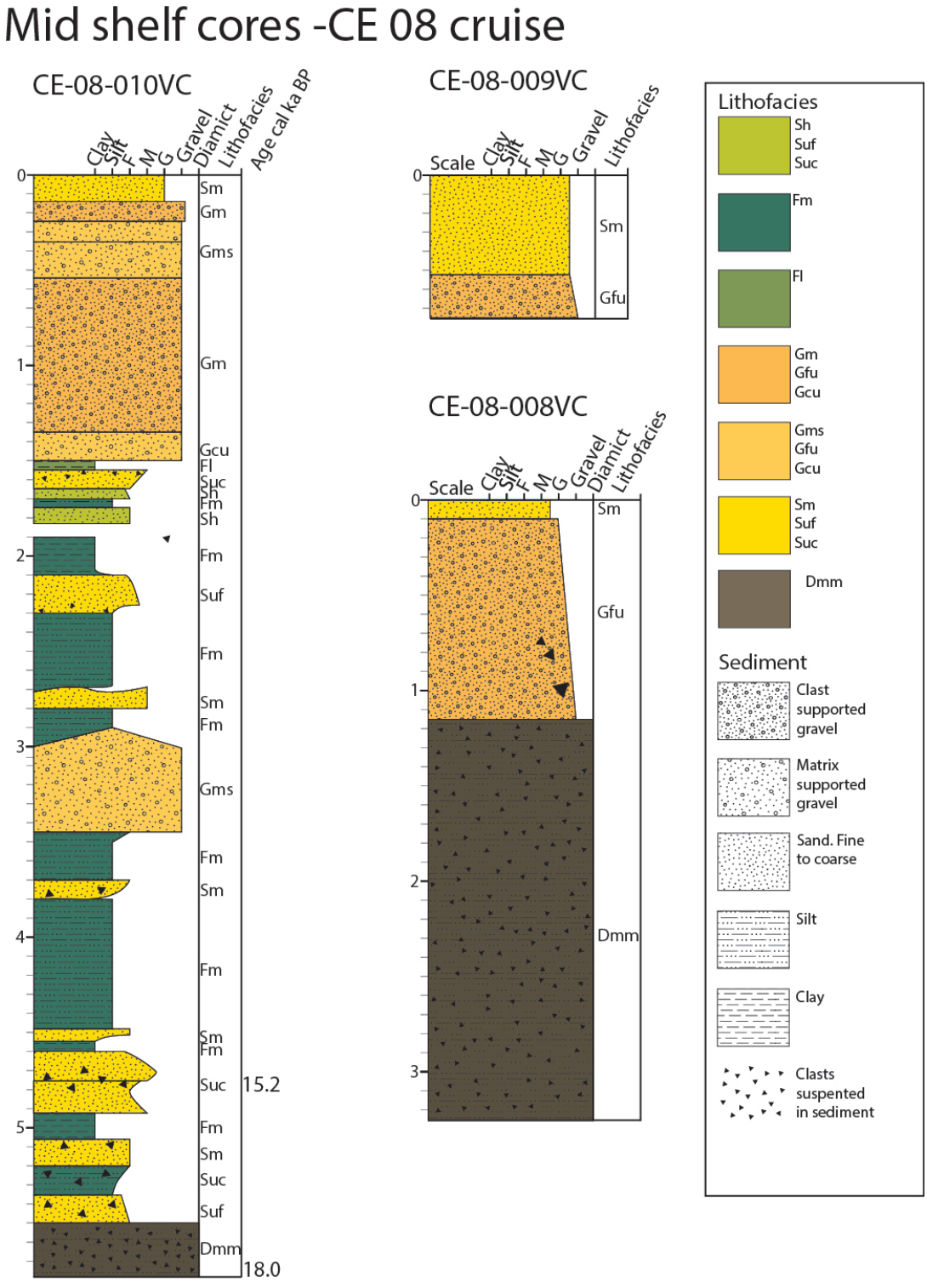

Figure 4.15: Core logs of the cores CE08-010, CE08-009 and CE08-008.

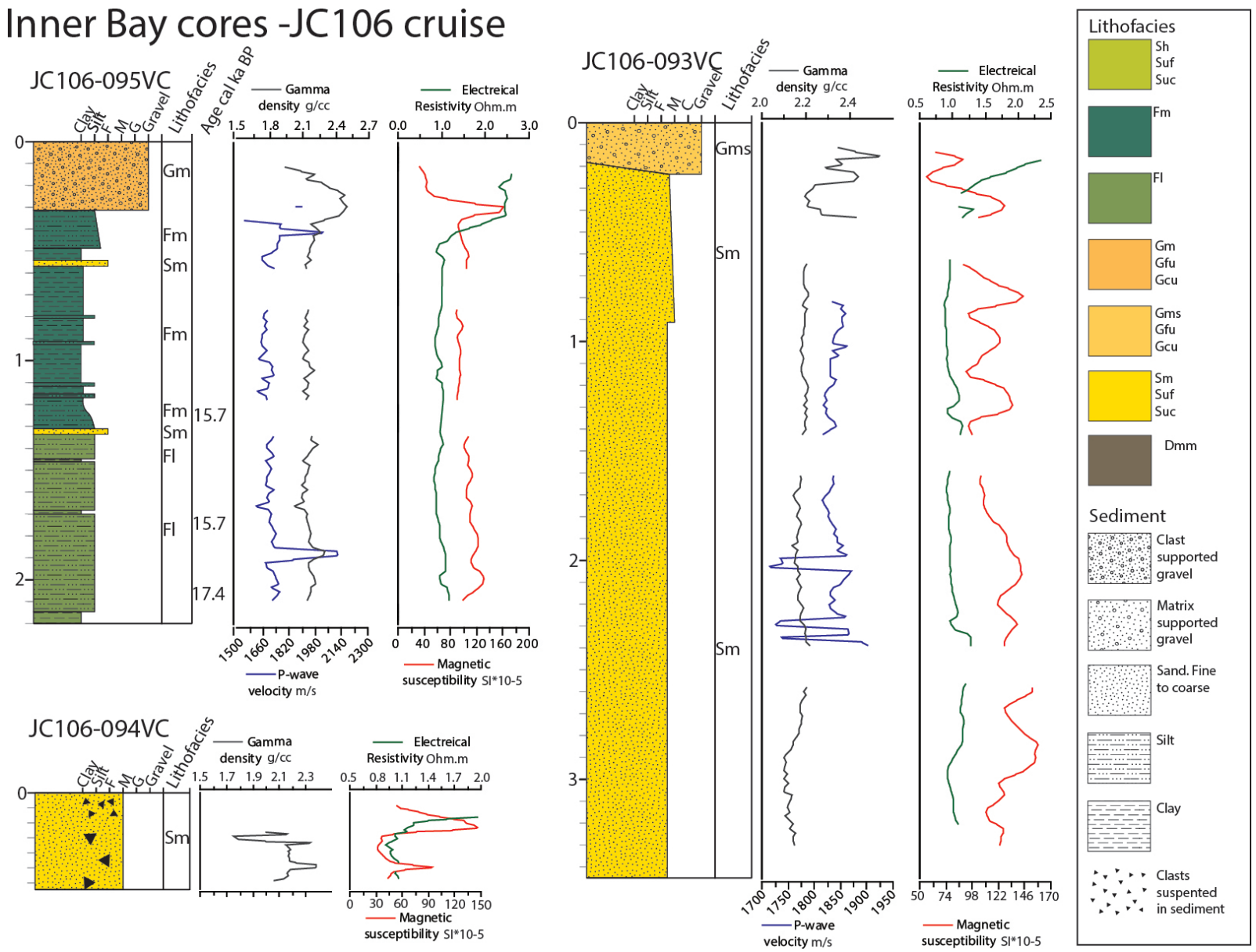

Figure 4.16: Core logs with MSCL data from the inner bay basin, on and east of the DBM, collected on the JC106 cruise.

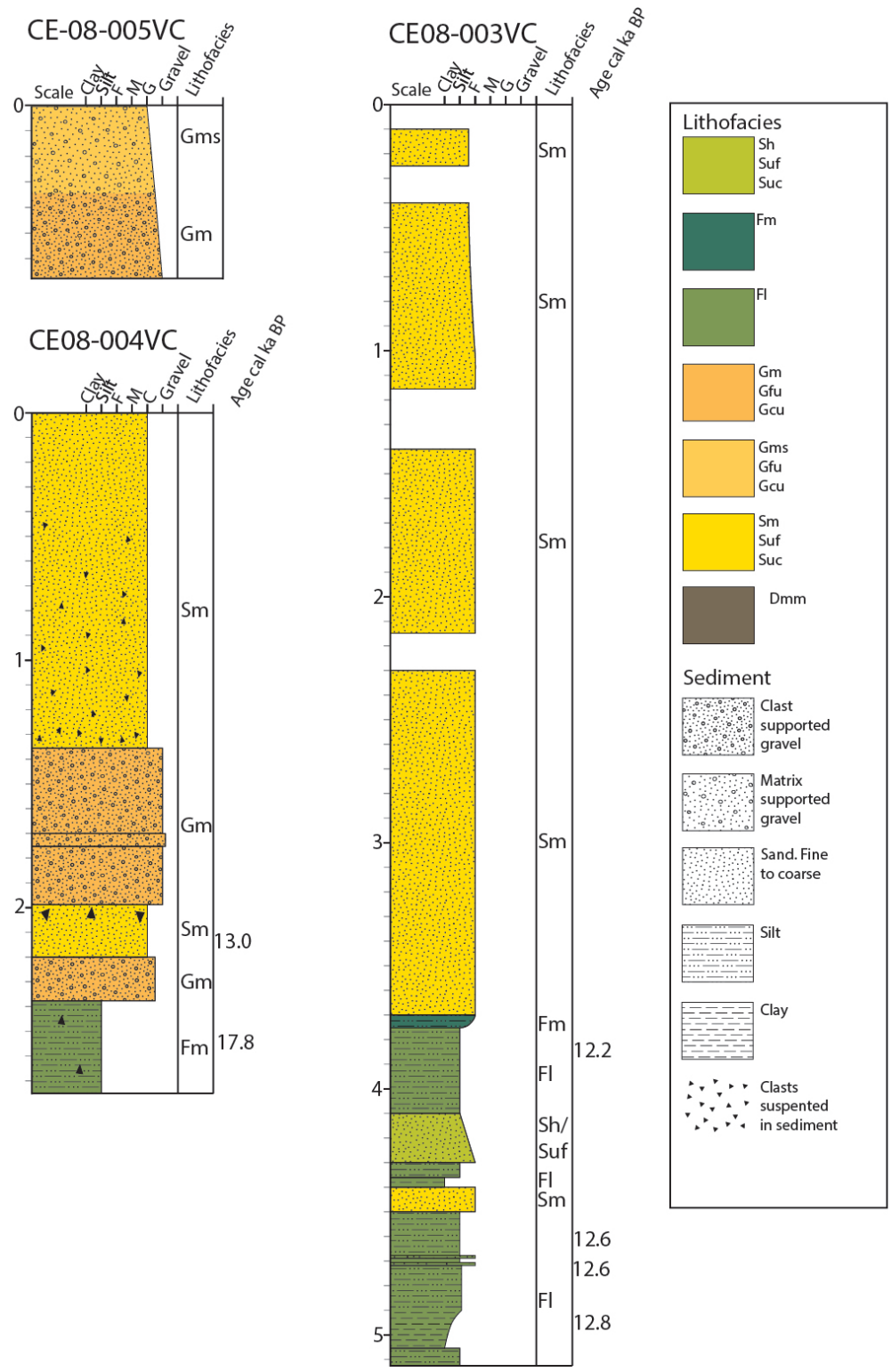

Figure 4.17: Core logs from the inner bay basin, on or east of the DBM, collected on the CE08 cruise.

Sediment	Description	Photo	X-ray	Lithofacies
Diamicton, matrix supported	Very firm, consisting of a mix of clay and silt, often with sand. Often abundant of clasts throughout the facies.		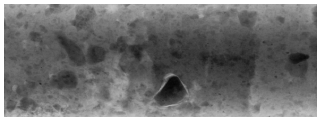	Diamict (Dmm)
Poorly sorted diamictic mud	Fine grained soft clay with a high abundance of angular clasts. Clast size range from mm to sub cm.		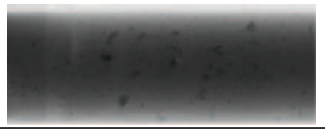	Diamictic mud (Fmd)
Clay or Silt	Laminated clay and/or silt. Variable in colour and firmness. Often horizontal sand laminations.		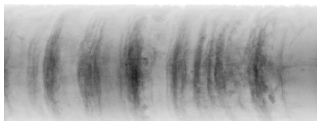	Laminated fines (Fl)
Clay or Silt	Massive clay and/or silt, structureless. This lithofacies is predominantly consisting of silt.		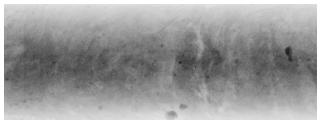	Massive fines (Fm)
Sand	Very fine to coarse sand. Horizontally stratified. Clasts and shell fragments are often absent in this facies.		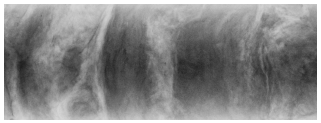	Laminated sand (Sh)
Sand	Very fine to coarse massive sand. Abundant in clasts and shells.		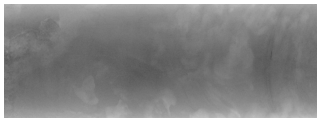	Massive sand (Sm)
Matrix supported gravel	Gravel of variable clast size, granular to pebble. Matrix of silt or sand.		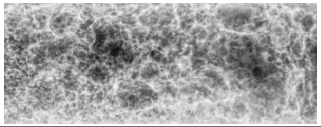	Gravel, matrix supported (Gms)
Clast supported gravel	Gravel of variable clast size, granular to pebble. Very little matrix, poorly mixed with clasts when present.		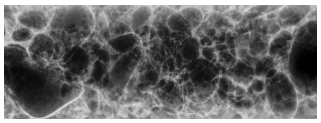	Gravel clast supported (Gm)

Table 4.3: Selection of eight of the twelve sedimentary lithofacies found in the study area. Grading in fine grained sediments is unrecognisable in X-rays and photos, and is therefore excluded from this table.

4.6 Lithofacies

Twelve lithofacies (Table 4.3) were identified according to Eyles *et al.* (1983) classification of lithofacies. Lithofacies were defined on the basis of sedimentary structures, grain size, lithology, sorting and shear strength.

4.6.1 Dmm- massive matrix supported diamicton

This lithofacies is characterised by a highly consolidated fine-grained silt and clay matrix. Both X-ray images and visual analysis reveal a high abundance of clasts. Clasts appear angular and in the X-rays they appear with no preferred orientation. The dominant clast size is sub-cm and up to 2 cm, with occasional clasts of up to 5 cm. The sediment is matrix supported. Shear strength ranges between 50-220 kPa, and is a key criteria that distinguishes this lithofacies from the Gms lithofacies. The Dmm lithofacies is up to 60 cm thick and is found at the base of cores from the outer shelf, and from the base of mid shelf cores from the northern profile, in thicknesses of up to 2 m (Figure 3.4). On the outer shelf, reworked marine shells are found in the Dmm lithofacies, and foraminifera samples from the mid shelf reveal a low biodiversity (Chapter 4.7). Magnetic susceptibility in the lithofacies is between 50 and 115 SI*10-5, and the Dmm facies has sharp boundaries with other lithofacies.

4.6.2 Fmd- Poorly sorted diamictic mud

This lithofacies is characterised by soft clay with a high abundance of clasts. Clasts are angular with no fabric. Clast sizes in this lithofacies range from mm to sub cm. Shear strength measurements range from 25 to 37.5 kPa. This lithofacies is only found at the lowermost 2 m of core JC106-100. On x-ray images the facies appears similar to Dmm. The lithofacies has a sharp boundary to the overlying lithofacies, Fl.

4.6.3 Fl- laminated silt and clay

This lithofacies consists of finely laminated mud, found primarily in the lower sections of cores from the mid-shelf from the southern transect (cores JC106-095, JC106-099, JC106-100, JC106-101, JC106-102 and JC106-106). Clasts in this lithofacies are uncommon and are of sub-cm size. Fl lithofacies ranges in thickness from 5 to 450 cm and it is the thickest lithofacies found in the sediment cores in the study area. The sediment is soft with low (∼10-15 kPa) shear strength values. Lamination is visually apparent as dark bands of silt

and/or fine sand in grey clay. In X-rays (Figure 4.19) lamination is clearly seen and appears as darker bands of higher density. Individual lamina are sub mm thick, and in some cores they are grouped together in layers of a few cm, with pure sand layers in between, also a few cm thick. This is clearly seen in X-rays (Figure 4.19A), and gives the appearance of a cyclicity to the sediment. Deformation of the laminae, where present, is minor however on X-rays the laminations appear to be slightly bent downwards along the sides of the core. This is likely a result of the coring process. Palaeoenvironmental samples from this lithofacies show a high biodiversity dominated by a few key environmental indicator species (see chapters 4.7 and 5.3.2). Magnetic susceptibility of this lithofacies varies between 70 to 120 SI*10-5.

4.6.4 Fm- massive silt and clay

This lithofacies is characterised by massive silt and clay. In some, cores sub-cm clasts are seen scattered throughout the sediment. Fm facies occurs in cores from all parts of the shelf, although it is most common on the mid shelf. Thicknesses range from a few cm up to a few meters. Visually this lithofacies show no bedding structures, but some X-ray images reveal deformed zones (Figure 4.19B). Boundaries with other lithofacies are often sharp. Samples show a relatively high biodiversity dominated by a few key environmental indicator species (see chapters 4.7 and 5.3.2). Fragmented and whole shells occur in X-rays from this lithofacies (Figure 4.19F). Magnetic susceptibility is relatively stable around 80 SI*10-5.

4.6.5 Sh- Laminated sand, Suf- upwards fining and Suc- upwards coarsening

These three lithofacies comprise laminated or graded sand, and are limited to a few cores primarily from the outer part of the mid shelf. Thicknesses rarely exceed 10 cm. These lithofacies are clast poor, and laminae appear weak on X-Rays (Figure 4.19). Although both upwards fining and upwards coarsening units are found in various depth in sediment cores from all parts of the shelf, there seems to be a trend of more upwards fining sections towards the top of the cores. No shear strength measurements were taken due to the sandy nature of the facies as no tension in the tore vane can be build up in this sediment. Contacts with other lithofacies are sharp. Magnetic susceptibility measurements in this lithofacies is approximately 80 SI*10-5.

4.6.6 Sm, massive sand

Massive sand are found in most of the cores. In cores from the inner bay, it dominates with thicknesses exceeding than 3 m. In cores from the mid and outer shelf, sand layers vary in thickness. Clasts are often present and range in size from sub-cm to the size of the core liner (70 mm). Shear strength measurements were not taken in sandy lithofacies as no tension can be build up in this sediment. Magnetic susceptibility measurements vary widely from 30 SI*10-5 to 200 SI*10-5. In general magnetic susceptibility is greater in landward cores.

4.6.7 Gms- matrix-supported gravel, Guf- upwards fining, Guc- upwards coarsening

Matrix-supported gravel is characterised by a textually variable matrix which most often comprises coarse sand and shell fragments in some cases. Grading is sometimes seen, either fining or coarsening upwards. Gms is often found on top of Gm, and below Sm lithofacies. As a result, Gms is often found as a thin mixing zone between Gm and Sm, although a 50 cm thick unit is seen in core CE08-010, with no associated Gm. No shear strength measurements were taken in this lithofacies due to high abundance of clasts. X-ray images reveal that clasts are predominantly sub angular to sub rounded (Figure 4.18). Magnetic susceptibility ranges from 80 to 100 SI*10-5.

4.6.8 Gm- Clast-supported massive gravel, Guf- upwards fining and Guc- upwards coarsening

These lithofacies are comprised of clast-supported gravel which often lack any matrix. Clast size ranges from mm sized granules to pebbles, and in some cases cobbles of the diameter of the core liner (70 mm) are found (Figure 4.18 D and E). In some cases the gravel are graded, either upwards fining or upwards coarsening. Where matrix is found, this is often as a result of mixing with finer grained lithofacies found above or below. Gm is often found as the capping facies in the sediment cores, with thicknesses between 10 and 120 cm. Clasts are predominantly sub-rounded to rounded. Whole shells or shell fragments are often seen within this lithofacies, and in the outer shelf cores, shell fragments constitute a coarse matrix. Due to the high clast content, no shear strength measurements were taken. Magnetic susceptibility is generally low compared to other lithofacies, at 25-60 SI*10-5, and clear drops in magnetic susceptibility are seen across boundaries with

other lithiofacies.

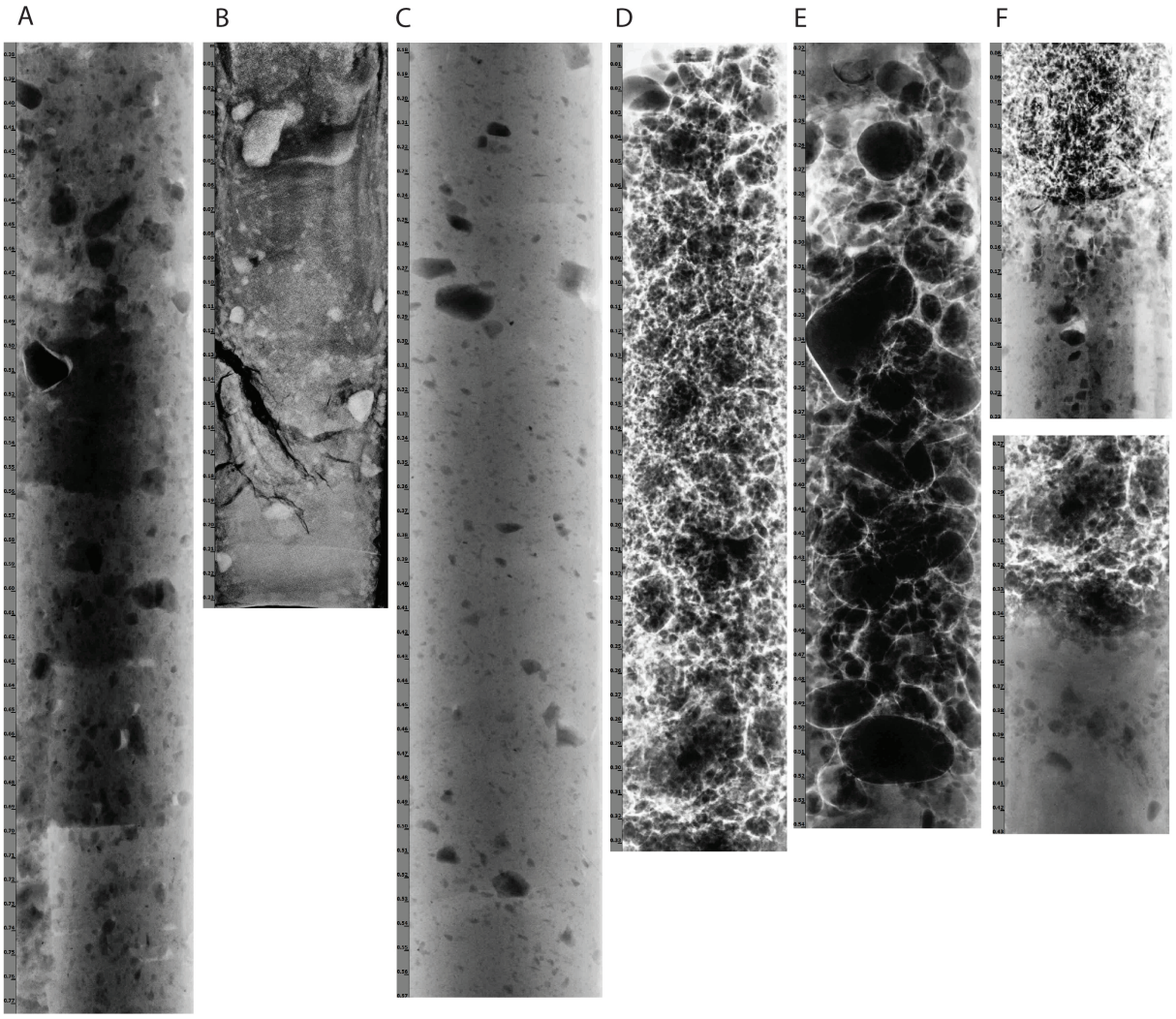

Figure 4.18: Examples of x-rays of coarse-grained and diamictic facies, and bedding contacts. A: Dmm (massive, matrix-supported diamicton) from bottom of core JC106-112 B: Dmm (massive, matrix-supported diamicton) from core CE08-010. Note the reversed contrasts, due to different x-ray technique. C: Fmd (Poorly sorted diamictic mud) from core JC106-100 Very soft mud, abundant in clasts. D: Guc (Clast supported gravel) from core JC106-095 E: Gm (Gravel, clast supported) from core JC106-106 F: Two examples of sharp boundaries between the gravel (Gm) and underlying fine massive (Fm) from the cores JC106-095 and JC106-101

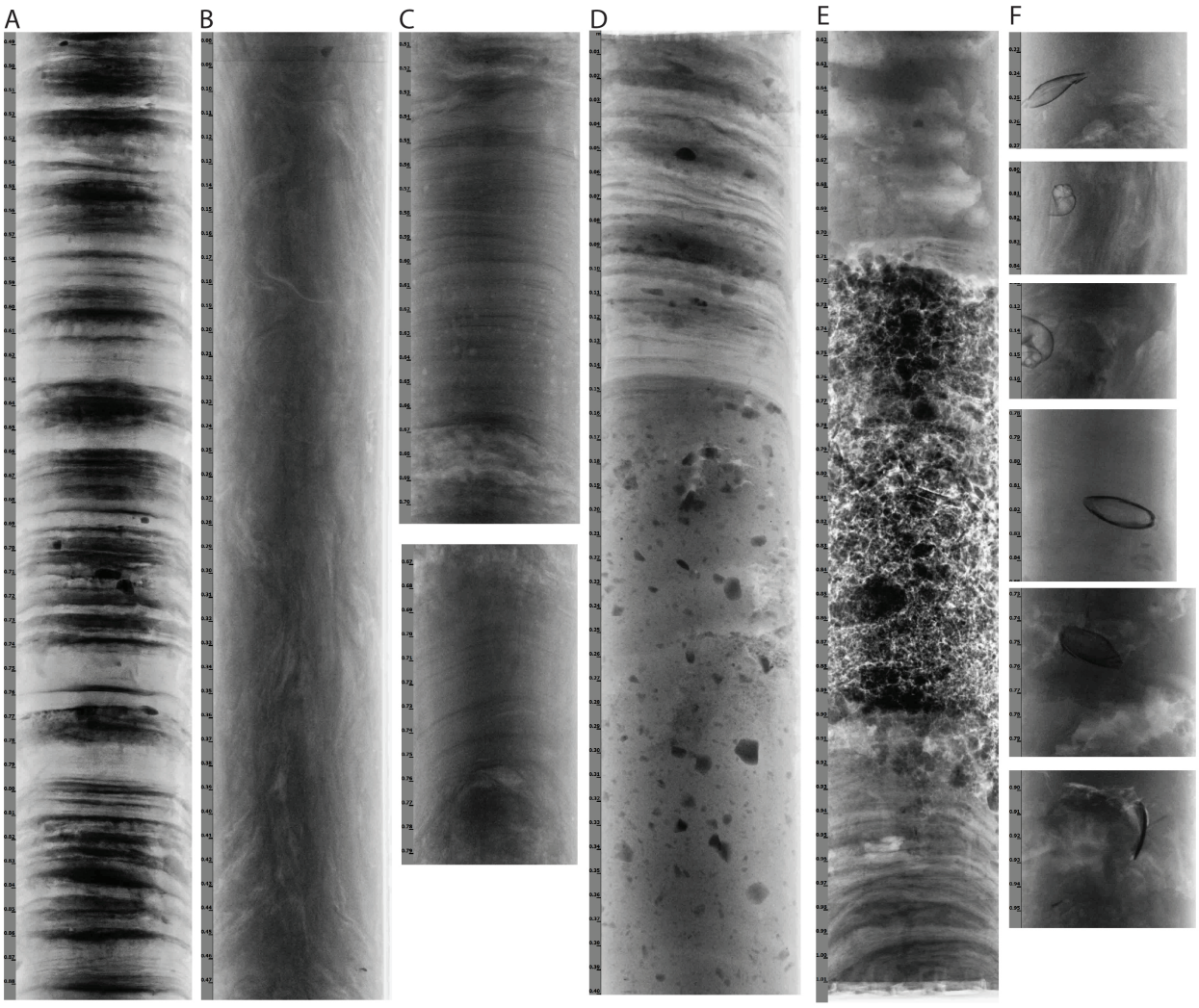

Figure 4.19: Examples of x-rays of fine-grained lithofacies and bedding contacts. A: Fl (Laminated silt and clay) primarily found in lower sections of cores from the mid-shelf basin. Clasts occur but are not always present. Clays are of higher density and appear as dark bands, while silt and fine sand appear light. B: Fm (Massive silt and clay) primarily found on the mid shelf. This lithofacies often appears chaotic or deformed in x-rays. C: Sh (laminated sand). Two examples of horizontally laminated sand from core JC106-105. The lamination can be very faint. Lamination appear to be bent downcore, but this could be a result of drawdown from the coring process. D: Sharp boundary between Fl (laminated silt and clay), and Fmd (poorly sorted diamictic mud) in core JC106-100. E: Section of core JC106-100 with faint laminated sand Fh, sharp boundary to Gms (Matrix-supported gravel), and Gm (Clast-supported gravel), and a sharp lower boundary to Fl (Fine laminated silt and clay). F: Six examples of snails, shells and shell fragments found in Sm lithofacies.

4.7 Foraminifera

To support the environmental interpretation of the lithofacies found in the sediment cores, palaeoenvironmental analysis on foraminifera from 5 sediment cores were carried out. Two of the cores, CE08-010 and

JC106-102 were selected due to their thick successions of fine grained laminated sediments, and changes in stratigraphy up through the cores. These two cores was both collected from the mid shelf basin (Figure 3.4) in water depths of $\sim$ 100 meters (Table 4.2). The cores were sub-sampled at 16 cm intervals from the base, up to coarse grained sand and gravels near the surface. Another three cores, CE08-018, JC106-095 and JC106-100 (Figure 3.4) were sub-sampled either towards the base of the fine grained sediments, or at depths where significant changes in the lithofacies were evident. Foraminifera were found in all lithofacies represented in the five sediment cores selected for sampling. A total of 50 species of benthic foraminifera, along with a collective group of planktic foraminifera were identified. Only benthic foraminifera have been identified to species level, as these are closely connected to the environment they live in (Murray, 2006), where as living conditions for planktic foraminifera tend to be less common on the continental shelf, and hence planktic foraminifera found in the samples are most likely carried in by ocean currents.

Most samples are dominated by no more than two to four species, in some samples making up to 80-90% of the total assemblage, resulting in a low alpha index. Exceptions are samples from coarser grained lithofacies, where foraminiferal diversity in general is higher. The dominant species found in the samples are: *Cassidulina reniforme*, *Elphidium excavatum f. clavata* and *Cibicides lobatulus*. Other abundant species, making up 10 to 20% of foraminiferal assemblages are *Elphidium sp.*, *Quinqueloculina seminulum*, *Textularia segittula* (only found in Gms in CE08-010) and few planktic species. Other common species found in most samples, making from less than one and up to just a few percent are: *Bolivina sp. Bulimina marginata*, *Cassidulina laevigata*, *Miliolinella sp. Nonionellina labradorica*, and *Quinqueloculina lata*. Other rare species are found but are limited to very few samples, and can be seen in the species list and count sheets in appendix I.

4.7.1 Core CE08-010

Core CE08-010 is the longest core in the northern transect, and recovered several lithofacies, bottoming out in Dmm (Figure 4.15) at a depth of 578 cm b.s.f. The core was sampled close to the bottom, at a depth of 576 cm b.s.f. in Dmm, through Sm and Fm lithofacies in the middle section of the core, to a depth of 144 cm b.s.f. where coarse grained Guc lithofacies begins to dominate. A total of 28 samples at 16 cm intervals were analysed from the core (Table 4.4). The highest abundance of foraminifera from one sample was from a depth of 176 cm b.s.f. where 517 tests yielded 18 different species. The lowest foraminifera abundance from the core was at 496 cm b.s.f. where only 16 tests were found, made up of three species (Table 4.4).

The highest species diversity found in the core was at a depth of 336 cm b.s.f. with 25 species (Table

4.4). This sample is however, somewhat questionable, as the sample size is considerably below the desired 300 individual tests and furthermore, the lithofacies at this depth consists of matrix supported gravel (Gms). The subsequent two samples above, at 320 cm and 304 cm b.s.f. also show a high species diversity, with 21 and 20 species respectively. These two samples were also taken in matrix supported gravel, and although the sample size shows 298 and 324 individual tests respectively, they still have a significantly higher alpha index than the average for this core (Table 4.4). Core CE08-010 has an average alpha index of 3.13 with a trend to increase up core, showing a higher species diversity towards the top of the sampled section (Figure 4.20).

Benthic foraminiferal species with an abundance $\geq$5% from core CE08-010 are shown in figure 4.20. The assemblage is dominated by *C. reniforme* and *E. excavatum f. clavata* through most of the core. At the base, from 576 cm to 540 cm b.s.f. in Dmm lithofacies (Figure 4.20), *E. excavatum f. clavata* dominates the assemblage with abundances up to 60%. The other abundant species in the Dmm lithofacies is *C. reniforme* (abundance of 30%). Abundance of *C. reniforme* increases upcore from approximately 30% in the Dmm at the base, to between 60 and 80% in Sm, Suf and Fm lithofacies, between 540 to 350 cm b.s.f. while the abundance of *E. excavatum f. clavata* decreases in the same interval (Figure 4.20). *C. lobatulus* has an abundance of between 5 and 15% from the base of the core through the Sm and Fm lithofacies with an increasing trend upcore. In the coarse-grained Gms lithofacies found at 345 to 290 cm b.s.f. *C. lobatulus* increases to an abundance of approximately 35%, while *T. sagittula* have an abundance of 30 to 40%. In this lithofacies, *E. excavatum f. clavata* and *C. reniforme* decrease to abundances of 10 to 15% (Figure 4.20). From 290 to 160 cm b.s.f. in Fm and Sm lithofacies, the assemblage is heavily dominated by *C. reniforme* with an abundance of up to 70%. At the top of the core, in lithofacies Suc and Guc at 160 to 144 cm b.s.f. *C. lobatulus* and *T. sagittula* becomes dominant with abundances up to 30% while both *E. excavatum f. clavata* and *C. reniforme* decreases to $\leq$10%. The absolute abundance of benthic foraminifera varies significantly through the core, and there appears to be no pattern in relation to specific lithofacies. Planktic foraminifera seem to be more abundant in coarse grained lithofacies.

Table4, CE08-010

Sample depth	**Nr. Tests**	**Nr. Species**	**alpha index**
144 cm	237	17	4.2
160 cm	160	12	3
176 cm	517	18	3.6
192 cm	19	5	2.2
208 cm	515	17	3.4
224 cm	151	8	1.8
240 cm	236	11	2.4
256 cm	19	7	4
272 cm	255	13	2.9
288 cm	109	15	4.7
304 cm	324	20	4.7
320 cm	298	21	5.2
336 cm	147	25	8.6
352 cm	413	12	2.3
368 cm	34	9	4
384 cm	220	10	2.2
400 cm	367	12	2.4
416 cm	166	12	3
432 cm	208	12	2.8
448 cm	452	17	3.5
464 cm	468	12	2.2
480 cm	221	11	2.4
496 cm	16	3	1.1
512 cm	431	16	3.3
528 cm	26	6	2.4
544 cm	47	6	1.8
560 cm	62	4	1
576 cm	108	10	2.7
Average	222	12	3.13

Table 4.4: Foraminifera collection in core CE08-010. Sample depth, nr. test, nr. species and alpha index.

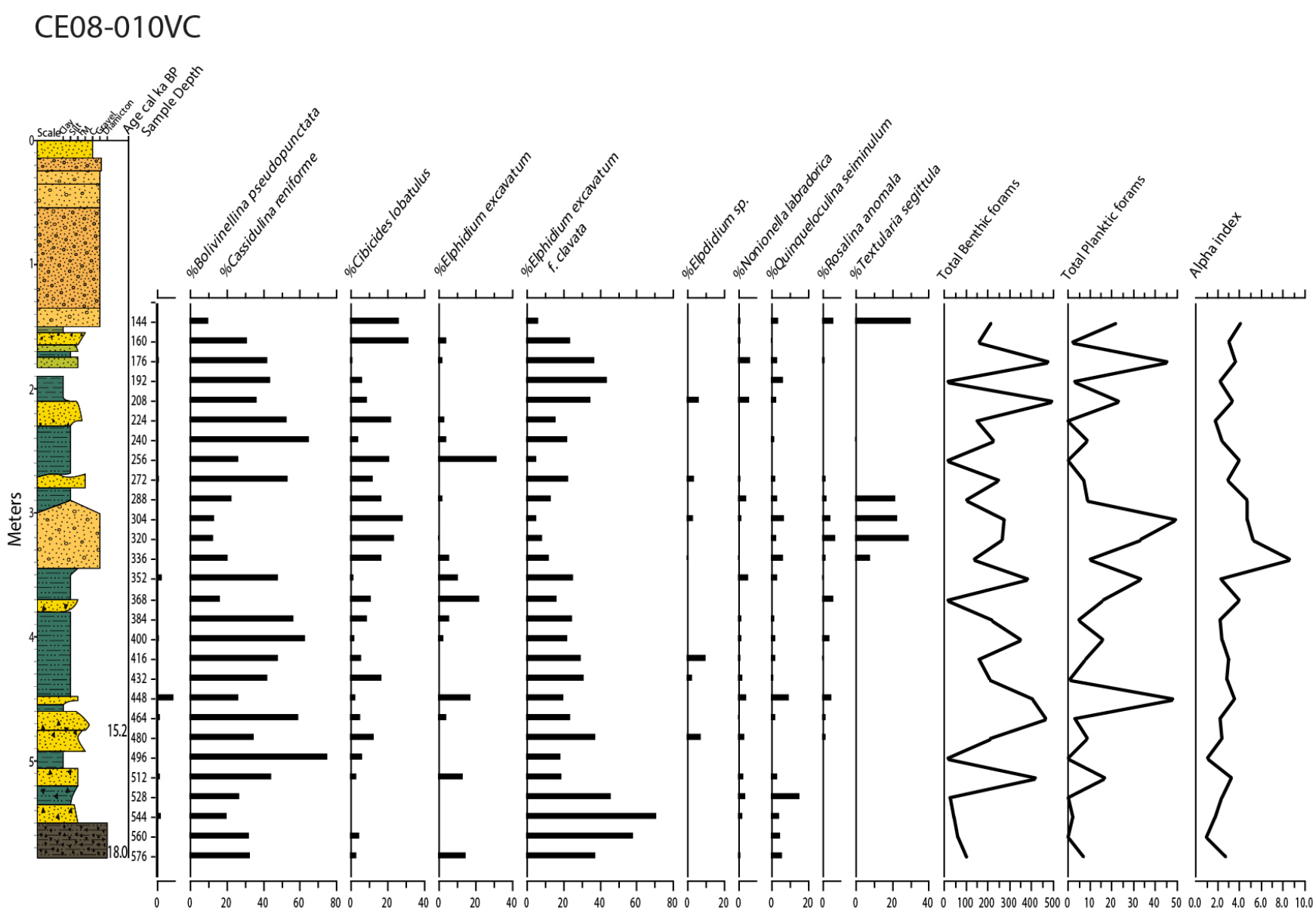

Figure 4.20: Abundant foraminifera assemblage greater than 5%, of core CE08-010.

4.7.2 Core JC106-102

Core JC106-102 has a length of 250 cm, and has a long succession of finely laminated silt and clay (lithofacies Fl). Foraminifera were examined from this core to provide additional information to support the palaeoenvironmental interpretation of lithofacies Fl, as well as to investigate the palaeoenvironmental evolution of the mid shelf. The core was sub sampled from the base at a depth of 248 cm b.s.f. in laminated mud (Fl), into massive fine grained silt and clay (lithofacies Fm) at a depth of 56 cm b.s.f. (Table 4.5). Samples taken above this depth yielded very few foraminifera, and were not counted in detail, or presented here. A total of 13 samples at 16 cm intervals were analysed from the core. The highest abundance of foraminifera collected from one sample was 72 cm. b.s.f. where 700 tests were found and yielded 13 species. The lowest foraminifera count presented here from the core was at depth 104 cm b.s.f. where 26 tests were present, including 8 different species (Table 4.5). The highest species diversity is found at 120 cm b.s.f. where 305 foraminiferal tests yielded 19 different species. The lithofacies throughout most of this core, from 75 cm b.s.f. to the base at 250 cm b.s.f, is fine grained laminated silt and clay (Fl). This consistency can also be seen in the relatively stable Alpha index, which is constant between 2 and 4 with an average of 3.34 down through the core. (Figure 4.21 Table4.5).

The dominant species in core JC106-102 are *C. reniforme* and *E. excavatum f. clavata* which both have abundances of approximately 40% in the base of the core in Fl lithofacies (Figure 4.21). Abundance of *C. reniforme* is relatively constant up through the core, while *E. excavatum f. clavata* is more variable with a slight decrease up core as *E. e. selseyensis* becomes increasingly more abundant, from less than 5% at the base to abundances over 20% at 152 cm b.s.f. and 104 cm b.s.f., and with a general abundances of about 10% (Figure 4.21). Total benthic foraminiferal abundance is relatively stable, with a drop at 104 cm b.s.f. where only 24 tests was counted, and a spike at 72 cm b.s.f. where 700 tests were counted. Alpha index in the core is stable with an average of 3.34.

Table5, JC106-102

Sample depth	**Nr. Tests**	**Nr. Species**	**alpha index**
56 cm	177	16	4.3
72 cm	700	13	2.3
88 cm	307	17	3.9
104 cm	26	8	4.5
120 cm	305	19	2.6
136 cm	375	13	2.4
152 cm	144	10	3.7
168 cm	285	16	3.7
184 cm	301	15	3.3
200 cm	375	14	2.9
216 cm	144	12	3.1
232 cm	326	15	3.2
248 cm	298	16	3.6
Average	289	14	3.34

Table 4.5: Foraminifera collection in core JC106-102. Sample depth, nr. test, nr. species and alpha index.

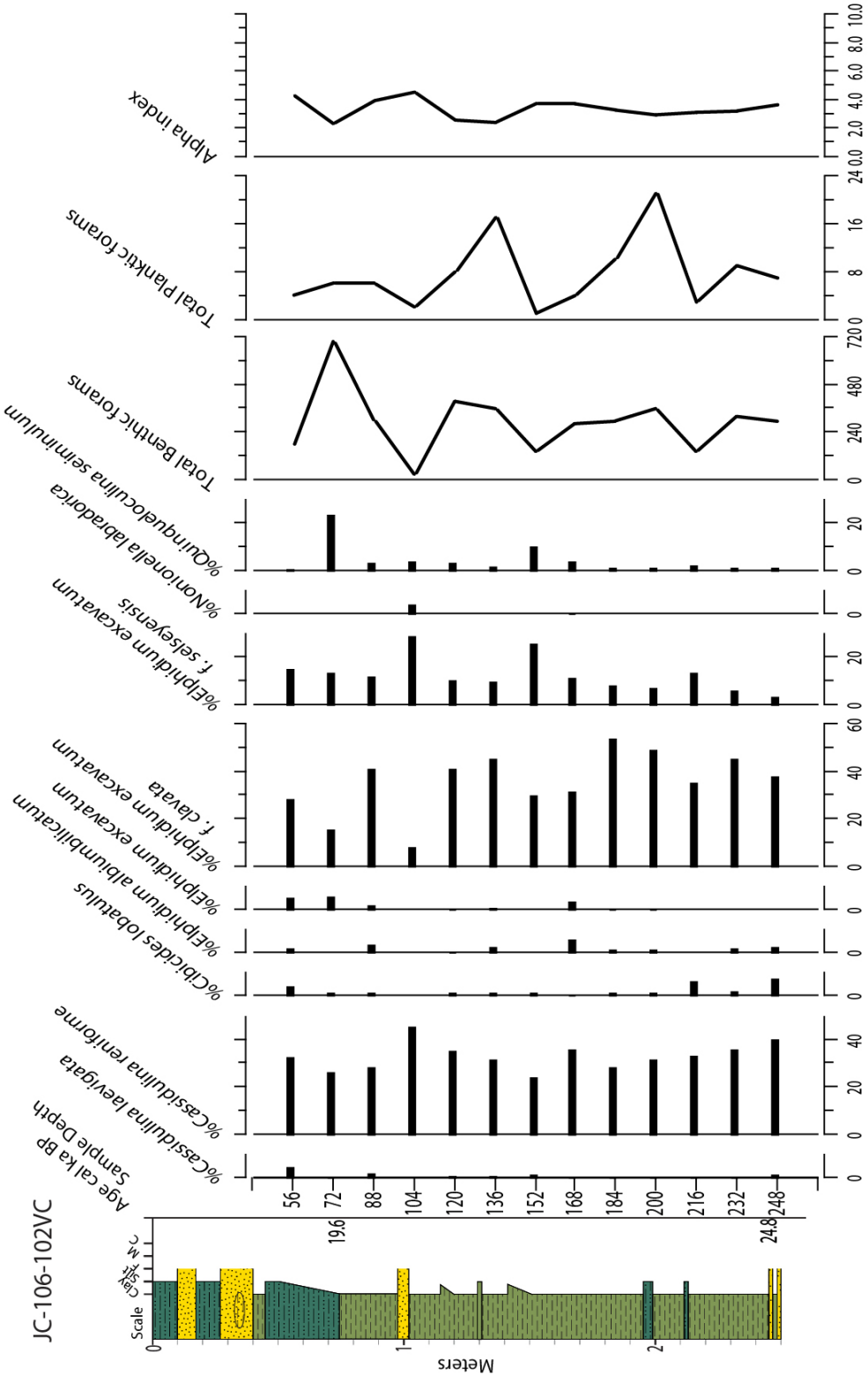

Figure 4.21: Foraminifera abundances greater than 5% of core JC106-102 and Alpha index.

4.7.3 Core CE08-018

Core CE08-018 from the outer shelf, was sub-sampled in its bottom 40 cm, from 100 cm b.s.f. to 62 cm b.s.f. in laminated sand (Sh) and massive sand (Sm), in order to provide information on the palaeoenvironmental changes shortly after deglaciation from the outer shelf. Four samples were taken at 100, 84, 72 and 62 cm b.s.f., avoiding the gravel unit found at 64 to 70 cm b.s.f. (Figure 4.22). The highest foraminifera count was found in the bottom sample, 100 cm b.s.f., with 297 tests and a diversity of 16 species. The lowest count was found in 72 cm b.s.f. with 19 tests and a diversity of 6 species (Table 4.6).

The assemblage is dominated by *C. lobatulus* and *E. excavatum f. clavata* with abundances ranging from 20 to 50% and 20 to 40% respectively (Figure 4.22). *C. reniforme* has an abundance of approximately 20% through the sampled section, and at 62 cm b.s.f. abundances of approximately 10% of *Q. seminulum* are found. Total benthic foraminifera found in the core are decreasing through the sampled section, and alpha index is stable with an average of 3.17 (Figure 4.22)

Table6, CE08-018

Sample depth	**Nr. Tests**	**Nr. Species**	**alpha index**
62 cm	60	10	3.4
72 cm	19	6	3
84 cm	217	12	2.7
100 cm	297	16	3.6
Average	148	11	3.17

Table 4.6: Foraminifera collection in core CE08-018. Sample depth, nr. test, nr. species and alpha index.

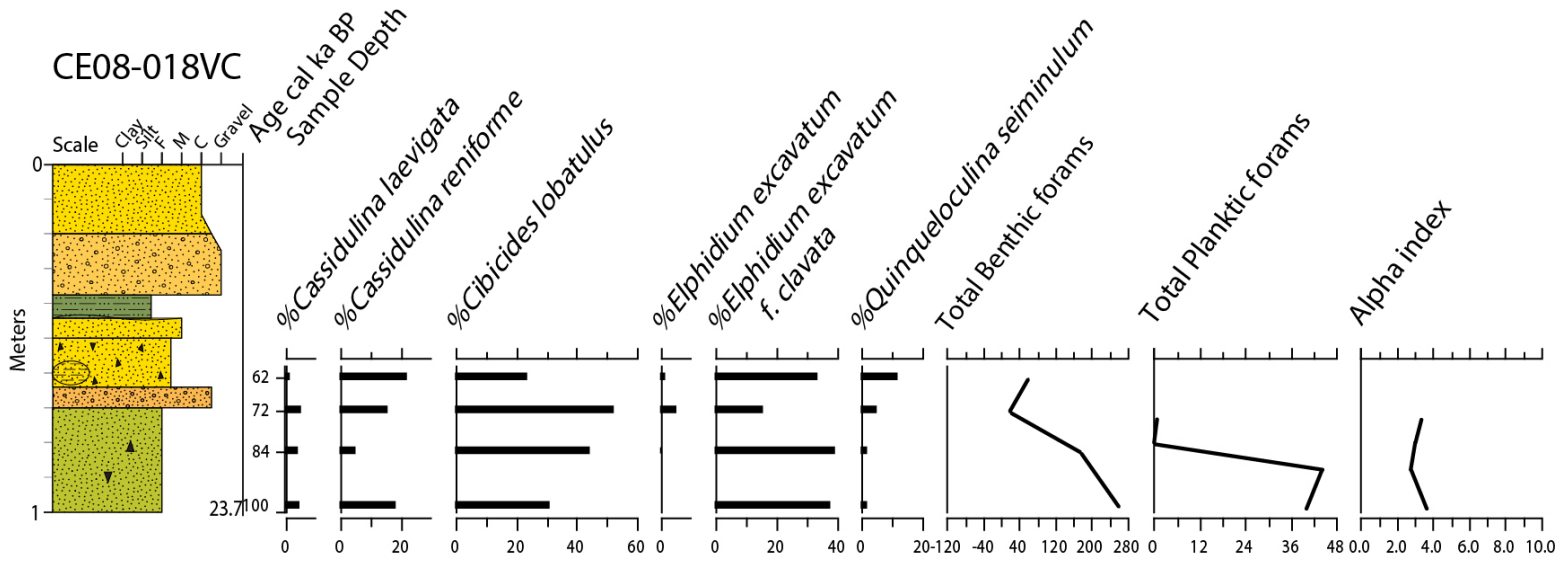

Figure 4.22: Foraminifera abundances greater than 5% of core CE08-018 and Alpha index.

4.7.4 Core JC106-095

Core JC106-095 was sampled in the bottom 1 m, in laminated fine grained silt and clay (lithofacies Fl). This core was selected due to its location on the DBM, in order to provide information of the plaaeoenvironmental changes across the inner bay basin and associated with the formation of the moraine. Samples were mostly taken in 16 cm increments, from 138 cm b.s.f. to 238 cm b.s.f. but two samples were taken at 12 cm increments, close to a sample depth for radiocarbon dating at 176 cm b.s.f. Foraminiferal abundance is relatively high but species diversity is low, with an average alpha index of 1.35 (Figure 4.23 Table 4.7). The highest foraminifera count was at 182 cm b.s.f. with 438 tests and a species diversity of 6. The lowest count was at 170 cm b.s.f with 268 foraminifera tests and a diversity of 8 species.

E. excavatum f. clavata dominates all of the sampled section, with abundances between 40% at 218 cm b.s.f. to 80% at 138 cm b.s.f. (Figure 4.23). *C. reniforme* is common through the core with a relatively stable abundance just below 20%, decreasing to 10% up through the section. Alpha index is relatively stable with an average of 1.35.

Table7, JC106-095

Sample depth	**Nr. Tests**	**Nr. Species**	**alpha index**
138 cm	341	6	1
154 cm	345	10	1.9
170 cm	268	8	1.6
182 cm	438	6	1
202 cm	390	6	1
218 cm	418	9	1.6
Average	367	7.5	1.35

Table 4.7: Foraminifera collection in core JC106-095. Sample depth, nr. test, nr. species and alpha index.

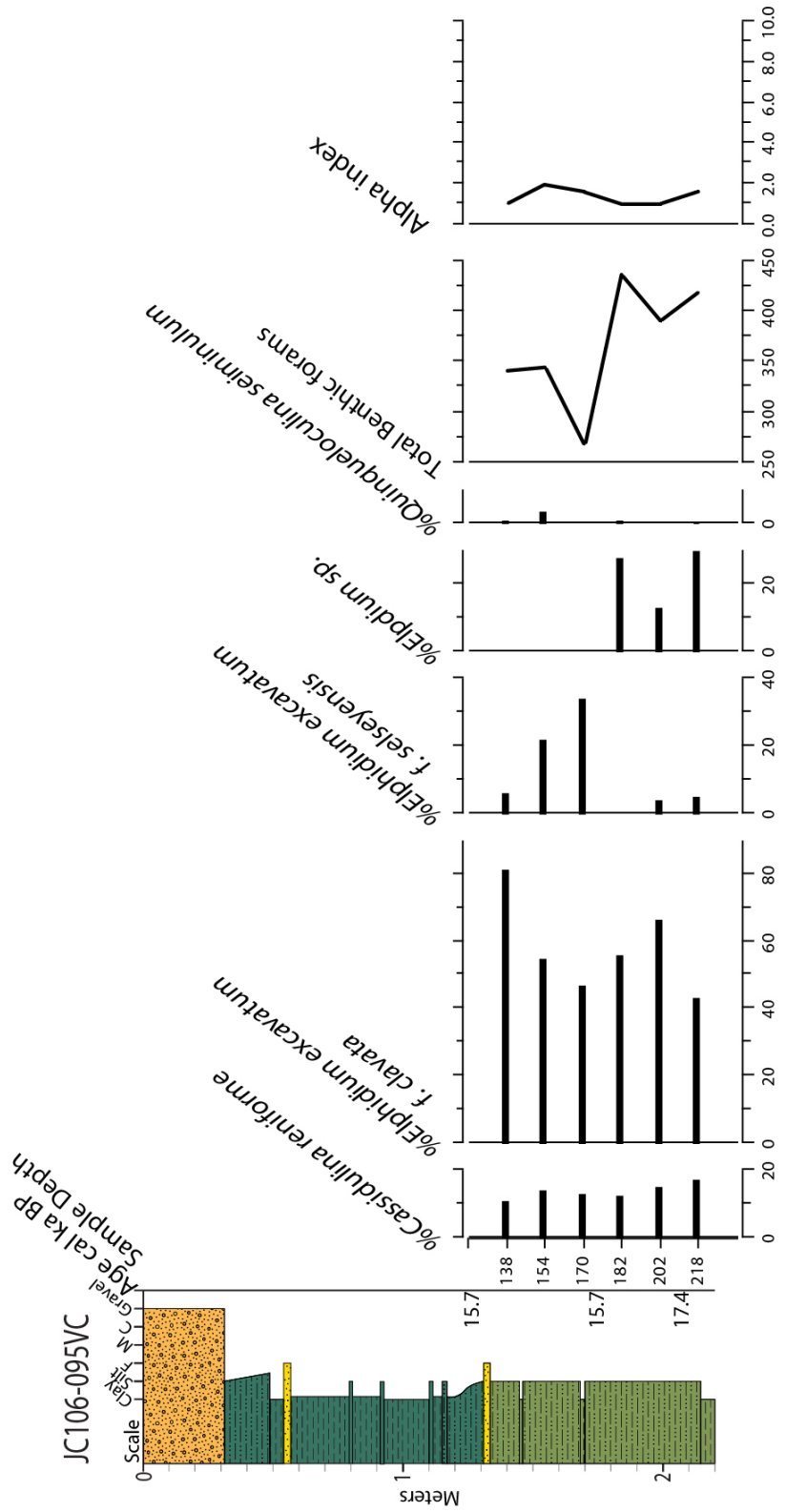

Figure 4.23: Abundant foraminifera assemblage greater than 5% of core JC106-095

4.7.5 Core JC106-100

Core JC106-100 was sampled across a very clear change in lithofacies at 310 cm b.s.f. from clast-rich, poorly-sorted diamictic mud(lithofacies Fmd) to clast-poor, laminated fine grained silt and clay (lithofacies Fl) (Figure 4.19. Four samples were taken, two above and two below the boundary. Samples were taken 10 cm from the boundary, and in subsequent 16 cm increments. The highest foraminiferal count was at 284 cm b.s.f. with 302 tests, and a diversity of 8 species. The lowest count was from 300 cm b.s.f. with 70 foraminiferal tests and a diversity of 7 species. There is no significant change in abundance or diversity over the boundary. The alpha index is relative low, with an average of 2 (Table 4.8). The assemblage throughout the core is dominated by *E. excavatum f. clavata* with 60% to $\geq$ 80% of the total assemblage (Figure 4.24). *C. reniforme* is also common with 10% to 20% up through the sampled section, and less abundant species such as *E. excavatum f selseyensis* and *Q. seminulum* are found with abundances of around 10% through the core (Figure 4.24). There are no apparent changes in total benthic foraminifera through the core, and the alpha index is relative stable with an average of 2.0.

Table8, JC106-100

Sample depth	**Nr. Tests**	**Nr. Species**	**alpha index**
284 cm	302	8	1.5
300 cm	70	7	1.9
320 cm	204	13	3.1
336 cm	138	8	1.8
Average	178	9	2

Table 4.8: Foraminifera collection in core JC106-100. Sample depth, nr. test, nr. species and alpha index.

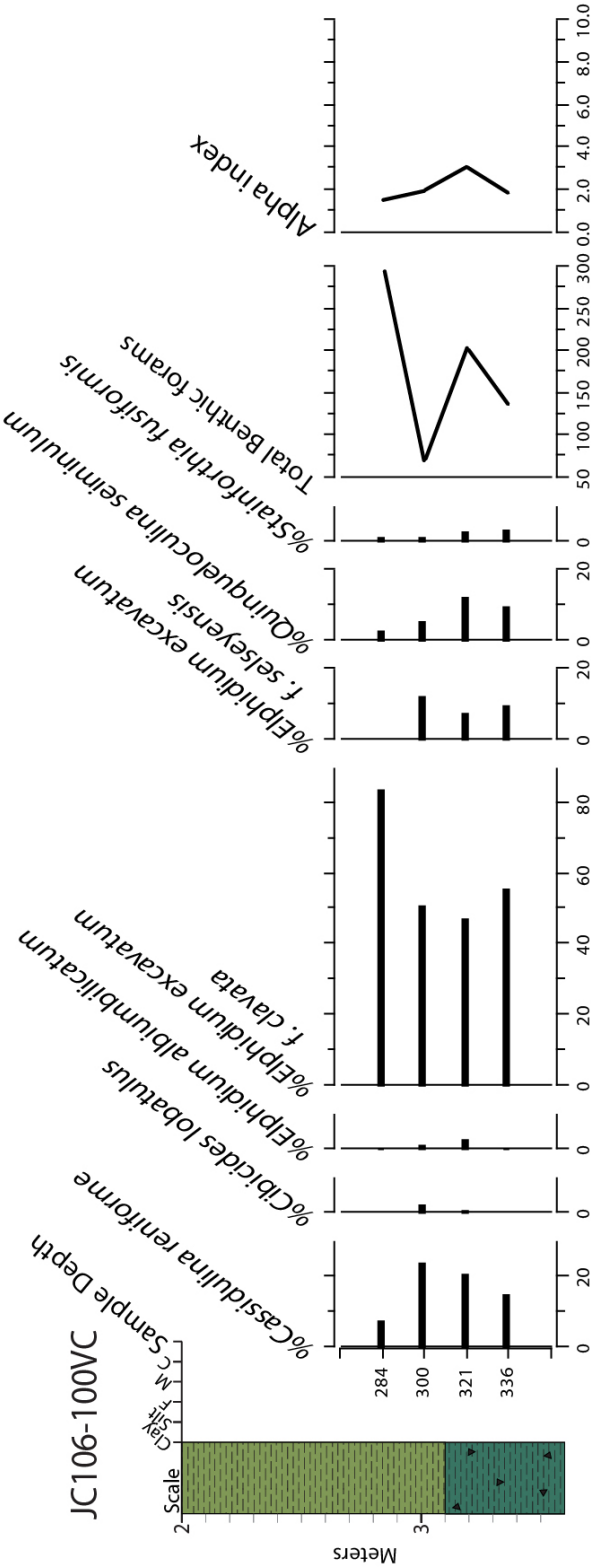

Figure 4.24: Abundant foraminifera assemblage greater than 1% of core JC106-100

4.8 Radiocarbon results

Twenty two radiocarbon dates were obtained on samples from the cores presented in this thesis. Samples consisted both of macro-fossils where present, and mixed species of benthic foraminifera in other selected locations. Samples were acquired from the deepest possible parts of the cores containing sediments interpreted as glacimarine, in order to provide a chronology for de-glaciation across the shelf. Depending on palaeoenvironmental interpretations of the sampled material, the dates may directly record the age of retreat from the area, or may provide a limiting date for glacial retreat. Some samples of reworked shells were also obtained for dating from deposits interpreted as tills (see Chapter 5 below), in order to provide a maximum age for the till and thus ice advance. Further, critical changes in lithofacies and thus changes in palaeoenvironmental conditions, were also targeted for dating in order to investigate timing of changes across the shelf. Nine of these samples were analysed for a previous project, in table 4.9 marked with a *, exclusively on the CE08 cores (Purcell, 2014) and used here, and the remaining thirteen were collected during data collection for this thesis, one from the CE08 cores and the remaining twelve from the JC106 cores (Table 4.9). Cores selected for radiocarbon dating is relatively even distributed across the study area, although as cores from the outer shelf in general are very short and predominantly consists of coarse grained sediments, only three of the twenty two samples have been selected in this area. Ten of the samples was selected from the mid shelf basin and distributed on eight cores, all with a sample taken at the very base of the core and two from higher up. The remaining nine samples was taken from the DBM and inner bay basin and was distributed on three cores, where only one of the samples was taken from the base and the remaining samples selected at lithological changes in the cores (Figure 4.25). All radiocarbon dates have been calibrated using Calib 7.1 with the Marine13 calibration curve (Stuiver & Reimer, n.d.), taking into account a 400 year global reservoir effect (Reimer *et al.*, 2013). For the variable local reservoir age calibration, see chapter 3; Methods, section 3.5, Radiocarbon dating. All calibrated ages have been calculated with $\Delta R=0$. Ages are quoted as the median value of the two σ range with uncertainty. The 22 radiocarbon dates and information about sample depth, sediment type, sample method, radiocarbon and calibrated age and uncertainties are shown in table 4.9.

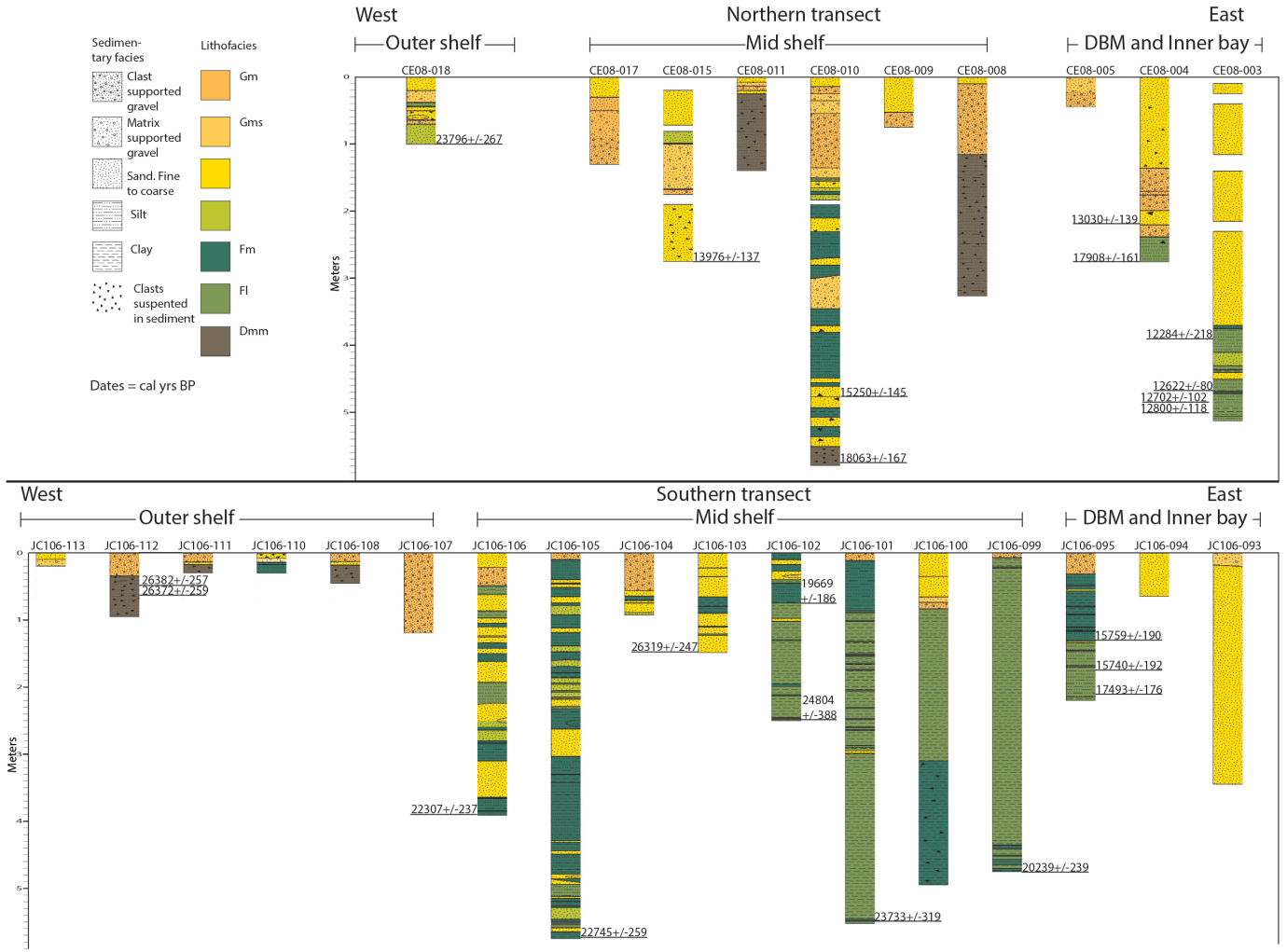

Figure 4.25: Profile of the sediment cores across the shelf, with shown distribution of radiocarbon dates.

Sample nr	**Sample depth (cm)**	**Litho-facies**	**Sample type**	**^{14}C Age (years BP)**	**$\pm 1\sigma$ (^{14}C yBP)**	**(Cal yrs BP) R = 0 years**	**$\pm 1\sigma$ (cal y. BP)**
JC106-095-128	128	Fm	Sf	13527	39	15759	190
JC106-095-175.5	175.5-177.5	Fl	Sf	13516	38	15740	192
JC106-095-209	209	Fm	F	14705	45	17493	176
JC106-099-474	474	Fm	F	17180	80	20239	239
JC106-101-548	548-551	Fl	F	20110	120	23733	319
JC106-102-72	72	Fl	Sf	16692	45	19669	186
JC106-102-247	247	Fl	F	21000	110	24804	388
JC106-103-145	145	Sm	F	22521	70	26319	247
JC106-105-572	572	Fm	F	19290	90	22745	259
Jc106-106-389	389	Fm	F	18850	90	22307	237
JC106-112-51	51	Dmm	Sf	22582	67	26382	257
JC106-112-59.5	59.5	Dmm	Ms	22572	71	26372	259
CE08-003-387*	387-390	Fl	Sf	10802	38	12284	218
CE08-003-466*	466	Fl	Sf	11091	38	12622	80
CE08-003-477*	477	Fl	Sf	11219	39	12702	102
CE08-003-493*	493-499	Fl	F	11345	30	12800	118
CE08-004-217*	217	Sm	Sf	11555	39	13030	139
CE08-004-264*	264-273	Fl	F	15130	44	17918	161
CE08-010-471*	471-478	Sm	F	13205	35	15250	145
CE08-010-573	573-578	Dmm	F	15263	43	18063	167
CE08-015-272*	272-275	Sm	Sf	12494	40	13976	137
CE08-018-CC*	core catcher	Sh	F	20170	90	23796	267

Table 4.9: Radiocarbon results form 22 samples. Samples marked * collected by Purcell (2014). Sample types: Sf: Shell fragment. F: Foraminifera. Ms: Marine snail. Ages are quoted as the median value of the two σ range with uncertainty. 14C ages are calibrated using Marine13 (Reimer *et al.*, 2013) with a 400 year reservoir effect.

5. *Interpretations*

5.1 Acoustic facies

5.1.1 Acoustic Facies A

Based on its homogeneous, structureless appearance, Acoustic Facies A is interpreted as subglacial till. Acoustic Facies A comprises a series of landforms across the mid-shelf basin, that are buried by the overlying acoustically stratified Facies B (Figure 5.2) This is consistent with similar findings from Arctic basins from Greenland and Canada, where an acoustically unstratified till unit with an irregular upper boundary is overlain by a well stratified deglacial facies (Gilbert, 1985; Syvitski & Praeg, 1989; Syvitski, 1991; Hein & Syvitski, 1992). These landforms are interpreted as moraines, and they possibly represent the buried southward extension of the ridges which are seen in the multibeam data in the northern part of the mid shelf (Benetti *et al.*, 2010; Ó Cofaigh *et al.*, 2012) (Figure 2.8). The presence of Acoustic Facies A just under the seafloor on the outer shelf is consistent with the sediment cores collected at this location, where stiff massive diamicton (Dmm) is present under a thin layer of coarse sand and gravel (Gm, Gms and Sm lithofacies) (Figures 4.8 and 4.9). The distribution, topographic expression and acoustic characteristics of Acoustic Facies A and its sedimentological composition as a stiff massive diamicton is consistent with its interpretation as a subglacial till (Shipp *et al.*, 2002; Ó Cofaigh *et al.*, 2005).

5.1.2 Acoustic Facies B

Acoustically well stratified facies have been documented in many currently glaciated Arctic fjords, where they have been interpreted as a product of ice-proximal glacimarine sedimentation (Gilbert, 1985; Syvitski, 1991; Josenhans & Lehman, 1999; Ó Cofaigh *et al.*, 2001; Ó Cofaigh & Dowdeswell, 2001). With the parallel reflectors and the onlapping relationship of Acoustic Facies B to the underlying topography, this facies is interpreted as a product of deposition in a subaquatic, probably ice-proximal glacimarine environment (Gilbert, 1985; Josenhans & Lehman, 1999). Sediment cores that penetrated Acoustic Facies B on the mid-shelf basin all recovered laminated and massive fine grained lithofacies (Fl, Fm and Sh) (Figures 4.10, 4.11, 4.12, 4.13 and 4.15), with a glacimarine foraminiferal assemblage (See section 5.3.4). Acoustic Facies B is therefore interpreted as glacimarine in origin.

5.1.3 Seafloor and Acoustic Facies C

Acoustic Facies C is consistent with findings in present day Arctic fjords (Gilbert, 1985; Syvitski, 1991; Hein & Syvitski, 1992) where a thin veneer of acoustically transparent sediment is seen overlying glacimarine sediments, and is interpreted as post-glacial muds and sand (Syvitski, 1991; Hein & Syvitski, 1992). This is consistent with the relatively thin layer of sand and gravel lithofacies (Gm, Gms and Sm) seen throughout the sediment cores across the shelf (Figures 4.8 to 4.17). Sediment cores from Facies C, especially those from the inner bay, show this to be composed of massive sand. Both the seafloor reflector and the Acoustic Facies C are thus composed of Gm, Gms and Sm lithofacies, and on that basis are interpreted as post-glacial sediments.

The 1 to 2 ms thick seafloor reflector seen through-out the profile (Figure 4.1), is equivalent to a ∼85 to ∼170 cm thick sedimentary unit on the seafloor. This is however, rarely seen in the sediment cores across the shelf. In many of the cores, a 10 to 50 cm thick clast-rich gravel unit (Gm and Gms) is seen at the top of the cores (Figures 4.8, to 4.17). The clear and thick reflector of the seafloor is therefore a result of the large acoustic contrast from seawater to sediment, and is furthermore, amplified as a ringing effect due to the high abundance of clasts in the sediment (Veeken, 2007).

5.2 Spatial distribution of acoustic facies

5.2.1 Outer shelf

The sub-bottom profile of the outer shelf moraine (Figure 5.1), shows the interpreted Acoustic Facies. The moraine is formed in Acoustic Facies A, subglacial till, with a thin veneer of acoustic Facies C, probably as a result of bottom currents. Cores from this part of the shelf bottomed out in Dmm lithofacies, and the geomorphology, acoustic facies and core sediments are all consistent with a grounded ice sheet margin on the outer shelf.

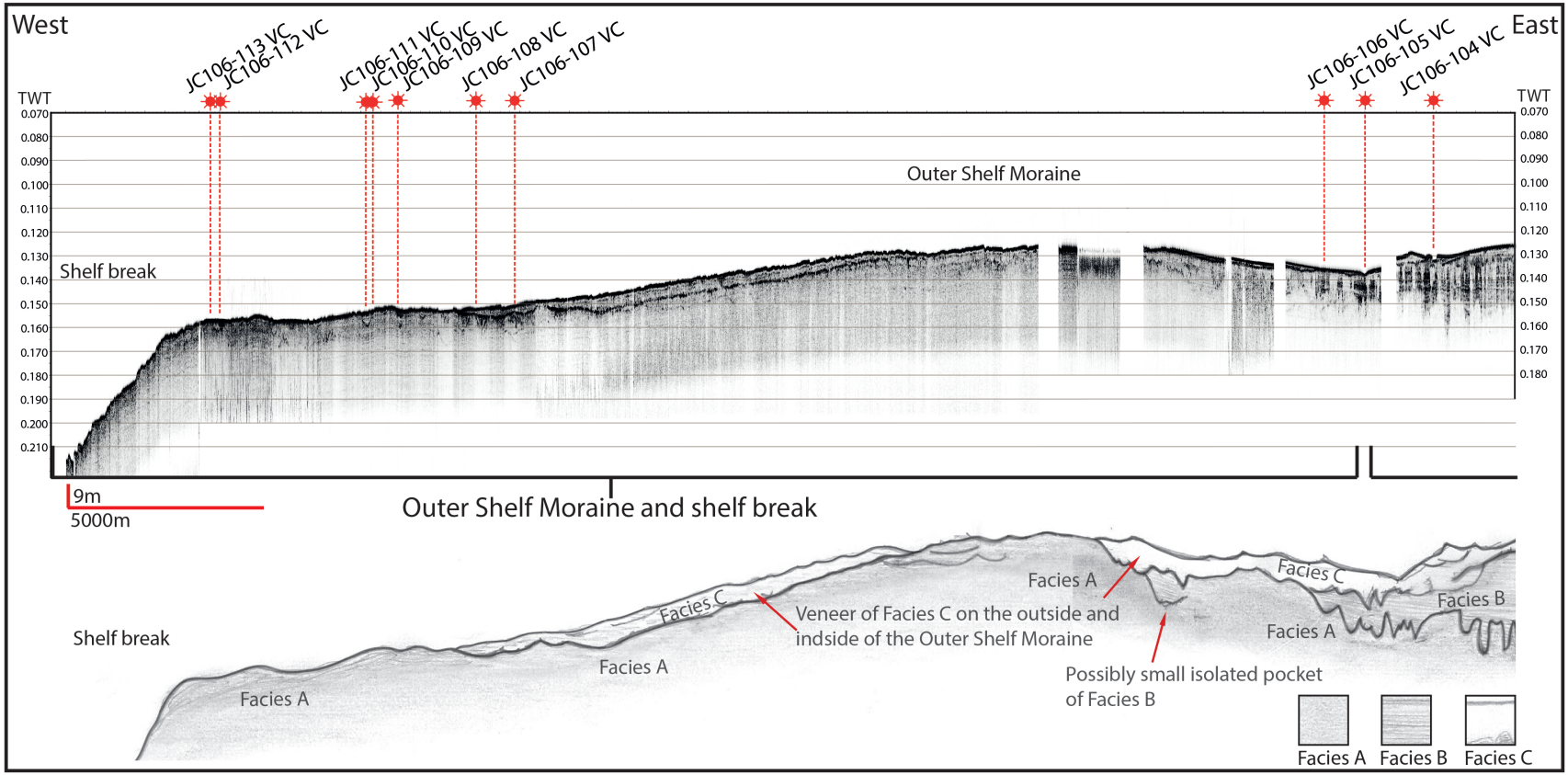

Figure 5.1: SBP of the Outer shelf with distribution of the interpreted acoustic facies. Note that with depth, the acoustic signal fades out, which may obscure identification of any units (if present) underlying Facies A. Note Two Way Time in seconds on the acoustic profile. Horizon to the east on the drawn profile represents the onlapping character of Facies B on to Facies A.

5.2.2 Mid-shelf Basin

The mid-shelf basin is characterised by the distinct topography of the buried moraines formed from Acoustic Facies A, and the overlying thick deposits of Acoustic Facies B (Figure 5.2). Although cores from the mid-shelf basin bottomed out in glacimarine sediments, the acoustic data from here shows the presence of Acoustic Facies A at the base of the sequence (Figure 5.2). The landforms created by Acoustic Facies A are consistent both in their geographical location and dimensions with the moraines found in the northern part of the basin, suggesting that they are the buried southern extension of these moraines (Ó Cofaigh *et al.*, 2012).

In the northern part of the basin, the moraines are 1 to 4 m high and 1 to 3.5 km wide. As the acoustic data show the landforms to the south are 500 to 1000 meters wide, and do not penetrate through the seafloor, indicating that the moraines decrease in both hight and width to the south (Figure 5.2). Burial is due to the thick sequence of glacimarine sediments (Acoustic Facies B), overlying them. This further supports the interpretation of Acoustic Facies B as glacimarine sediment deposited after the formation of the moraines and infilling the low lying areas between them and in the case of the southern transect, draping the moraines as well. The onlapping character of Acoustic Facies B on to the moraines is then a result of deposition in a glacimarine environment. The nested pattern of these moraines indicates slow retreat with repeated stillstands and even minor re-advances of the ice sheet margin across the shelf during deglaciation (Dowdeswell *et al.*, 2008; Ó Cofaigh *et al.*, 2012). Facies B between the moraines indicate that retreat occurred in a glacimarine environment.

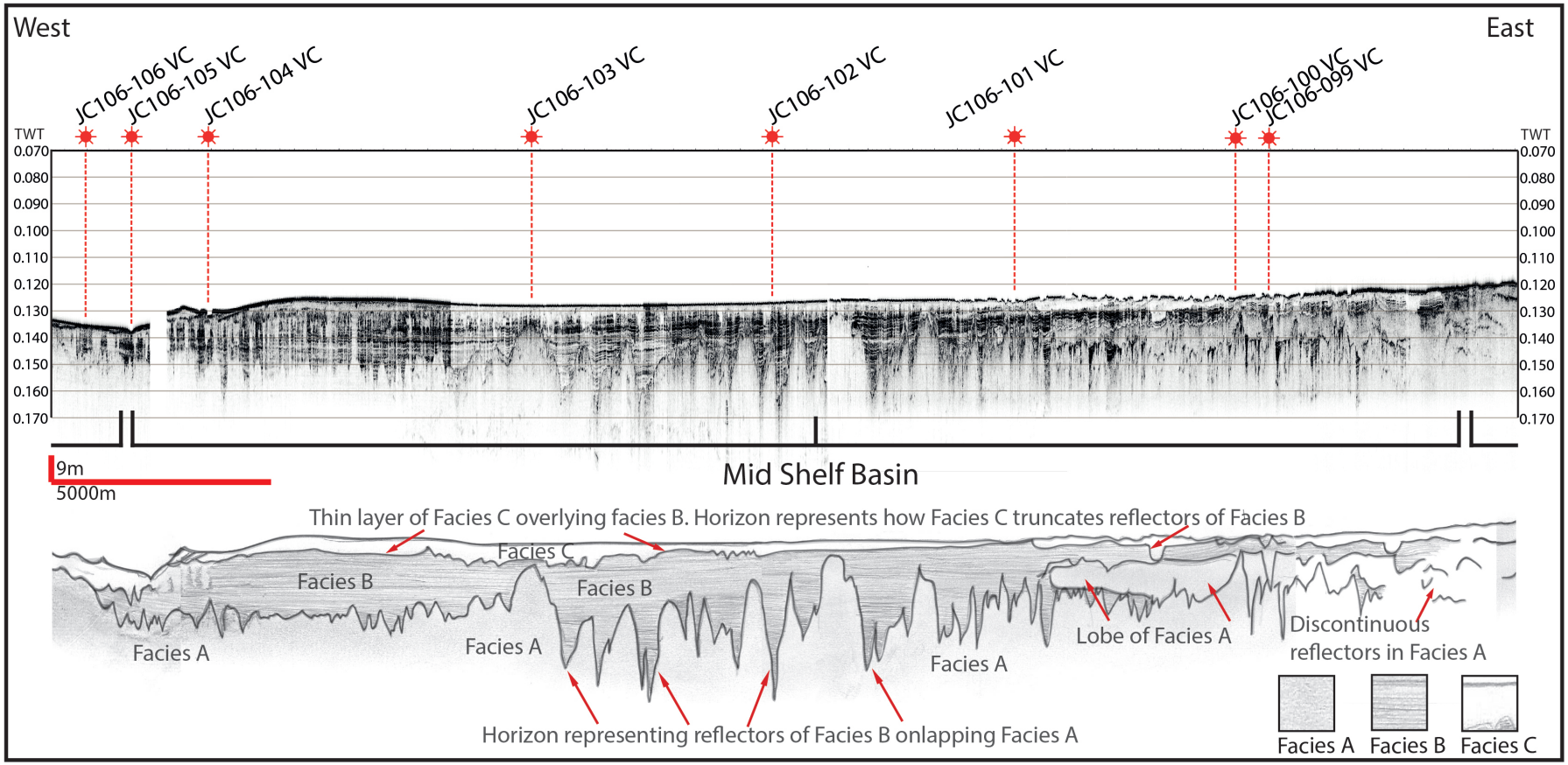

Figure 5.2: SBP of the mid-shelf basin, with distribution of the interpreted acoustic facies. Note that with depth, the acoustic signal fades out, which may obscure identification of any units (if present) underlying Facies A. Note Two Way Time in seconds on the acoustic profile. THe interpreted horizon on the drawn profile seperating Facies A and B represents the onlap of reflectors in Facies B. It is clearly seen how Facies B infill the topography of Facies A across the Mid Shelf Basin.

5.2.3 Donegal Bay Moraine

The morphology of the large sediment ridge at the mouth of Donegal Bay is consistent with its interpretation as a moraine, termed here the 'Donegal Bay Moraine' (DBM) (cf. Benetti *et al.* 2010; Dunlop *et al.* 2011; Ó Cofaigh *et al.* 2012), and this interpretation is supported by the new acoustic data from this study. Figure 5.3 shows that Acoustic Facies A constitutes the core of the western ridge. Acoustic Facies B onlaps the eastern flank, with faint isolated and deformed pockets incorporated into the eastern ridge. With the interpretation of Acoustic Facies A as subglacial till, it is inferred that formation of the DBM must have taken place either during an ice marginal still-stand and/or as a result of a re-advance(s). Acoustic Facies B is also seen folded and deformed between the two ridges of the DBM (Figure 5.3), and this, in conjunction with the segmented reflectors seen on the western slope of the moraine (Figure 4.4 insert A and B), suggests a re-advance which cannibalised and deformed previously deposited glacimarine sediments into the DBM. This is further supported by the two NW-SE profiles from the eastern ridge of the DBM (Figures 4.5 and 4.6) which show that it consists of glacimarine sediments. On both these profiles, Acoustic Facies B can be traced almost as a continuous facies, onlapping the western ridge of DBM. In line 0542 (Figure 4.5), the reflectors of Acoustic Facies B can be seen to have been deposited directly on the eastern flank of the western ridge. These two profiles (Figures 4.5 and 4.6) indicate that, in contrast to the western ridge of the DBM, the eastern ridge does not consist of till, but rather glacimarine sediments.

The very strong, discontinuous reflector seen under the eastern ridge in these profiles (Figures 4.5 and 4.6) can be followed westward for about 1 km and eastward for about 3 km. This reflector could have one of two possible origins. Previously acquired SPB data from Donegal Bay, collected by the Marine Institute and the Geological Survey of Ireland in 2002 (see section 5.2.5 below), have shown evidence of high lying and outcropping bedrock in other parts of the bay (Marine Institute, and Geological Survey of Ireland, 2002). There is therefore the possibility that this reflector could represent a pre-glacial surface, possibly a bedrock high, onto which the re-advancing ice, forming the western ridge of the DBM was hinged onto. A second explanation could be that this reflector could be correlated to the reflector separating Acoustic Facies A and B in the mid-shelf basin, i.e. it separates subglacial morainic sediments from stratified deglacial glacimarine sediments. This interpretation supports the formation of the western ridge of the DBM as a result of a re-advance deforming pre-existing glacimarine sediments. The DBM can therefore be regarded as a two part feature, with formation of the ridges as a result of the reworking of glacimarine sediments, followed by further proximal glacimarine sedimentation on the eastern flank of the moraine after the re-advance.

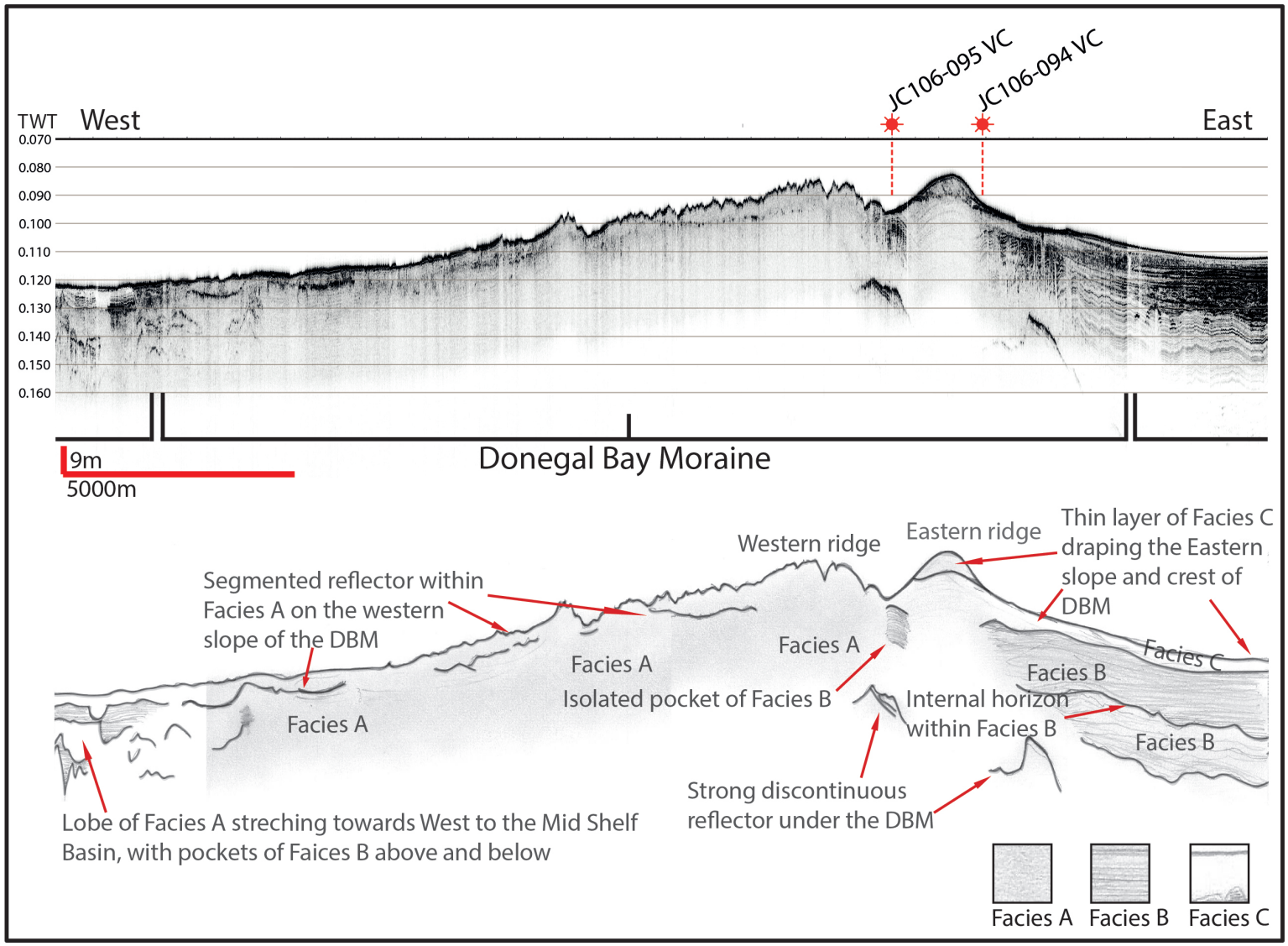

Figure 5.3: SBP of the DBM with a hand drawn sketch showing the distribution of the interpreted acoustic facies. Note that with depth, the acoustic signal fades out, which may obscure identification of any units (if present). This could be the case to the east, where no facies can be recognised below facies B. Note Two Way Time in seconds on the Acoustic profile. The drawn sketch have some exaggeration to better visualise the Facies. Internal horizon within Facies B to the east, show a shift from dense to less dense reflectors, and are not a shift in Facies.

5.2.4 Inner bay basin

The inner bay basin is dominated by the glacimarine sediments of Acoustic Facies B (Figure 5.4). Deposition of this facies must have taken place in front of the retreating ice margin, suggesting that the near horizontal reflectors, which on-lap Acoustic Facies A, have been deposited in a glacimarine environment as the glacial margin retreated back. Truncation of the horizontal reflectors of Acoustic Facies B against the overlying Acoustic Facies C, indicates erosion associated with emplacement of this capping facies, due to post glacial bottom current reworking. The thin 'spikes' or blank zones seen protruding up through Acoustic Facies B in the eastern part of the basin (Figure 5.4) are unlike any landforms associated with Acoustic Facies A, and are therefore interpreted as zones of gas blanking (Riedel *et al.*, 2002).

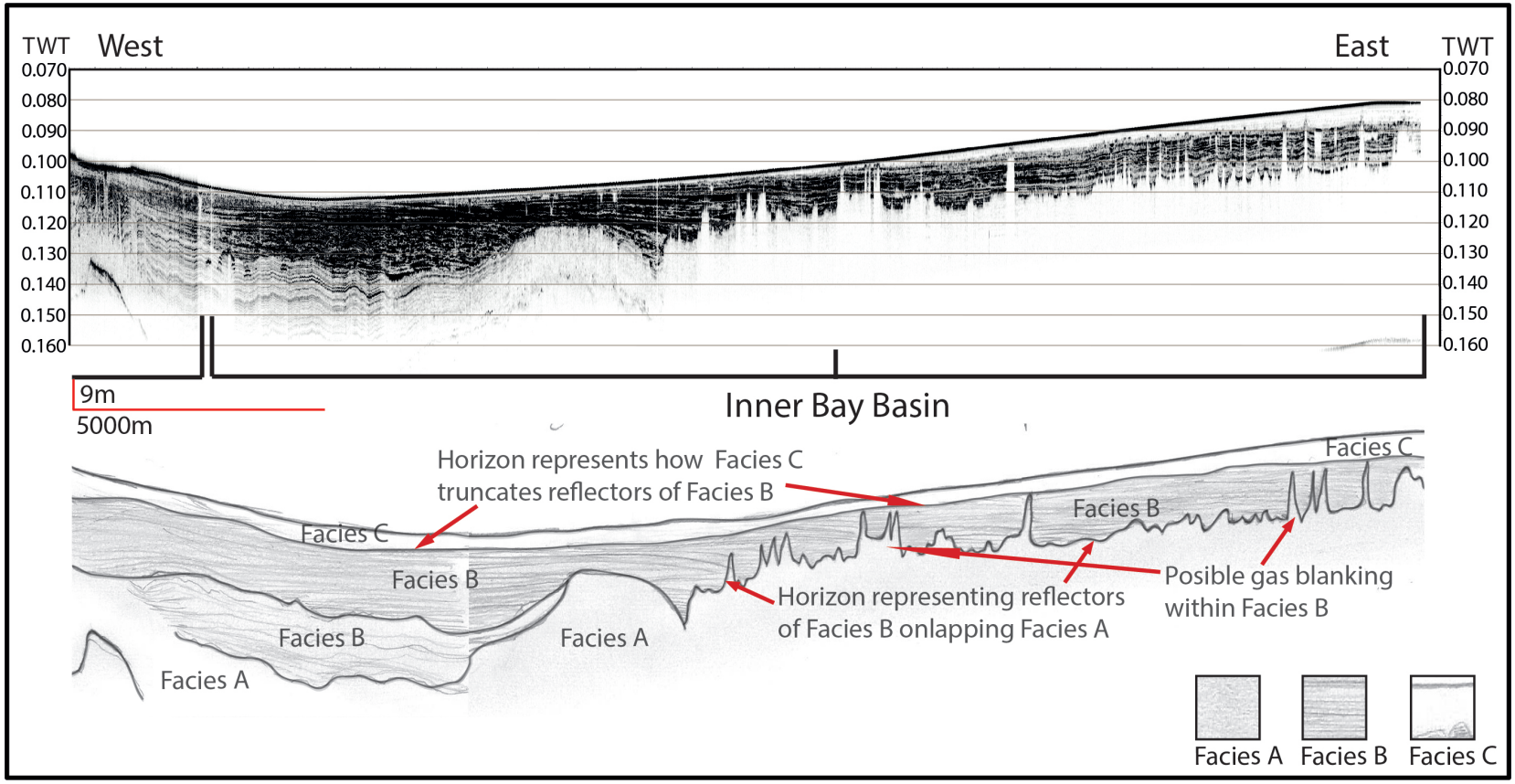

Figure 5.4: Acoustic facies and associated interpretation from the inner bay basin. Note Two Way Time in seconds on the acoustic profile.

5.2.5 Additional SBP data

These three Acoustic Facies described in this thesis, have also been recognised in previously acquired SBP data from Donegal Bay, collected by the Marine Institute and the Geological Survey of Ireland in 2002. Here the top most Acoustic Facies is described as acoustically transparent and distributed as a veneer overlying well-layered sediments, with increasing thickness towards the inner bay, where it in places exceeds 15 m. This facies is interpreted as comprising clays, silt and sands of post-glacial or Holocene age, probably formed in open marine conditions (Marine Institute, and Geological Survey of Ireland, 2002).

Underlying this facies, the Marine Institute, and Geological Survey of Ireland (2002) describes a facies characterised as acoustically well layered. The most extensive distribution of this facies is in the inner bay and mid shelf basins, where it attains thicknesses of up to 35 m. The base of the facies is described as unconformable, and it is indicated that this facies infills the underlying topography. The facies is interpreted as comprising clays, silts and fine sand, and the age has been interpreted as late-Pleistocene to Holocene, deposited in a variety of glacimarine and open marine conditions.

The third acoustic facies, described by the Marine Institute, and Geological Survey of Ireland (2002) as underlying the previous two, is characterised as being acoustically chaotic and structureless. In places it its seen to outcrop at, or close to the seabed. The top of the facies is described as unconformably underlying the well layered sediments of the overlying facies, and where seen, the base is a marked unconformity with a highly irregular rock surface. This facies is interpreted as comprising glacial till of Pleistocene age, and with a marine/glacimarine origin.

Further, the Marine Institute, and Geological Survey of Ireland (2002) also describes outcropping bedrock at several locations in the bay, most extensive in the coastal areas. Bedrock is also described in the inner bay and mid shelf basins, but here limitations in the data make it impossible to discriminate between bedrock and the overlying acoustically chaotic facies, and material interpreted as bedrock could therefore in those places alternatively represent till.

The Marine Institute and the Geological Survey of Ireland acquired SBP data from most of Donegal Bay, and the shelf, both north and south of the JC106 line (Figure 3.4). With the similarities between the Acoustic Facies in the two data sets, it can be implied that distribution of the three facies recognised in the JC106 SBP data, can also be extended to a much wider part of Donegal Bay.

5.3 Sedimentology, lithofacies associations and foraminifera assemblages

Twelve lithofacies (Dmm, Fmd, Gms, Gm, Guf, Guc, Sm, Sh, Suf, Suc, Fm and Fl) were identified, based on the distinctive combination of visual and physical characteristics, outlined in chapter 3 and described in chapter 4. Based on the interpretations of the lithofacies, these are built into three lithofacies associations (LFA), which represent the depositional environment from ice sheet advance, through retreat, to post-glacial marine sedimentation. Foraminiferal assemblages in the sediment are a result of the depositional environment, and specific indicator species are therefore expected to be found associated with the LFAs.

5.3.1 LFA 1 *Subglacial till*

Based on its massive, over-consolidated, matrix-supported structure (Figure 4.18 A and B), the Dmm in the base of cores JC106-112, JC106-111, JC106-108 from the outer shelf, and from cores CE08-011, CE08-010 and CE08-008 from the mid-shelf basin, are interpreted as subglacial till, deposited by grounded ice (Ó Cofaigh *et al.*, 2001; Evans *et al.*, 2005). Highly consolidated diamictons, similar to those found in the base of these cores, have also been documented in cores from the Antarctic shelf where they have been interpreted as subglacial tills (e.g., Shipp *et al.* 2002; Ó Cofaigh *et al.* 2005). As seen in the sub-bottom profile of the outer shelf moraine (Figure 5.1) Acoustic Facies A (sub-glacial till) is found under the seafloor reflector. Cores that penetrated Acoustic Facies A on the outer shelf recovered Dmm lithofacies in the base, thereby supporting the interpretation of Acoustic Facies A as sub-glacial till. The presence of marine shell fragments in the till in core JC106-112 from the shelf edge indicates that the advancing ice-sheet incorporated pre-existing marine sediments into the till during advance (cf. Peters *et al.* 2016). Foraminifera were only acquired from LFA 1 in two samples from the base of core CE08-010 (Figure 4.20), and was dominated by *Elphidium excavatum f. clavata* and *Cassidulina reniforme*, species indicative of cold glacimarine conditions (see also LFA 2 below).

5.3.2 LFA 2 *Glacimarine mud and sand*

Finely laminated clay and silt are common in contemporary glacimarine systems, from temperate to high polar regions (Mackiewicz *et al.*, 1984; Domack, 1990; Dowdeswell *et al.*, 2000; Ó Cofaigh *et al.*, 2001; Ó Cofaigh & Dowdeswell, 2001), as well as from mid- to high-latitude Quaternary and pre-Quaternary sedimentary sequences interpreted to be glacimarine in origin (McCabe *et al.*, 1986; Hambrey & McKelvey,

2000). The Fl lithofacies seen in cores JC106-106, JC106-102, JC106-101, JC106-100 and JC106-099 in the mid-shelf basin, are therefore interpreted as having been deposited in a glacimarine environment during retreat of an ice margin, that was extended offshore and grounded on the continental shelf. Suspension settling from turbid meltwater plumes, turbidity-current deposition and contour-current activity are all known for producing laminated glacimarine sequences (Gilbert *et al.*, 1998; Cowan *et al.*, 1999; Howe & Pudsey, 1999), and it is therefore difficult to interpret the depositional environment of the Fl lithofacies based solely on the characteristics of the lithofacies, although it is inferred that they occurred during deglaciation when the ice sheet retreated across the shelf in a glacimarine setting. Foraminiferal assemblage data from this lithofacies supports this interpretation, and will be discussed below.

The laminated silt and clay have an on-lapping relationship with the underlying lithofacies (Figures 4.3 and 5.2), and the laminae are horizontal to sub-horizontal with little deformation. These characteristics are compatible with sedimentation through suspension settling from turbid overflow meltwater plumes (Mackiewicz *et al.*, 1984; Cowan *et al.*, 1999). The thick succession of Fl lithofacies, seen in the sediment cores (up to 4.5 m) (Figures 4.12 and 4.13), but as thick as ∼40 m in the SBP data (Acoustic Facies B) (Figure 5.4), implies high sedimentation rates on the shelf. Such high sedimentation rates would inhibit macrofaunal colonisation and bioturbation of the sediment, which would otherwise destroy the parallel lamination (Ó Cofaigh & Dowdeswell, 2001). This suggests that deposition of the Fl lithofacies occurred in ice proximal rather than ice distal glacimarine environment.

The massive silt and clay facies (Fm) generally occurs in successions up to 1 m thick, although in two cores (JC106-105 and JC106-100) successions up to 2 m are seen. This lithofacies often has a more silty component than the Fl facies and contains shells and shell fragments, as seen in the x-radiographs (Figure 4.19). The change from Fl to more massive Fm facies could indicate slower sedimentation with macrofaunal colonisation and bioturbation in a more distal glacimarine setting, and the increase of silt could be an indication of a greater increase in the delivery of iceberg-rafted sediment. The relatively constant magnetic susceptibility throughout this lithofacies supports mixing from bioturbation, which has resulted in a magnetically homogeneous sediment.

Horizontally laminated sand (Sh), shows many characteristics consistent with sediments deposited by turbidity currents. These include: a variable lamina geometry and thickness, convoluted lamination, disrupted lamination by injection of mud from underlying lithofacies, sharp lower and upper boundaries, and massive internal structure (Figure 4.19) (Stow & Shanmugam, 1980; Ó Cofaigh *et al.*, 2001). However, these characteristics are not indicative of turbidity currents alone, as mass or debris flows and slumps from the

side of moraines, could also produce these features in the sediment. However, as most of the Sh lithofacies was acquired from the mid shelf basin with no moraines in the near vicinity, such interpretations are most unlikely.

Sediment cores with Fl, Fm, Sh, and Sm lithofacies were recovered from Acoustic Facies B across the shelf and are primarily found in the mid-shelf basin (Figures 4.10 to 4.15). This supports the interpretation of Acoustic Facies B as a product of ice-proximal glacimarine sedimentation, and these lithofacies are therefore grouped inro LFA 2; glacimarine mud and sand.

Foraminifera assemplages of LFA 2

Foraminiferal samples from LFA 2 are dominated by *Elphidium excavatum f. clavata* and *Cassidulina reniforme* (Figures 5.5, and 5.6). These two species are opportunistic (Murray, 1991; Kowalczuk *et al.*, 2013) and are associated with modern Arctic and glacimarine conditions from Svalbard (Hald & Korsun, 1997; Kowalczuk *et al.*, 2013), tidewater glaciers from northern Siberia (Korsun & Hald, 1998) sediments from the Central and Northern Barents Sea (Hald & Steinsund, 1996) and late Quaternary shelf sediments from Canada (Mudie *et al.*, 1984). *E. excavatum f. clavata* often dominates these samples with an abundance of over 50 % and is known to thrive in glacimarine conditions (Feyling-Hanssen, 1972; Vilks, 1981).

Both *E. excavatum f. clavata* and *C. reniforme* are strongly related to temperature, and *C. reniforme* also seems to be restricted to waters with normal marine salinity (Mudie *et al.*, 1984; Hald & Steinsund, 1996). *E. excavatum f. clavata* adopts both epifaunal and infaunal strategies to live and thrive in highly variable environments with high turbidity, high sedimentation rates, changing salinity, low ($\leq 1°$C) water temperatures and changing sea ice cover, typical of ice proximal, glacimarine conditions (Murray, 1991; Hald & Steinsund, 1996). *C. reniforme* is quick to respond to seasonal and environmental changes, such as pulses of organic material, oxygen starvation or seasonal sea-ice cover, and it is abundant in cold waters ($\leq 2°$C) with normal marine salinity, low turbidity and soft seafloor sediments (Hald & Steinsund, 1996; Kowalczuk *et al.*, 2013).

5.3.3 LFA 3 *Post glacial marine sand and gravel*

Based on its stratigraphic position, coarseness, thickness and spatial distribution, the massive structureless sand (Sm facies) found in the inner bay cores, and which cap of many cores from across the shelf, is interpreted as post-glacial reworked sand. The thin (up to 50 cm) successions of Sm lithofacies found in cores JC106-106, JC106-105 and CE08-010 from the mid-shelf basin are in terms of their sedimentary structures, grain size

and sorting, the same as the thick successions of Sm found in the inner bay. However, in the mid-shelf basin Sm lithofacies is also seen interbedded with facies Fm or Fl lower in the cores. This cyclicity between finer and coarser sediments, could indicate close proximity to an oscillating ice margin, and the Sm facies found in these cores would therefore have a different depositional environment to the capping post-glacial sands from inner bay. The Sm lithofacies found in these cores is therefore interpreted as part of LFA 2, which is related to glacimarine deposition.

The distribution of these lithofacies, with thick successions in the inner bay and thin caps in many cores across the shelf, is consistent with the spatial distribution of Acoustic Facies C, which overly glacimarine facies (facies B). This supports the interpretation of this lithofacies as post-glacial reworked sand and gravel and can be regarded as LFA 3; post-glacial sand and gravel.

Cores from the northern transect have relatively thick caps of LFA 3, while cores from the southern transect tend to have a thin cap in the top. Facies Gms often form a mixing zone between overlying Gm and underlying Sm or Fm lithofacies. Facies Gm is interpreted as current reworked gravel, based on the palaeoenvironmental analysis which show high abundance of *Cibicides lobatulus*, a species which prefers strong bottom currents (Hald & Steinsund, 1996), as well as its well sorted, clast-supported nature and association with capping coarse-grained deposits (Sm and Gms) which form the uppermost part of the cores.

Foraminifera assemplages of LFA 3

Foraminiferal samples from LFA 3 show a higher diversity than LFA 1 and 2, with high abundance of *Cibicides lobatulus* and *Textularia sagittula*, a clear decrease in *E. excavatum f. clavata* and *C. reniforme*, and a relatively high abundance of planktic species (Figure 5.5). *C. lobatulus* thrives in coarse-grained sediments with high hydrodynamic activity (Hald & Steinsund, 1996; Gooday & Hughes, 2002; Schonfeld, 2002). As *C. lobatulus* is found both in the Barents Sea (Hald & Steinsund, 1996) and from temperate waters from the Gulf of Cadiz (Schonfeld, 2002) its presence cannot be used as a proxy for temperature, but with the high abundance of planktic species, this foraminifera assemblage indicates highly active bottom current conditions.

5.3.4 Interpretation of foraminiferal assemblages

Korsun & Hald (1998) find that the *C. reniforme* to *E. excavatum f. clavata* ratio increases with an increase of organic carbon and phytoplankton, and it is thus inferred that *C. reniforme* exceeds *E. excavatum f. clavata* in food-rich environments, where glacial activity is moderate. This correlation can therefore be

interpreted as a proxy for ice margin proximity. *E. excavatum f. clavata* dominates proximal to the glacier margin where high sedimentation rates, high turbidity and changing salinity due to meltwater discharge are the dominant environmental condition (Korsun & Hald, 1998). More distal to the ice margin, although still influenced by seasonal ice cover and temperatures of $\leq 2°C$ (Hald & Steinsund, 1996), *C. reniforme* becomes more dominant, due to more stable salinity conditions and an abundance of organic material.

This relationship can be seen in samples from core CE08-010 (Figure 5.5). Here *E. excavatum f. clavata* dominates at the base of the core with over 50% abundance, but decreases up through the core in LFA 2, to an abundance of ∼20% at 352 cm b.s.f. The abundance of *C. reniforme* increases up through LFA 2, from ∼25% at the base of the core, to abundances of ∼60% at 352 cm b.s.f. (Figure 5.5) Above this, *C. lobatulus* and *T. sagittula* become dominant, due to the coarse grained, bottom current reworked Gms lithofacies in the core. A peak in planktic foraminifera is also evident at 352 cm b.s.f. This could indicate open marine waters, possible with high hydrodynamic activity at the seabed. From 272 cm b.s.f. *C. reniforme* again becomes dominant, with a low abundance of *E. excavatum f. clavata*, but towards the top of the core, bands of coarse grained sediment of LFA 3 give a more mixed signal, with equal abundance of *C. reniforme* and *E. excavatum f. clavata* and a relatively high abundance of *C. lobatulus*.

Like the glaciamarine sections of core CE08-010, palaeoenvironmental analysis of core JC106-102 also show a high abundance of *E. excavatum f. clavata* and *C. reniforme* (Figure 5.6), with up to 40% of each species in some samples. The sediments in the core comprise LFA 2- glacimarine, and the foraminiferal assemblage clearly supports this, with very low abundance of planktic species or benthic species such as *C. lobatulus*. In the bottom half of the core, a decrease in *C. reniforme* corresponds with an increase in *E. excavatum f. clavata*, but this trend is reversed in the upper half of the core (Figure 5.6). This change in species abundance could be an indication of small changes in the distance to the ice margin. Samples from this core show a relatively high abundance of *Elphidium excavatum f. selseyenses* (up to about 30 % in some samples)(Figure 5.6). *E. e. selseyensis* is common in boreal environments (Feyling-Hanssen, 1972; Murray, 1991), and is therefore not to be expected in a sediment interpreted as glacimarine, such as LFA2 in core JC106-102. However, this species can be confused with *E. excavatum f. clavata*, as their morphologies often appear similar (See chapter 3.4) (Feyling-Hanssen, 1972); indeed *E. excavatum f. clavata* has been interpreted as a juvenile form of *E. e. selseyenses* in previous studies (Feyling-Hanssen, 1972). There is therefore a good reason to believe that the high abundance of *E. e. selseyenses* in reality is an intermorph form of *E. excavatum f. clavata*.

Quinqueloculina seminulum makes up 10 to 20 % of assemblages in some samples. This species, along

with other less common species such as *Textularia sagittula, Cassidulina lavigata, Bolivina sp. Bulimena marginata, Miliolinella sp. Nonionella labradoraca and Quinqueloculina lata*, have all been identified in Arctic or Subarctic environments (Korsun & Hald, 1998), and from glacimarine clays interpreted as high Arctic (Feyling-Hanssen, 1953). Thus, based on the primarily Arctic species assemblage and the lack of any warm water indicator species in any of the samples, the depositional environment during formation of LFA 2 and during deglaciation is interpreted as glacimarine.

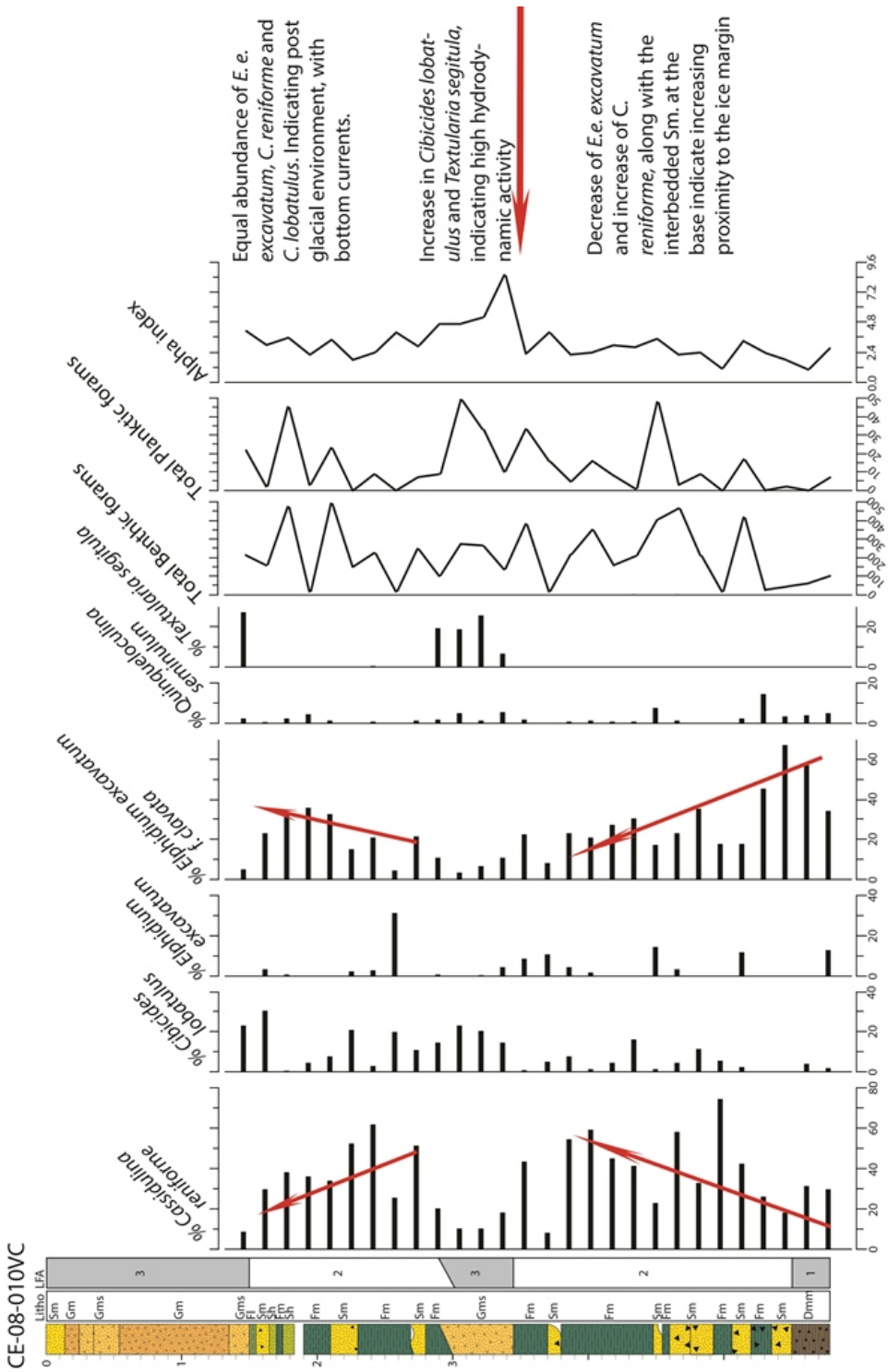

Figure 5.5: Foraminiferal assemblage data from core CE08-010 with accompanying lithofacies log.

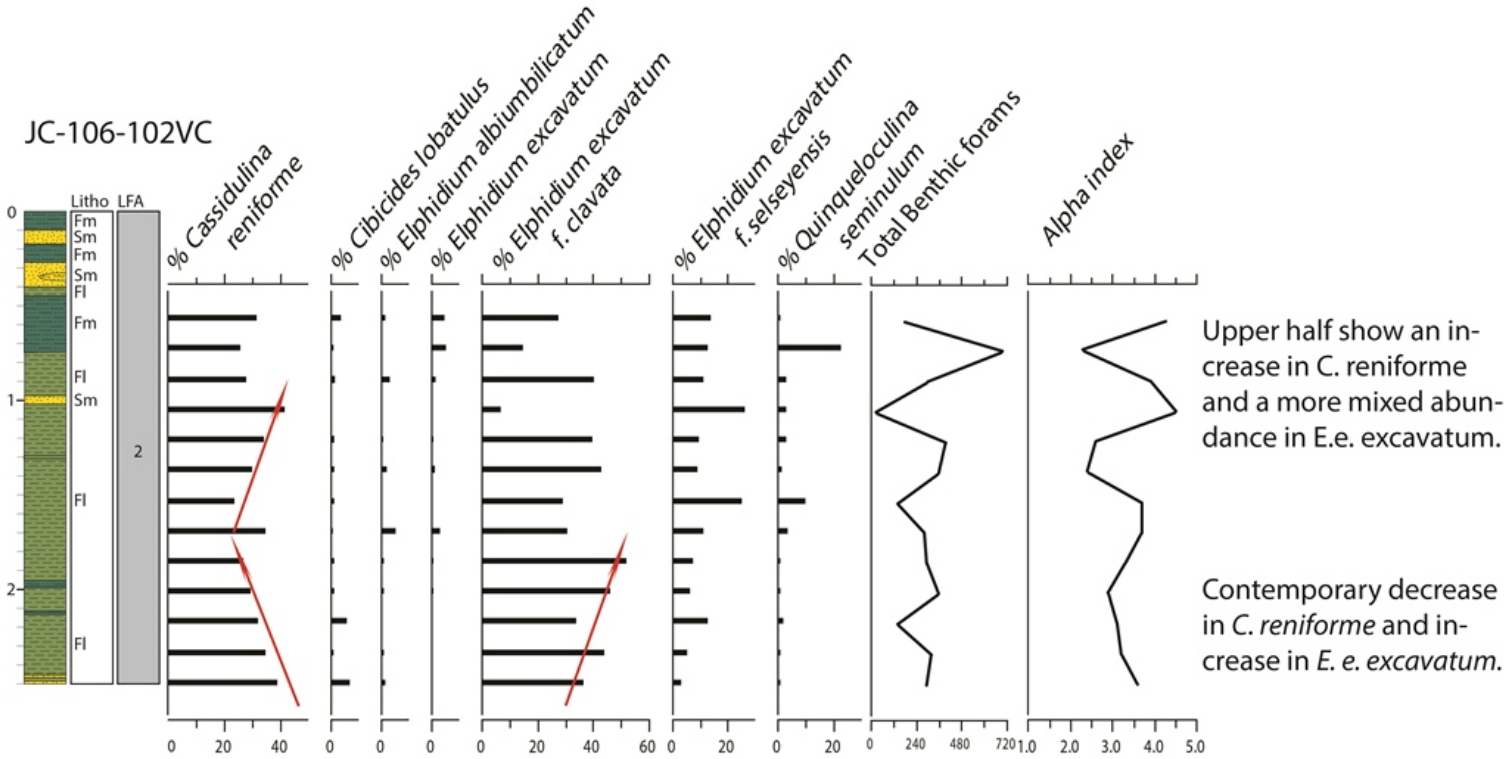

Figure 5.6: Foraminiferal assemblage data from core CE08-102 with accompanying lithofacies log.

5.4 Distribution of LFAs across the shelf

5.4.1 *Southern transect*

Interpretations of the LFAs enables correlation between the sediment cores and allows for extrapolation of the LFAs across the shelf, making it possible to visualize the spatial distribution of different depositional environments (Figure 5.7). In the southern transect (Figure 5.7) a clear division in the LFAs is seen, following the three areas: outer shelf, mid-shelf basin and inner bay.

On the outer shelf, extrapolation show thick units of subglacial till, overlain by a thin layer of post-glacial sediment (LFA3). This is also seen in the SBP data (Figure 5.1), where thick units of Acoustic Facies A is overlain by a thin veneer of Acoustic Facies C. This suggest initial deposition of subglacial till (LFA1) at the shelf edge by a grounded ice-margin, with the subsequent removal of any glacimarine sediment due to strong bottom-current reworking which eroded the deglacial sediments. The overlying thin layer of post-glacial sediments (LFA3), is most likely a result of bottom current reworking and removal of fine grained material, rather than post-glacial deposition.

Thick units of glacimarine sediments (LFA2) occur across the mid-shelf, where they are overlain by a thin cap of post-glacial sediments. Subglacial till was not recovered in the cores but it likely underlies LFA2 at depth, as the cores from here bottomed out in glacimarine sediment, and as Acoustic facies A is clearly seen on the SBP data on the mid shelf basin (Figure 5.2). The thick units of glacimarine sediments indicate a slow retreat across the mid-shelf basin, an interpretation that is consistent with the presence of the closely spaced nested arcuate recessional moraines imaged on the multibeam data (Benetti *et al.*, 2010; Ó Cofaigh *et al.*, 2012) (Figure 2.8). The interbedded units of Sh and Sm lithofacies within Fl and Fm lithofacies in the cores JC106-106 and JC106-105 (Figure 5.7) could be the result of suspension settling from turbid overflows, or sandy turbidites from sediment-rich underflows, both deposited in relatively close proximity to the ice margin, (Ó Cofaigh & Dowdeswell, 2001). The other cores in the mid-shelf basin show thick sequences of Fl facies at the base, overlain by Fm facies towards the top. This indicate an increasingly ice distal setting, where laminated silts and clay grade up into massive bioturbated mud (Ó Cofaigh & Dowdeswell, 2001).

The massive diamictic mud (Fmd) at the base of core JC106-100 which is then overlain by laminated silt and clay, displays a reverse stratigraphy to that seen elsewhere in the mid-shelf basin. The Fmd facies are very soft and shear strength values ranges from 25 to 37.5 kPa. This facies could be the result of rain-out of clast-rich iceberg-rafted debris. The deposits of LFA 3 in the top of the mid-shelf cores, show thicker units

than on the outer shelf (Figure 5.7), suggesting greater reworking and sediment removal by bottom currents on the outer shelf. Alternatively this could also be related the topography of the deepened mid shelf basin, where more accommodation space have resulted in thicker units of LFA3.

Palaeoenvironmental analysis of LFA 3, from core CE08-010 show a high abundance of *Cibicides lobatulus* and *Textularia sagittula*, two species that thrive in conditions with high hydrodynamic activity (Hald & Steinsund, 1996; Peters *et al.*, 2015), indicating that LFA 3 on the mid-shelf basin, is a result of bottom current reworking.

The inner bay is characterised by thick successions of post-glacial sediments (LFA 3). No other LFAs are seen in cores from this part of the bay, although SBP data show thick sequences of the stratified Acoustic Facies B, which is interpreted as glacimarine, underlying LFA 3 (see section 5.2). With the interpretation of LFA 1 as subglacial till, which in the SBP-data forms the lowermost stratigraphic unit across the shelf, it can be assumed that this would also be the case here. The thick deposits of post-glacial marine sediments in the inner bay, indicate extensive post-glacial reworking of marine sediments into thick accumulations.

5.4.2 *Northern transect*

In the case of the northern transect (Figure 5.7), thick sequences of LFA 3 occur in the top of all the cores from across the shelf. LFA 2 is seen in only a few cores from across the shelf, and is usually significantly thinner than in cores from the southern transect. However, thick deposits of LFA 2 are observed in core CE08-010, from the trough between two moraines on the mid-shelf basin. This suggests the presence of glacimarine conditions across the shelf where-ever LFA 2 is observed. LFA 1 is found in three cores (Cores CE08-008, CE08-010 and CE08-011) from the mid-shelf basin, two of which are taken from the crest of a moraine. The presence of LFA 1 in these two cores (CE08-011 and CE08-008) show that the moraines contain subglacial till. It can therefore be interpreted that LFA 1 was deposited during ice sheet advance across the shelf. Subsequent oscillations and minor re-advances of the retreating ice margin have glacitectonised sediment of LFA 1 into the series of moraines seen across the shelf. With the generally thin sequences of LFA 2 seen in the mid-shelf in the northern transect (Figure 5.7)(except in the trough between two moraines (core CE08-010)) it can be interpreted that thicker sequences of LFA 2 was deposited between the moraines, with a thin cover over the crest of the moraines, as it is seen in the SBP data from the mid-shelf basin in the southern profile.

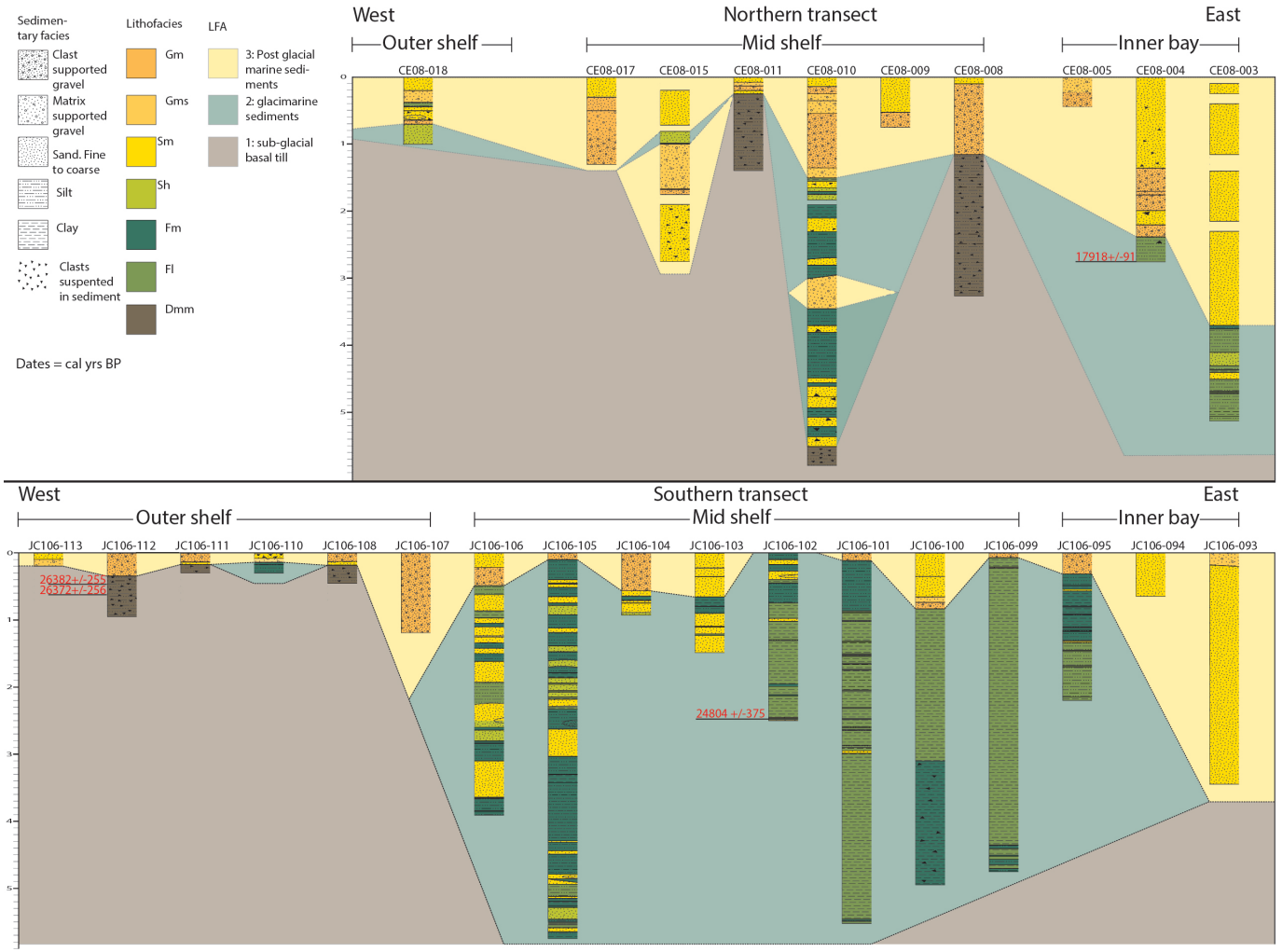

Figure 5.7: Extrapolations of LFAs across the shelf for the northern and the southern transects. Key radiocarbon dates are here shown in red.

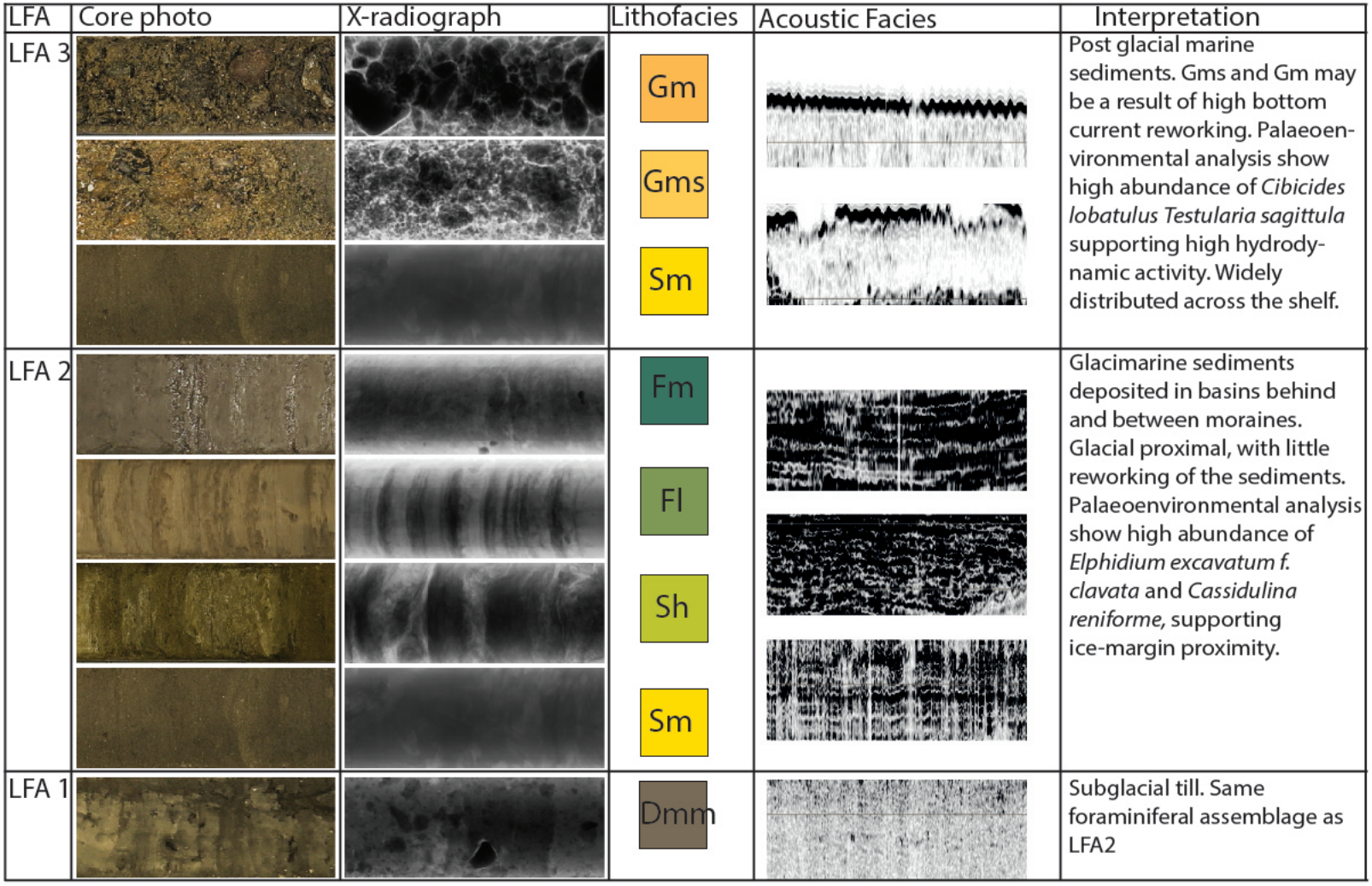

Figure 5.8: Summary information for the three Lithofacies Associations recovered in cores from the study area, showing core photos, X-radiographs, associated Acoustic Facies, lithofacies code and interpretation

5.5 Geochronology

The two radiocarbon dates on reworked shells from subglacial till in core JC106-112 on the outer shelf dated 26,382 cal BP ±257 and 26,372 cal BP± 259 (Figure 5.9 and Table 4.9). These shells were fragments and had been reworked into the till. They therefore provide a maximum age for the till and the presence of grounded ice at the shelf edge occurring after ∼26.3 cal ka BP.

Across the mid-shelf basin, radiocarbon dates generally fall into two groups (Figure 5.9 and Table 4.9). In cores from the northern core transect, three samples (one from Dmm and two from sand lithofacies), have been dated post LGM, in ages between ∼18.0 cal ka BP and ∼13.9 cal ka BP (Table 4.9). From the southern transect, seven samples all taken from glacimarine sediments (LFA 2) result in ages between 26.3 cal ka BP and 19.6 cal ka BP. Samples from the southern transect are generally taken deeper in the cores, although the sample with an age of 19.6 cal ka BP from core JC106-102 was taken towards the top of the core (Table 4.9). In core JC106-103 a mixed benthic foraminiferal sample from Sm lithofacies, taken at the base of the core, 145 cm b.s.f. dated 26.3 cal ka BP. The shallow depth compared to dates from surrounding core sites, and the sedimentary composition of the core consisting of massive coarse sand which is consistent with a subaqueous mass flow, suggests that the enclosing sediment may be reworked. The foraminiferal assemblage in the core could therefore represent an older fauna that provide a maximum age for the surrounding sediment. Furthermore, the standard error for this date is ±247 which potentially overlap the two dates from till at the shelf edge, thus making it likely that the sample is reworked, recording a maximum deglacial age.

The oldest date recording deglaciation of the mid-shelf basin is from benthic foraminifera in laminated glacimarine clay (Fl lithofacies) at the base of core JC106-102. This sample dated 24.8 cal ka BP. (Figure 5.9) and the composition of the lithofacies in the core along with no deformation of the laminae in the sediment, gives no reason to believe any reworking had taken place during or after deposition. This date constrains the timing of retreat from the mid-shelf basin and also provides a minimum date for ice sheet recession from the outer-shelf. Maximum glaciation at the shelf edge and subsequent retreat to the mid-shelf basin must therefore have taken place after 26.3 cal ka BP and before 24.8 cal ka BP. There is ca. 50 km from the location of core JC106-112 on the shelf edge to core JC106-102. Errors in the dates from core JC106-112 gives the oldest possible grounding of ice at 26639 y BP., and errors from the mid-shelf gives the youngest possible retreat at 24618 y BP (Table 4.9). This is a difference of 2021 years thus the slowest possible retreat rate must be 24 m per year circa. The youngest possible grounding at the shelf edge given from the errors in core JC106-122 gives an age of 26113 y BP, and the oldest possible retreat at the mid-shelf basin date to

24990 y BP (Table 4.9). This is difference of 1123 years, and the fastest possible retreat rate must be 44 m per year circa. The retreat rate from the shelf edge to the mid-shelf basin was therefore between 44 and 24 m/y.

The youngest age from the mid-shelf basin, from glacimarine sediments, are from the bottom of core JC106-099 ca. 20 km west of the DBM. A sample taken in laminated glacimarine silt (Fl) dated to 20.2 cal ka BP. Two cores, CE08-004 and JC106-095 are taken directly from the top of, or immediately behind the eastern ridge of the DBM (Figures 4.25 and 5.9). A total of five samples have been radiocarbon dated from these two cores. Four of the dates fall between 17.9 cal ka BP and 15.7 cal ka BP, and are all taken in glacimarine sediments (Figure 4.25 and Table 4.9), and one is significantly younger (13.0 cal ka BP). These dates constrain the age of the formation of the DBM to some time between 20.2 cal ka BP and 17.9 cal ka BP, with the DBM being ice free prior to the later date.

In the inner bay basin, four radiocarbon dates were obtained from Fl lithofaces in core CE08-003 (Figure 5.9). All four dates are within 600 years of each other (4.9), and date 12.8 to 12.2 cal ka BP. These all fall within the global Younger Dryas cooling event, which from δ^{18}O records from Greenland ice cores has been dated to 12.9 to 11.7 (Rasmussen *et al.*, 2006).

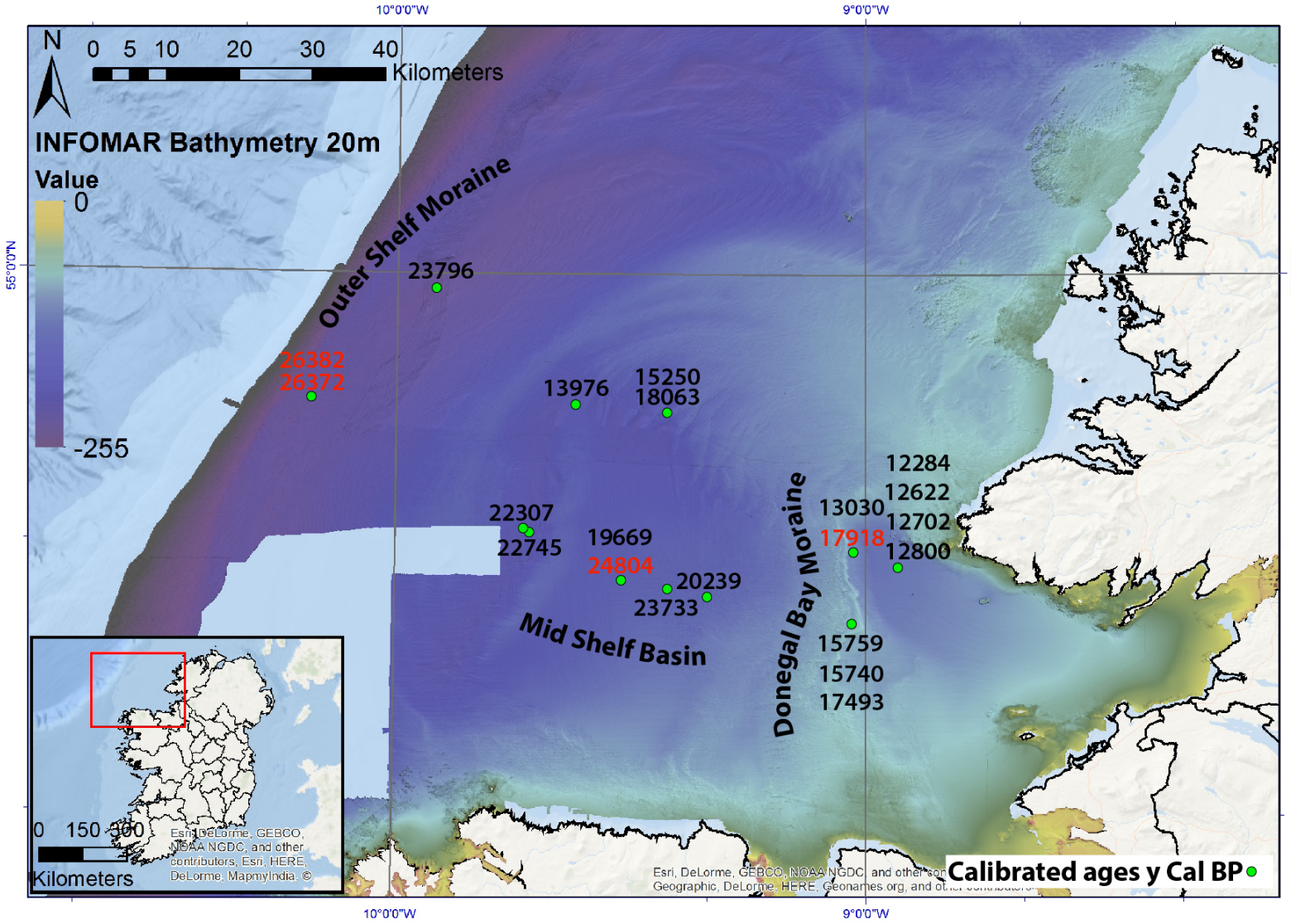

Figure 5.9: Radiocarbon dates from across the shelf. All dates are in y. Cal. PB. Red dates show minimum age on retreat across the shelf. www.infomar.ie.

6. *Discussion*

This chapter will bring together the results and interpretations presented in the previous two chapters in order to create a coherent reconstruction for the Late Quaternary glacial history of Donegal Bay and the adjoining continental shelf. Based on radiocarbon dates presented in the results, it will discuss the timing of ice sheet advance and retreat across the shelf, and in particular ice extent at the LGM, as well as assessing the drivers of retreat. The acoustic facies interpreted from the sub-bottom profiles, and the lithofacies interpreted from the sediment cores, will be used to determine the nature of deglaciation and to provide insights into the retreat dynamics of large ocean-terminating ice sheets, in this case the BIIS along its northwestern margin.

6.1 BIIS extent at the LGM offshore of NW Ireland

As discussed in chapter 2, extent of the Irish part of the BIIS prior to, and at, the LGM has been a source of considerable debate (Figure 6.1). Through the use of terrestrial surface exposure dating, Bowen *et al.* (2002) reported 24 ^{36}Cl exposure ages of onshore areas from widely scattered sample sites lying both within and outside the limits of the traditional ice limits proposed by Bowen *et al.* (1986) (Figure **??**) (Ballantyne, 2010). Bowen *et al.* (2002) grouped these 24 exposure ages in to five groups, each related to a particular deglaciation age (Ballantyne, 2010), with the oldest group consisting of six ^{36}Cl surface exposure dates between 36.5 ±3.6 ka to 25.1 ±1.1 ka. These samples was obtained from ice-moulded bedrock or erratic bounders from various locations in Ireland and were critical as they underpin the interpretation placed by Bowen *et al.* (2002), that the BIIS reached its maximum extent sometime before ∼40 ka BP (during MIS3), with the ice margin fluctuating during the 40-25 ka. period and that the subsequent LGM ice sheet was restricted to the mainland, with its maximum westerly extent marked by terrestrial end moraines on the western and north western peninsulas of Ireland (Bowen *et al.*, 2002).

This interpretation was supported by a series of radiocarbon dates from stratigraphic sequences on the south side of Donegal Bay. Eleven dates from reworked single Arctica Islantica shells from till or deglacial outwash, ranged from 43.8 to 26.1 cal ka BP. and further four dates from in situ *Elphidium excavatum f. clavata* from raised marine muds dating 27.7 to 25.3 cal ka BP. The dates was obtained at c. 80 m OD at Glenulra Farm on the south coast of Donegal Bay (Figure 2.5) (McCabe *et al.*, 2007b). This led to the interpretation by McCabe *et al.* (2007b) that a localised ice dome in North-west Ireland overran the Glenulra

Farm site, and the date of ∼43.8 ka BP. provided a maximum age for this. The altitude of the samples from which these dates have been acquired implies high relative sea level (RSL) due to isostatic depression caused by the proximity of an ice sheet, which depressed the area to a depth of at least 140 m (McCabe *et al.*, 2007b). McCabe *et al.* (2007b) argued that the Glenulra Farm site was not overrun by glacier ice again after 28 cal ka BP. thus supporting the interpretation by Bowen *et al.* (2002) of a restricted ice sheet during the LGM.

There are, however, some problems with these terrestrial surface exposure dates (Ballantyne, 2010), as well as with the deglacial and marine radiocarbon dates found at the Glenulra Farm site, that make the associated interpretations outlined above problematic (cf. Ballantyne & Ó Cofaigh 2017). The six ^{36}Cl exposure dates, critical for the interpretation by Bowen *et al.* (2002), were collected from boulders and glacially-polished bedrock from widely separated locations in Ireland and the uncertainties of ±17ka and ±13ka for two of these dates make it difficult to draw any solid inferences pertaining to age (Ballantyne, 2010; Ballantyne & Ó Cofaigh, 2017). Another of the six ^{36}Cl exposure dates from polished bedrock at Malin Head with an age of 25.1 ±1.1 does not provide any evidence for extensive glaciation during MIS 3, and is furthermore also inconsistent with both radiocarbon dates (McCabe & Clark, 2003) and ^{10}Be exposure dates from the area (Ballantyne *et al.*, 2007), which indicate offshore extension of ice during the LGM in the northern most part of Ireland (Ballantyne, 2010). Subsequent exposure dates collected from neighbouring sites in Ireland (Figure 6.2) imply that the LGM ice sheet actually extended offshore across the shelf, and the pre-LGM exposure dates have thus been interpreted to reflect nuclide inheritance (Ballantyne, 2010). In addition, the radiocarbon dates at Glenulra Farm on the south coast of Donegal Bay were acquired from a combination of reworked *Arctica islandica* shells and apparently in situ *Elphidium excavatum f. clavata* tests. The *Arctica islandica* dates ranges from 43.3 to 26.1 cal. ka BP, and McCabe *et al.* (2007b) infered from this wide range, that high relative sea level caused by isostatic depression due to the proximity of a thick ice sheet, persisted throughout most of this period (McCabe *et al.*, 2007b). However, as the death age of *Arctica islandica* can pre-date re-working by several millennia, these dates cannot be used as indicators for early glaciation (Ballantyne & Ó Cofaigh, 2017); rather they only indicate a maximum age for the sediment. The *Elphidium excavatum f. clavata* dates however, range from 27.7 to 25.3 cal ka BP, with the youngest age aberrant from the other three. These dates could record the growth of a substantial land-based ice sheet by 27.8 to 27.6 cal ka BP, causing isostatic depression accounting for the deposition of apparently *in situ* marine muds at Glenulra Farm c. 80 m OD (Ballantyne & Ó Cofaigh, 2017). As stated by McCabe *et al.* (2007b), these dates appear to indicate that the Glenulra Farm site was indeed not over-run by glacier ice

during the LGM. However, a few kilometres to the west of the Glenulra Farm site, at Belderg, radiocarbon ages obtained on marine shells from glacimarine successions from two separate locations, have yielded ages which indicate deglaciation at around 20.4 to 19.2 cal ^{14}C ka (McCabe *et al.*, 2005), indicating retreat of the ice margin from the shelf edge after $\sim$ 24 ka (Ballantyne & Ó Cofaigh, 2017). If the *Elphidium excavatum f. clavata* dates from the Glenulra Farm site c. 80 m OD, is an indication of isostatic depression due to the proximity of a thick land based ice sheet, and the dates from glacimarine successions at Belderg to the west of Glenulra, is an indication of retreat of the ice margin from the shelf edge after $\sim$ 24 ka, then the deposits found at the Glenulra Farm site must have been preserved, possibly by permafrost under the advancing ice (Ballantyne & Ó Cofaigh, 2017).

The radiocarbon dates acquired in this study, from tills near the shelf edge and from deglacial glacimarine sediments from the mid-shelf basin, directly contradict the notion of a restricted ice sheet in west and northwest Ireland during the LGM. They demonstrate that the Irish Ice Sheet extended to the shelf edge at some point after $\sim$26.3 cal ka BP. with subsequent retreat in a glacimarine environment under way before $\sim$24.8 cal ka BP. IRD records from the Barra-Donegal Fan and the Porcupine Bank (Scourse *et al.*, 2009), indicate the existence of a small BIIS throughout MIS 4 to the onset of the LGM, with marine calving margins and localised ice domes (Scourse *et al.*, 2009). Thus although there does appear to have been ice in existence in Ireland prior to the LGM (cf. Bowen *et al.* 2002 and McCabe *et al.* 2007b) it does not appear to have reached its maximum extent at least along its north-western margin until the LGM. During MIS 2 these ice domes merged into a coherent BIIS, which between $\sim$29.0 cal ka BP and $\sim$27.0 cal ka BP advanced across the shelf. The timing of this maximum extent was inferred to have been between $\sim$27 and $\sim$24 cal ka BP based on deep sea IRD records from along the western margin (Scourse *et al.*, 2009). The two radiocarbon dates from till in core JC106-112 at the shelf edge supports this and allows a more definitive interpretation constraining ice sheet extent at the shelf edge to $\leq$ 26.3 cal ka BP.

As described in section 1.1, the global LGM is traditionally defined as the most recent interval in Earth history when global ice sheets reached their maximum integrated volume (Mix *et al.*, 2001; Clark *et al.*, 2009b). This is based on two independent methods; either by estimating changes in sea level from direct observational evidence of past sea level relative to the present (Figure 6.3), or indirectly from temporal variations in oxygen isotopic composition of the mean ocean water (mow), δ^{18}O_*mow* (Mix *et al.*, 2001; Lambeck *et al.*, 2014), either measured on benthic foraminifera from deep sea sediment cores (Waelbroeck *et al.*, 2002), or directly in the ice cores from, for example, the Greenland Ice Sheet (Figure 6.4) (Svensson *et al.*, 2006; Rasmussen *et al.*, 2008). The RSL curves (Figure 6.3) show a $\sim$120-130 m drop in SL between

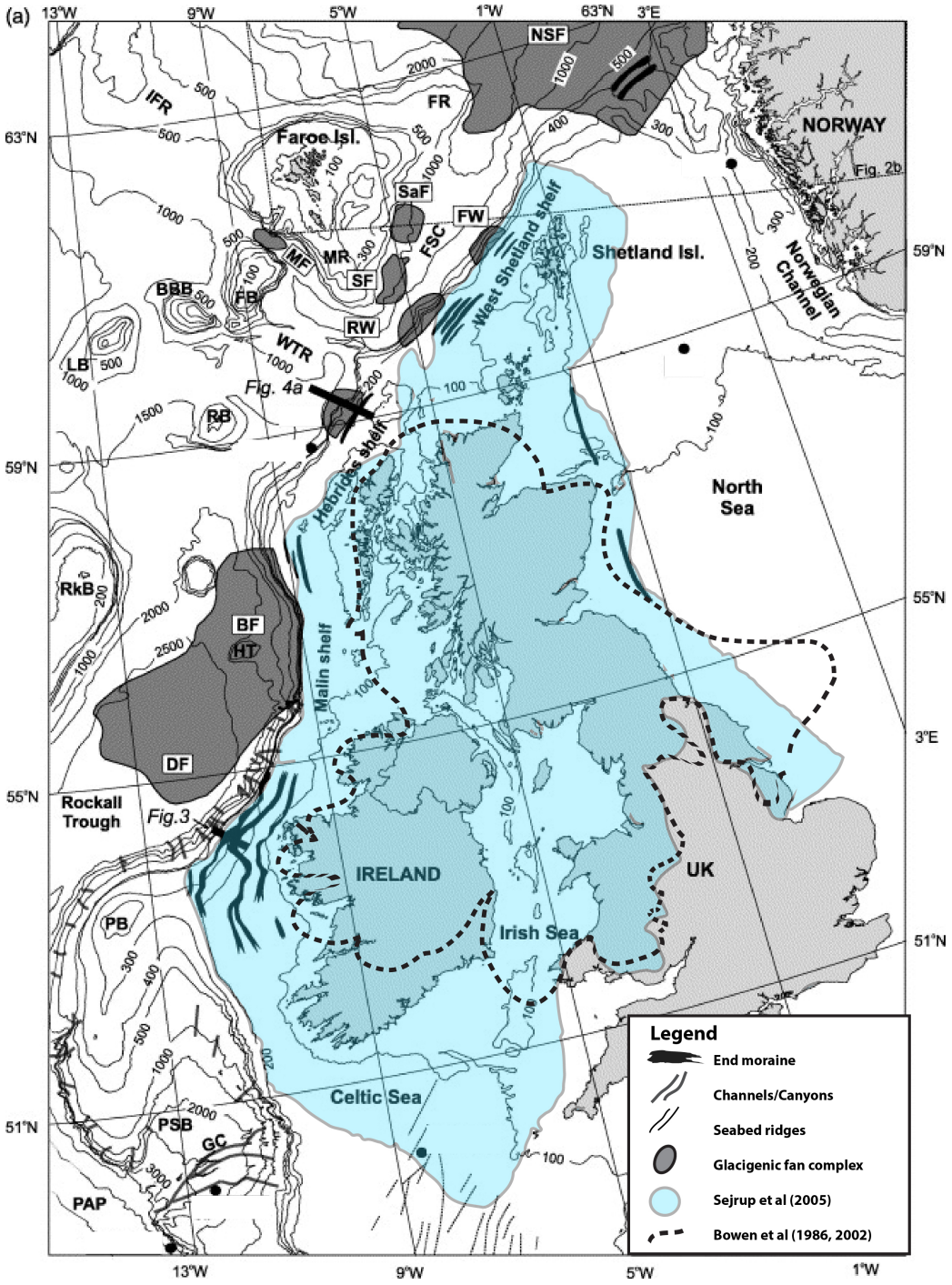

Figure 6.1: The two interpretations of the BIIS extent during the LGM. Dashed line is the interpretation of Bowen *et al.* (1986) while the light blue represent the extensive shelf edge interpretation of Sejrup *et al.* (2005) This large LGM extent is interpreted based on offshore locations of end-moraines, channels and canyons and glacigenic fan complexes. Modified from (Sejrup *et al.*, 2005) and based on (Ballantyne, 2010).

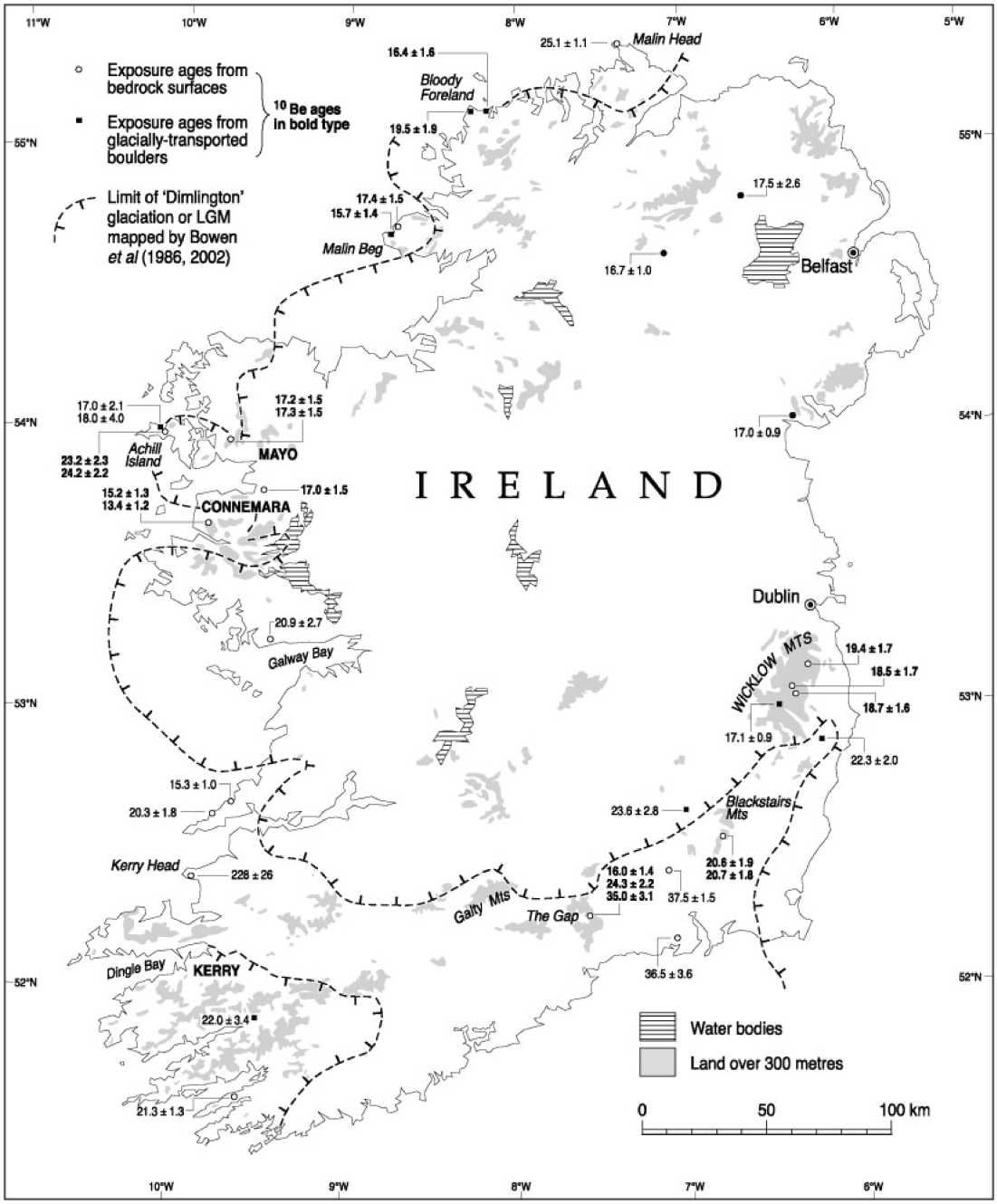

Figure 6.2: Exposure ages obtained from bedrock surfaces and glacially transported boulders in Ireland. ^{36}Cl exposure ages are from Bowen *et al.* (2002), with two dates with large uncertainties (36 ±13 ka. and 31 ±17 ka.) omitted. ^{10}Be exposure ages are from Ballantyne *et al.* (2006, 2007, 2008). Dashed line is the ice limit during the LGM as depicted by Bowen *et al.* (1986). From (Ballantyne, 2010)

~30.0 ka BP and 19.0 ka BP. with the maximum lowstand SL at ~ 21.0 ka BP (Lambeck *et al.*, 2002, 2014; Peltier & Fairbanks, 2006; Clark *et al.*, 2009b), and δ^{18}O curves from the GRIP and NGRIP ice core drilling projects shown on figure 6.4 record a rapid enrichment of δ^{18}O between 24120 and 23440 YB2K, followed by a steady increase, indicating a termination of the LGM after this time. There is therefore a good coherence between the global RSL curves presented by Peltier & Fairbanks (2006); Clark *et al.* (2009b) and Lambeck *et al.* (2014) (Figure 6.3) and the Greenland ice core records (Figure 6.4), both showing that the global LGM occurs between ~30.0 cal ka BP and ~19.0 cal ka BP. However, there is considerable variation in the timing of regional and local last glacial maximum, and some ice sheets, such as the Laurentide Ice Sheet, might have reached its maximum as early as ~33.0 ka BP (Clark *et al.*, 2009b). This variation is also evident in the sea level curves presented by Clark *et al.* (2009b) and by Lambeck *et al.* (2014), which show significant differences in the timing of the onset of the LGM, as shown above. This may also have been the case with the BIIS which began its westward extension in the very early stages of the global LGM as proposed by Lambeck *et al.* (2014) (Figure 6.3). This is supported by the radiocarbon results in this thesis, which indicate that the north-western sector of the Irish Ice Sheet reached its maximum extent at <26.3 cal ka BP, during the global LGM (Lambeck *et al.*, 2014).

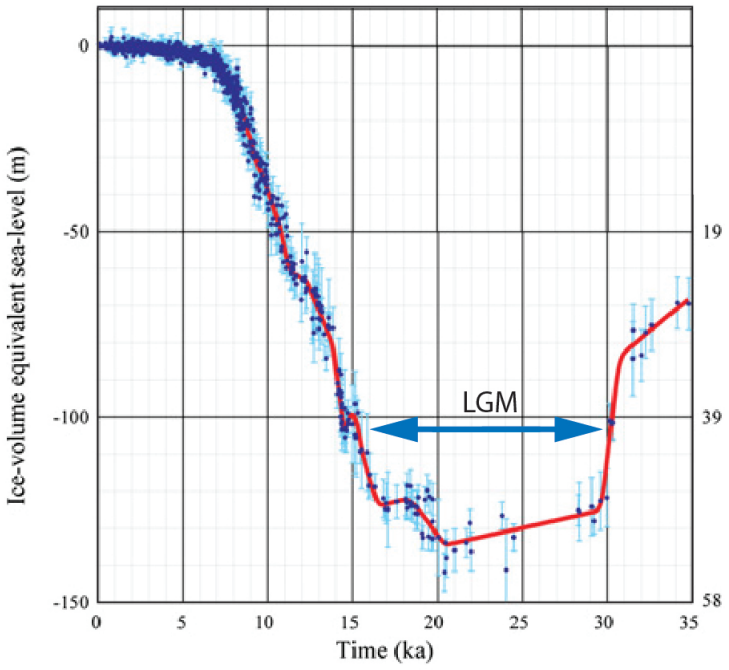

Figure 6.3: Composite global RSL curve from corals from Barbados, Tahiti, Papua New Guinea, Northwest Australia, New Zealand, the western Indian Ocean, the Great Barrier Reef, and the Sunda Shelf. After Lambeck *et al.* (2014).

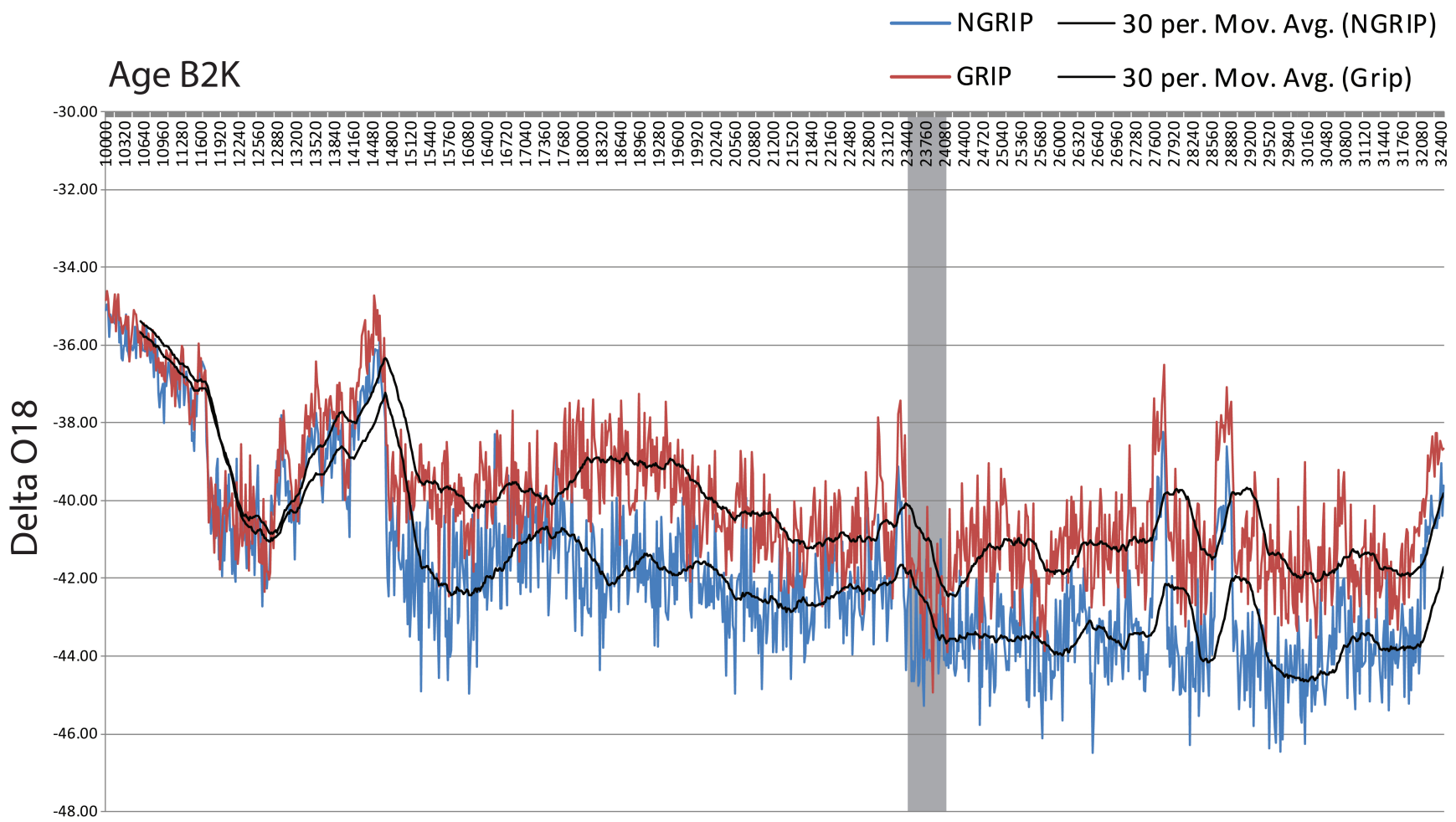

Figure 6.4: $\delta\ ^{18}$O record from the GRIP and NGRIP ice cores. The grey zone marks a rapid enrichment in $\delta\ ^{18}$O at 24120 YB2K, followed by a steady enrichment, leading to the termination of the LGM around 19 ka BP. Data after Svensson *et al.* (2006) and Rasmussen *et al.* (2008)

6.2 Controls on advance and retreat of the BIIS and onset of the LGM

From North Atlantic sediment cores and Greenland ice cores, there is a clear indication that, at least over the last 80,000 years, the atmosphere and ocean surface temperature in the North Atlantic were a coupled system (Bond *et al.*, 1993), and that meridional migration of the Polar Front had a direct influence on the growth and decay of circum-North Atlantic ice-sheets (Ruddiman & McIntyre, 1981; Bond *et al.*, 1993; Scourse *et al.*, 2009). The North Atlantic polar front has a direct control on the supply of heat and moisture delivered to Britain and Ireland, as it is connected to the mid-latitude westerlies and therefore the location of the polar front is likely to have been one of the major controlling factors in BIIS growth and decay (Scourse *et al.*, 2009). Variations in the position of the polar front throughout MIS 4 to 2 would, given the maritime location of Britain and Ireland at the margin of the NE Atlantic, have resulted in a dynamic behaviour of the ice sheet, which would have been sensitive to climatic changes and oceanic control. The ice sheet may therefore have responded sensitively to early signs of cooling leading up to the LGM ((Knutz *et al.*, 2001; Thierens *et al.*, 2012), and this could be one explanation for the westward expansion of the ice sheet, in the early stages of the LGM (Lambeck *et al.*, 2014). From the record of Heinrich events in marine sediments, and the Greenland ice cores, it is evident that large-scale ice sheets around the North Atlantic persisted throughout MIS 4-2 (Scourse *et al.*, 2009), indicating that these ice sheets did not undergo full scale deglaciation prior to the LGM. With the Polar Front adjacent to Britain and Ireland, high precipitation and oscillating temperatures would have resulted in ice sheet growth, while a further shift south would have led to colder temperatures, low precipitation, and a steady state or very slow growth. Conversely a northern shift in the polar front, would lead to a rapid negative mass balance of the ice sheet, and result in deglaciation (Scourse *et al.*, 2009). The polar front must therefore have been located adjacent to Britain and Ireland leading up to the LGM, resulting in a rapid westward growth of the BIIS from ∼30.0 ka BP onwards. The increase in δ^{18}O seen in the Greenland ice cores after 24120 YB2K (Figure 6.4), could therefore be an indication of a northward shift in the polar front, delivering more moisture to the North Atlantic ice sheets, thereby driving a later LGM in the North Atlantic than otherwise the case with the BIIS. Increased influx of BIIS sourced IRD following H2 indicates rapid deglaciation, possibly as a result of this northward shift of the polar front, and further as a response to a LIS-forced eustatic sea level rise of ∼15-30 m (Scourse *et al.*, 2009). As indicated by the radiocarbon dates acquired from tills near the shelf edge and glacimarine sediments from the mid-shelf basin,

presented in chapter 4, the BIIS did not retain its maximum position at the shelf edge offshore of Donegal Bay over a prolonged period, but rather experienced a short lived, shelf edge-position some-time after 26.3 cal ka BP, followed by a retreat that had reached the mid-shelf by 24.8 cal ka BP. This retreat from the shelf occurs almost at the same time as the increased IRD flux to the Barra Donegal Fan (Scourse *et al.*, 2009), and shortly before the increase in δ^{18}O seen in the Greenland ice cores (Figure 6.4). This implies that the ice sheet was highly sensitive towards external forcing, and in tune with surrounding environmental changes.

6.3 Ice sheet retreat: drivers and dynamics

From the radiocarbon dates obtained at the continental shelf edge and the mid-shelf basin, offshore of NW Ireland, it is evident that initial ice-sheet retreat took place during a period of falling global SL, nearing the minimum LGM global sea level of ∼130 m below present, (Figure 6.3) (Lambeck *et al.*, 2002, 2014; Peltier & Fairbanks, 2006; Clark *et al.*, 2009b). The δ^{18}O increase in the Greenland ice cores (Figure 6.4) does not happen until around 24120 YB2K, and if this is an indication of a northward shift in the polar front, it falls too late to be considered as the main driver for the retreat. Benthic foraminiferal data from Disko Bugt in West Greenland show a close correlation between subsurface ocean temperature changes and glacial ice margin positions, when warm water moves onto the shelf and interact with the ice sheet (e.g Holland *et al.* (2008); Lloyd *et al.* (2011)). However, the lack of warm water indicator species in the foraminiferal assemblage data from cores on the outer continental shelf edge and the mid-shelf basin, offshore of NW Ireland is notable, and indicates that ocean warming was probably not a driver of retreat.

Palaeoenvironmental analysis of glacimarine facies in sediment cores from across the shelf, clearly show the dominance of the two key cold water/glacimarine indicator species *Elphidium excavatum f. clavata* and *Cassidulina reniforme* (Figures 5.5 5.6). Both species are associated with modern day Arctic and glacimarine conditions from Svalbard (Murray, 1991; Hald & Korsun, 1997; Kowalczuk *et al.*, 2013). They seem to thrive in glacimarine conditions characterised by fluctuating seasonal changes, temperatures $\leq$2°C, oxygen starvation and high sedimentation rates (Murray, 1991; Hald & Steinsund, 1996; Kowalczuk *et al.*, 2013). Glacimarine sediments as young as 19.5 cal ka BP (core JC106-102), 18.0 cal ka BP and 15.2 cal ka BP (core CE08-010), have been found on the mid-shelf. In these cores the foraminiferal assemblages are dominated by the two glacimarine indicator species, thereby supporting the interpretation of continuous glacimarine conditions across the shelf during deglaciation.

Sedimentological, micropalaeontological and acoustic data presented in this thesis thus indicate that

retreat of the ice sheet across the shelf occurred in a glacimarine environment with high relative sea level. The boundary between Acoustic Facies A and B lies in the mid-shelf basin ∼128 m below current sea level (Figure 4.3). This is very close to the reconstructed global eustatic sea level minimum of ∼130 m below present during the LGM (Figure 6.3) (Lambeck *et al.*, 2014). Hence the high relative sea level indicated by the glacimarine sediments on the shelf implies substantial isostatic depression at this time. As discussed above, glacimarine muds have been found at locations on the south coast of Donegal Bay (McCabe *et al.*, 1986). At Glenulra Farm, *Elphidium excavatum f. clavata* tests from glacimarine muds at 80 m OD dated 27.7 to 27.6 cal ka BP (McCabe *et al.*, 2007b) indicate isostatic depression caused by the build up of a thick land based ice sheet at this time with a subsequent advance to the shelf edge, preserving the deposits in permafrost (Ballantyne & Ó Cofaigh, 2017). Further to the west, at Belderg, dates from marine shells obtained from glacimarine successions at 20 m OD, have yielded ages of ∼20.4 to 19.2 cal ka BP (McCabe *et al.*, 2005), indicating retreat of the ice margin back from the shelf edge (Ballantyne & Ó Cofaigh, 2017). These dates therefore infer isostatic depression of at least 140 m (McCabe *et al.*, 2007b), and possibly a maximum of 210 m at the time in Donegal Bay (Ballantyne & Ó Cofaigh, 2017).

A shelf-edge terminating ice sheet offshore of northwest Ireland could have been relatively thin given the distance from its source area in the Donegal mountains and is therefore also likely to have been sensitive to external forcing, such as oceanic changes and sea level fluctuations. It could be expected to have responded rapidly to sea level rise either eustatically or isostatically driven (cf. Scourse *et al.* 2000).

Substantial millennial-scale fluctuations in RSL, reconstructed from dated coral terraces on Papua New Guinea and Barbados record a 10-15 m sea level change correlated with H events (Hemming, 2004), and a ∼15-30 m sea level rise has been suggested as a consequence of LIS discharge, correlated with the H2-event (Flückiger *et al.*, 2006). There are relatively few data points constraining sea level at the time of the H2-event and the existing points have significant vertical errors (Figure6.3) (Lambeck *et al.*, 2014). Indeed the H2-event is not visible in the curve, which rather shows a steady sea level fall until ∼20 ka BP. If discharge from the LIS was responsible for a 15-30 m rise in global sea level at the time of H2, it can be argued that this only slowed the overall rate of eustatic sea level fall. Thus the net relative sea level rise recorded by the glacimarine sediments across the shelf and onshore in southern Donegal Bay (McCabe *et al.*, 2005, 2007b), must have been a consequence of local glacioisostatic depression. Chronologically the H2-event occurs sometime between 24-25 ka BP (Hemming, 2004; Bradwell *et al.*, 2008; Scourse *et al.*, 2009) and thus onset of the H2-event falls after the ice sheet reached its maximum position at the shelf edge < 26.3 cal ka BP. However the timing of retreat does fall within the time interval of the H2, making it highly plausible

that the sea level fluctuations caused by the H2-event had an influence on retreat from the continental shelf edge, albeit subsidiary to glacioisostatic depression.

Along the shelf break, immediately west of the outer shelf moraine, there is a zone of irregular, cross-cutting iceberg ploughmarks (Ó Cofaigh *et al.*, 2012). They range from a few hundred meters up to 15 km in length, up to 0.3 km wide and have depths of up to 3 m. These iceberg ploughmarks suggests a phase of rapid ice sheet break-up and a calving event during initial retreat from the shelf edge. This indicate a reorganisation of the ice-sheet following a rapid RSL rise (Bradwell *et al.*, 2008; Dunlop *et al.*, 2011; Ó Cofaigh *et al.*, 2012), and this indirectly supports the interpretation that the ice-sheet in Donegal Bay was highly sensitive to external forcing.

The arcuate moraines on the mid-shelf (Figure 2.8), indicate a dynamic ice margin during deglaciation, with retreat across the shelf punctuated by several stillstands or minor re-advances. (Dunlop *et al.*, 2011; Ó Cofaigh *et al.*, 2012) Radiocarbon dates indicate that the ice margin had retreated to the mid shelf by 24.8 cal ka BP. and further had reached the DBM, sometime before 17.9 cal ka BP, where it was stabilised.

6.4 Implications for the ice sheet extent during the Killard Point Readvance in NW Ireland

Records of post-LGM ice sheet readvances in Ireland have been a subject of considerable controversy over the last decade. It has been proposed that the last Irish Ice Sheet underwent several climatically-controlled ice marginal readvances during deglaciation from its LGM position (McCabe & Clark, 1998; McCabe *et al.*, 1998, 2005, 2007a; Clark *et al.*, 2012b). These comprised the Clogher Head Readvance dated 19.3 cal ka BP to 18.4 cal ka BP and the Killard Point Readvance dated 16.5 cal ka BP to 15 cal ka BP (McCabe *et al.*, 1998, 2007b; McCabe & Clark, 1998; Clark *et al.*, 2009a), and both were interpreted as products of rapid climatic cooling in the North Atlantic. The Killard Point Readvance has been correlated with the H1-event (McCabe *et al.*, 1998), and if a product of external forcing, shows that the BIIS, even late in deglaciation was still sensitive to oceanic and climatic forcing. A number of terrestrial moraines in Ireland have been related to the Killard Point Readvance through radiocarbon and cosmogenic dating (McCabe *et al.*, 1998), and linked to offshore undated glacial moraines (Clark *et al.*, 2009a). In western Ireland the Tawnywaddyduff moraine system extends northwards from Clew Bay to just west of Killala Bay on the south coast of Donegal Bay. This moraine system was dated by Clark *et al.* (2009a) using cosmogenic ^{10}Be, to between 15.6 and 15.5 cal ka BP, thus interpreted as being formed during the Killard Point Readvance. Due to its north-south

orientation and location just west of Killala Bay McCabe (2008) and Clark *et al.* (2009a) infer that the DBM is actually the offshore extension of the Tawnywaddyduff moraine, and thus the DBM dates to be Killard Point Readvance.

The new radiocarbon dates presented in this thesis directly counter this interpretation. Glacimarine sediments were deposited behind the moraine as early as 1800 years prior to the Killard Point Readvance. From the east-west oriented moraines superimposed upon the south end of the DBM (Figure 2.8), there is good evidence that the Tawnywaddyduff moraine indeed does extend offshore into the southern margin of Donegal Bay, creating a small ice lobe extending north from Killala Bay (Ó Cofaigh *et al.*, 2012).
The new radiocarbon dates from glacimarine sediments from cores either side of the DBM (Table 4.9), constrain the timing of its formation to between 20.2 and 17.8 cal ka BP (see section 4). Indeed the latter date was from core CE08-004 recovered east of the DBM and indicates that the ice sheet had pulled back from the moraine by this time. The previous interpretation of the DBM as a moraine by Benetti *et al.* (2010); Dunlop *et al.* (2011); Ó Cofaigh *et al.* (2012) is supported by the presence of Acoustic Facies A which constitutes the core of the western part of the moraine. Formation was, at least in part, the result of a re-advance, which reworked glacimarine sediments into the moraine. This is evident by a segmented reflector with underlying lamination on the western flank of the moraine (Figure 4.4). Formation of the eastern ridge of the moraine as a result of later deposition of glacimarine sediments, is evident in the onlapping Acoustic Facies B onto the eastern flank of the western ridge, and in the three profile lines penetrating the ridge (Figures 4.4, 4.5, 4.6). Formation of the DBM as a result of a re-advance is supported by the nature of the glacial margin being sensitive to fluctuating sea level, as discussed above. The global sea level curve by Lambeck *et al.* (2014) display minor fluctuations during sea level rise after 20 ka (Figure 6.3). The timing of some of these fluctuations fall within the timing of the formation of the DBM, between 20.2 cal ka BP and 17.9 cal ka BP, and could be one driver for the re-advance of a grounded glacial front. Another likely alternative could be that the topographic configuration of Donegal Bay and adjoining coastline slowed retreat of the ice margin once it had reached this far back into the Bay. Cosmogenic ^{10}Be exposure dates, sampled from rock slope failures in the Donegal mountains, suggests terrestrial deglaciation occurred at ∼17.4 ka to ∼16.3 ka BP (Ballantyne *et al.*, 2013). This suggests that the ice sheet was on-land at the time of the Killard Point Readvance and could be one explanation for why no evidence for the Killard Point Readvance is seen in the Inner Bay, since the ice sheet margin was land-based by that time.

7. *Conclusions*

The aim of this thesis was to reconstruct the extent, timing, and nature of the British-Irish Ice Sheet (BIIS) on the continental shelf offshore of North-west Ireland, and in Donegal Bay, during the Last Glacial Maximum (LGM). As part of this aim a series of research questions were put forward in chapter 1.2:
1: What was the timing of the maximum extent of the last BIIS on the continental shelf offshore of NW Ireland and did this occur during the LGM or an earlier glaciation? How does this compare to other sectors of the BIIS and the LGM more widely?
2: What was the timing and cause(s) of ice retreat across the shelf, and how does this compare to other sectors of the BIIS?
3: What was the nature of the depositional environment during deglaciation? Did the ice sheet retreat in a marine-based or terrestrial-based setting?
4: What can be inferred about the retreat dynamics from the distribution and age of dated glacial landforms on the continental shelf?

Through the data presented in the chapters: 4 and 5, answers to these research questions can now be summarised as follows:

The orientation and dimensions of glacial landforms - especially the moraines, present on the continental shelf offshore of NW Ireland (Figure 2.8), indicate that an ice lobe extended from dispersal centres in the Donegal mountains (Figures 2.4 and 2.6) across the shelf to the shelf edge, where it formed a large moraine. Acoustic data and sediment cores containing till from this moraine (Figures 5.1 and 4.8 and 4.9) indicate that the ice sheet margin was grounded at the shelf edge. Marine shells reworked into the till further supports this interpretation, and radiocarbon dates from these shells constrain this grounding to some time after 26.3 cal ka BP and before 24.8 cal ka BP. (Figure 7.1 A). This timing is consistent with a eustatic sea level lowstand during the LGM (Figure 6.3). This demonstrates that the BIIS reached its maximum shelf-edge extent offshore of NW Ireland during the LGM, and thereby refutes previous work Bowen *et al.* (2002) and McCabe *et al.* (2007b) which argued for a larger pre-LGM ice advance and restricted LGM extent for NW Ireland.

Radiocarbon dates from the mid shelf, dated to 24.8 cal ka BP, constrain the timing of the initial retreat from the shelf edge to <26.3 and >24.8 cal ka BP (Figure 7.1B). Glacimarine sediments in cores from the shelf and emergent glacimarine sediments found on the south coast of Donegal Bay with LGM ages (McCabe *et al.*, 2005, 2007b) imply glacioisostatic depression of at least 140 m, and possible as high as 210 m. Iceberg ploughmarks west of the outer shelf moraine suggests an initial phase of rapid ice sheet break-up and calving from the shelf edge. The timing of this retreat is probably contemporary and associated with the H2-event, and indicates a reorganisation of the ice sheet margin following a RSL fluctuation, possibly associated with the H2 event (Bradwell *et al.*, 2008; Dunlop *et al.*, 2011; Ó Cofaigh *et al.*, 2012). Retreat thus occurred in a glacimarine setting and the driver for initial retreat appears to have been relative sea level rise, in large part due to local glacioisostatic depression

Acoustically laminated sediments overlying a series of moraines on the mid-shelf (Figure 5.2), indicate that the retreat was characterised by still stands and re-advances in a glacimarine environment (Figure 7.1B). Foraminiferal analysis of the sediments show a clear dominance of two key cold water/glacimarine indicator species *Elphidium excavatum f. Clavata* and *Cassidulina reniforme* (Figures 5.5 5.6). With no warm water indicator species found in the sediments, there is no evidence for warm Atlantic water to be introduced onto the shelf during deglaciation, and thus ocean warming as a driver for retreat can be ruled out.

The presence of a segmented reflector with partial lamination underneath the western flank of the DBM (Figure 4.4A and B), show that glacimarine sediments were reworked into the moraine during its formation. This means that the moraine was, at least in part, the result of a re-advance(s) across a substrate of glacimarine sediments deposited prior to the re-advance during deglaciation (Figure 7.1C). Radiocarbon dates from glacimarine sediments both in front of, and behind, the DBM, constrain its formation to between 20.2 cal ka BP and 17.9 cal ka BP (Figure 7.1D).

During retreat from the DBM prior to 17.9 cal ka BP, glacimarine sediments were deposited on the eastern flank of the moraine (Figure 4.5), in thick successions immediately behind the moraine, and throughout the the inner bay (Figure 7.1E), before the final retreat onshore. From ^{10}Be exposure dates in the Donegal mountains (Ballantyne *et al.*, 2013), it can be inferred that the transition from a marine- to a terrestrially-terminating ice sheet margin occurred sometime between 17.9 cal ka BP and 16.3 cal ka BP. The DBM thus pre-dates the Killard Point Readvance. East-west orientated moraines superimposed on the southern part of

the DBM (Figure 2.8) suggest that an ice lobe extended north from Killala Bay into Donegal Bay, and exposure dates on the terrestrial Tawnywaddyduff moraine system suggests a Kilard Point Readvance age for this.

The contemporary environment across the continental shelf from Donegal Bay to the shelf edge, can thus be visualised as an area dominated by the outer shelf moraine and the DBM, with basins behind each (Figure 7.1F). The shelf edge moraine and the DBM are built up by subglacial tills and the basins are dominated by glacimarine sediments, overlying till. To the north the arcuate nested moraines indicate that retreat was dominated by several still stands and minor re-advances. Post-glacial sediments consisting of coarse grained sands and gravels are seen throughout the area, possible as a result of bottom current reworking.

Figure 7.2 summarises the retreat history for Donegal Bay and the adjoining shelf and presents a series of isochrones based on the radiocarbon dates and the ice marginal positions reconstructed from the geophysical and core data. The ice sheet was present at the shelf edge after 26.3 cal ka BP, and by 24.8 cal ka BP it had retreated to a position east of core JC106-102 (Figures 3.4 7.2) on the mid-shelf. Through a series of stillstands and re-advances, it retreated to the DBM between 20.2 cal ka BP and 17.9 cal ka BP. Further retreat and transition to a terrestrial ice margin occurred sometime after 17.9 cal ka BP. Exposure dates from the Donegal mountains imply a terrestrial margin between 17.4 ka and 16.3 ka BP (Ballantyne *et al.*, 2013). East-west orientated moraines are superimposed on the southern end of the DBM and suggest a possible readvance into the bay from the Killala Bay to the south, possibly as an extension of the Killard Point readvance.

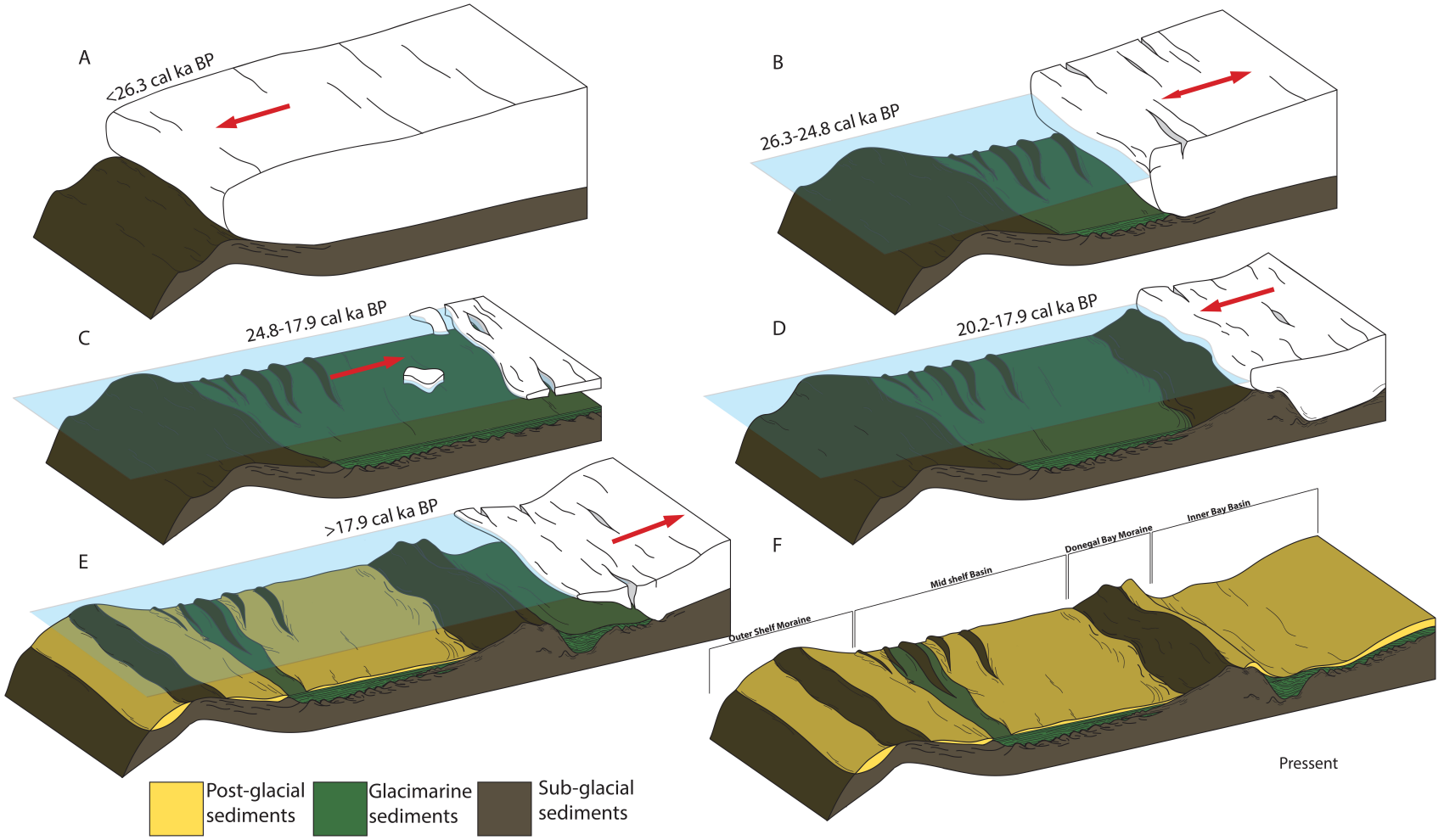

Figure 7.1: A graphic interpretation for ice sheet retreat from the shelf edge, to present day environment

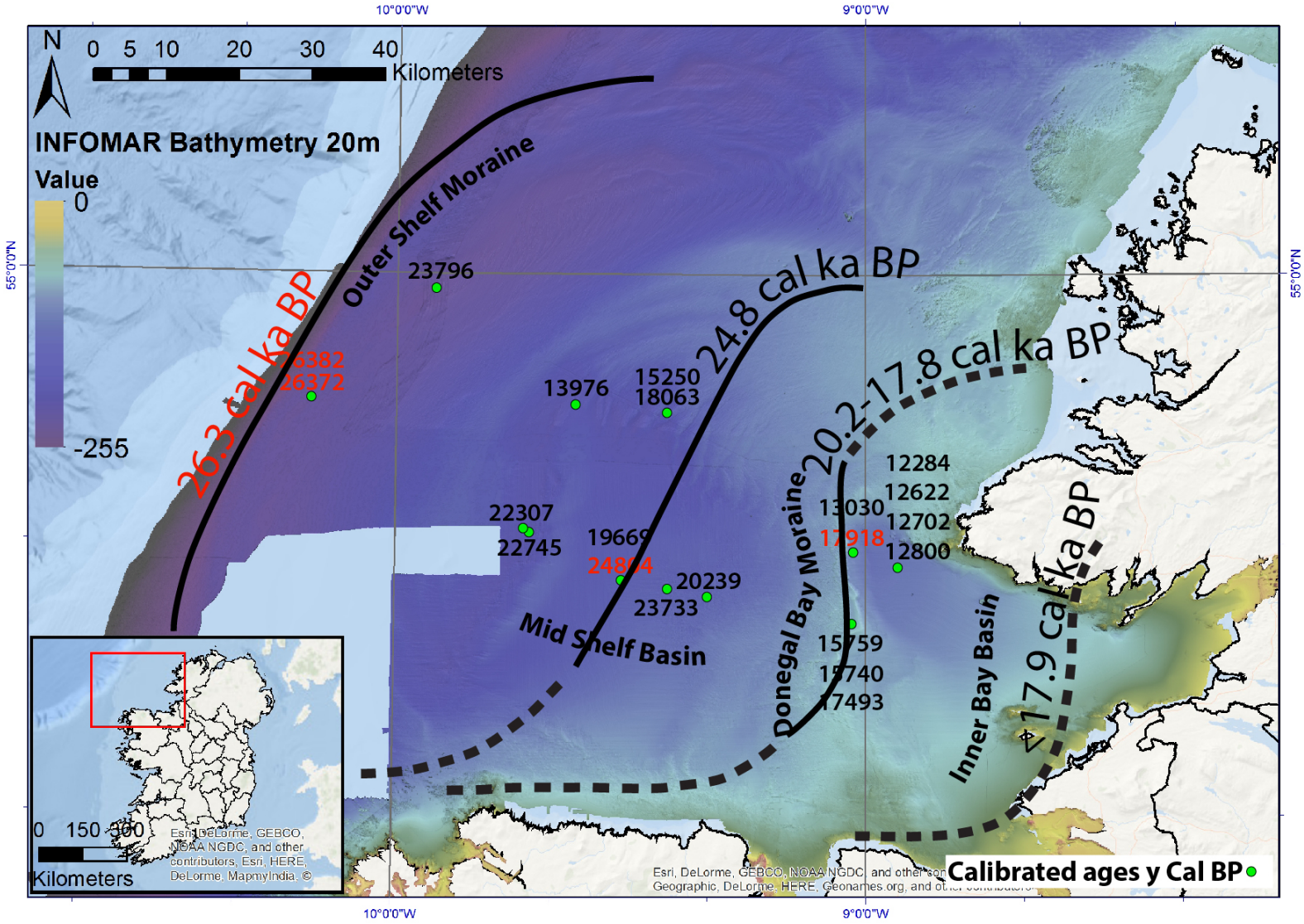

Figure 7.2: Isochron map of the continental shelf and Donegal Bay, showing dated positions of the ice sheet margin from LGM to deglaciation, based on the acoustic, sedimentological and radiocarbon dates presented in this thesis (INFOMAR, 2017).

7.1 Future work

As the palaeoenvironmental analysis in this thesis shows, introduction of warm water onto the shelf has been ruled out as a driver for retreat. However, since this sector of the BIIS is exposed to the North Atlantic and the Gulf Stream branch of the thermohaline circulation, some oceanographic influence could be expected. Further investigations of sediment cores acquired on the continental slope and in the Rockall Trough could potentially reveal if warm water influenced the grounded ice margin at the shelf edge during the LGM, or if and when ocean warming from the Gulf Stream grew strong enough to influence the North Atlantic ocean temperature.

Acquisition of deep seismic data in Donegal Bay could be acquired in order to investigate the record of pre-LGM glaciation of the NW shelf and reveal if deglaciation of earlier glacial margins had a similar dynamic regime to that of the LGM.

In the study area, four additional sediment cores were collected during the JC106 cruise, to the south of the DBM on the east-west orientated ridges, extending north from Killala Bay. As these ridges, have been interpreted as a north-ward extension of an ice lobe during the Killard Point Readvance, chronological data from these sediment cores, would give a better understanding of the Killard Point Readvance in this part of Ireland, and the possible link with the dated terrestrial moraines found to the south of Donegal Bay.

Results from the lithofacies show that deglaciation of Donegal Bay occurred in a glacimarine environment, and chronological data show that sometime between 17.9 cal ka BP and 16.3 cal ka BP., the ice sheet margin changed from marine- to terrestrially-terminating. Further investigation of the timing of this transition, and any associated changes in retreat dynamics could provide a useful analogue for contemporary tidewater glacier retreat in Greenland fjords today. Chronological data from core CE08-003 show four dates of Younger Dryas age from glacimarine sediments, considerably younger than the interpreted deglaciation of the Bay. This provisionally suggests the presence of marine-terminating ice that delivered sediment into the bay during the Younger Dryas Stadial, implying a more extensive Younger Dryas ice cover than previously thought. Chronological investigations of additional near shore, or inner bay sediment cores, could reveal the maximum extent of the Younger Dryas ice cover in this part of Ireland, and further palaeoenvironmeltal analysis could shed light on the nature of such an ice cover.

Bibliography

Armstrong, H., A., & Brasier, M., D. 2005. *Microfossils.* Blackwell.

Ballantyne, C. K. 2010. Extent and deglacial chronology of the last BritishIrish Ice Sheet: implications of exposure dating using cosmogenic isotopes. *Journal of Quaternary Science*, **25**(4), 515–534.

Ballantyne, C. K., & Ó Cofaigh, C. 2017. *The Last Irish Ice Sheet: Extent and Chronology.* Paris: Atlantis Press. Pages 101–149.

Ballantyne, C. K., McCarroll, D., Nesje, A., Dahl, S. O., Stone, J. O., & K, Fifield L. 1998a. High-resolution reconstruction of the last ice sheet in NW Scotland. *Terra Nova*, **10**, 63–67.

Ballantyne, C. K., McCarroll, D., Nesje, A., Dahl, S. O., & Stone, J. O. 1998b. The Last Ice Sheet in North-West Scotland: Reconstruction and Implicatios. *Quaternary Science Reviews*, **17**(12), 1149 – 1184.

Ballantyne, C. K., McCarroll, D., & Stone, J. O. 2006. Vertical dimensions and age of the Wicklow Mountains ice dome, Eastern Ireland, and implications for the extent of the last Irish Ice Sheet. *Quaternary Science Reviews*, **25**(1718), 2048 – 2058.

Ballantyne, C. K., McCarroll, D., & Stone, J. O. 2007. The Donegal ice dome, northwest Ireland: dimensions and chronology. *Journal of Quaternary Science*, **22**(8), 773–783.

Ballantyne, C. K., Stone, J. O., & McCarroll, D. 2008. Dimensions and chronology of the last ice sheet in Western Ireland. *Quaternary Science Reviews*, **27**(34), 185 – 200.

Ballantyne, C. K., Wilson, P., Schnabel, C., & Xu, S. 2013. Lateglacial rock slope failures in north-west Ireland: age, causes and implications. *Journal of Quaternary Science*, **28**(8), 789–802.

Bamber, J.L., Alley, R. B., & Joighin, I. 2007. Rapid response of modern day ice sheets to external forcing. *Earth and Planetary Science Letters*, **257**(12), 1 – 13.

Bartoli, G., Sarnthein, M., Weinelt, M., Erlenkeuser, H., Garbe-Schnberg, D., & Lea, D. W. 2005. Final closure of Panama and the onset of northern hemisphere glaciation. *Earth and Planetary Science Letters*, **237**, 33–44.

Beaman, R. J., & Harris, P. T. 2003. Seafloor morphology and acoustic facies of the George V Land shelf. *Deep Sea Research Part II: Topical Studies in Oceanography*, **50**(89), 1343 – 1355. Recent investigations of the Mertz Polynya and George Vth Land continental margin, East Antarctica.

Benetti, S., Dunlop, P., & Ó Cofaigh, C. 2010. Glacial and glacially-related features on the continental margin of northwest Ireland mapped from marine geophysical data. *Journal of Maps*, **6**(1), 14–29.

Bentley, Michael J., Cofaigh, Colm , Anderson, John B., Conway, Howard, Davies, Bethan, Graham, Alastair G.C., Hillenbrand, Claus-Dieter, Hodgson, Dominic A., Jamieson, Stewart S.R., Larter, Robert D., Mackintosh, Andrew, Smith, James A., Verleyen, Elie, Ackert, Robert P., Bart, Philip J., Berg, Sonja, Brunstein, Daniel, Canals, Miquel, Colhoun, Eric A., Crosta, Xavier, Dickens, William A., Domack, Eugene, Dowdeswell, Julian A., Dunbar, Robert, Ehrmann, Werner, Evans, Jeffrey, Favier, Vincent, Fink, David, Fogwill, Christopher J., Glasser, Neil F., Gohl, Karsten, Golledge, Nicholas R., Goodwin, Ian, Gore, Damian B., Greenwood, Sarah L., Hall, Brenda L., Hall, Kevin, Hedding, David W., Hein, Andrew S., Hocking, Emma P., Jakobsson, Martin, Johnson, Joanne S., Jomelli, Vincent, Jones, R. Selwyn, Klages, Johann P., Kristoffersen, Yngve, Kuhn, Gerhard, Leventer, Amy, Licht, Kathy, Lilly, Katherine, Lindow, Julia, Livingstone, Stephen J., Mass, Guillaume, McGlone, Matt S., McKay, Robert M., Melles, Martin, Miura, Hideki, Mulvaney, Robert, Nel, Werner, Nitsche, Frank O., O'Brien, Philip E., Post, Alexandra L., Roberts, Stephen J., Saunders, Krystyna M., Selkirk, Patricia M., Simms, Alexander R., Spiegel, Cornelia, Stolldorf, Travis D., Sugden, David E., van der Putten, Nathalie, van Ommen, Tas, Verfaillie, Deborah, Vyverman, Wim, Wagner, Bernd, White, Duanne A., Witus, Alexandra E., & Zwartz, Dan. 2014. A community-based geological reconstruction of Antarctic Ice Sheet deglaciation since the Last Glacial Maximum. *Quaternary Science Reviews*, **100**(Supplement C), 1 – 9. Reconstruction of Antarctic Ice Sheet Deglaciation (RAISED).

Bond, G., Broecker, W., Johnsen, S., McManus, J., Labeyrie, L., Jouzel, J., Bonani, G., *et al.* 1993. Correlations between climate records from North Atlantic sediments and Greenland ice. *Nature*, **365**(6442), 143–147.

Boulton, G. S., Smith, G. D., Jones, A. S., & Newsome, J. 1985. Glaciated geology and glaciology of the last mid-latitude ice sheets. *Journal of the Geological Society*, **142**, 447–474.

Bowen, D. Q., Phillips, F. M., McCabe, A. M., Knutz, P. C., & Sykes, G. A. 2002. New data for the Last Glacial Maximum in Great Britain and Ireland. *Quaternary Science Reviews*, **21**(13), 89 – 101.

Bowen, D.Q., Rose, J., McCabe, A.M., & Sutherland, D.G. 1986. Correlation of Quaternary glaciations in England, Ireland, Scotland and Wales. *Quaternary Science Reviews*, **5**, 299 – 340.

Bradwell, T., Stoker, M. S., Golledge, N. R., Wilson, C. K., Merritt, J. W., Long, D., Everest, J. D., Hestvik, O. B., Stevenson, A. G., Hubbard, A. L., Finlayson, A. G., & Mathers, H. E. 2008. The northern sector of the last British Ice Sheet: Maximum extent and demise. *Earth-Science Reviews*, **88**(34), 207 – 226.

Brooks, A. J., Bradley, S. L., Edwards, R. J., & Milne, G. A. 2008. Postglacial relative sea-level observations from Ireland and their role in glacial rebound modelling. *Journal of Quaternary Science*, **23**, 175–192.

Carvill Lewis, H. 1894. *Papers and Notes on the Glacial Geology of Great Britain and Ireland.* Green and Co.

Charlesworth, J.K. 1924. The geology of the north-west of Ireland. *Proceedings of the Royal Irish Academy*, **B36**, 174–314.

Chew D., M, Daly, J., S., Flowerdew, M., J., Kennedy, M., J., & Page, L., M. 2004. Crenulation-slip development in a Caledonian shear zone in NW Ireland: evidence for a multi-stage movement history. *Geological Society, London, Special Publications*, **224**(1), 337–352.

Chi, J., & Mienert, J. 1996. Linking physical property records of Quaternary sediments to Heinrich events. *Marine Geology*, **131**(12), 57 – 73. Ice Rafting and Paleocengraphy of the Northeast Atlantic Ocean Selected papers presented at the 7th European Union of Geosciences.

Chiverrell, R. C., & Thomas, G. S. P. 2010. Extent and timing of the Last Glacial Maximum (LGM) in Britain and Ireland: a review. *Journal of Quaternary Science*, **25**(4), 535–549.

Church, J.A., Clark, P.U., Cazenave, A., Gregory, J.M., Jevrejeva, S., Levermann, A., Merrifield, M.A., Milne, G.A., Nerem, R.S., Nunn, P.D., Payne, A.J., Pfeffer, W.T., Stammer, D., & Unnikrishnan, A.S. 2013. *Climate Change 2013: The Physical Science Basis. Contribution of Working Group I to the Fifth Assessment Report of the Intergovernmental Panel on Climate Change.* Cambridge University Press, Cambridge, United Kingdom and New York, NY, USA. Chap. Sea Level Change.

Clark, C. D., Hughes, A. L. C., Greenwood, S. L., Jordan, C., & Sejrup, H. P. 2012a. Pattern and timing of retreat of the last British-Irish Ice Sheet. *Quaternary Science Reviews*, **44**(0), 112 – 146. Quaternary Glaciation History of Northern Europe.

Clark, J., McCabe, A. M., Schnabel, C., Clark, P.U., McCarron, S., Freeman, S.P.H.T., Maden, C., & Xu, S. 2009a. Cosmogenic 10Be chronology of the last deglaciation of western Ireland, and implications for sensitivity of the Irish Ice Sheet to climate change. *Geological Society of America Bulletin*, **121 no 1-2**, 3–16.

Clark, J., McCabe, A. M., Bowen, D. Q., & Clark, P. U. 2012b. Response of the Irish Ice Sheet to abrupt climate change during the last deglaciation. *Quaternary Science Reviews*, **35**, 100 – 115.

Clark, P. U., & Mix, A. C. 2002. Ice sheets and sea level of the Last Glacial Maximum. *Quaternary Science Reviews*, **21**(13), 1 – 7.

Clark, P. U., Dyke, A. S., Shakun, J. D., Carlson, A. E., Clark, J., Wohlfarth, B., Mitrovica, J. X., Hostetler, S. W., & McCabe, A. M. 2009b. The Last Glacial Maximum. *Science*, **325**(5941), 710–714.

Close, M. H. 1866. Notes on the general glaciation of Ireland. *Journal of the Royal Geological Society of Ireland*, **1**, 207–242.

Colhoun, E. A. 1971. The Glacial Stratigraphy of the Sperrin Mountains and Its Relation to the Glacial Stratigraphy of North-West Ireland. *Proceedings of the Royal Irish Academy. Section B: Biological, Geological, and Chemical Science*, **71**, 37–52.

Cowan, A. E., Seramur, K. C., Cai, J., & Powell, R. D. 1999. Cyclic sedimentation produced by fluctuations in meltwater discharge, tides and marine productivity in an Alaskan fjord. *Sedimentology*, **46**(6), 1109–1126.

Coxall, H. K., Wilson, P. A., Palike, H., Lear, C. H., & Backman, J. 2005. Rapid stepwise onset of Antarctic glaciation and deeper calcite compensation in the Pacific Ocean. *Nature*, **433**, 53–57.

Dansgaard, W., Johnsen, S. J., Clausen, H. B., Dahl-Jensen, D., Gundestrup, N .S., Hammer, C. U., Hvidberg, C. S., Steffensen, J. P., Sveinbjörnsdottir, A .E., Jouzel, J., & Bond, G. 1993. Evidence for general instability of past climate from a 250-kyr ice-core record. *Nature*, **364**(6434), 218–220.

De Moustier, C., & Matsumoto, H. 1993. Seafloor acoustic remote sensing with multibeam echo-sounders and bathymetric sidescan sonar systems. *Marine Geophysical Researches*, **15**(1), 27–42.

Domack, E. W. 1990. Laminated terrigenous sediments from the Antarctic Peninsula: the role of subglacial and marine processes. *Geological Society, London, Special Publications*, **53**, 91–103.

Dowdeswell, J. A., Whittington, R. J., Jennings, A. E., Andrews, J. T., Mackensen, A., & Marienfeld, P. 2000. An origin for laminated glacimarine sediments through sea-ice build-up and suppressed iceberg rafting. *Sedimentology*, **47**(3), 557–576.

Dowdeswell, J. A., Ottesen, D., Evans, J., Ó Cofaigh, C., & J.B., Anderson. 2008. Submarine glacial landforms and rates of ice-stream collapse. *Geology*, **36 no. 10**, 819–822.

Dunlop, P., Shannon, R., McCabe, M., Quinn, R., & Doyle, E. 2010. Marine geophysical evidence for ice sheet extension and recession on the Malin Shelf: New evidence for the western limits of the British Irish Ice Sheet. *Marine Geology*, **276**, 86–99.

Dunlop, P., Sacchetti, F., Benetti, S., & Ó Cofaigh, C. 2011. *Mapping Ireland's glaciated continental margin using marine geophysical data. In: Geomorphological Mapping: Methods and Applications: A Professional Handbook of Techniques and Applications (Developments in Earth Surface Processes).* Elsevier.

Dyke, A. S., Andrews, J. T., Clark, P. U., England, J. H., Miller, G. H., shaw, J., & Veillette, J. J. 2002. The Laurentide and Innuitian ice sheets during the Last Glacial Maximum. *Quaternary Science Reviews*, **21**, 9–31.

Edwards, K. J, & Warren, W. P. 1985. Quaternary Studies in Ireland. *Pages 1–16 of:* Edwards, K. J, & Warren, W. P. (eds), *The Quaternary History of Ireland.* Academic Press.

Evans, J., Pudsey, J. C., Ó Cofaigh, C., Morris, P., & Domack, E. 2005. Late Quaternary glacial history, flow dynamics and sedimentation along the eastern margin of the Antarctic Peninsula Ice Sheet. *Quaternary Science Reviews*, **24**(56), 741 – 774.

Eyles, N., & Lazorek, M. 2013. Glacial Landforms, Sediments. Glaciogenic Lithofacies. *Pages 946–958 of:* Elias, S., A. (ed), *Encyclopedia of Quaternary science. Volume 2.* Elsevier.

Eyles, N., Eyles, C. H., & Miall, A. D. 1983. Lithofacies types and vertical profile models; an alternative approach to the description and environmental interpretation of glacial diamict and diamictite sequences. *Sedimentology*, **30**(3), 393–410.

Feyling-Hanssen, R. W. 1953. Late-Pleistocene Foraminifera from the Oslofjord area, southeast Norway. *Norges Geologiske Tidsskrift*, **33**, 109–155.

Feyling-Hanssen, R. W. 1972. The Foraminifer Elphidium excavatum (Terquem) and Its Variant Forms. *Micropaleontology*, **18**(3), 337–354.

Fisher, R. A., Steven A. Corbet-C., & Williams, B. 1943. The Relation Between the Number of Species and the Number of Individuals in a Random Sample of an Animal Population. *Journal of Animal Ecology*, **12**(1), 42–58.

Flückiger, J., Knutti, R., & White, J. W.C. 2006. Oceanic processes as potential trigger and amplifying mechanisms for Heinrich events. *Paleoceanography*, **21**(2).

Foraminifera.eu, Project The. 2017. *The Foraminifera.eu Project Foraminifera Gallery - illustrated catalog.*

Geikie, J. 1878. On the glacial phenomena of the Long Isle or Outer Hebrides. *Journal of the Geological Society of London*, **34**, 819–866.

GEOTEK. 2016. *Geotek MSCL Systems. Techinical Specifications http://www.geotek.co.uk/.* Tech. rept.

Gilbert, R. 1985. Quaternary Glaciomarine Sedimentation Interpreted from Seismic Surveys of Fiords on Baffin Island, N.W.T. *Arctic*, **38**(4).

Gilbert, R., Nielsen, N., Desloges, J. R., & Rasch, M. 1998. Contrasting glacimarine sedimentary environments of two arctic fiords on Disko, West Greenland. *Marine Geology*, **147**(14), 63 – 83.

Gooday, A. J., & Hughes, J. A. 2002. Foraminifera associated with phytodetritus deposits at a bathyal site in the northern Rockall Trough (NE Atlantic): seasonal contrasts and a comparison of stained and dead assemblages. *Marine Micropaleontology*, **46**(12), 83 – 110.

Greenwood, S. L., & Clark, C. D. 2008. Subglacial bedforms of the Irish Ice Sheet. *Journal of Maps*, **4**(1), 332–357.

Greenwood, S. L., & Clark, C. D. 2009a. Reconstructing the last Irish Ice Sheet 1: changing flow geometries and ice flow dynamics deciphered from the glacial landform record. *Quaternary Science Reviews*, **28**(2728), 3085 – 3100.

Greenwood, S. L., & Clark, C. D. 2009b. Reconstructing the last Irish Ice Sheet 2: a geomorphologically-driven model of ice sheet growth, retreat and dynamics. *Quaternary Science Reviews*, **28**(2728), 3101 – 3123.

GSI. 2017. *GSI Bedrock Geology 1 Million ArcGIS Map service https://secure.dcenr.gov.ie/arcgis/services.* Tech. rept.

Gunn, E., D., & Best, I., A. 1998. A new automated nondestructive system for high resolution multi-sensor core logging of open sediment cores. *Geo-Marine Letters*, **18**(1), 70–77.

Hald, M., & Korsun, S. 1997. Distribution of modern Arctic benthic foraminifera from fjords of Svalbard, European Arctic. *The Journal of Foraminiferal research*, **27, no 2**, 101–122.

Hald, M., & Steinsund, P. I. 1996. Benthic foraminifera and carbonat dissolution in the surface sediments of Barents and Kara seas. *Pages 285–307 of:* Ruediger Stein, Gennadij I. Ivanov, Michael A. Levitan, & Fahl, Kirsten (eds), *Surface-sediment composition and sedimentary processes in the central Arctic Ocean and along the Eurasian Continental Margin.* Reports of Polar Research. 212.

Hall, A. M., & Bent, A. J. A. 1990. The limits of the last British ice sheet in Northern Scotland and the adjacent shelf. *Quaternary Newsletter*, **61**, 2–11.

Hambrey, M. J., & McKelvey, B. 2000. Neogene fjordal sedimentation on the western margin of the Lambert Graben, East Antarctica. *Sedimentology*, **47**(3), 577–607.

Hein, F.J., & Syvitski, J.P.M. 1992. Sedimentary environments and facies in an arctic basin, Itirbilung Fiord, Baffin Island, Canada. *Sedimentary Geology*, **81**(12), 17 – 45.

Hemming, S. R. 2004. Heinrich events: Massive late Pleistocene detritus layers of the North Atlantic and their global climate imprint. *Reviews of Geophysics*, **42**(1).

Hibbert, F. D., Austin, W. E. N., Leng, M. J., & Gatliff, R. W. 2010. British Ice Sheet dynamics inferred from North Atlantic ice-rafted debris records spanning the last 175000 years. *Journal of Quaternary Science*, **25**(4), 461–482.

Hinch, J. de W. 1913. The shelly drift of Glenulra and Belderrig Co. Mayo. *Irish Naturalists Journal*, **22**, 1–16.

Holland, D. M., Thomas, R. H., De Young, B., Ribergaard, M. H., & Lyberth, B. 2008. Acceleration of Jakobshavn Isbrae triggered by warm subsurface ocean waters. *Nature geoscience*, **1**(10), 659–664.

Howe, J. A., & Pudsey, C. J. 1999. Antarctic circumpolar deep water: a Quaternary paleoflow record from the northern Scotia Sea, South Atlantic Ocean. *Journal of Sedimentary Research*, **69**, 847–861.

INFOMAR. 2017. *INSS INFOMAR 20m Bathymetry http://www.infomar.ie/data/DataAccess.php.* Data acquired april 2017.

Josenhans, H., & Lehman, S. 1999. Late glacial stratigraphy and history of the Gulf of St. Lawrence, Canada. *Canadian Journal of Earth Sciences*, **36**(8), 1327–1345.

Joughin, I., Smith, B. E., & Medley, B. 2014. Marine Ice Sheet Collapse Potentially Under Way for the Thwaites Glacier Basin, West Antarctica. *Science*, **344**(6185), 735–738.

King, E.L., Haflidason, H., Sejrup, H.P., Austin, W.E.N., Duffey, M., Helland, H., Klitgaard-Kristensen, D., & Scourse, J.D. 1998. End moraines on the northwest Irish continental shelf. *In: Poster Presented at Third ENAM II Workshop, Edinburgh.*

Knight, J., & McCabe, A. M. 1997a. Drumlin evolution and ice sheet oscillations along the NE Atlantic margin, Donegal Bay, western Ireland. *Sedimentary Geology*, **111**(14), 57 – 72.

Knight, J., & McCabe, A. M. 1997b. Identification and significance of ice-flow-transverse subglacial ridges (Rogan moraines) in northern central Ireland. *Journal of Quaternary Science*, **12**, 519–524.

Knight, J., Coxon, P., McCabe, A. M., & McCarron, S. G. 2004. Pleistocene glaciations in Ireland. *Pages 183 – 191 of:* Ehlers, J., & Gibbard, P.L. (eds), *Quaternary Glaciations Extent and Chronology Part I: Europe.* Developments in Quaternary Sciences, vol. 2, Part 1. Elsevier.

Knutz, P. C., Austin, W. E. N., & Jones, E. J. W. 2001. Millennial-scale depositional cycles related to British Ice Sheet variability and North Atlantic paleocirculation since 45 kyr B.P., Barra Fan, U.K. margin. *Paleoceanography*, **16 (1)**, 53–64.

Kongsberg, Maritime, AS. 2016. *SBP 120 Sub-Bottom Profiler Techinical Specifications www.kongsberg.com.* Tech. rept. Kongsberg Maritime AS.

Korsun, S., & Hald, M. 1998. Modern Benthic Foraminifera off Novaya Zemlya Tidewater Glaciers, Russian Arctic. *Arctic and Alpine Research*, **30**(1), 61–77.

Kowalczuk, M. W., Pawowska, J., & Zajczkowski, M. 2013. Do foraminifera mirror diversity and distribution patterns of macrobenthic fauna in an Arctic glacial fjord? *Marine Micropaleontology*, **103**, 30 – 39.

Kutzbach, J. E., Prell, W. L., & Ruddiman, W. M. F. 1993. Sensitivity of Eurasian climate to surface uplift of the Tibetan Plateau. *The Journal of Geology*, 177–190.

Lambeck, K., Yokoyama, Y., & Purccell, T. 2002. Into and out of the Last Glacial Maximum: Sea-level change during Oxygen Isotope Stages 3 and 2. *Quaternary Science Reviews*, **21**, 343–360.

Lambeck, K., Rouby, H., Purcell, T., Sun, Y., & Sambridge, M. 2014. Sea level and global ice vvolume from the Last Glacial Maximum to the Holocene. *Proceedings of the National Academy of Sciences*, **111**, 15296–15303.

Lear, C. H., Rosenthal, Y., & Wright, J. D. 2003. The closing of a seaway: ocean water masses and global climate change. *Earth and Planetary Science Letters*, **210**, 425–436.

Lecavalier, B. S., Milne, G. A., Simpson, M. J. R., Wake, L., Huybrechts, P., Tarasov, L., Kjeldsen, K. K., Funder, S., Long, A. J., Woodroffe, S., Dyke, A. S., & Larsen, N. K. 2014. A model of Greenland ice sheet deglaciation constrained by observations of relative sea level and ice extent. *Quaternary Science Reviews*, **102**, 54 – 84.

Leoblich, Jr. A., R., & Tappan, H. 1987. *Foraminiferal Genera and their Classification.* Van Nostrand Reinhold. New York.

Libby, W., F., Anderson, E., C., & Arnold, J., R. 1949. Age Determination by Radiocarbon Content: World-Wide Assay of Natural Radiocarbon. *Science*, **109**(2827), 227–228.

Lloyd, J., Moros, M., Perner, K., Telford, R. J., Kuijpers, A., Jansen, E., & McCarthy, D. 2011. A 100 yr record of ocean temperature control on the stability of Jakobshavn Isbrae, West Greenland. *Geology*, **39**(9), 867–870.

Loubere, P., & Austin, W. 2007. PALEOCEANOGRAPHY, {BIOLOGICAL} {PROXIES} — Benthic Foraminifera Palaeoceanography, Biological proxies/ Benthic Foraminifera. *Pages 1618 – 1627 of:* Elias, Scott A. (ed), *Encyclopedia of Quaternary Science.* Oxford: Elsevier.

Mackiewicz, N. E., Powell, R. D., Carlson, P. R., & Molnia, B. F. 1984. Sedimentation on High-latitude Continental Shelves Interlaminated ice-proximal glacimarine sediments in Muir Inlet, Alaska. *Marine Geology*, **57**(1), 113 – 147.

Marine Institute, and Geological Survey of Ireland. 2002. *The Irish National Seabed Survey - 2002 Donegal Bay, Ireland. Survey Report.* Tech. rept. The Irish National Seabed Survey GeoLab Technical Services Ltd. August-October 2002 R.V. Celtic Voyager.

Max, M. D., & Riddihough, R. P. 1975. Continuation of the Highland Boundary fault in Ireland. *Geology*, **3**(4), 206–210.

McCabe, A. M. 1999. Chapter 10: Ireland. *Pages 115–125 of:* Bowen, D., Q. (ed), *A revised Correlation of Quaternary Deposits in the British Isles.* The Geological society.

McCabe, A. M., & Clark, P. U. 1998. Ice-sheet variability around the North Atlantic Ocean during the last deglaciation. *Nature*, **392**, 373–377.

McCabe, A. M., & Clark, P. U. 2003. Deglacial chronology from Country Donegal, Ireland: Implications for deglaciation of the British-Irish ice sheet. *Journal of the Geological Society, London*, **160**, 847–855.

McCabe, A. M., Haynes, J. R., & Macmillan, N. F. 1986. Late-Pleistocene tidewater glaciers and glaciomarine sequences from north County Mayo, Republic of Ireland. *Journal of Quaternary Science*, **1**, 73–84.

McCabe, A. M., Bowen, D. Q., & Penney, D. N. 1993. Glaciomarine facies from the western sector of the last British ice sheet, Malin Beg, County Donegal, Ireland. *Quaternary Science Reviews*, **12**(1), 35 – 45.

McCabe, A. M., Knight, J., & McCarron, S. 1998. Evidence for Heinrich event 1 in the British Isles. *Journal of Quaternary Science*, **13**, 549–568.

McCabe, A. M., Clark, P. U., & Clark, J. 2005. AMS 14C dating of deglacial events in the Irish Sea Basin and other sectors of the BritishIrish ice sheet. *Quaternary Science Reviews*, **24**, 1673–1690.

McCabe, A. M., Clark, P. U., Clark, J., & Dunlop, P. 2007a. Radiocarbon constraints on readvances of the British-Irish Ice Sheet in the northern Irish Sea Basin during the last deglaciation. *Quaternary Science Reviews*, **26**(910), 1204 – 1211.

McCabe, A. M., Clark, P. U., & Clark, J. 2007b. Radiocarbon constraints on the history of the western Irish ice sheet prior to the Last Glacial Maximum. *Geology*, **35**(2), 147–150.

McCabe, A.M. 1987. Quaternary deposits and glacial stratigraphy in Ireland. *Quaternary Science Reviews*, **6**(3), 259 – 299.

McCabe, A.M. 2008. *Glacial Geology and Geomorphology: The Landscapes of Ireland.* Dunedin Academic Press Ltd, Edinburgh.

Mitchum, R. M., Vail, P. R. Jr., & Sangree, J. B. 1977a. *Seismic Stratigraphy–Applications to Hydrocarbon Exploration.* AAPG Special Volumes. Chap. Seismic Stratigraphy and Global Changes of Sea Level: Part 6. Stratigraphic Interpretation of Seismic Reflection Patterns in Depositional Sequences: Section 2. Application of Seismic Reflection Configuration to Stratigraphic Interpretation, pages 117–133.

Mitchum, R. M., Vail, P. R. Jr., & Thomson, S., III. 1977b. *Seismic Stratigraphy–Applications to Hydrocarbon Exploration.* AAPG Special Volumes. Chap. Seismic Stratigraphy and Global Changes of Sea Level: Part 2. The Depositional Sequence as a Basic Unit for Stratigraphic Analysis: Section 2. Application of Seismic Reflection Configuration to Stratigraphic Interpretation, pages 53–62.

Mix, A. C., Edouard, B., & Ralph, S. 2001. Environmental processes of the ice age: land, oceans, glaciers (EPILOG). *Quaternary Science Reviews*, **20**(4), 627 – 657.

Monahan, D. 2009. *Marine Geology and Geophysics. A derivative of Encyclopedia of Ocean Sciences, 2nd Edition.* Academic Press. Chap. Bathymetry, pages 7–15.

Mudie, P. J., Keen, C. E., Hardy, I. A., & Vilks, G. 1984. Multivariate analysis and quantitative paleoecology of benthic foraminifera in surface and late Quaternary shelf sediments, Northern Canada. *Micropaleontology*, **8**, 283–313.

Murray, J. W. 1991. *Ecology and Palaeoecology of Benthic Foraminifera.* Pearson Education.

Murray, J. W. 2006. *Ecology and applications of benthic foraminifera.* Cambridge University Press.

Myhre, G., D. ans Shindell F.-M., Bron, W., Collins, J., Fuglestvedt, J., Huang, D., Koch, J.-F., Lamarque, D., Lee, B., Mendoza, T., Nakajima, A., Robock, G., Stephens, T., Takemura, & Zhang, H. 2013. *Climate Change 2013: The Physical Science Basis. Contribution of Working Group I to the Fifth Assessment Report of the Intergovernmental Panel on Climate Change.* Cambridge University Press, Cambridge, United Kingdom and New York, NY, USA. Chap. Anthropogenic and Natural Radiative Forcing.

Naafs, B.D.A., Stein, R., Hefter, J., Khlifi, N., De Schepper, S, & G.H., Haug. 2010. Late Pliocene changes in the North Atlantic Current. *Earth and Planetary Science Letters*, **298**(34), 434 – 442.

Ó Cofaigh, C, & Dowdeswell, J.A. 2001. Laminated sediments in glacimarine environments: diagnostic criteria for their interpretation. *Quaternary Science Reviews*, **20**(13), 1411 – 1436.

Ó Cofaigh, C, & Evans, D. J. A. 2001. Sedimentary evidence for deforming bed conditions associated with a grounded Irish Sea glacier, southern Ireland. *Journal of Quaternary Science*, **16**(5), 435–454.

Ó Cofaigh, C., & Evans, D. J. A. 2007. Radiocarbon constraints on the age of the maximum advance of the British-Irish Ice Sheet in the Celtic Sea. *Quaternary Science Reviews*, **26**(910), 1197 – 1203.

Ó Cofaigh, C, Dowdeswell, J.A., & Grobe, H. 2001. Holocene glacimarine sedimentation, inner Scoresby Sund, East Greenland: the influence of fast-flowing ice-sheet outlet glaciers. *Marine Geology*, **175**(14), 103 – 129.

Ó Cofaigh, C., Dowdeswell, J. A., Allen, C. S., Hiemstra, J. F., Pudsey, C. J., Evans, J., & Evans, D. J. A. 2005. Flow dynamics and till genesis associated with a marine-based Antarctic palaeo-ice stream. *Quaternary Science Reviews*, **24**(56), 709 – 740.

Ó Cofaigh, C., Dunlop, P., & Benetti, S. 2012. Marine geophysical evidence for Late Pleistocene ice sheet extent and recession off northwest Ireland. *Quaternary Science Reviews*, **44**, 147–159.

Ó Cofaigh, C., Benetti, S., Dunlop, P., & Monteys, X. 2016. *Arcuate moraines on the continental shelf NW of Ireland. In: Atlas of Submarine Glacial Landforms.* Geological Society, London. Pages 253–254.

Owen, L.A. 2013. Glaciation, Causes, Tectonic Uplift and Continental Configurations. *Pages 127 – 135 of:* Elias, Scott A., & Mock, Cary J. (eds), *Encyclopedia of Quaternary Science (Second Edition)*, second edition edn. Amsterdam: Elsevier.

Peck, V. L., Hall, I. R., Zahn, R., Grousset, F., Hemming, S. R., & Scourse, J. D. 2007. The relationship of Heinrich events and their European precursors over the past 60 ka BP: a multi-proxy ice-rafted debris provenance study in the North East Atlantic. *Quaternary Science Reviews*, **26**(7-8), 862–875.

Peltier, W. R., & Fairbanks, R. G. 2006. Global glacial ice volume and Last Glacial Maximum duration from an extended Barbados sea level record. *Quaternary Science Reviews*, **25**, 3322 – 3337.

Peters, J. L., Benetti, S., Dunlop, P., & Ó Cofaigh, C. 2015. Maximum extent and dynamic behaviour of the last BritishIrish Ice Sheet west of Ireland. *Quaternary Science Reviews*, **128**, 48 – 68.

Peters, J. L., Benetti, S., Dunlop, P., Ó Cofaigh, C., Moreton, S. G., Wheeler, A. J., & Clark, C. D. 2016. Sedimentology and chronology of the advance and retreat of the last British-Irish Ice Sheet on the continental shelf west of Ireland. *Quaternary Science Reviews*, **140**, 101 – 124.

Petit, J. R., Jouzel, J., Raynaud, D., Barkov, N. I., Barnola, J.-M., Basile, I., Bender, M., Chappellaz, J., Davis, M., Delaygue, G., Delmotte, M., Kotlyakov, V. M., Legrand, M., Lipenkov, V. Y., Lorius, C., PEpin, L., Ritz, C., Saltzman, E., & Stievenard, M. 1999. Climate and atmospheric history of the past 420,000 years from the Vostok ice core, Antarctica. *Nature*, **399**(6735), 429–436.

Portlock, J. E. 1843. *Report on the geology of Londonderry and parts of Tyrone and Fermanagh, Dublin, 784 pp.* Andrew Milliken and Hodges and Smith Dublin.

Praeg, D., McCarron, S., Dove, D., Ó Cofaigh, C., Scott, G., Monteys, X., Facchin, L., Romeo, R., & Coxon, P. 2015. Ice sheet extension to the Celtic Sea shelf edge at the Last Glacial Maximum. *Quaternary Science Reviews*, **111**, 107 – 112.

Praeger, R. L. 1896. Report of the sub-committee appointcd to investigate the gravels of Ballyrudder, County Antrim. 198-209. *Proceedings Belfast Naturalists Field Club*, 198–209.

Purcell, C. 2014. *Late Quaternary glaciation of the continental shelf offshore of NW Ireland.* M.Phil. thesis, Durham University, Department of Geography.

Ramsey, C. B., Staff, R. A., Bryant, C. L., Brock, F., Kitagawa, H., van der Plicht, J., Schlolaut, G., Marshall, M. H., Brauer, A., Lamb, H. F., Payne, R. L., Tarasov, P. E., Haraguchi, T., Gotanda, K., Yonenobu, H., Yokoyama, Y., Tada, R., & Nakagawa, T. 2012. A Complete Terrestrial Radiocarbon Record for 11.2 to 52.8 kyr B.P. *Science*, **338**(6105), 370–374.

Rasmussen, S. O., Andersen, K. K., Svensson, A. M., Steffensen, J. P., Vinther, B. M., Clausen, H. B., Siggaard-Andersen, M.-L., Johnsen, S. J., Larsen, L. B., Dahl-Jensen, D., Bigler, M., Rthlisberger, R., Fischer, H., Goto-Azuma, K., Hansson, M. E., & Ruth, U. 2006. A new Greenland ice core chronology for the last glacial termination. *Journal of Geophysical Research: Atmospheres*, **111**(D6), 1–16. D06102.

Rasmussen, S.O., Seierstad, I.K., Andersen, K.K., Bigler, M., Dahl-Jensen, D., & Johnsen, S.J. 2008. Synchronization of the NGRIP, GRIP, and GISP2 ice cores across MIS 2 and palaeoclimatic implications. *Quaternary Science Reviews*, **27**(12), 18 – 28. Integration of Ice-core, Marine and Terrestrial records (INTIMATE): Refining the record of the Last Glacial-Interglacial Transition.

Reimer, P., Bard, E., Bayliss, A., Beck, J. W., Blackwell, P., Ramsey, C. B., Buck, C., Cheng, H., Edwards, R. L., Friedrich, M., Grootes, P., Guilderson, T., Haflidason, H., Hajdas, I., Hatt, C., Heaton, T., Hoffmann, D., Hogg, A., Hughen, K., Kaiser, K., Kromer, B., Manning, S., Niu, M., Reimer, R., Richards, D., Scott, E., Southon, J., Staff, R., Turney, C., & Plicht, vd.J. 2013. IntCal13 and Marine13 Radiocarbon Age Calibration Curves 0 50,000 Years cal BP. *Radiocarbon*, **55**(4).

Riedel, M., Spence, G. D., Chapman, N. R., & Hyndman, R. D. 2002. Seismic investigations of a vent field

associated with gas hydrates, offshore Vancouver Island. *Journal of Geophysical Research: Solid Earth*, **107**(B9), EPM 5–1–EPM 5–16. 2200.

Rignot, E., Koppes, M, & Velicogna, I. 2010. Rapid submarine melting of the calving faces of West Greenland glaciers. *Nature Geoscience*, **3**, 187–191.

Robinson, S., G. 1993. Lithostratigraphic applications for magnetic susceptibility logging of deep-sea sediment cores: examples from ODP Leg 115. *Geological Society, London, Special Publications*, **70**(1), 65–98.

Rothwell, R., G., & Rack, F. R. 2006. New techniques in sediment core analysis: an introduction. *Geological Society, London, Special Publications*, **267**(1), 1–29.

Ruddiman, W., F. 2001. *Earths Climate. Past and Future*. Freeman.

Ruddiman, F. W., & McIntyre, A. 1981. The North Atlantic Ocean during the last deglaciation. *Palaeogeography, Palaeoclimatology, Palaeoecology*, **35**, 145–214.

Sacchetti, F., Benetti, S., Georgiopoulou, A., Shannon, P. M., O'Reilly, B. M., Dunlop, P., Quinn, R., & Ó Cofaigh, C. 2012. Deep-water geomorphology of the glaciated Irish margin from high-resolution marine geophysical data. *Marine Geology*, **291294**(0), 113 – 131.

Scher, H. D., Whittaker, J. M., Williams, S. E., Latimer, J. C., Kordesch, W. E. C, & Delaney, M. L. 2015. Onset of Antarctic Circumpolar Current 30 million years ago as Tasmanian Gateway aligned with westerlies. *Nature*, **523**, 580–583.

Schonfeld, J. 2002. A new benthic foraminiferal proxy for near-bottom current velocities in the Gulf of Cadiz, northeastern Atlantic Ocean. *Deep Sea Research Part I: Oceanographic Research Papers*, **49**(10), 1853 – 1875.

Schonfeld, J., Alve, E., Geslin, E., Jorissen, F., Korsun, S., & Spezzaferri, S. 2012. The FOBIMO (FOraminiferal BIo-MOnitoring) initiativeTowards a standardised protocol for soft-bottom benthic foraminiferal monitoring studies. *Marine Micropaleontology*, **9495**, 1 – 13.

Scourse, J. D., Hall, I. R., McCave, I. N., Young, J. R., & Sugdon, C. 2000. The origin of Heinrich layers: evidence from H2 for European precursor events. *Earth and Planetary Science Letters*, **182**(2), 187 – 195.

Scourse, J. D., Haapaniemi, A. I., Colmenero-Hidalgo, E., Peck, V. L., Hall, I. R., Austin, W. E. N., Knutz, P. C., & Zahn, R. 2009. Growth, dynamics and deglaciation of the last British-Irish Ice Sheet: the deep-sea ice-rafted detritus record. *Quaternary Science Reviews*, **28**(2728), 3066 – 3084.

Sejrup, H. P., Hjelstuen, B. O., Dahlgren, K. I. T., Haflidason, H., Kuijpers, A., Nygrd, A., Praeg, D., Stoker, M. S., & Vorren, T. O. 2005. Pleistocene glacial history of the NW European continental margin. *Marine and Petroleum Geology*, **22**(910), 1111 – 1129. The STRATAGEM Project.

Sejrup, H., P., & Guilbault, J-P. 1980. Cassidulina reniforme and C. obtusa (Foraminifera), Taxonomy, Distribution, and Ecology. *Sarsia*, **65**, 79–85.

Shipp, S. S., Wellner, J. S., & Anderson, J. B. 2002. Retreat signature of a polar ice stream: sub-glacial geomorphic features and sediments from the Ross Sea, Antarctica. *Special oublications, Geological Society, London*, **203**, 277–304.

Smith, A.G., & Pickering, K.T. 2003. Oceanic gateways as a critical factor to initiate icehouse Earth. *Journal of the Geological Society*, **160**(3), 337–340.

Stocker, T.F., Qin, D., Plattner, G.-K., Tigner, M., Allen, S.K., Boschung, J., Nauels, A., Xia, Y., Bex, V., & Midgley, P.M. (eds). 2013. *Climate Change 2013: The Physical Science Basis. Contribution of Working Group I to the Fifth Assessment Report of the Intergovernmental Panel on Climate Change*. Cambridge University Press, Cambridge, United Kingdom and New York, NY, USA. Chap. Summary for Policymakers.

Stow, D.A.V., & Shanmugam, G. 1980. Sequence of structures in fine-grained turbidites: Comparison of recent deep-sea and ancient flysch sediments. *Sedimentary Geology*, **25**(1), 23 – 42.

Stroeven, A. P., Httestrand, C., Kleman, J., Heyman, J., Fabel, D., Fredin, O., Goodfellow, B. W., Harbor, J.M., Jansen, J. D., Olsen, L., Caffee, M. W., Fink, D., Lundqvist, J., Rosqvist, G. C., Strmberg, B., & Jansson, K. N. 2016. Deglaciation of Fennoscandia. *Quaternary Science Reviews*, **147**, 91 – 121. Special Issue: PAST Gateways (Palaeo-Arctic Spatial and Temporal Gateways).

Stuiver, M., & Braziunas, T., F. 1993. Modeling Atmospheric^ 1^ 4C Influences and^ 1^ 4C Ages of Marine Samples to 10,000 BC. *Radiocarbon*, **35**, 137–137.

Stuiver, M., Reimer P.J., & Reimer, R.W. *CALIB7.1 www.calib.org/calib/.*

Svensson, A., Andersen, K.A., Bigler, M., Clausen, H.B., Dahl-Jensen, D., Davies, S.M., Johnsen, S.J., Muscheler, R., Rasmussen, S.O., Rthlisberger, R., Steffensen, J.P., & Vinther, B.M. 2006. The Greenland Ice Core Chronology 2005, 15-42 ka. Part 2: comparison to other records. *Quaternary Science Reviews*, **25**(2324), 3258 – 3267.

Syvitski, J. M. P. 1991. Towards an understanding of sediment deposition on glaciated continental shelves. *Continental Shelf Research*, **11**(810), 897 – 937. Proceedings of the Canadian Continental Shelf Seabed Symposium (C2S3).

Syvitski, J. P. M., & Praeg, D. B. 1989. Quaternary Sedimentation in the St. Lawrence Estuary and Adjoining Areas, Eastern Canada: An Overview Based on High-Resolution Seismo-Stratigraphy. *Geographie physique et Quaternaire*, **43**, 291–310.

Taschek, J. 2011. *Visualization of how multibeam bathymetry is collected. Deep-Water Mid-Atlantic Canyons. http://oceanexplorer.noaa.gov.*

Thierens, M., Pirlet, H., Colin, C., Latruwe, K., Vanhaecke, F., Lee, J. R., Stuut, J.-B., Titschack, J., Huvenne, V.A.I., Dorschel, B., Wheeler, A.J., & Henriet, J.-P. 2012. Ice-rafting from the British-Irish ice sheet since the earliest Pleistocene (2.6 million years ago): implications for long-term mid-latitudinal ice-sheet growth in the North Atlantic region. *Quaternary Science Reviews*, **44**, 229 – 240. Quaternary Glaciation History of Northern Europe.

Traill, W. A. 1875. On the occurrence of a lower boulder-clay or till, with shells, in the counties of Down and Mayo, Ireland. *British Association Report*, 83–84.

Vail, P. R., Mitchum, R. M., & Thomson, S. III. 1977. *Seismic Stratigraphy–Applications to Hydrocarbon Exploration.* AAPG Special Volumes. Chap. Seismic Stratigraphy and Global Changes of Sea Level, Part 3: Relative Changes of Sea Level from Coastal Onlap: Section 2. Application of Seismic Reflection Configuration to Stratigrapic Interpretation, pages 63–81.

Vaughan, D.G., Comiso, J.C., Allison, I., Carrasco, J., Kaser, G., Kwok, R., Mote, P., Murray, T., Paul, F., Ren, J., Rignot, E., Solomina, O., Steffen, K., & Zhang, T. 2013. *Climate Change 2013: The Physical Science Basis. Contribution of Working Group I to the Fifth Assessment Report of the Intergovernmental Panel on Climate Change.* Cambridge University Press, Cambridge, United Kingdom and New York, NY, USA. Chap. Observations: Cryosphere.

Veeken, P.C.H. 2007. *Seismic Stratigraphy, Basin Analysis and Reservoir Characterisation.* Eslevier.

Vilks, G. 1981. Late Glacial-Postglacial Foraminiferal Boundary in Sediments of Eastern Canada, Denmark and Norway. *Geoscience Canada*, **8**(2), 48–55.

Waelbroeck, C., Labeyrie, L., Michel, E., Duplessy, J. C., McManus, J. F., Lambeck, K., Balbon, E., & Labracherie, M. 2002. Sea-level and deep water temperature changes derived from benthic foraminifera isotopic records. *Quaternary Science Reviews*, **21**(13), 295 – 305.

Warren, B.A. 1983. Why is no deep water formed in the North Pacific? *Journal of Marine Research*, **41**(2), 327–347.

Weber, M., E., Niessen, F., Khun, G., & Wiedicke, M. 1997. Calibration and application of marine sedimentary physical properties using a multi-sensor core logger. *Marine Geology*, **136**, 151–172.

8. *Apendix I*

This Appendix lists all the identified foraminiferal species found in the 55 samples from the five sediment cores: CE08-010, CE08-018, JC106-095, JC106-100 and JC106-102 along with count sheets from each of the five sampled cores. Count sheets are presented with species name on the X-axis and sample depth on the Y-axis. As the number of identified species exceeds the page size, tables have been divided into two parts:

8.1 Identified foraminifera

Biloculina depressa
Bolivina
Bolivina spathulata
Bolivinellina pseudopunctata
Buccella frigida
Bulimena marginata
Cassidulina laevigata
Cassidulina obtusa
Cassidulina reniforme
Cibicides lobatulus
Cibicides sp
Cyclogyra
Elphidium Albiumbilicatum
Elphidium Crispum
Elphidium Excavatum
Elphidium Excavatum clavatum
Elphidium Excavatum selseyensis
Elphidium Subarcticum
Elphidium Gerthi
Elphidium Macellum
Elphidium Williamsoni Haynes
Elphidium sp.
Fissurina orbignyana
Haynesina germanica
Lagena laevis
Lagena semilineata
Lagena sp
lagena sulcata
Lamarckina sp
Laryngosigma
Melonis barleeanum
Miliolinella
Noniunella labradorica
Oolina Borealis
Oolina Globosa
Oolina melo
Oolina sp.
Oolina williamsoni
Planorbulina distoma
Quinqueloculina nata
Quinqueloculina seminulum
Quinqueloculina sp
Rosalina anomala
Stainforthia fusiformis
Stainforthia sp.
Spiroloculina excavata
Textularia segitula
Textularia trancata
Trifarina angulosa
Triloculina
Vulvulina fusca (agglutinated)

8.2 Core CE08-010

Sample Depth	Species Name	*Biloculina depressa*	*Bolivina*	*Bolivina spathulata*	*Bolivinellina pseudopunctata*	*Buccella frigida*	*Bulimena marginata*	*Cassidulina laevigata*	*Cassidulina obtusa*	*Cassidulina reniforme*	*Cibicides lobatulus*	*Cibicides sp*	*Cyclogyra*	*Elphidium Albiumbilicatum*	*Elphidium Crispum*	*Elphidium Excavatum*	*Elphidium Excavatum f. clavata*	*Elphidium Excavatum f. selseyensis*	*Elphidium Subarcticum*	*Elphidium Gerthi*	*Elphidium Macellum*	*Elphidium Williamsoni Haynes*	*Elphidium sp.*	*Fissurina orbignyana*	*Haynesina germanica*	*Lagena laevis*
144			4			1	1	22	57							14	14									
160			1				2	49	50			3		7	38											
176				4				200	4					9	176		10			1		1		1		
192								7	1						7											
208							1	180	43	1					172		8				30					
224							2	80	33			2		5	24					1						
240				1			2	148	9					9	51							1				
256								5	4		1			6	1											
272			1	2			2	133	30						57						9					
288							1	23	17					2	13											
304			1				5	36	78						14						9	1				
320		1	2				7	33	63					2	22							2				
336			1		1		2	28	23		1			8	17	3		1			1	2				
352				9			2	183	6					40	96								9			
368								3	2					4	3								1			
384							1	122	19					12	53							1				
400			1	3				221	7					10	79											
416			1	1			1	76	9						47						16					
432				1			1	88	35						65		4				5					
448				36				108	10		7			70	82					1		1				
464				7			1	276	25					20	111		6									
480								74	27						80		1				16					
496								12	1						3											
512				6			1	185	13		2			55	80						1					
528								7							12											
544				1				9							32											
560								20	3						36											
576								33	3			2		15	38											

Sample Depth	Species Name	*Lagena semilineata*	*Lagena sp.*	*Lagena sulcata*	*Lamarckina sp.*	*Laryngosigma sp.*	*Melonis barleeanum*	*Miliolinella*	*Nonionella labradorica*	*Oolina Borealis*	*Oolina Globosa*	*Oolina melo*	*Oolina sp.*	*Oolina Williamsoni*	*Planorbulina distoma*	*Quinqueloculina lata*	*Quinqueloculina seminulum*	*Quinqueloculina sp.*	*Rosalina anomala*	*Stainforthia fusiformis*	*Stainforthia sp.*	*Spiroloculina excavata*	*Textularia agglutinata*	*Textularia sagittula*	*Textularia truncata*	*Trifarina angulosa*	*Triloculina*	*Valvulina Fusca (agglutinated)*	Unidentified	Planktic	Total
144					1			2							2	8		12	4			65	7				1	22	215
160							2								1								1					4	2	158
176								30		3	1		1		2	16	8	5											45	472
192																1													3	16
208							3	28		4		1	1	3		12			2									3	23	492
224																												4		151
240										1						4						1							9	227
256							1																					1		19
272								3			1					5		4	1										7	248
288				2				4		1					3	3		2				22	4			3			9	100
304			1	4			1	5								19		11	8	2	1	63	9			7			49	275
320				1			6		1	1						7		18	6		1	78	11			2	1		33	265
336				3			1	1			1				5	9		2	2			11	4		7	3			10	137
352								19		3						11		2											33	380
368																	3	1									1		16	18
384								3								3											1		5	215
400								6	1							8		13									2		16	351
416								2		1						3		1											8	158
432								4		1						2								1					1	207
448							4	17		6	1				3	38		19									1		48	404
464								2	1							9		7											3	465
480	1	1						7		2								3											9	212
496																														16
512								10					1		4	14	16		1								25	17	414
528							1	1		1						4														26
544								1								2													2	45
560																3														62
576							2	1								6											1	7	101

8.3 Core CE08-018

Sample Depth	Species Name	*Biloculina depressa*	*Bolivina*	*Bolivina spathulata*	*Bolivinellina pseudopunctata*	*Buccella frigida*	*Bulimena marginata*	*Cassidulina laevigata*	*Cassidulina obtusa*	*Cassidulina reniforme*	*Cibicides lobatulus*	*Cibicides* sp	*Cyclogyra*	*Elphidium Albiumbilicatum*	*Elphidium Crispum*	*Elphidium Excavatum*	*Elphidium Excavatum f. clavata*	*Elphidium Excavatum f. selseyensis*	*Elphidium Subarcticum*	*Elphidium Gerthi*	*Elphidium Macellum*	*Elphidium Williamsoni Haynes*	*Elphidium* sp.	*Fissurina orbignyana*	*Haynesina germanica*	*Lagena laevis*
62		1					1	13	14					1	20											
72							1	3	10					1	3											
84							7	9	77					1	68						1					
100						1	12	47	81				1		97	3			1		2		2			

Sample Depth	Species Name	*Lagena semilineata*	*Lagena sp.*	*Lagena sulcata*	*Lamarckina sp.*	*Laryngosigma sp.*	*Melonis barleeanum*	*Miliolinella*	*Nonionella labradorica*	*Oolina Borealis*	*Oolina Globosa*	*Oolina melo*	*Oolina sp.*	*Oolina Williamsoni*	*Planorbulina distoma*	*Quinqueloculina lata*	*Quinqueloculina seminulum*	*Quinqueloculina sp.*	*Rosalina anomala*	*Stainforthia fusiformis*	*Stainforthia sp.*	*Spiroloculina excavata*	*Textularia sagittula*	*Trifarina truncata*	*Trilocullina angulosa*	*Vulvulina Fusca (agglutinated)*	Unidentified	Planktic	Total
62				1				1							7												1		59
72															1														19
84					3	1	1			1					4												44		173
100					1	1			1						6											1	40		257

8.4 CoreJc106-095

Sample Depth	Species Name *Biloculina depressa*	*Bolivina*	*Bolivina spathulata*	*Bolivinellina pseudopunctata*	*Buccella frigida*	*Bulimena marginata*	*Cassidulina laevigata*	*Cassidulina obtusa*	*Cassidulina reniforme*	*Cibicides lobatulus*	*Cibicides sp*	*Cyclogyra*	*Elphidium Albiumbilicatum*	*Elphidium Crispum*	*Elphidium Excavatum*	*Elphidium Excavatum f. clavata*	*Elphidium Excavatum f. selsegensis*	*Elphidium Subarcticum*	*Elphidium Gerthi*	*Elphidium Macellum*	*Elphidium Williamsoni Haynes*	*Elphidium sp.*	*Fissurina orbignyana*	*Haynesina germanica*	*Lagena laevis*
138							37								278	21									
154							49	1					13		189	76	1								
170							35								126	92	5								
182							55								245		10			121					
202							59								260	16				51					
218		1					73								181	23				125					

Sample Depth	Species Name	*Lagena semilineata*	*Lagena sp.*	*Lagena sulcata*	*Lamarckina sp.*	*Laryngosigma sp.*	*Melonis barleeanum*	*Miliolinella*	*Nonionella labradorica*	*Oolina Borealis*	*Oolina Globosa*	*Oolina melo*	*Oolina sp.*	*Oolina Williamsoni*	*Planorbulina distorta*	*Quinqueloculina lata*	*Quinqueloculina seminulum*	*Quinqueloculina sp.*	*Rosalina anomala*	*Stainforthia fusiformis*	*Stainforthia sp.*	*Spiroloculina excavata*	*Textularia segitula*	*Triforina truncata*	*Triloculina angulosa*	*Vulvulina Fusca (agglutinated)*	Unidentified	Planktic	Total
138										1				1		3													341
154				1		2										12											1		344
170							1												3						5	1			267
182																5										2			436
202																1									3				390
218						2										2			5						6				418

8.5 CoreJc106-100

Sample Depth	Species Name	*Biloculina depressa*	*Bolivina*	*Bolivina spathulata*	*Bolivinellina pseudopunctata*	*Buccella frigida*	*Bulimena marginata*	*Cassidulina laevigata*	*Cassidulina obtusa*	*Cassidulina reniforme*	*Cibicides lobatulus*	*Cibicides sp*	*Cyclogyra*	*Elphidium Albiumbilicatum*	*Elphidium Crispum*	*Elphidium Excavatum*	*Elphidium Excavatum f. clavata*	*Elphidium Excavatum f. selseyensis*	*Elphidium Subarcticum*	*Elphidium Gerthi*	*Elphidium Macellum*	*Elphidium Williamsoni Haynes*	*Fissurina orbignyana*	*Haynesina germanica*	*Lagena laevis*
284								23			2	1	248												
300								17	2		1		36	9											
321					1	1		42	2		6		96	16							1				
336								21			1		77	14											

Sample Depth	Species Name	*Lagena semilineata*	*Lagena sp.*	*Lagena sulcata*	*Lamarckina sp.*	*Laryngosigma sp.*	*Melonis barleeanum*	*Miliolinella*	*Nonionella labradorica*	*Oolina Borealis*	*Oolina Globosa*	*Oolina melo*	*Oolina sp.*	*Oolina Williamsoni*	*Planorbulina distoma*	*Quinqueloculina lata*	*Quinqueloculina seminulum*	*Quinqueloculina sp.*	*Rosalina anomala*	*Stainforthia fusiformis*	*Stainforthia sp.*	*Spiroloculina excavata*	*Textularia sagittula*	*Textularia truncata*	*Trifarina angulosa*	*Triloculina*	*Vulvulina Fusca (agglutinated)*	Unidentified	Planktic	Total
284			8												9		4											7	295
300															4		1												70
321			4												25		6									2		2	202
336			5												14		5											1	137

8.6 CoreJc106-102

Sample Depth	Species Name	*Biloculina depressa*	*Bolivina*	*Bolivina spathulata*	*Bolivinellina pseudopunctata*	*Buccella frigida*	*Bulimena marginata*	*Cassidulina laevigata*	*Cassidulina obtusa*	*Cassidulina reniforme*	*Cibicides lobatulus*	*Cibicides sp*	*Cyclogyra*	*Elphidium Albiumbilicatum*	*Elphidium Crispum*	*Elphidium Excavatum*	*Elphidium Excavatum f. clavata*	*Elphidium Excavatum f. selseyensis*	*Elphidium Subarcticum*	*Elphidium Gerthi*	*Elphidium Macellum*	*Elphidium Williamsoni Haynes*	*Elphidium sp.*	*Fissurina orbignyana*	*Haynesina germanica*	*Lagena laevis*
56							8	57	7	1		4	9	50	26						2	1				
72			1				4	183	11				39	109	95											
88		1	2		1		6	87	4	2		11	7	125	36						2					
104								11						2	7											
120			1		1		3	106	4	1		1	1	123	31											1
136			3				4	114	5			10	3	163	36											
152							2	35	2					43	37											
168			1				2	101	1			16	11	90	33						1					
184			3				2	83	4	1		4	1	158	24							1				
200			4				1	113	6			6	2	175	26											
216					3		1	47	9					50	19											
232			5		1		2	115	6	1		6		145	20							1				
246			2		1		4	117	22			7		111	11			1				1				

Sample Depth	Species Name	*Lagena semilineata*	*Lagena sp.*	*Lagena sulcata*	*Lamarckina sp.*	*Laryngosigma sp.*	*Melonis barleeanum*	*Miliolinella*	*Nonionella labradorica*	*Oolina Borealis*	*Oolina Globosa*	*Oolina melo*	*Oolina sp.*	*Oolina Williamsoni*	*Planorbulina distorma*	*Quinqueloculina lata*	*Quinqueloculina seminulum*	*Quinqueloculina sp.*	*Rosalina anomala*	*Stainforthia fusiformis*	*Stainforthia sp.*	*Spiroloculina excavata*	*Textularia agglutinata*	*Textularia sagittula*	*Trifarina angulosa*	*Triloculina*	*Vulvulina Fusca (agglutinated)*	Unidentified	Planktic	Total
56						1				1						2		2									2	4	173
72						4	1								34	163											50	6	694
88						2										11		1									3	6	301
104							1								1	1		1										2	24
120						6				1					1	11	1					1					3	8	297
136						9				1						7											3	17	35
152				2		3										15		4										1	143
168						5	1								1	12		3									3	4	281
184						3										5	1	1										10	291
200						8									3	6		1									3	21	354
216				2		2									3	4		1										3	141
232						7										5		1									2	9	317
246						3				1						4		1									5	7	291

9. *Appendix II*

Following appendix consists core logs of the sediment cores, described in the thesis, along with photos and X-radiographs of cores, where available.

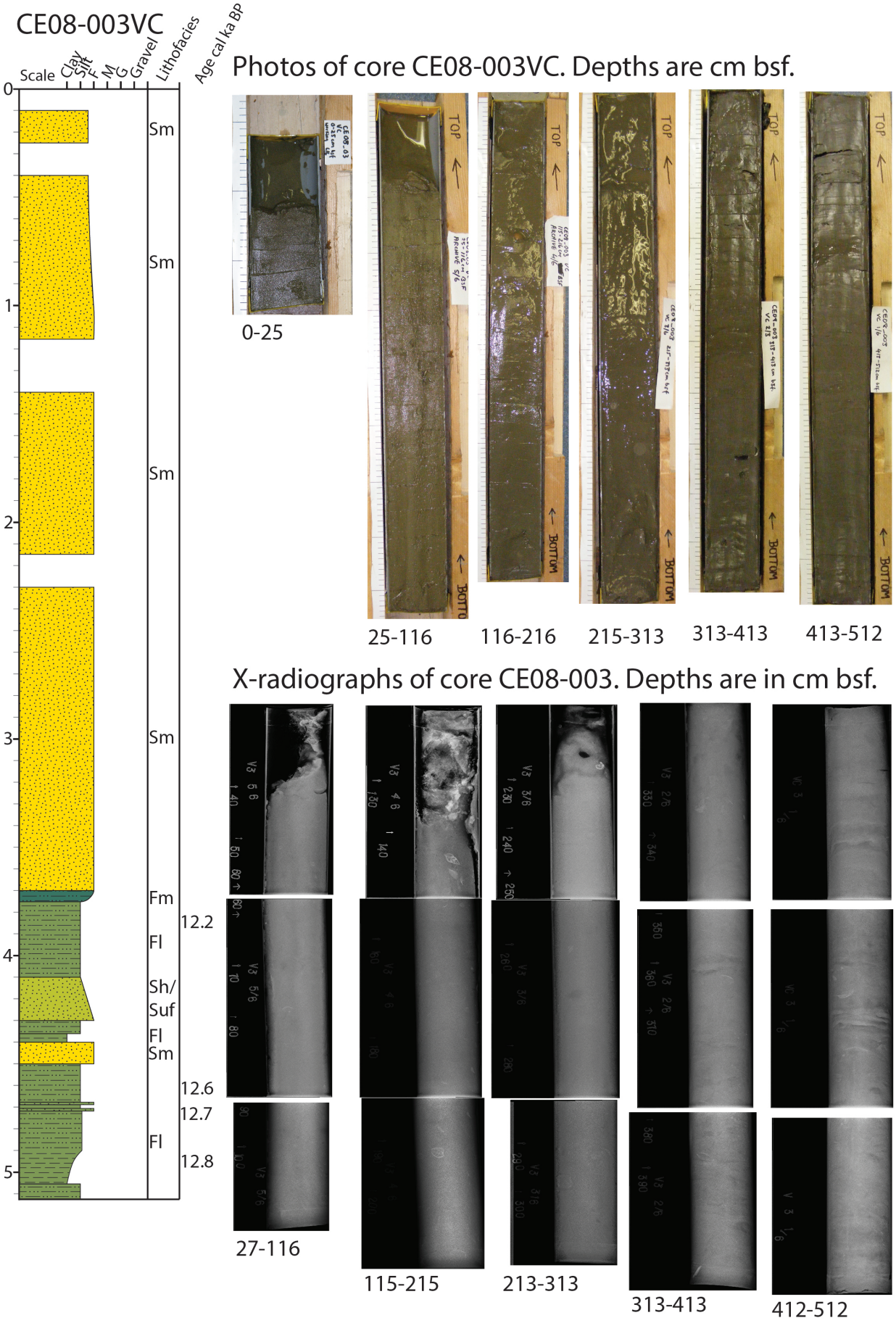

Figure 9.1: Corelog, photos and X-radiographs of core CE08-003.

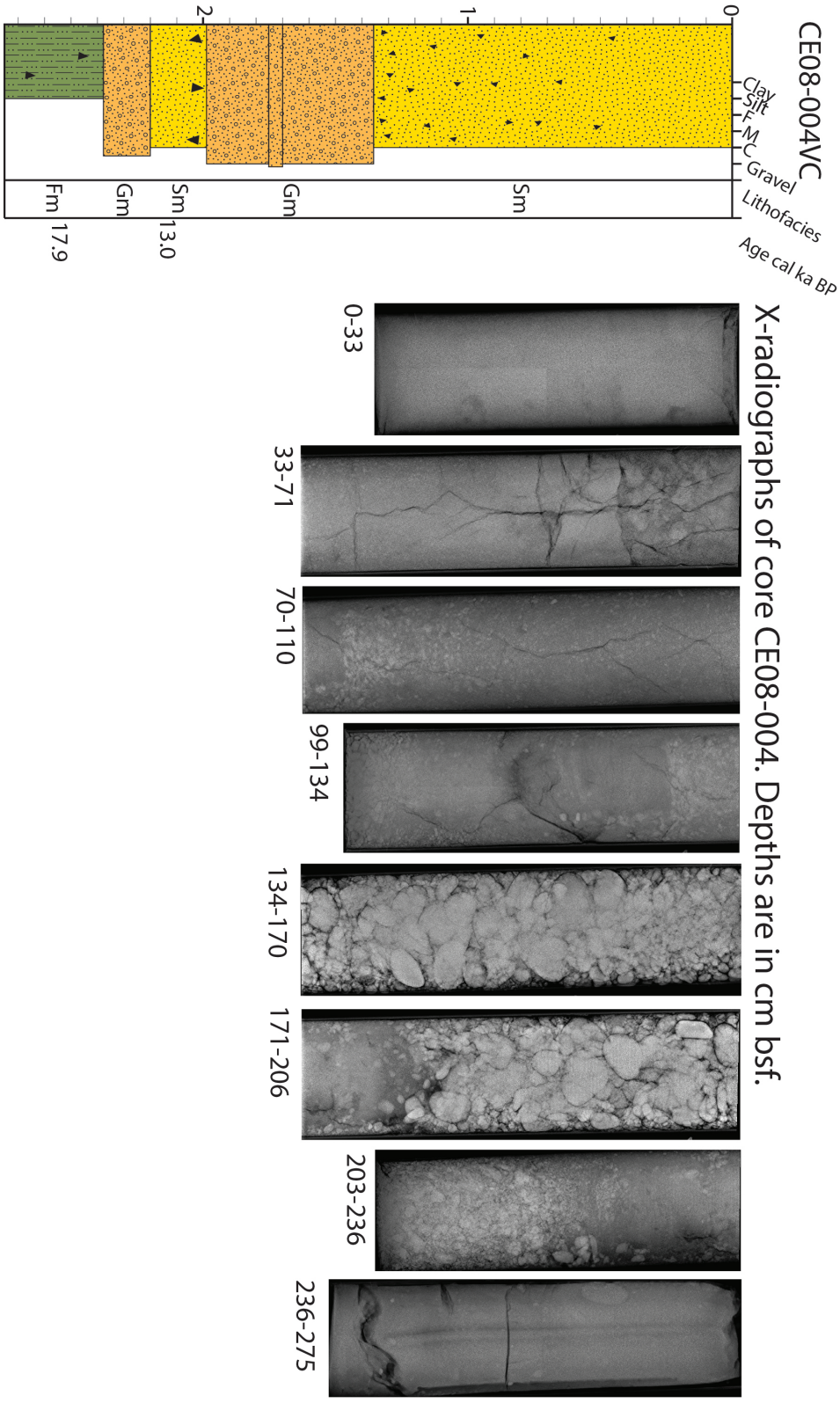

Figure 9.2: Corelog and X-radiographs of core CE08-004.

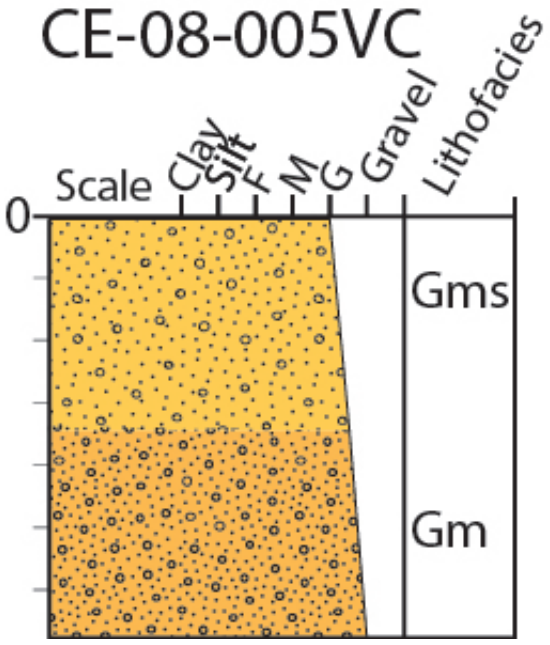

Figure 9.3: Corelog of core CE08-005.

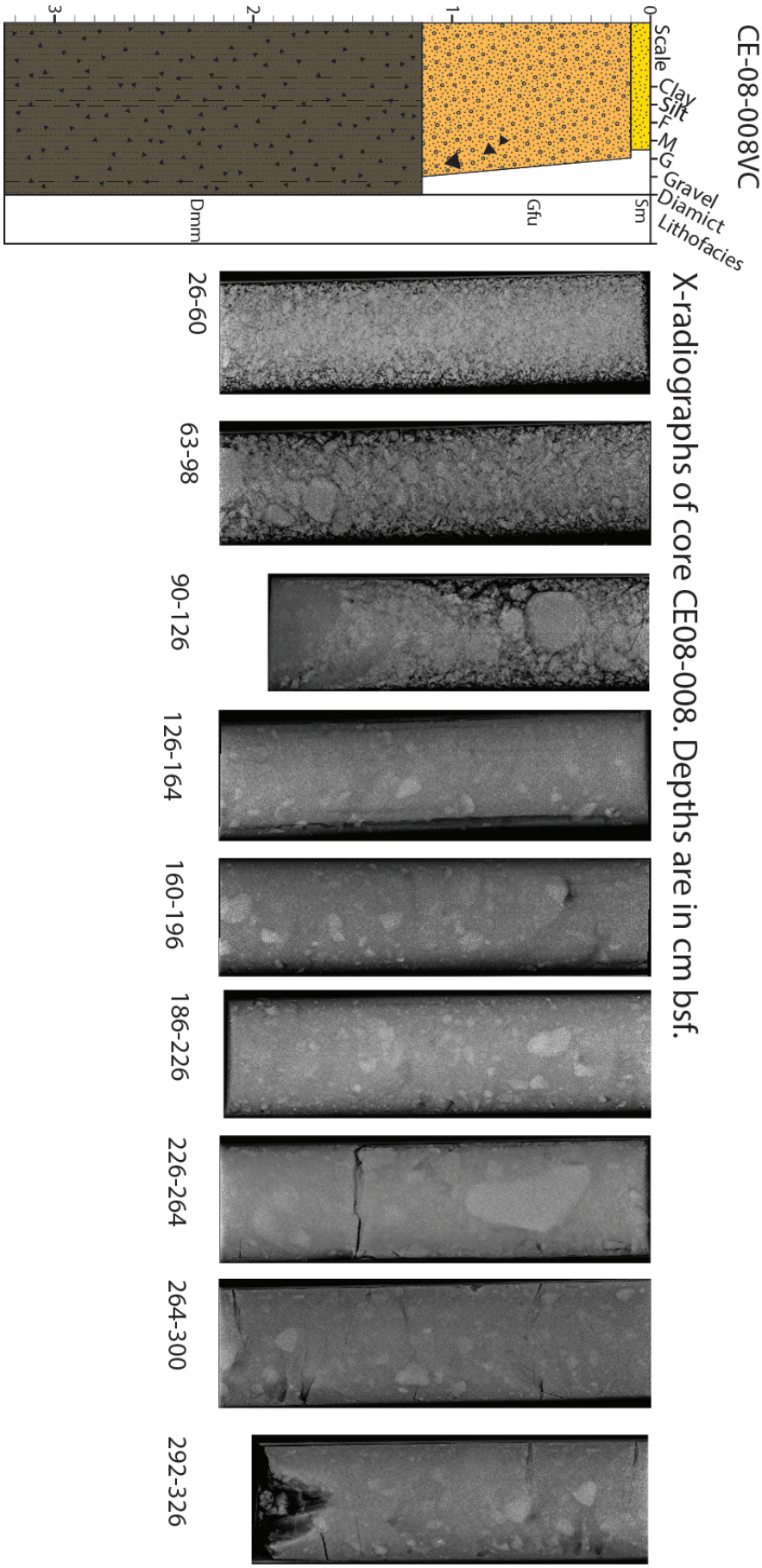

Figure 9.4: Corelog and X-radiographs of core CE08-008.

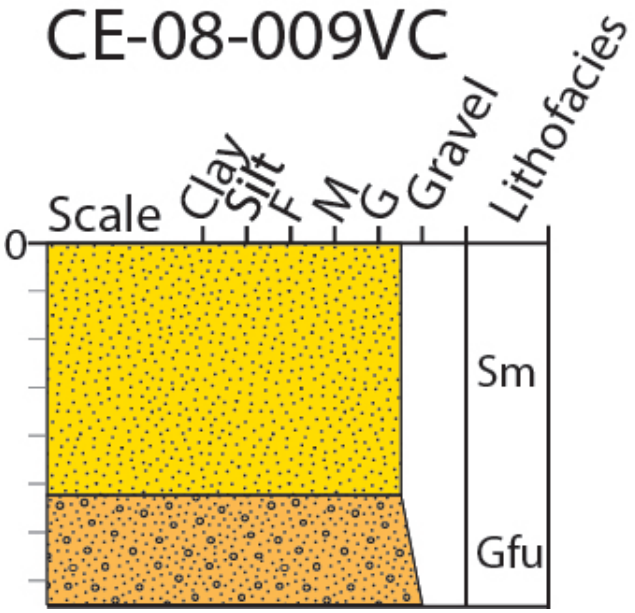

Figure 9.5: Corelog of core CE08-009.

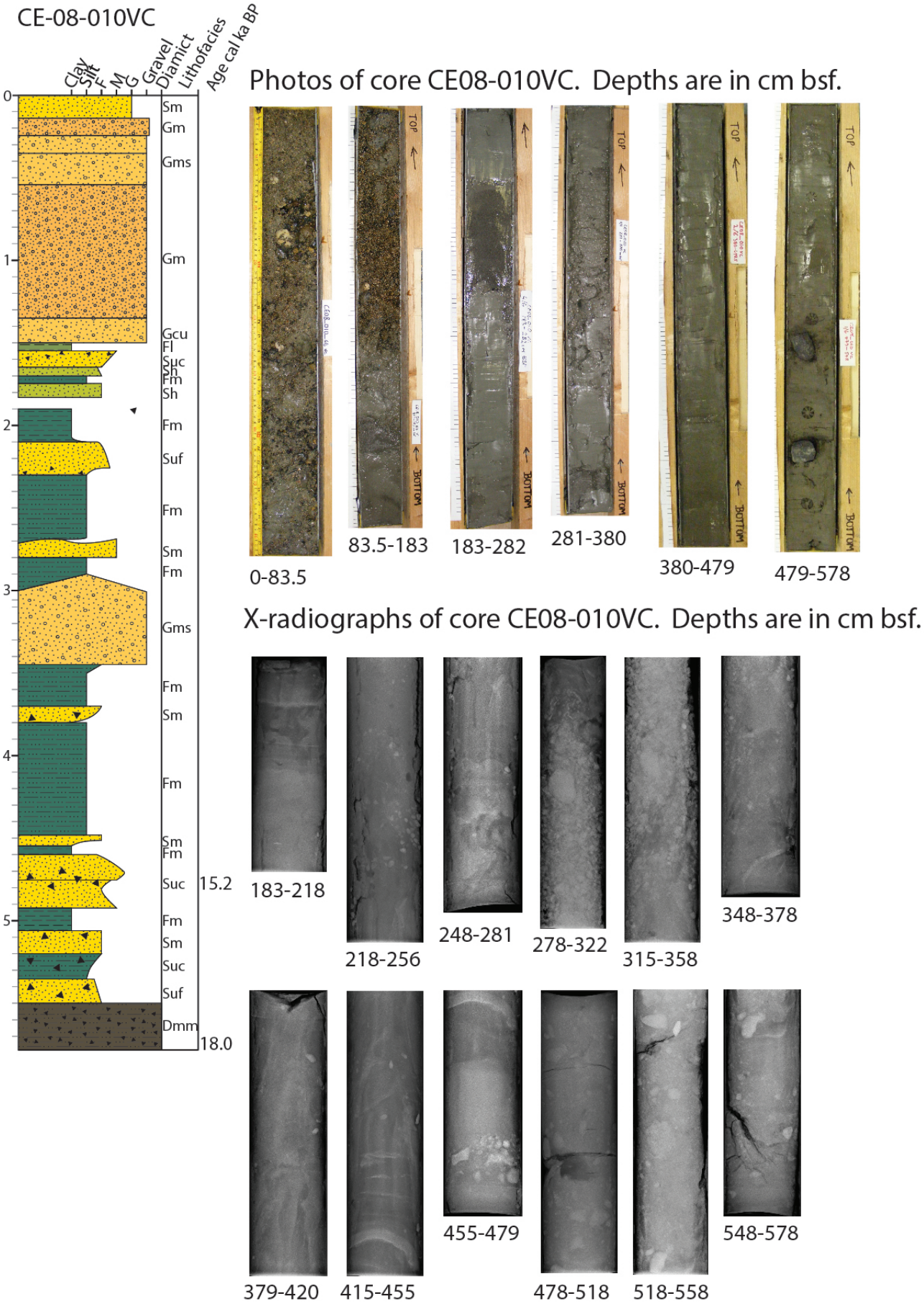

Figure 9.6: Corelog, photos and X-radiographs of core CE08-010.

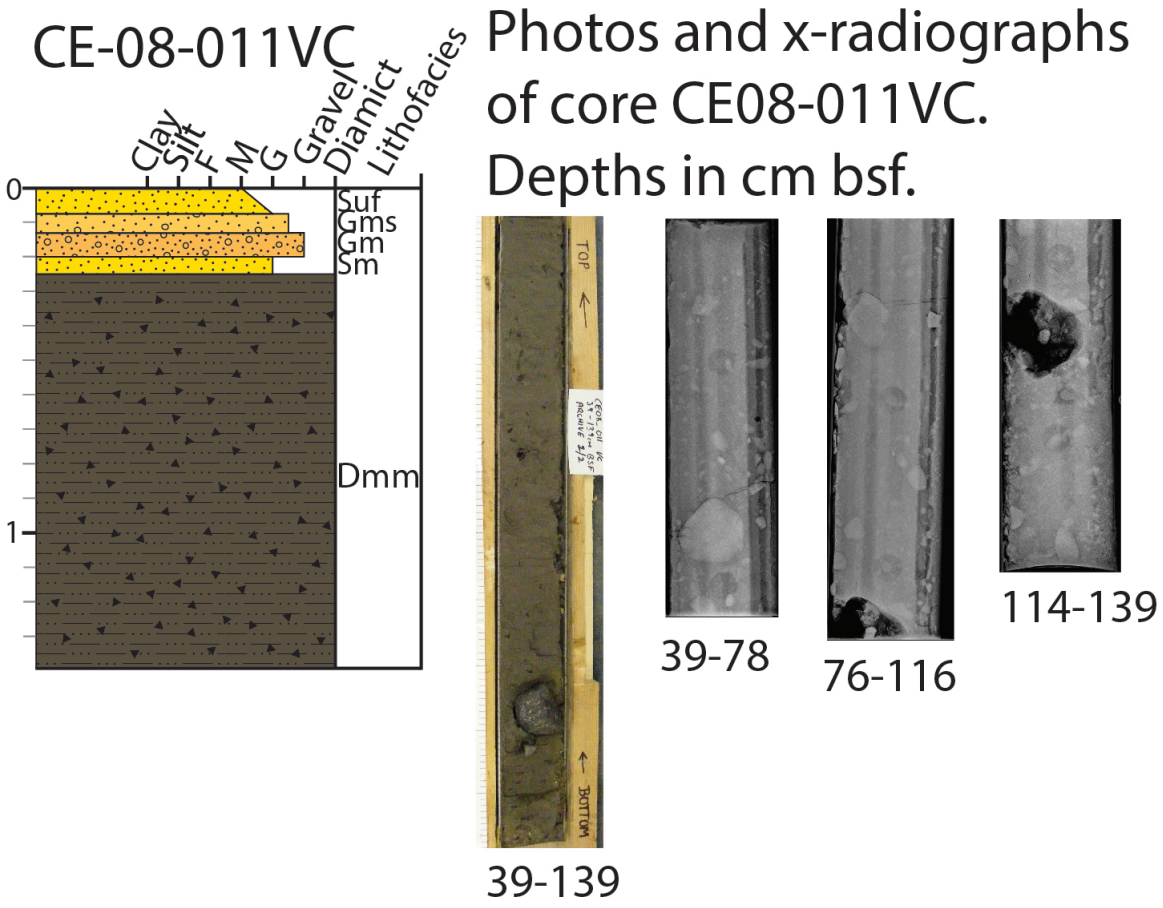

Figure 9.7: Corelog, photos and X-radiographs of core CE08-011.

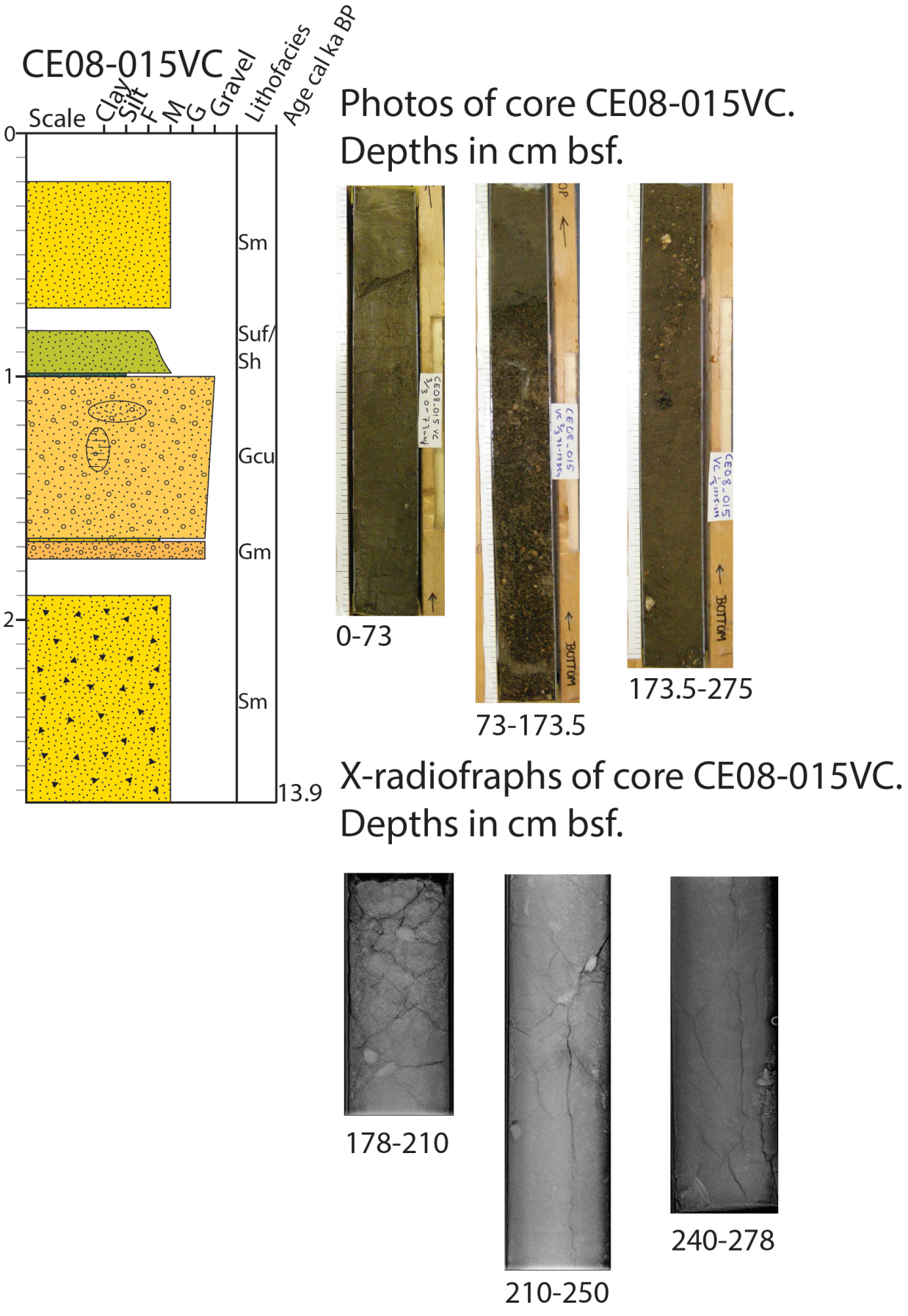

Figure 9.8: Corelog, photos and X-radiographs of core CE08-015.

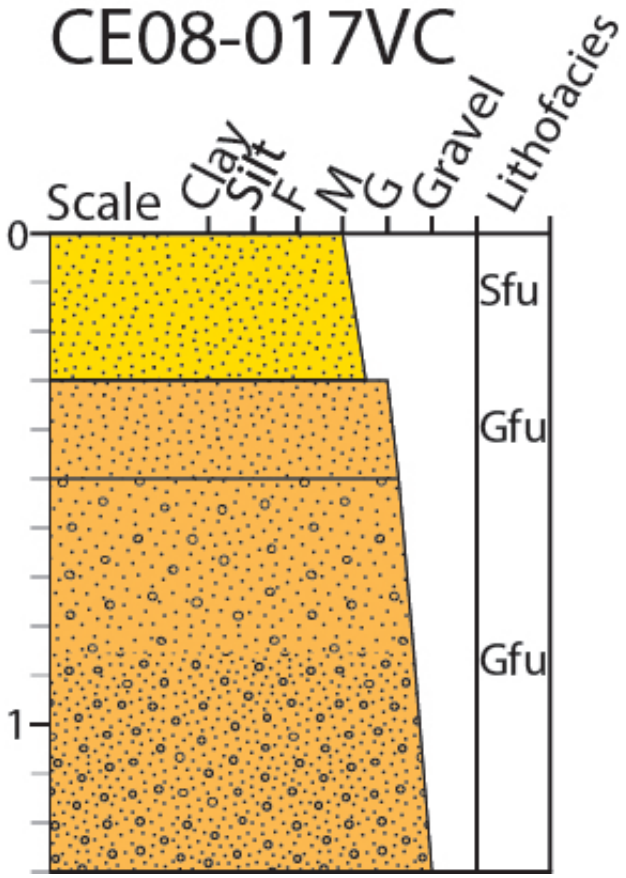

Figure 9.9: Corelog of core CE08-017.

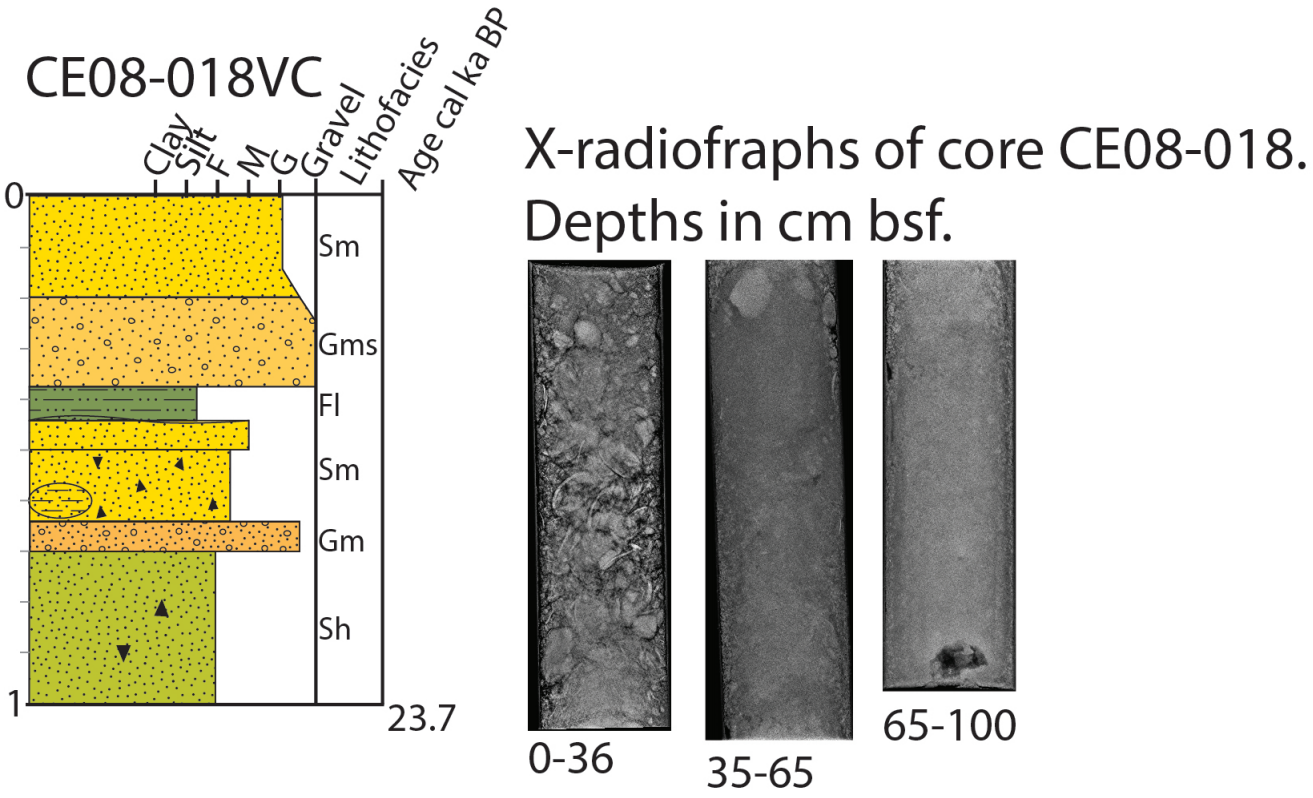

Figure 9.10: Corelog and X-radiographs of core CE08-018.

Figure 9.11: Corelog and photos of core JC106-093.

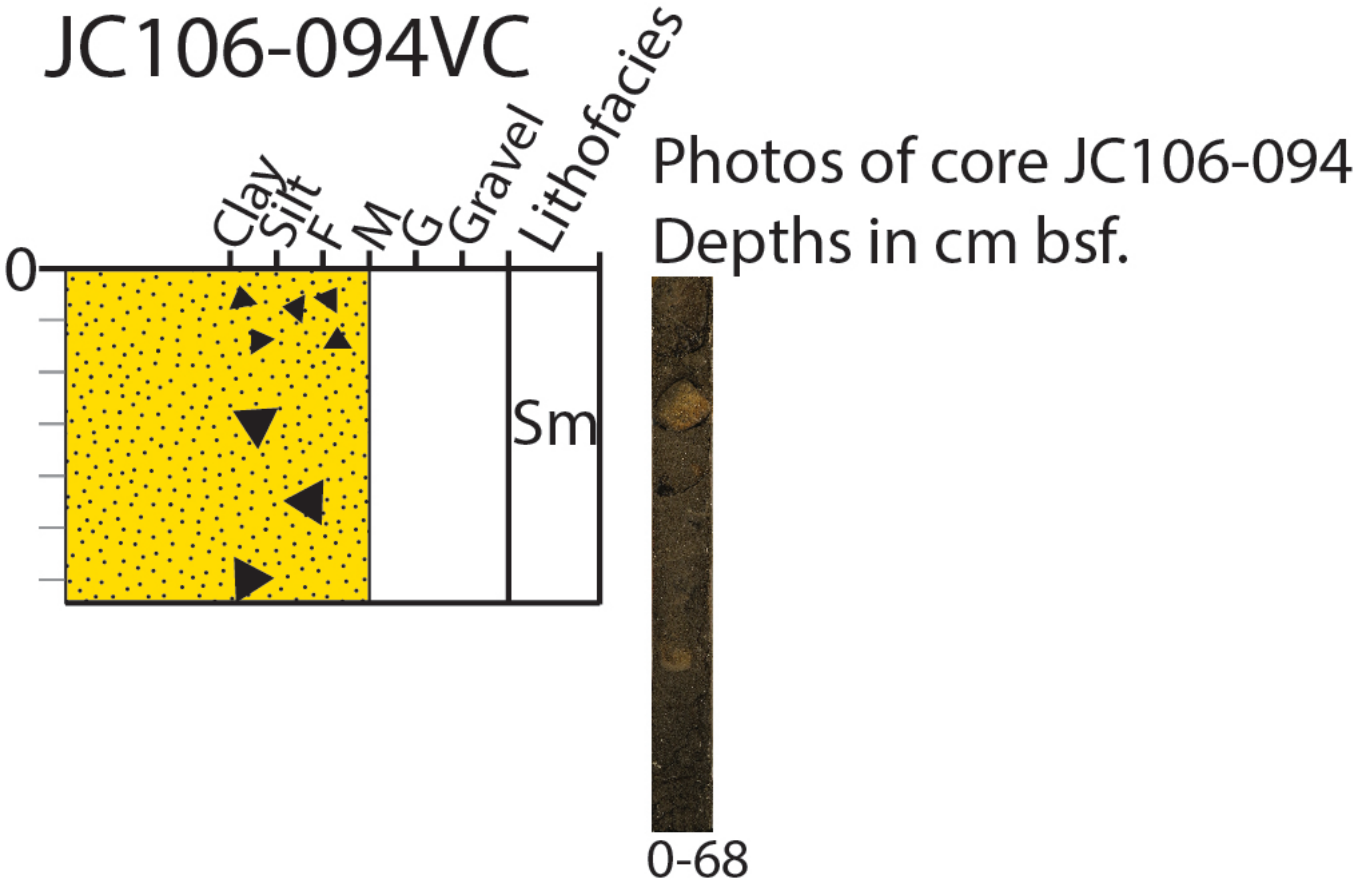

Figure 9.12: Corelog and photos of core JC106-094.

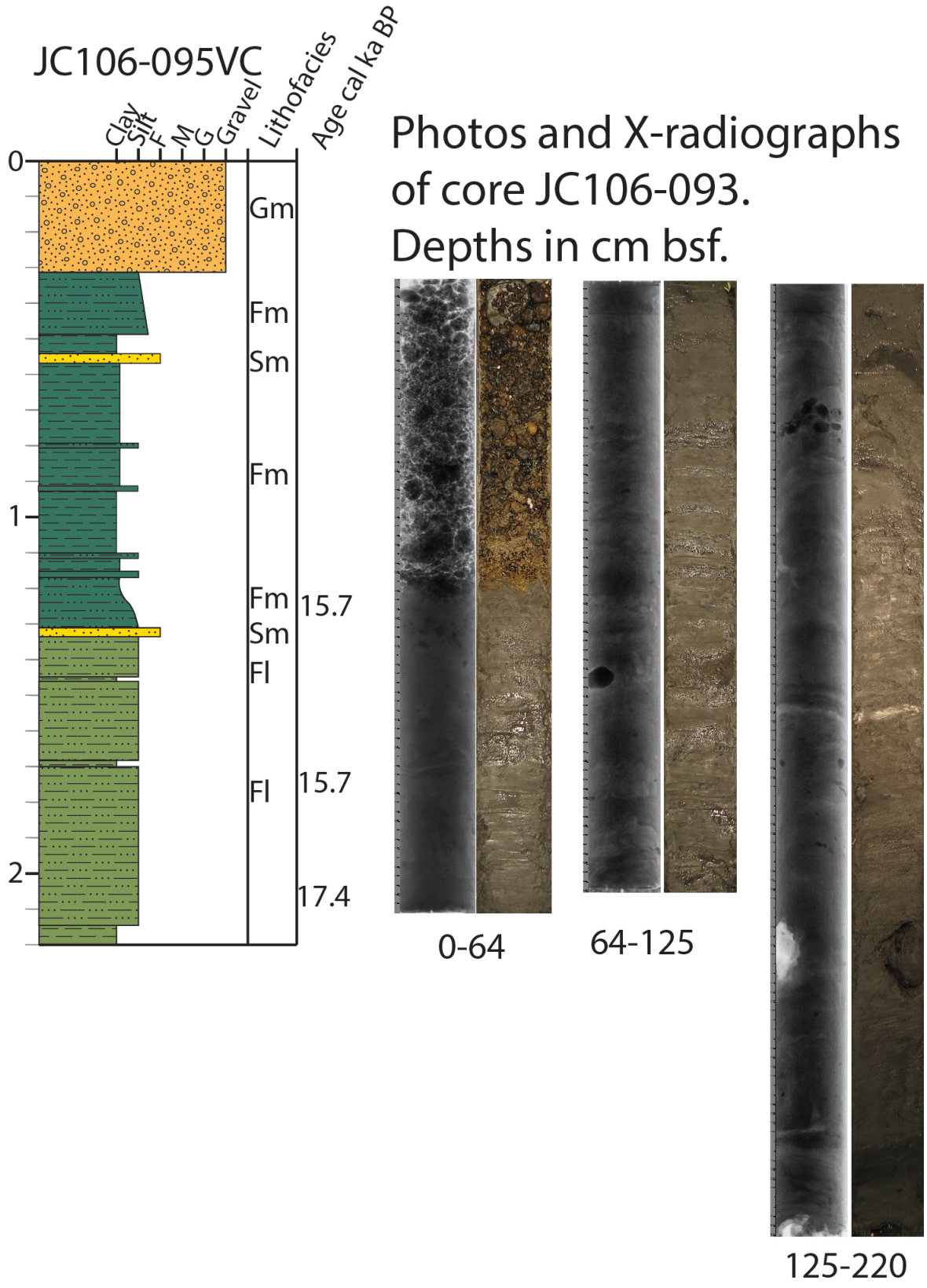

Figure 9.13: Corelog, photos and x-radiographs of core JC106-095.

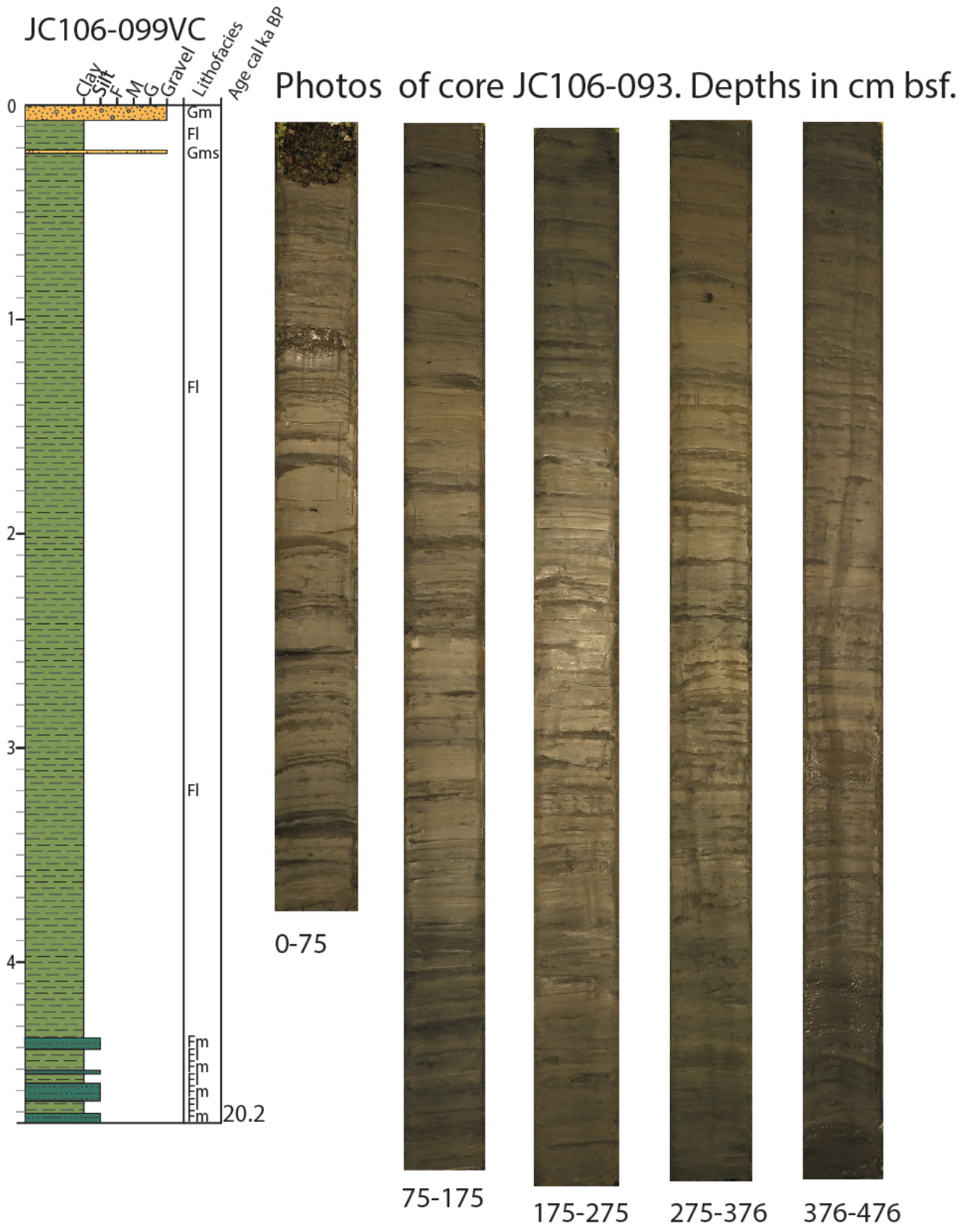

Figure 9.14: Corelog and photos of core JC106-099.

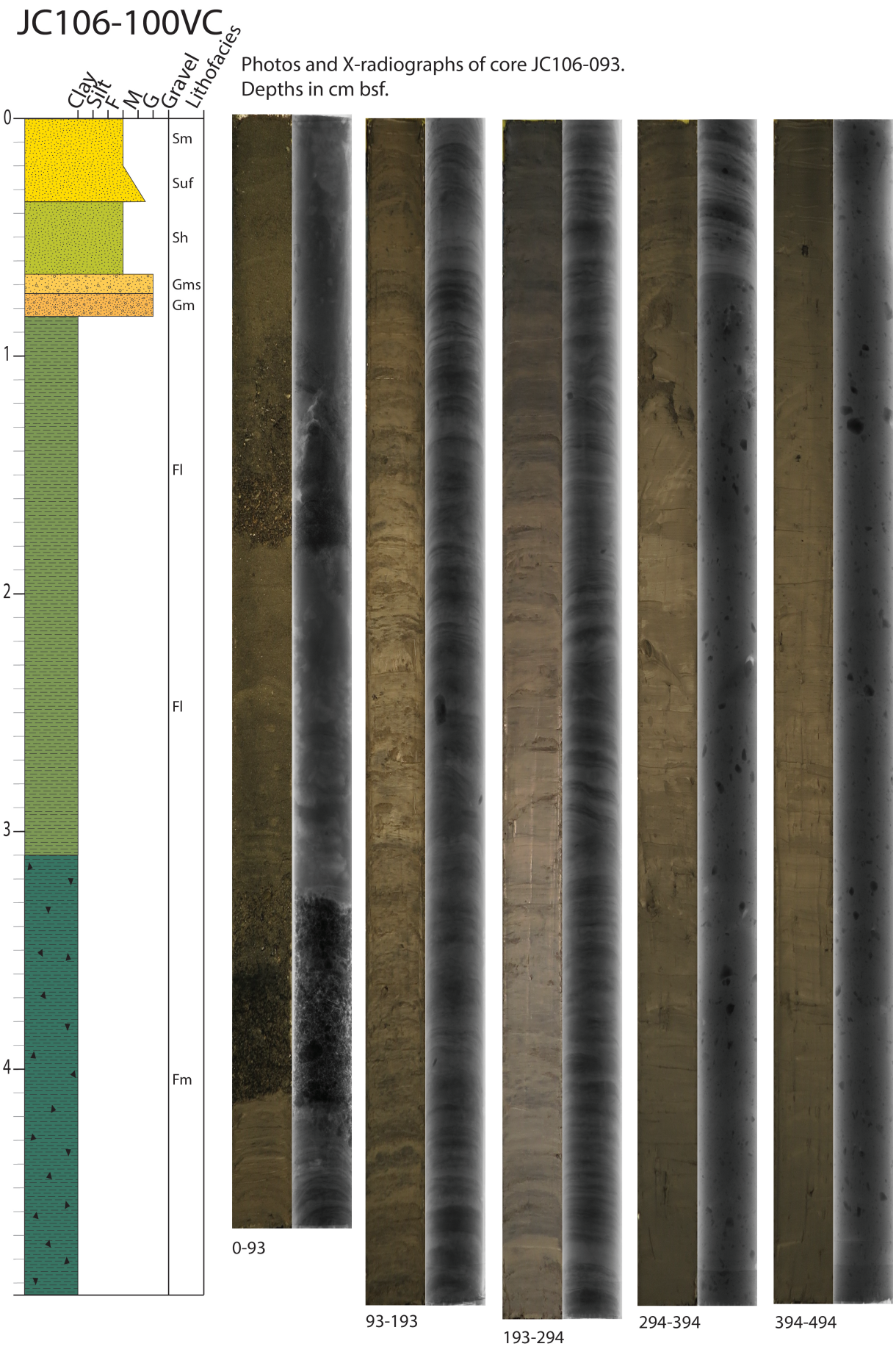

Figure 9.15: Corelog and photos of core JC106-100.

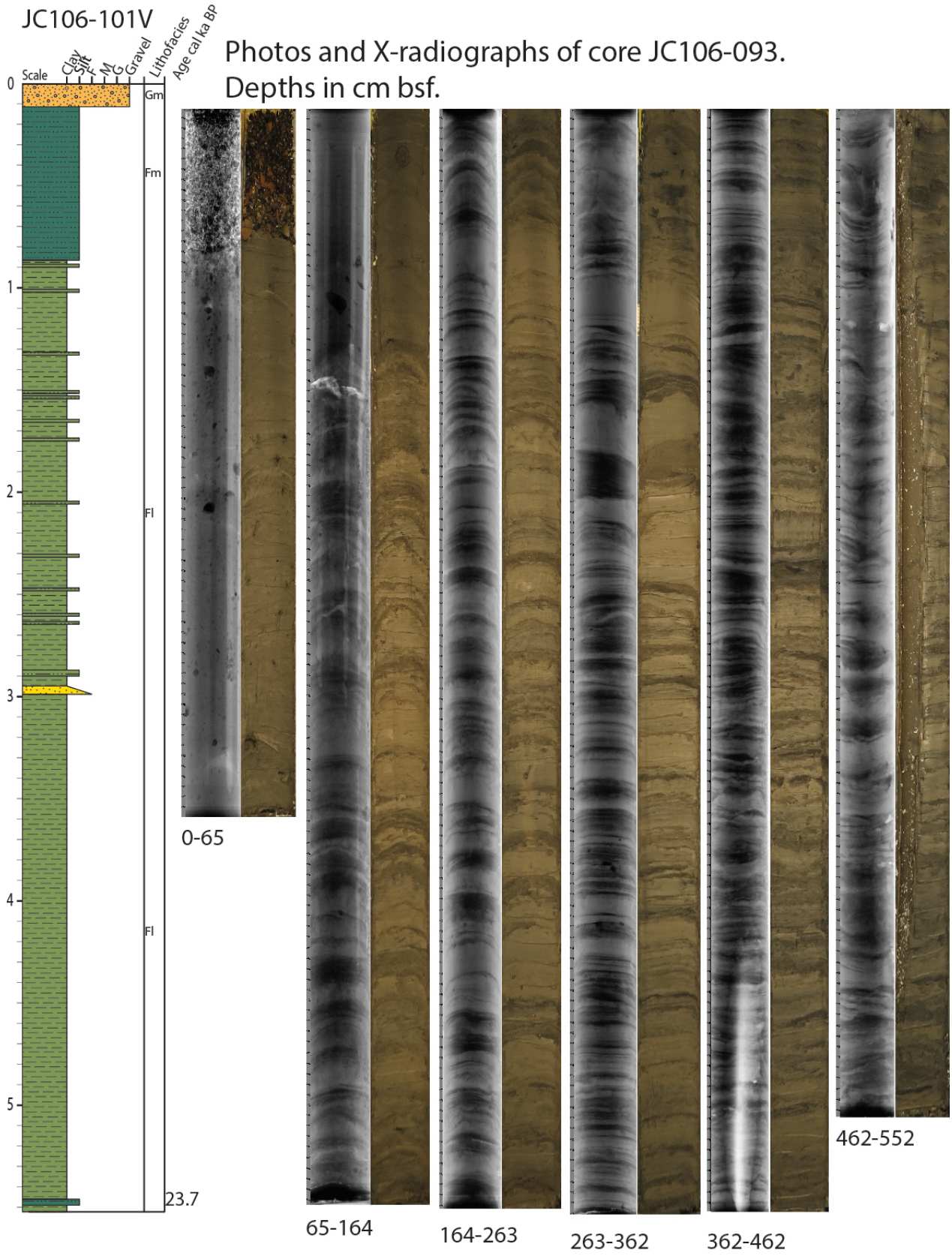

Figure 9.16: Corelog, photos and x-radiographs of core JC106-101.

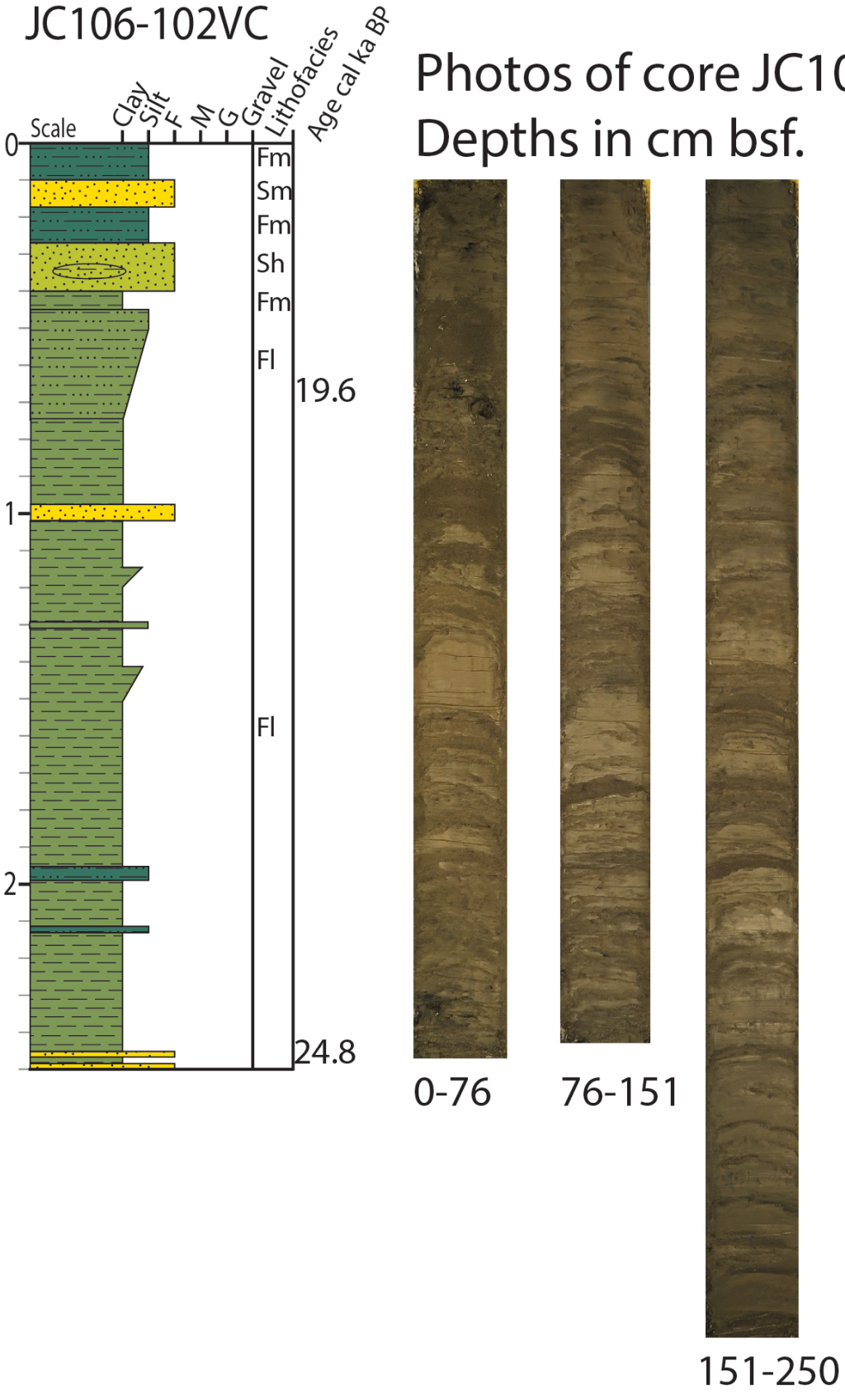

Figure 9.17: Corelog and photos of core JC106-102.

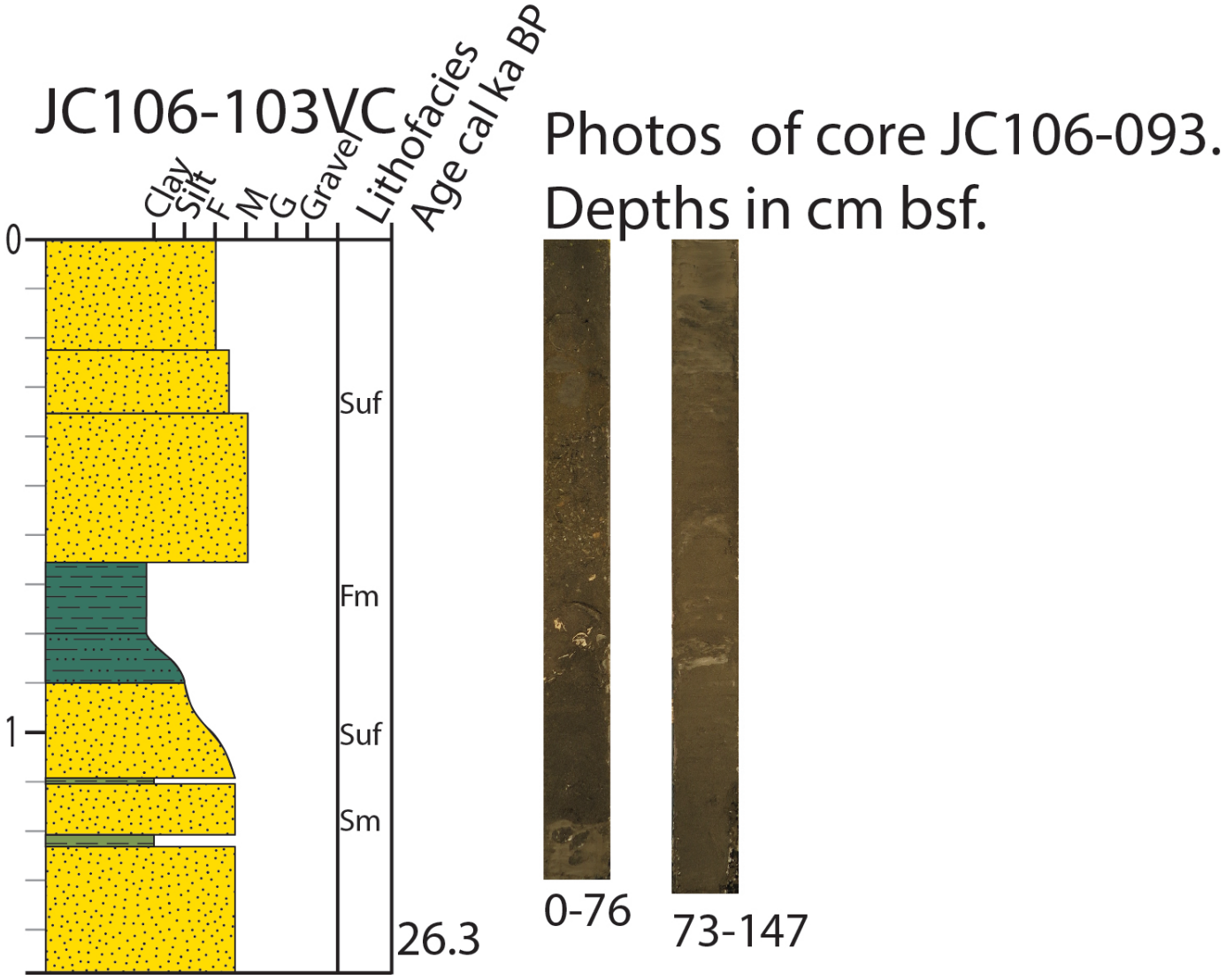

Figure 9.18: Corelog and photos of core JC106-103.

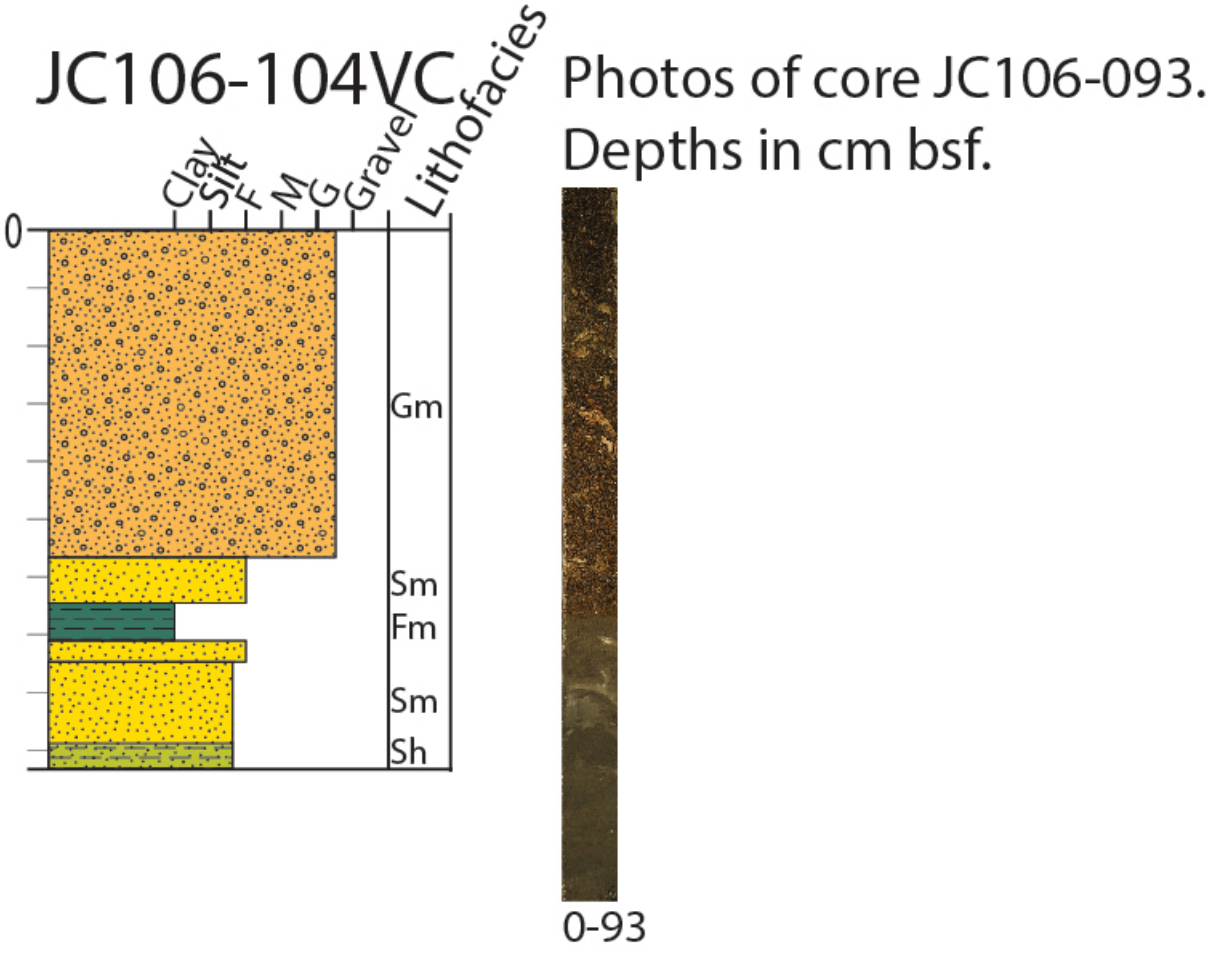

Figure 9.19: Corelog and photos of core JC106-104.

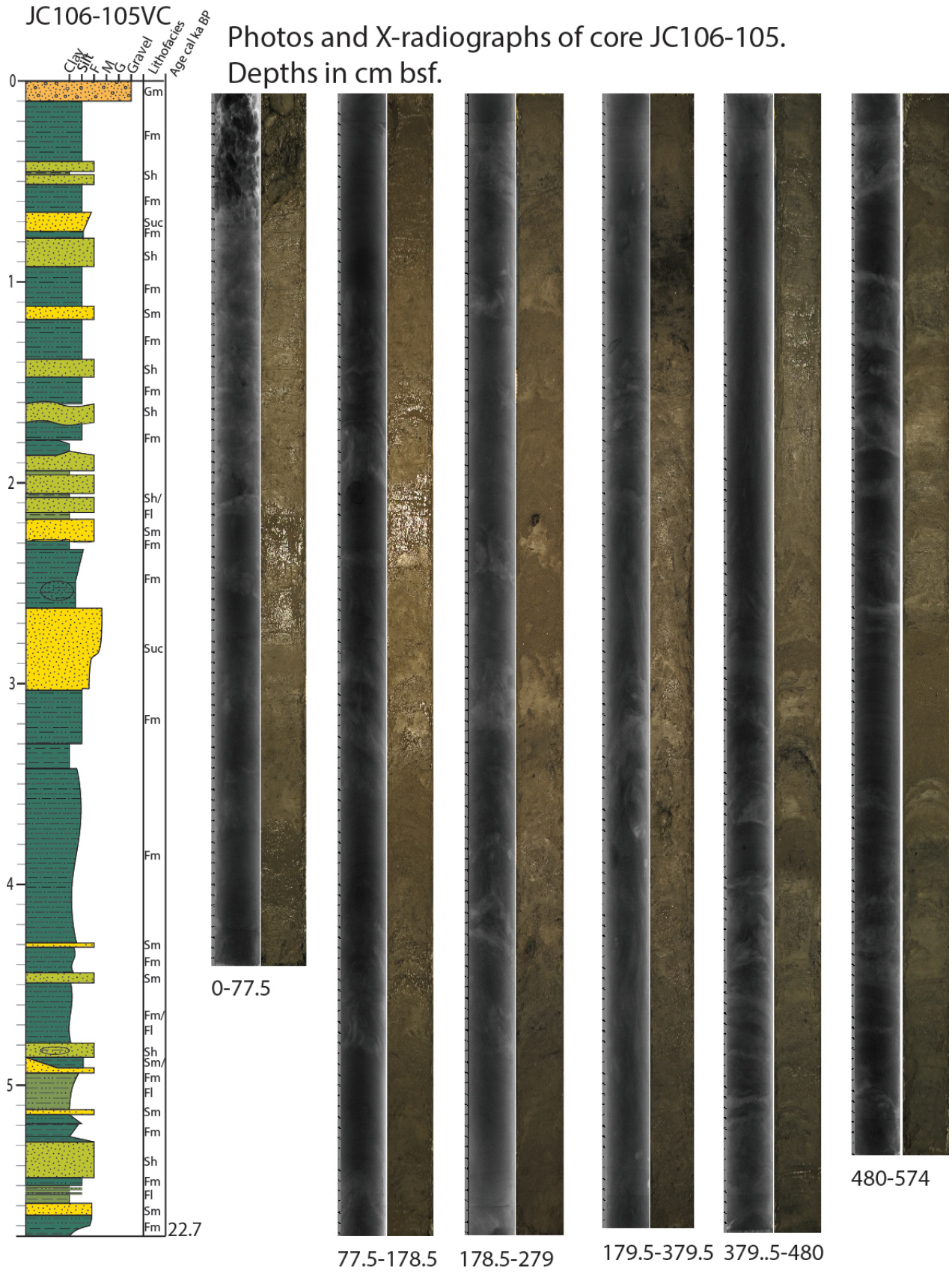

Figure 9.20: Corelog, photos and x-radiographs of core JC106-105.

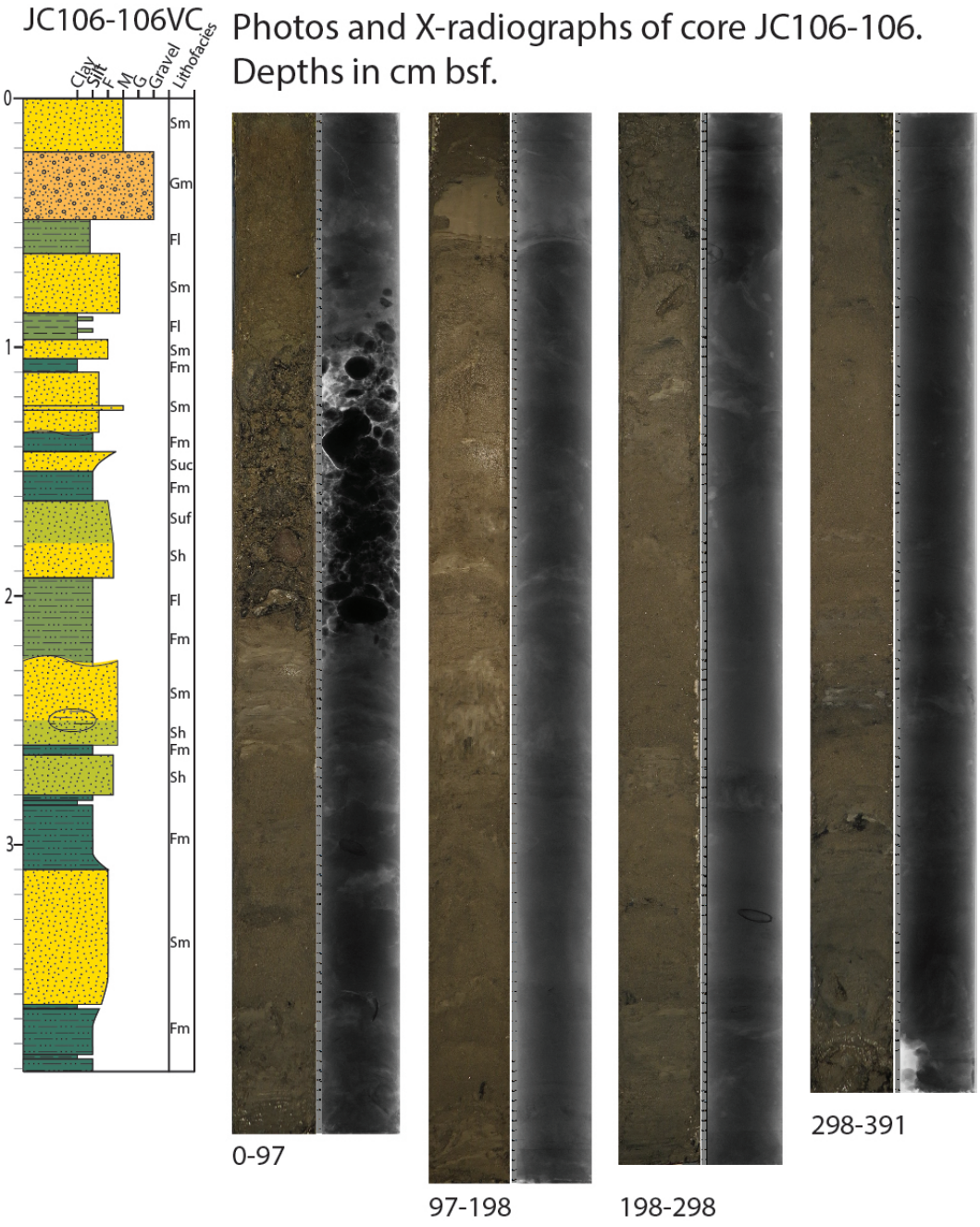

Figure 9.21: Corelog, photos and x-radiographs of core JC106-106.

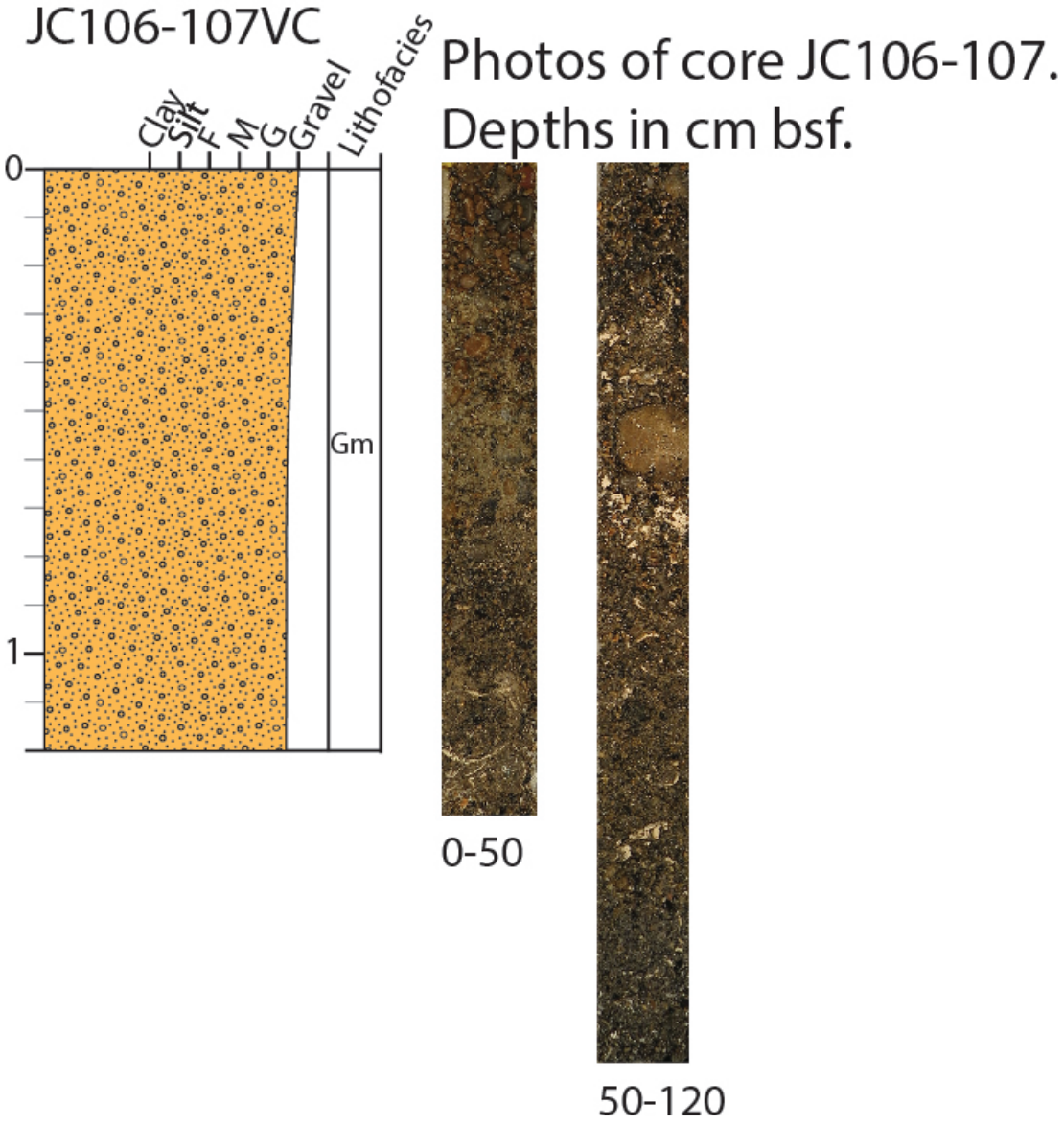

Figure 9.22: Corelog and photos of core JC106-107.

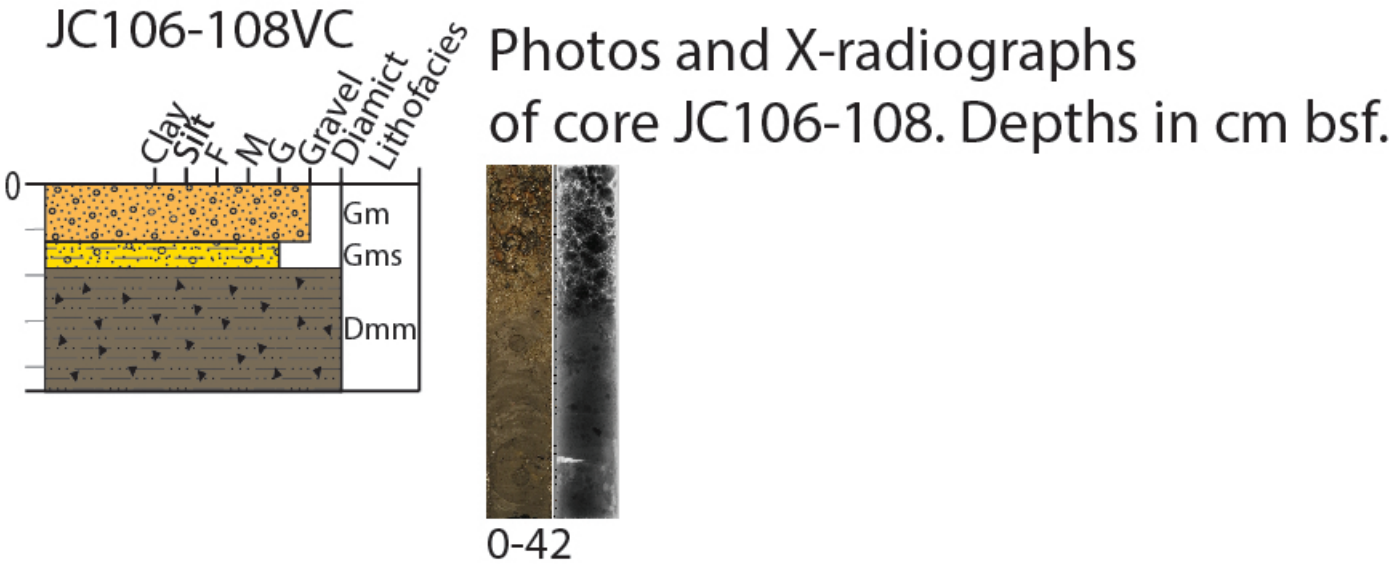

Figure 9.23: Corelog, photos and x-radiographs of core JC106-108.

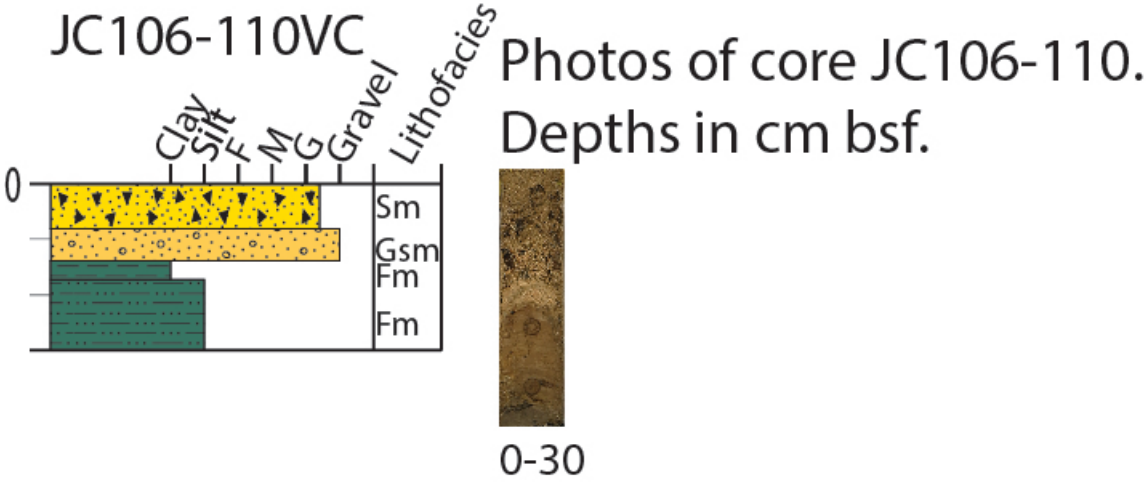

Figure 9.24: Corelog and photos of core JC106-110.

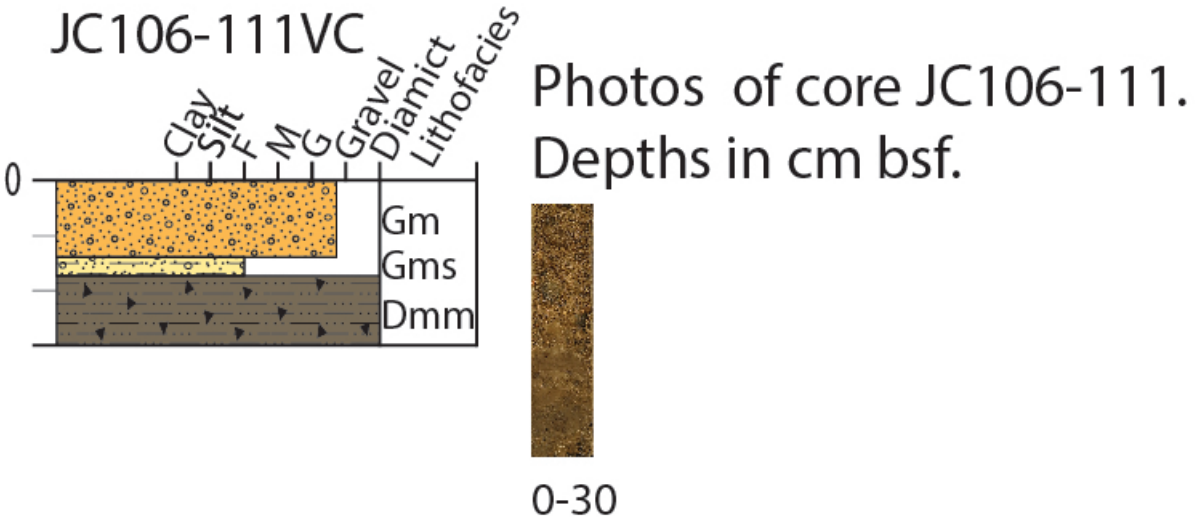

Figure 9.25: Corelog and photos of core JC106-111.

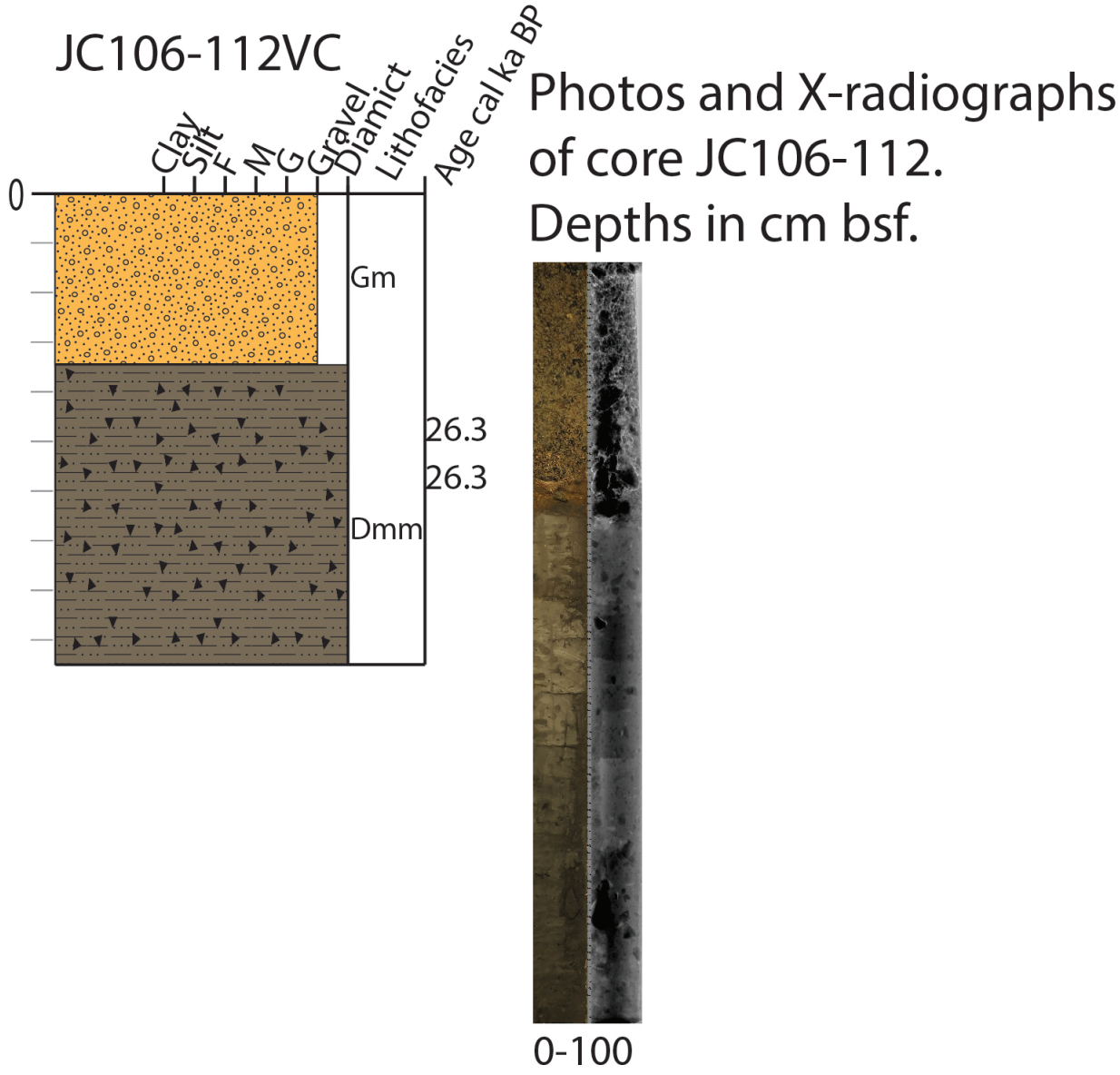

Figure 9.26: Corelog, photos and x-radiographs of core JC106-11.